

Aus der Klinik für Anästhesiologie
Abteilung für Transfusionsmedizin, Zelltherapeutika und Hämostaseologie
Klinikum der Ludwig-Maximilians-Universität München
Direktor: Prof. Dr. med. Andreas Humpe



**From Harmful to Useful:
Exploiting a Leukemia-Associated Transcription Factor
for Large-Scale Manufacture of Functional Human Macrophages**

Dissertation
zum Erwerb des Doktorgrades der Naturwissenschaften
an der Medizinischen Fakultät der
Ludwig-Maximilians-Universität München

vorgelegt von
Roland Windisch
aus
Augsburg

2022

Mit Genehmigung der Medizinischen Fakultät
der Universität München

Betreuer: PD Dr. rer. nat. Christian Kellner

Zweitgutachter: Prof. Dr. rer. nat. Jürgen Bernhagen

Dekan: Prof. Dr. med. Thomas Gudermann

Tag der mündlichen Prüfung: 04. Mai 2023

Table of Contents

Table of Contents	I
Abstract	IV
Zusammenfassung	V
List of Figures	VI
List of Tables	VIII
List of Abbreviations	IX
1. Introduction	1
1.1 Hematopoietic Stem Cells	1
1.1.1 Development, Location and Function	1
1.1.2 Regulation of Hematopoietic Differentiation by Transcription Factors	3
1.1.3 Hematological Malignancies	5
1.2 Chromosomal Translocations Involving MLL1	8
1.2.1 Structure and Function of MLL1	8
1.2.2 <i>Ex vivo</i> Expansion of Monocytic Progenitor Cells by MLL-ENL	10
1.3 Macrophages	11
1.3.1 Ontogeny and Classification	11
1.3.2 Phenotypes and Functions	13
1.3.3 Macrophages in Cancer.....	16
1.4 Cell-Based Immunotherapy	17
1.4.1 Non-Stem Cell-Based Therapy.....	18
1.4.2 Stem Cell-Based Therapy.....	20
1.4.3 Limitations and Challenges.....	23
1.4.4 Aims and Objectives	27
2. Materials and Methods	29
2.1 Materials	29
2.1.1 Chemicals	29
2.1.2 Kits	31
2.1.3 Buffers and Solutions.....	31
2.1.4 DNA Oligonucleotides.....	33
2.1.5 Cell Lines	34
2.1.6 Primary Cells.....	34
2.1.7 Cell Culture Media, Supplements and Reagents.....	34
2.1.8 Antibodies	36
2.1.9 Enzymes	37
2.1.10 Consumables	38
2.1.11 Devices	39
2.1.12 Bacterial strains	41
2.1.13 Plasmids	41
2.1.14 Software.....	42
2.2 Methods	43
2.2.1 Molecular Biology Techniques.....	43
2.2.1.1 Polymerase Chain Reaction (PCR).....	43

Table of Contents

2.2.1.1.1	Conventional PCR.....	43
2.2.1.1.2	Real-time Quantitative PCR (qPCR).....	44
2.2.1.1.3	Ligation-Mediated PCR (LM-PCR).....	44
2.2.1.2	TOPO Cloning.....	46
2.2.1.3	Heat Shock Transformation of <i>E. coli</i>	48
2.2.1.4	Culture and Storage of <i>E. coli</i>	48
2.2.1.5	Isolation of Plasmid DNA from <i>E. coli</i>	48
2.2.1.6	Isolation of RNA from Mammalian Cells.....	49
2.2.1.7	Isolation of Genomic DNA from Mammalian Cells.....	49
2.2.1.8	Photometric Analysis of Nucleic Acids.....	49
2.2.1.9	Enzymatic Restriction Digestion.....	50
2.2.1.10	Ligation of DNA Fragments.....	50
2.2.1.11	Agarose Gel Electrophoresis.....	50
2.2.1.12	Sanger Sequencing of DNA.....	51
2.2.1.13	Whole Exome Sequencing.....	51
2.2.1.14	Gene expression profiling.....	52
2.2.1.15	Cell Lysate Preparation.....	54
2.2.1.16	Protein Quantification via Bradford assay.....	54
2.2.1.17	Sodium Dodecyl Sulfate Polyacrylamide Gel Electrophoresis.....	55
2.2.1.18	Western Blot Experiment.....	55
2.2.2	Cell Biology Techniques.....	56
2.2.2.1	Cell Culture.....	56
2.2.2.2	Mammalian Cell Transfection with Polyethylenimine.....	58
2.2.2.3	Retroviral Transduction of Hematopoietic Stem Cells.....	59
2.2.2.4	Differentiation of DD-MLL-ENL Expressing Monocytic Precursor Cells.....	60
2.2.2.5	Cytospin Technique.....	61
2.2.2.6	Flow Cytometry.....	62
2.2.2.7	Karyotyping.....	63
2.2.2.8	Colony-Forming Unit Assay.....	63
2.2.2.9	Flow Chamber Adhesion Assay.....	64
2.2.2.10	Cell Migration Assay (Chemotaxis).....	65
2.2.2.11	<i>E. coli</i> BioParticles™ Uptake Assay.....	66
2.2.2.12	Efferocytosis Assay.....	67
2.2.2.13	Isolation of Mononuclear Cells from Peripheral Blood.....	67
2.2.2.14	Generation of M0 and M1 Macrophages.....	68
2.2.2.15	FcγR Binding Assay.....	68
2.2.2.16	Antibody-Dependent Cellular Phagocytosis.....	69
2.2.2.16.1	Analysis by Fluorescence Microscopy.....	69
2.2.2.16.2	Analysis by Live Cell Imaging.....	70
2.2.2.17	Statistical Analysis.....	70
3.	Results.....	71
3.1	HSPC Expansion via Stable Expression of DD-MLL-ENL.....	71
3.1.1	Analysis of Shield-1 Dependent Proliferation Advantage.....	71
3.1.2	Comparison with <i>HOX</i> Gene Overexpression in HSPCs.....	74
3.2	Characterization of DD-MLL-ENL Expressing Progenitor Cells ...	75
3.2.1	Analysis of Sustained Proliferative Ability.....	75

3.2.2	Phenotypical Characterization of DD-MLL-ENL Expressing Progenitor Cells	76
3.2.2.1	Morphologic Classification by Cytochemical Stains	77
3.2.2.2	Immunophenotyping	78
3.2.3	Investigation of Chromosome Number and Structure	79
3.2.4	Genome Integrity of DD-MLL-ENL Expanded Monocytic Progenitors	79
3.2.5	Retroviral Integration Site Analysis.....	82
3.3	Differentiation of DD-MLL-ENL Myeloid Progenitor Cells	84
3.3.1	Differentiation upon Shield-1 Deprivation	85
3.3.2	Macrophage Differentiation Mediated by GM-CSF, LPS and IFN- γ	87
3.3.3	Analysis of Colony-Forming Capacity.....	88
3.4	Characterization of Differentiated DD-MLL-ENL Derived Macrophages	90
3.4.1	Immunophenotyping	90
3.4.2	Gene Expression Profiling	92
3.4.2.1	Expression of Inflammatory Genes	93
3.4.2.2	Expression of Innate Immunity-Related Genes	94
3.4.3	Functional Characteristics of Differentiated DD-MLL-ENL Macrophages ..	102
3.4.3.1	Adhesion under Shear Stress.....	102
3.4.3.2	Chemokine-Guided Migration	103
3.4.3.3	Phagocytic Properties	105
3.4.3.3.1	Phagocytosis of Bacterial Particles	105
3.4.3.3.2	Efferocytosis.....	106
3.4.3.3.3	Antibody-Dependent Cellular Phagocytosis (ADCP)	107
4.	Discussion	114
4.1	Characteristics of DD-MLL-ENL Expanded Progenitor Cells.....	115
4.2	How Natural Are DD-MLL-ENL Derived Macrophages?	118
4.3	Risk Assessment of Oncogenes as Expansion Factors	123
4.4	Comparison with Established Expansion Methods	126
4.5	Consideration for Clinical Application: What Follow-Up Steps Are Required?.....	130
	List of References	133
	Acknowledgements.....	156
	Affidavit.....	157
	List of Publications	158

Abstract

Expansion of hematopoietic stem and progenitor cells outside the body is hardly possible due to spontaneous differentiation. Therefore, *ex vivo* production of immune cells in sufficient quantities for cell therapeutic approaches is limited. Exploitation of oncogenic fusion proteins represents a new, promising possibility for *ex vivo* propagation of human blood progenitor cells. These chromosomal translocation-derived chimeric transcription factors are capable of driving hematopoietic progenitor cell expansion by blocking differentiation. In this context, it was investigated to what extent a controllable designed leukemia-associated fusion protein can be exploited for *ex vivo* proliferation of human hematopoietic progenitor cells to generate functional macrophages on a large scale after switching off the protein. As such a fusion gene, MLL-ENL was stably integrated into the genome of human hematopoietic progenitor cells via retroviral gene transfer. A destabilization domain fused to MLL-ENL was used to target protein stability using the specific small molecule ligand Shield-1. In the presence of Shield-1, late monocytic progenitor cells were expanded in a large scale in *ex vivo* cultures in a controlled manner. The cells exhibited an immature monocyte immunophenotype, a normal karyotype, and permanent Shield-1 dependence. Genome-wide sequencing and viral integration site analysis also confirmed the absence of copy number alterations, mutations, or integration-activated proto-oncogenes that could promote cell proliferation. Shield-1 withdrawal allowed the expanded progenitor cells to be specifically differentiated into functional macrophages with appropriate cytokines. These phagocytes expressed macrophage-associated cell surface proteins and upregulated a variety of genes that play critical roles in the innate immune response. Functionally, adhesion under shear stress, migration along a chemokine gradient, and clearance of inactivated bacteria and apoptotic cells were demonstrated. Furthermore, macrophages were able to efficiently phagocytose antibody-loaded lymphoma or leukemia cells derived from patient blood. In summary, functional human phagocytes were produced for the first time from MLL-ENL expanded monocytic progenitor cells and characterized in detail by molecular and cell biology. This successful proof of concept suggests that such acute leukemia-derived and modified transcription factors have the potential to be used as molecular tools to generate functional immune cells for cell therapy approaches.

Zusammenfassung

Die Expansion hämatopoetischer Stamm- und Vorläuferzellen außerhalb des Körpers ist aufgrund spontaner Differenzierung kaum möglich. Daher ist die *ex vivo* Herstellung von Immunzellen in ausreichenden Mengen für zelltherapeutische Ansätze limitiert. Eine neue, vielversprechende Möglichkeit zur *ex vivo* Vermehrung humaner Blutvorläuferzellen stellt die Ausnutzung onkogener Fusionsproteine dar. Diese durch chromosomale Translokationen entstehenden chimären Transkriptionsfaktoren sind in der Lage, durch Blockade der Differenzierung die Expansion von hämatopoetischen Vorläuferzellen anzutreiben. In diesem Zusammenhang wurde untersucht, inwiefern ein regulierbar gestaltetes, Leukämie-assoziiertes Fusionsprotein für die *ex vivo* Vermehrung humaner hämatopoetischer Vorläuferzellen ausgenutzt werden kann, um nach Abschaltung funktionelle Makrophagen in großem Maßstab zu generieren. Als solches Fusionsgen wurde MLL-ENL mittels retroviralem Gentransfer stabil in das Genom humaner hämatopoetischer Vorläuferzellen integriert. Durch eine an MLL-ENL fusionierte Destabilisierungsdomäne konnte die Proteinstabilität mit Hilfe des spezifischen niedermolekularen Liganden Shield-1 gezielt reguliert werden. In Anwesenheit von Shield-1 wurden späte monozytäre Vorläuferzellen in großem Maßstab in *ex vivo* Kulturen kontrolliert vermehrt. Die Zellen wiesen einen unreifen monozytären Immunphänotyp, einen normalen Karyotyp sowie eine permanente Shield-1 Abhängigkeit auf. Genomweite Sequenzierungen und die Analyse der viralen Integrationsstellen bestätigten zudem die Abwesenheit von Kopienzahlvariationen, Mutationen oder durch Integration aktivierten Proto-Onkogenen, welche die Proliferation der Zellen begünstigen könnten. Durch Shield-1 Entzug konnten die expandierten Vorläuferzellen mit geeigneten Zytokinen gezielt zu funktionellen Makrophagen differenziert werden. Diese Phagozyten exprimierten Makrophagen-assoziierte Zelloberflächenproteine und regulierten eine Vielzahl an Genen hoch, welche eine entscheidende Rolle bei der angeborenen Immunantwort spielen. Funktionell konnte Adhäsion unter Scherspannung, die Migration entlang eines Chemokingradienten sowie das Beseitigen inaktiver Bakterien und apoptotischer Zellen gezeigt werden. Des Weiteren waren die Makrophagen in der Lage, aus Patientenblut gewonnene, Antikörper-beladene Lymphom- oder Leukämiezellen effizient zu phagozytieren. Zusammenfassend wurden erstmals funktionelle humane Phagozyten aus MLL-ENL expandierten monozytären Vorläuferzellen hergestellt und eingehend molekular- und zellbiologisch charakterisiert. Dieses erfolgreiche *Proof of Concept* legt nahe, dass solche von akuten Leukämien abgeleiteten und modifizierten Transkriptionsfaktoren das Potenzial haben, als molekulare Werkzeuge zur Herstellung funktioneller Immunzellen für zelltherapeutische Ansätze eingesetzt zu werden.

List of Figures

Figure 1: Evolution of hematopoiesis models.	4
Figure 2: Overview of the cellular origins of hematological malignancies.	6
Figure 3: Scheme of MLL1 functional domains and their involvement in multi-protein complexes.	9
Figure 4: Mode of action of the fusion protein MLL-ENL.	11
Figure 5: Graphical representation of the different origins of human macrophages.	12
Figure 6: Schematic of M1 and M2 macrophage polarization.	15
Figure 7. Graphical abstract illustrating the different steps during an LM-PCR.	46
Figure 8: Nanostring's CodeSet chemistry enabling specific target mRNA detection.	53
Figure 9: Graphical depiction of the regulable DD-Shield-1 interplay with MLL-ENL as protein of interest.	57
Figure 10: Tracking of DD-MLL-ENL transduced, GFP+ cells in the presence or absence of Shield-1.	72
Figure 11: Outgrowth tracking of DD-MLL-ENL transduced, GFP+ cells in the presence of Shield-1.	73
Figure 12: Tracking of HOXB4, HOXB8 and HOXA9 transduced, GFP+ cells.	75
Figure 13: Long-term and large-scale proliferation capacity of DD-MLL-ENL expressing progenitor cells in the presence of Shield-1.	76
Figure 14: Cytochemical staining of DD-MLL-ENL progenitor cells.	77
Figure 15: Immunophenotype of DD-MLL-ENL cells cultivated in the presence of Shield-1.	78
Figure 16: Representative karyogram of a DD-MLL-ENL progenitor cell sample at day 72 of expansion derived from a female HSC donor.	79
Figure 17: CNA comparison of outgrown DD-MLL-ENL progenitor cells with donor-matched untransduced HSCs.	80
Figure 18: Allele frequency of cancer-related genetic variants prior to transduction and after complete outgrowth of DD-MLL-ENL cells.	82
Figure 19: Agarose gel electrophoresis of amplified LM-PCR products from genomic DNA of DD-MLL-ENL cells.	83
Figure 20: Graphical scheme illustrating the hypothetical two-step procedure for large-scale manufacture of human macrophages.	85
Figure 21: Flow cytometry and western blot after Shield-1 deprivation.	86
Figure 22: Flow cytometry analyses of DD-MLL-ENL cells after withdrawal of Shield-1 in different cytokine settings.	87
Figure 23: Morphology of DD-MLL-ENL cells prior and after a six-day differentiation.	87
Figure 24: Differentiation progress of DD-MLL-ENL progenitor cells upon Shield-1 withdrawal and stimulation with GM-CSF, LPS and IFN- γ	88
Figure 25: Colony-forming capacity of DD-MLL-ENL cells prior and upon Shield-1 deprivation and differentiation.	89
Figure 26: Immunophenotypical characterization of DD-MLL-ENL derived macrophages.	90
Figure 27: Analysis of Fc γ receptor and MHC class I and II surface expression on DD-MLL-ENL derived macrophages.	92
Figure 28: qPCR analysis for mRNA expression of inflammatory genes.	93
Figure 29: mRNA expression levels of 730 innate immunity-related genes in the four different cell types.	95
Figure 30: Analysis of the macrophage abundance score by cell type profiling based on specific gene expression.	96

Figure 31. Gene expression volcano plots of sample groups versus annotated reference.....	97
Figure 32: Directed global significance score of innate immunity-related gene subsets in the analyzed sample groups.	98
Figure 33: mRNA expression levels of core proliferation genes.	99
Figure 34: Heatmaps of differentially expressed genes involved in selected immunity-related pathways.	100
Figure 35: Adhesion properties of DD-MLL-ENL derived macrophages under shear stress.	103
Figure 36: Chemotaxis of DD-MLL-ENL macrophages towards the chemoattractant CCL2.	104
Figure 37: Proof of phagocytosis of bacterial particles by DD-MLL-ENL macrophages.	105
Figure 38: Efferocytosis of apoptotic Jurkat cells mediated by DD-MLL-ENL macrophages.	106
Figure 39: Binding of IgGs by FcγR expressed on DD-MLL-ENL macrophages.	107
Figure 40: ADCP of lymphoma cells by DD-MLL-ENL macrophages.	109
Figure 41: ADCP progression of DD-MLL-ENL and PBMC-derived M0 and M1 macrophages.	110
Figure 42: Influence of CD47 blockade on ADCP of Daudi cells by DD-MLL-ENL macrophages.	111
Figure 43: ADCP of patient-derived CLL cells by DD-MLL-ENL macrophages.	112
Figure 44: Graphical scheme of the macrophage manufacturing process for potential cell therapeutic approaches.	132

List of Tables

Table 1: Common genetic alterations in hematological malignancies.....	7
Table 2: Overview of chemicals	29
Table 3: Overview of kits	31
Table 4: Overview of buffers and solutions.....	31
Table 5: Overview of primers	33
Table 6: Overview of cell lines	34
Table 7: Overview of primary cells	34
Table 8: Overview of cell culture media, supplements and reagents	34
Table 9: Overview of antibodies	36
Table 10: Overview of enzymes	38
Table 11: Overview of consumables	38
Table 12: Overview of devices	39
Table 13: Overview of bacterial strains.....	41
Table 14: Overview of the vectors	41
Table 15: Overview of software.....	42
Table 16: Components for conventional PCR reactions	43
Table 17: Cycling conditions for <i>HOXA9</i> amplification.....	44
Table 18: Components for TOPO cloning.....	48
Table 19: BSA dilutions for the Bradford assay calibration curve.....	55
Table 20: Composition of the PEI transfection solutions	58
Table 21: Shear stress settings for the flow chamber adhesion assay.....	65
Table 22: Composition of the rat tail collagen I solution	66
Table 23: LM-PCR-based identification of genes affected by retroviral integration. ...	84

List of Abbreviations

ACT	Adoptive cell therapy
ADCP	Antibody-dependent cellular phagocytosis
AHD	ANC1 homology domain
AhR	Aryl hydrocarbon receptor
ALL	Acute lymphoblastic leukemia
AML	Acute myeloid leukemia
APC	Allophycocyanin
APS	Ammonium persulfate
ARG1	Arginase
ASC	Adult stem cell
BCMA	B cell maturation antigen
BCR	Breakpoint cluster region
BET	bromodomain and extraterminal proteins
BRD	Bromodomain
BSA	Bovine serum albumin
CAR	Chimeric antigen receptor
CCL	C-C motif ligand
CCR	C-C motif chemokine receptor
CD	Cluster of differentiation
cDNA	Complementary DNA
CFU	Colony-forming unit
CLL	Chronic lymphocytic leukemia
CML	Chronic myelogenous leukemia
CMP	Common myeloid progenitor
CMV	Cytomegalovirus
CNA	Copy number alteration
CRISPR	Clustered Regularly Interspaced Short Palindromic Repeats
CRS	Cytokine release syndrome
CTLA4	Cytotoxic T-lymphocyte-associated protein 4
CXCL	C-X-C motif ligand
CXCR	C-X-C motif chemokine receptor
DAMPS	Damage-associated molecular pattern
DD	Destabilization domain
ddH ₂ O	Double-distilled water
DMSO	Dimethyl sulfoxide
DNA	Deoxyribonucleic acid
dNTPs	Deoxynucleoside triphosphates
DSMZ	Deutsche Sammlung von Mikroorganismen und Zellkulturen
E. coli	Escherichia coli

List of Abbreviations

E:T	Effector to target
ECM	Extracellular matrix
EGC	Embryonic germ cell
ENL	Eleven-nineteen-leukemia
EpiSC	Epiblast-derived stem cell
ESC	Embryonic stem cell
EST	Esterase
FAB	French-American-British
FACS	Fluorescence Activated Cell Sorting
FcR	Fc receptor
FDA	Food and Drug Administration
FLT3	Fms like tyrosine kinase 3
Flt3-L	Fms like tyrosine kinase 3 ligand
FMEV	combination of Friend Mink cell focus-forming viruses (FMCF) and murine embryonic stem cell virus (MESV)
FSC	Forward scatter
FYRC	FY-rich C-terminal
FYRN	FY-rich N-terminal
GALV	Gibbon ape leukemia virus
G-CSF	Granulocyte colony-stimulating factor
gDNA	Genomic DNA
GFP	Green fluorescent protein
GM-CSF	Granulocyte-macrophage colony-stimulating factor
GMP	Granulocyte/monocyte progenitor
GvHD	Graft-versus-host disease
HBSS	Hanks' Balanced Salt Solution
HL	Hodgkin lymphoma
HLA	Human leukocyte antigen
HOX	Homeobox
HRP	Horseradish peroxidase
HSC	Hematopoietic stem cell
HSCT	Hematopoietic stem cell transplantation
HSPC	Hematopoietic stem and progenitor cell
IFN	Interferon
IgG	Immunoglobulin G
IL	Interleukin
iNOS	Inducible nitric oxide synthase
iPSC	Induced pluripotent stem cell
IRES	Internal ribosomal entry site
LB	Lysogeny broth
LBD	Lens epithelium-derived growth factor binding domain

List of Abbreviations

LM-PCR	Ligation-mediated polymerase chain reaction
LPS	Lipopolysaccharide
LRS	Leukocyte reduction system
LT-HSC	Long-term repopulating hematopoietic stem cell
LTR	Long terminal repeat
MBM	Menin-binding motif
MCL	Mantle cell lymphoma
M-CSF	Macrophage colony-stimulating factor
MDS	Myelodysplastic syndrome
MEN1	Menin
MFI	Mean fluorescence intensity
MHC	Major histocompatibility complex
MLL	Mixed-lineage leukemia
MPN	Myeloproliferative neoplasm
MPS	Mononuclear phagocytic system
mRNA	Messenger RNA
MSC	Mesenchymal stem/stromal cell
MSCV	Murine Stem Cell Virus
NHL	Non-Hodgkin lymphoma
NK cell	Natural killer cell
NOD-SCID	Non-Obese Diabetic-Severe Combined Immunodeficiency
NSC	Neural stem cell
NSG	NOD scid gamma
OCT	Octamer-binding transcription factor
PAMPS	Pathogen-associated molecular pattern
PBMC	Peripheral blood mononuclear cell
PBS	Phosphate buffered saline
PBST	Phosphate buffered saline tween 20
PCR	Polymerase chain reaction
PE	Phycoerythrin
PEI	Polyethylenimine
PGE2	Prostaglandin E2
PHD	Plant homeodomain
PI	Propidium iodide
POX	Myeloperoxidase
PSC	Pluripotent stem cell
qPCR	Quantitative polymerase chain reaction
RNA	Ribonucleic acid
ROS	Reactive oxygen species
rpm	Rounds per minute
RUNX1	Runt-related transcription factor 1

List of Abbreviations

RVI	Retroviral vector integration site
SCF	Stem cell factor
scFv	Single chain variable fragment
SDF1	Stromal cell-derived factor 1
SDS	Sodium dodecyl sulfate
SDS-PAGE	Sodium dodecyl sulfate polyacrylamide gel electrophoresis
SEC	Super elongation complex
SET	Su(Var)3-9, enhancer-of-zeste, trithorax
SIRP	Signal regulatory protein
SOX2	Sex determining region Y (SRY)-box 2
SR1	StemRegenin 1
SSC	Side scatter
SSC	Skin stem cell
ST-HSC	Short-term repopulating hematopoietic stem cell
TAD	Transactivation domain
TAL1	T-cell acute lymphocytic leukemia protein 1
TAM	Tumor-associated macrophage
TCR	T cell receptor
TIL	Tumor-infiltrating lymphocyte
TLR	Toll-like receptor
TME	Tumor microenvironment
TNF	Tumor necrosis factor
TPO	Thrombopoietin
Treg	Regulatory T cell
USD	US dollar
UTD	Untransduced
VAF	Variant allele frequency
VCAM	Vascular cell adhesion molecule
VLA	Very late antigen
WES	Whole exome sequencing
WHO	World Health Organization
X-CGD	X-linked chronic granulomatous disease
YEATS	Yaf9, ENL, AF9, Taf14, Sas5

1. Introduction

1.1 Hematopoietic Stem Cells

1.1.1 Development, Location and Function

Hematopoietic stem cells (HSCs) constitute a rare population of cells with an occurrence of approximately 0.01% of nucleated cells within the bone marrow (Rossi et al., 2011). HSCs are essential for life-long hematopoiesis by giving rise to all progeny blood cells. Their collective hallmark is the maintenance of self-renewal activity and their ability to differentiate into mature blood cells (Seita and Weissman, 2010, Weissman and Shizuru, 2008). HSCs display the apex of the hematopoietic hierarchy by possessing a multipotent character presiding over a distinctive variety of progenitor cells. Evidence of the existence of cells capable of self-renewal that coordinate the regulation of the hematopoietic system arose in 1949 when Jacobsen and colleagues demonstrated that fatal marrow aplasia in mice could be rescued by protecting the spleen from total body irradiation, the organ in which murine hematopoiesis occurs (Jacobson et al., 1953). In 1961 the presence of HSCs was predicted by Till et al. who found the presence of clonogenic mixed colony formation in the spleen followed injection of bone marrow cells into irradiated mice (Till and Mc, 1961), while in 1963 Becker and colleagues stated a clonal origin of blood cells (Becker et al., 1963). During embryogenesis in vertebrates, first primitive hematopoietic cells emerge from the yolk sac, mainly consisting of nucleated erythrocytes, inside so-called yolk sac blood islands (Haar and Ackerman, 1971). In contrast, definitive self-renewing HSCs first originate from the ventral aortic endothelium wall of the Aorta-Gonad-Mesonephros region (de Bruijn et al., 2000, Medvinsky and Dzierzak, 1996). This process is known as endothelial-to-hematopoietic transition indicating the definitive HSCs' origin from endothelial precursors (Jaffredo et al., 1998). The relinquished cells proceed to colonize the fetal liver and the adult bone marrow where they reside and ensure long-term hematopoiesis (Zovein et al., 2008). Within the bone marrow, HSCs are responsible for replenishing the cellular blood constituents both in steady state and upon infection or injury (Wilson et al., 2008, Baldrige et al., 2010). HSCs represent a cell population dividing in both symmetric and asymmetric manners (Loeffler and Schroeder, 2021). The latter results in a daughter HSC and a committed progenitor cell, a more restricted descendant (Cheshier et al., 1999). Within the HSC compartment, two different homogeneous pools were defined with long-term reconstituting HSCs (LT-HSCs) that stay comparatively quiescent to prevent constant cell-cycle related DNA damage and short-term HSCs (ST-HSCs) (Morrison and Weissman, 1994). These ST-HSCs feature a limited self-renewal capacity and possess restricted lineage differentiation ability towards mature blood cells (Laurenti

and Gottgens, 2018). This way, around $4-5 \times 10^{11}$ hematopoietic cells are formed each day (Kaushansky, 2006). A distinct balance between differentiation and self-renewal is of paramount importance to maintain the HSC reservoir on the one side and to guarantee sufficient differentiation on the other side. Disturbed balance may result in hematopoietic malignancies where differentiation is impaired combined with unrestricted self-renewal.

The activity of HSCs is governed by intrinsic factors including transcriptional and epigenetic cues as well as by extrinsic factors from the interaction with the bone marrow microenvironment, known as the hematopoietic stem cell niche, originally proposed by Ray Schofield in 1978 (Schofield, 1978). Nowadays, the HSC niche is described as a network encompassing various hematopoietic and non-hematopoietic cells interacting with each other both physically and by molecular cues. These processes take place in the cavities of primarily axial bones, which constitute the major hematopoiesis sites (Asada et al., 2017b). Vascularization for removal of waste products as well as for supply of nutrients, oxygen and growth factors within the bone cavity is ensured by the periosteum, which orchestrates entry and exit of blood vessels (Chanavaz, 1995). In the hematopoietic niche itself, HSCs are intertwined by various types of supportive cells playing a decisive role for HSC quiescence, maintenance as well as mobilization. These include mesenchymal stem and progenitor cells, osteolineage cells (osteoblasts and osteocytes), adipocytes, endothelial cells, adrenergic nerve-associated cells as well as hematopoietic HSC progeny cells such as macrophages and megakaryocytes forming a complex network influencing HSC status via either direct or indirect mechanisms (Wei and Frenette, 2018). Apart from direct receptor-ligand interaction soluble factors substantially contribute to HSC activity (Boulais and Frenette, 2015). As such, the proteins CXCL12, also known as stromal cell-derived factor 1 binding the cognate receptor CXCR4 and stem cell factor (SCF), the ligand for c-KIT, both mainly secreted by mesenchymal stem cells, display relevant cues for HSC maintenance (Mendez-Ferrer et al., 2010, Asada et al., 2017a). Moreover, the glycoprotein hormone thrombopoietin (TPO), produced by the liver and kidney, is primarily associated with the production of megakaryocytes which positively regulate HSC maintenance through CXCL4 (Wang et al., 2018). Recently, an additional major role of TPO in directly impacting HSC self-renewal was ascertained by inducing the shift from the G0 to the G1 cell cycle phase (Wang et al., 2018). In contrast, the granulocyte colony-stimulating factor (G-CSF) disturbs the binding of CXCL12 to the cognate receptor CXCR4 expressed on HSCs leading to mobilization and egress into the circulation (Petit et al., 2002). This process is mainly controlled by both peripheral sympathetic nerve-derived noradrenaline signaling (Katayama et al., 2006) and nociceptor nerve-derived neurotransmitter release further highlighting a complex regulatory niche interaction network (Gao et al., 2021).

1.1.2 Regulation of Hematopoietic Differentiation by Transcription Factors

HSCs sit on top of the hematopoiesis and are therefore responsible for the production of all mature blood cells. Back in 1868, the term “stem cell” was originally used by Ernst Haeckel to describe a unicellular organism giving rise to multicellular life (Haeckel, 1873). This concept was subsequently adopted by histopathologists to describe hematopoiesis resulting in tree-like model with a common progenitor of both red and white blood cells (Laurenti and Gottgens, 2018). This tree-like model portrayed a multi-level descent from the multipotent stem cells to their progeny by several discrete branching steps. Until the early 2000s, this model served as traditional mapping of hematopoiesis with the classical first branch point that separates lymphoid potential from other lineages including myeloid, erythroid and megakaryocytic (Akashi et al., 2000). In a distinct tree-like manner subsequent branches lead to progression from multi- over bi- to ultimately unipotent progenitor cells (Orkin and Zon, 2008). During the hematopoiesis process mature blood cells are produced in a step-wise behavior (Laurenti and Gottgens, 2018). In terms of the two diverse lineages, myeloid progenitors give rise to erythrocytes, megakaryocytes and innate immune cells. Erythrocytes are responsible for the oxygen transport and guarantee supply throughout the whole body. Megakaryocytes represents the cell type which is in charge of producing and releasing platelets, which are essential for blood clotting. The cells associated with innate immunity consist of granulocytes as well as monocytes and dendritic cells. Their two main functions are to warrant a broad first-line defense against pathogens and to activate the adaptive immune system through antigen presentation. The adaptive immune system includes B and T cells originated from common lymphoid precursors representing the second major branch (Liggett and Sankaran, 2020). In recent years this old stringent hierarchical concept with its binary decisions has been overhauled by a new paradigm proposing a more continuous model. Single-cell RNA sequencing, transcriptional analyses and the introduction of other surface markers revealed that the traditional progenitor cells include several subpopulations with transcriptional profiles related to definite lineage commitment stepping back from the binary fate decision which was demonstrated by Velten and colleagues (Velten et al., 2017). These observations led to an updated vision of hematopoietic differentiation as a continuous distribution of cells without punctuated phenotypic changes and a switch from a homogeneous population assumption to a rather heterogeneous one. Thus, progenitors could be considered as rather transitory states within the hematopoietic stem and progenitor cell (HSPC) compartment (Weinreb et al., 2020, Dong et al., 2020, Laurenti and Gottgens, 2018). Moreover, stringent linear differentiation was questioned by verifying the existence of myeloid cells in early

lymphoid populations and vice versa (Adolfsson et al., 2005, Doulatov et al., 2010). Additionally, a direct differentiation of HSCs towards megakaryocytes has been suggested (Haas et al., 2015, Sanjuan-Pla et al., 2013). Although the given model proposes a continuum, punctuated transitions may still be existent resulting in a third model that combines the previous two and states functionally distinct heterogeneous cell populations (Pietras et al., 2015, Laurenti and Gottgens, 2018) (Figure 1).

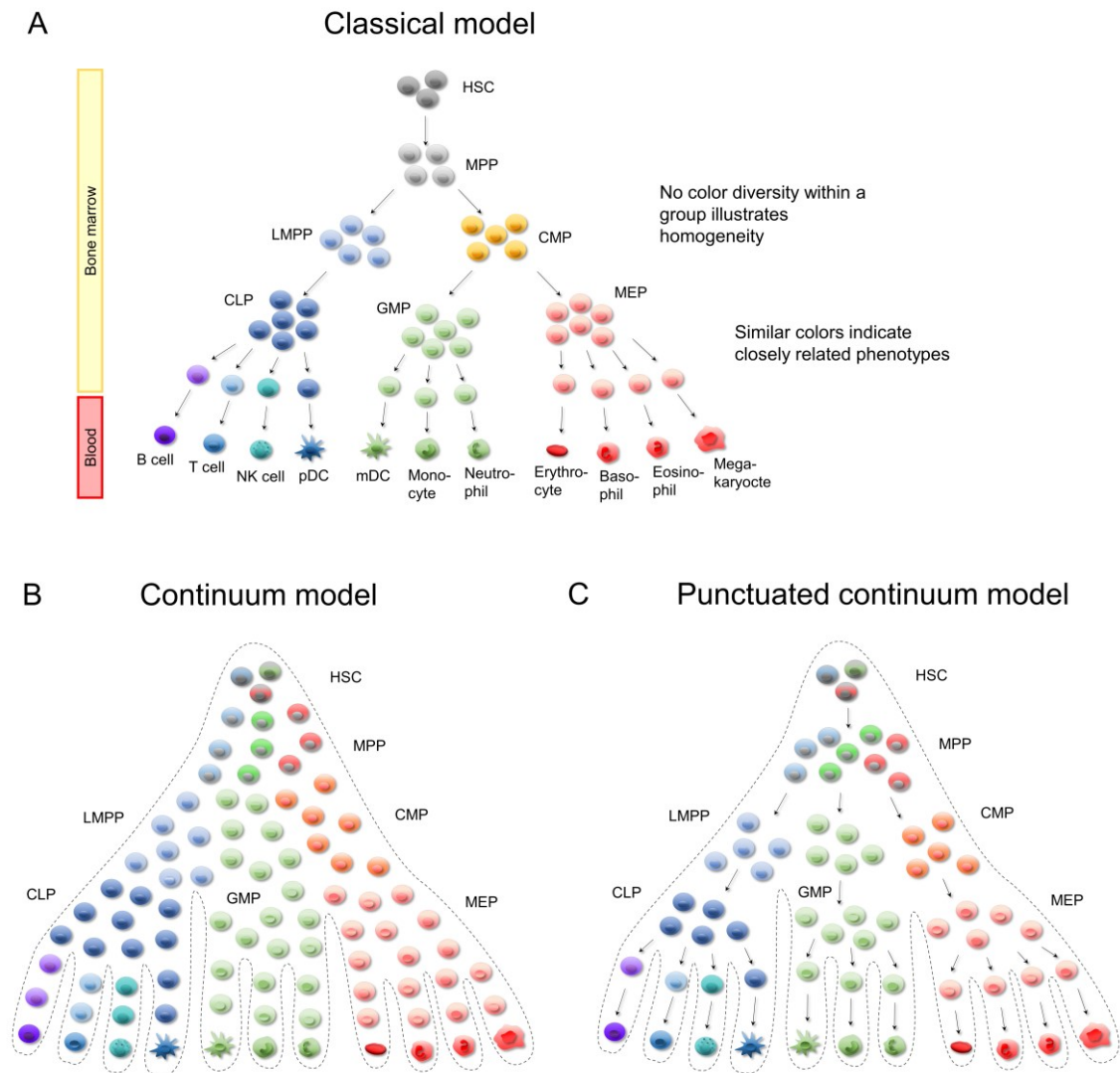


Figure 1: Evolution of hematopoiesis models. (A) The classical model of hematopoiesis is characterized by a stringent hierarchy with punctuated transition from one phenotype to a more differentiated one. Cell populations are separated by each other marked with different colors and show uniform potential. (B) In the continuum model punctuation is abrogated and replaced by a continuous differentiation process. The more immature cell populations display heterogeneity. (C) The punctuated continuum model combines the previous models with heterogeneous pools giving rise to different lineages as illustrated by punctuation. HSC, hematopoietic stem cell; MPP, multipotent progenitor; CMP, common myeloid progenitor; MEP, megakaryocyte/erythroid progenitor; GMP, granulocyte/macrophage progenitor; CLP, common lymphoid progenitor; LMPP, lymphoid-primed multi-potential progenitor; pDC, plasmacytoid dendritic cell; mDC, myeloid dendritic cell. Based on Liggett and Sankaran, 2020.

This differentiation process starting from HSCs is regulated by both internal and external signaling cues and is tightly controlled by the activity of transcription factors (Krumsiek et al., 2011). Cell type specific gene expression plays a pivotal role in orchestrating differentiation programs, which are governed by various transcription factors. The critical contribution of these proteins in hematopoiesis is highlighted by the fact that changes in activity such as a loss of function mutation impair stem cell properties and alter lineage choices. In this context, key hematopoietic transcription factors such as RUNX1 (runt-related transcription factor 1), TAL1 (T-cell acute lymphocytic leukemia 1) and GATA2 are essential for both primitive and adult definitive hematopoiesis. As crucial regulators of hematopoiesis they control HSC maintenance (GATA2) and organize differentiation into functional blood cells (RUNX1, TAL1). Another vital transcription factor orchestrating HSPC self-renewal is MLL (mixed-lineage leukemia), a regulator of multiple homeobox (*HOX*) genes. These *HOX* genes in turn encode for transcription factors contributing to HSPC proliferation (Ernst et al., 2004). Therefore, perturbed transcription factor activity in form of chromosomal translocations or mutations has been associated with the onset of hematological malignancies (Zhu and Emerson, 2002).

1.1.3 Hematological Malignancies

The normal hematopoiesis process can be disrupted resulting in the aberrant production and/or deficient maturation of blood cells in a malignant manner. Various forms of these so-called blood neoplasms exist which are summarized under the term hematological malignancies (Taylor et al., 2017). According to the World Health Organization (WHO) these malignancies are categorized due to the localization of origin, the lineage of the neoplastic cell, their stage within the hematopoietic differentiation hierarchy, their chronic or acute development and additionally their genetic and morphological characteristics (Arber et al., 2016, Swerdlow et al., 2016). Dependent on the cell type and the localization where the cancer originates, these malignancies comprise leukemias (affecting hematopoietic progenitor cells in the bone marrow) and lymphomas (originated mainly in the lymph node niche). In relation to the two major lineages (lymphoid and myeloid), acute lymphoblastic leukemias (ALL) and lymphomas including chronic lymphocytic leukemias (CLL) and multiple myeloma pertain to the lymphoid line, whereas chronic myelogenous leukemia (CML), acute myeloid leukemia (AML) are of myeloid origin. Two additional neoplasms which are associated with the myeloid lineage but develop in the HSC compartment are the myeloproliferative neoplasm (MPN) and the myelodysplastic syndrome (MDS) (Mead and Mullally, 2017). The exact origin of the given malignancy is depicted in Figure 2. Although some of the malignancies share the

same affected cell type they differ in terms of maturity state of the proliferating cells, causes, treatment and progression velocity.

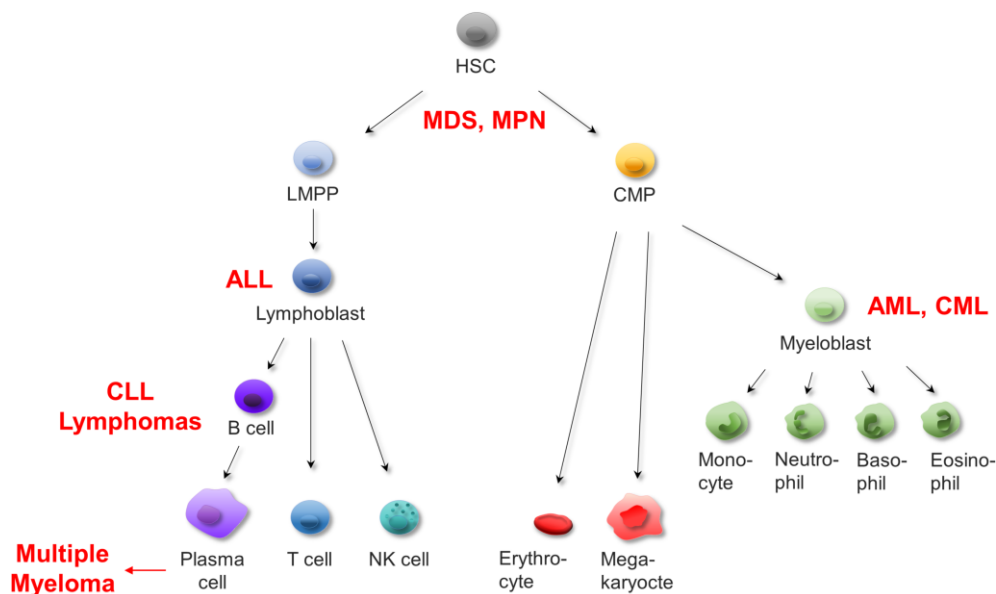


Figure 2: Overview of the cellular origins of hematological malignancies. For each delineated neoplasm the cellular origin is depicted within this simplified hematopoietic hierarchy. MDS, myelodysplastic syndrome; MPN, myeloproliferative neoplasm; ALL, acute lymphoblastic leukemia; AML, acute myeloid leukemia; CML, chronic myelogenous leukemia; CLL, chronic lymphocytic leukemia.

The cause for the malignant transformation of these hematopoietic cells represent genetic alterations disturbing the cell's physiological functions. According to the hallmarks of cancer, malignant cells feature acquired biological capabilities such as sustaining proliferative signaling, resisting cell death and enabling replicative immortality. The acquisition of these functions mainly originate from two enabling characteristics: the tumor-promoting inflammation driven by immune cells and the genome instability and mutations (Hanahan and Weinberg, 2011). The latter is the most prominent cause for the transformation and include abnormalities of the genomic structure provoked by chromosomal alterations and translocations, copy number alterations (CNAs) and specific point mutations (Taylor et al., 2017). In particular, chromosomal rearrangements including deletions, duplications, inversions and translocations frequently contribute to malignant transformation by abnormal expression of proliferation-associated oncogenes or by yielding tumor-specific fusion transcripts in a step-wise manner (He et al., 2016, Jan and Majeti, 2013). Chromosomal rearrangements represent a group of genomic alterations which arise as a result of defective repair of DNA breaks at two distinct loci by non-homologous end joining (Betermier et al., 2014). These rearrangements can be either balanced or unbalanced. They are classified as balanced when an equal exchange of genetic information appears between the two different loci, which is the case for

reciprocal translocations (co-existing breaks on different chromosomes) and inversions (breaks on the same chromosome). Unbalanced rearrangements display an uneven gain or loss of genetic information and therefore comprise insertions, deletions, and duplications (Li et al., 2020). As a consequence of such chromosomal rearrangements, tumorigenesis can be prompted by either generating an oncogenic fusion gene, disrupting essential tumor-suppressor genes or modifying gene copy numbers. Since the discovery of the first cytogenetic abnormality in patients with CML, known as Philadelphia chromosome, described by David Hungerford and Peter Nowell in 1960, a broad scope of various rearrangements was identified by genomic analyses (Nowell, 2007, Nowell and Hungerford, 1960). The Philadelphia chromosome emerges as a result from a translocation of chromosomes 9 and 22 leading to a fusion tyrosine kinase protein consisting of the breakpoint cluster region (BCR) and the tyrosine-protein kinase ABL1 (BCR-ABL). Based on such translocation products new subtypes of hematological malignancies could be defined.

Table 1: Common genetic alterations in hematological malignancies.

APL, acute promyelocytic leukemia; HL, Hodgkin lymphoma; FL, follicular lymphoma; DLBCL, diffuse large B cell lymphoma; MCL, mantle cell lymphoma. Based on Taylor et al., 2017.

Disease type	Genetic alteration	Genes	Frequency
APL	t(15;17)	<i>PML-RARα</i>	95%
AML	ITD, point mutation in TKD	<i>FLT3</i>	37%
	Frameshift due to insertion	<i>NPM1</i>	29%
	t(8;21)	<i>RUNX1-ETO</i>	7%
	t(11q23) translocations	<i>KMT2A (MLL1)</i>	5%
	t(16;16) (p13.1q22)	<i>CBFB-MYH11</i>	5%
CML	t(9;22)	<i>BCR-ABL</i>	100%
B-ALL	t(9;22)	<i>BCR-ABL</i>	25%
	t(11q23) translocations	<i>KMT2A (MLL1)</i>	2-10%
	t(12;21)	<i>ETV6-RUNX1</i>	20-30% (children)
T-ALL	Activating mutations	<i>NOTCH1</i>	50-60%
	Recurrent deletions	<i>CDKN2A/B</i>	50-60%
CLL	Activating mutations	<i>NOTCH1</i>	15%
	Point mutations	<i>SF3B1</i>	15-20%
HL	copy-number alterations	<i>PD-L1/L2</i>	95%
FL/DLBCL	t(14;18)	<i>BCL2</i>	50-90%
Burkitt	t(8;14)	<i>MYC</i>	80-100%
MCL	t(11;14)	<i>IG/CCND1</i>	80-19%

Although some translocations were detected in multiple forms of leukemia and lymphomas such as the existence of BCR-ABL in AML, a handful of common fusion proteins as well as other chromosomal rearrangements exist, which are characteristic for a specified subtype. The most frequent chromosomal rearrangements as well as cytogenetic abnormalities for the various hematological malignancies are summarized in Table 1 (Taylor et al., 2017).

1.2 Chromosomal Translocations Involving MLL1

1.2.1 Structure and Function of MLL1

One of these recurrent chromosomal rearrangements involves the histone-lysine N-methyltransferase 2A (*KMT2A*) gene, also known as mixed-lineage leukemia 1 (*MLL1*) gene, on band 23 of the longer arm (q arm) of chromosome 11 (11q23). First described in 1992, the gene encodes a multi-domain transcriptional coactivator with 3,969 amino acids and a molecular weight of 500 kDa essential for chromatin modification and regulating gene expression in hematopoiesis and early development (Ballabio and Milne, 2014). Once translated, the protein is cleaved by the enzyme taspase 1, a threonine aspartase, generating two fragments: an N-terminal 320 kDa MLL-N and a C-terminal 180 kDa MLL-C. Both fragments associate through the FY-rich N-terminal (FYRN) and FY-rich C-terminal (FYRC) domains composing a heterodimeric complex (Hsieh et al., 2003). The protein's N-terminal residues containing 1400 amino acids include domains of the menin-binding motif (MBM) and lens epithelium-derived growth factor (LEDGF)-binding domain (LBD), three AT hooks, nuclear-localization signals 1 and 2 (SNL1 and 2), a CxxC motif, four plant homeodomain (PHD) fingers, a bromodomain (BRD) and the FYRN (Chan and Chen, 2019). MBM and LBD are responsible for the recruitment of menin (MEN1) and LEDGF interacting with the DNA/chromatin complex. AT hooks bind to AT-rich DNA regions, while the CxxC motif interacts with unmethylated CpG DNA sequences and is associated with the polymerase-associated factor complex (PAFc) enabling target gene recognition (Cosgrove and Patel, 2010, Muntean et al., 2010). The four PHD fingers recognize di- or tri-methylated lysine 4 of histone 3 (H3K4) enabling gene transcription and interact with cyclophilin CYP33 important for negative regulation of MLL-induced transcription, while the BRD mediate recognition of acetylated lysine residues (Chang et al., 2010). The C-terminus contains the transactivation domain (TAD) and the Su(Var)3-9, enhancer-of-zeste, trithorax (SET) domain, a homolog of *Drosophila* trithorax (Chan and Chen, 2019). TAD recruits the histone acetyltransferases CBP/p300 and MOF, both crucial for MLL1 target gene expression such as the *HOX* genes (Mishra

et al., 2014). The SET domain catalyzes the tri-methylation of H3K4. (Krivtsov and Armstrong, 2007). This methyltransferase activity of MLL1 and the other family members SETD1A, SETD1B, MLL2, MLL3, and MLL4, relies on the involvement in multi-subunit protein complexes called COMPASS (**complex of proteins associated with SET1**). COMPASS features core subunits consisting of the four proteins ASH2L, RBBP5, WDR5 and DPY30 and the additional above-mentioned subunits Menin and LEDGF for MLL1 (Figure 3). This multiprotein complex is required to ensure and stabilize a catalytically efficient form (Southall et al., 2009).

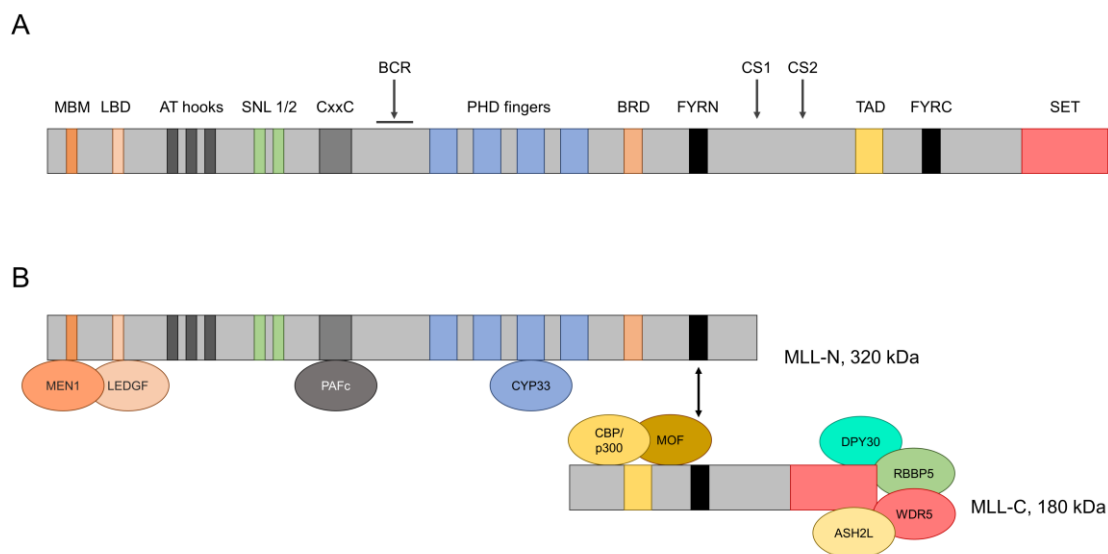


Figure 3: Scheme of MLL1 functional domains and their involvement in multi-protein complexes. (A) Full-length MLL1 protein before cleavage by taspase 1. **(B)** Generation of MLL-N and MLL-C after cleavage by taspase 1. Both fragments reassemble via FYRN and FYRC and interact with various proteins forming complexes regulating transcription. MBM, menin-binding motif; LBD, lens epithelium-derived growth factor (LEDGF)-binding domain; SNL, nuclear-localization signal; BCR, breakpoint cluster region; PHD, plant homeodomain; BRD, bromodomain; CS, cleavage site; TAD, transactivation domain; FYR, FY-rich; SET, Su(Var)3-9, enhancer-of-zeste, trithorax. Based on Winters and Bernt, 2017.

The *MLL1* gene is frequently altered by chromosomal rearrangements causing over 70% of pediatric AML and ALL and account for 10% of adult AML as well as therapy-induced acute leukemias (Meyer et al., 2018). These rearrangements encompass translocations generating oncogenic fusion proteins where the N-terminal part of MLL1 is fused to a broad variety of more than 100 fusion partners, ranging from transcription factors to cytoplasmic proteins (Meyer et al., 2018). The most frequent partners comprise nuclear proteins associated with the regulation of transcriptional elongation via interaction with the positive transcription elongation factor b (pTEFb) complex and recruitment of the H3K79 histone methyltransferase DOT1L (Erfurth et al., 2004, Yokoyama et al., 2010). Among these, the transcription cofactors AF9 and ENL, AF4, AFF4 and ELL cover over 70% of MLL1-related rearrangements (Krivtsov and Armstrong, 2007).

1.2.2 *Ex vivo* Expansion of Monocytic Progenitor Cells by MLL-ENL

One of the recurrent MLL fusion protein partner is the eleven-nineteen-leukemia (ENL) protein. The formed fusion protein MLL-ENL, originated as a consequence of the balanced chromosomal translocation t(11;19), is linked with explicit subsets of acute leukemias (Slany et al., 1998). Various chromosomal breakpoints were identified fusing the N-terminal part of MLL to the almost full-length ENL. Within the *MLL* gene, a distinct breakpoint cluster region (BCR) spans intron 9, 10 and exon 11 whereas the breakpoints in the *ENL* gene were found to be most frequently located in intron 1 and additionally up to 26 kb upstream of the *ENL* gene (Meyer et al., 2007). The resulting fusion protein features dissimilar transcriptional and chromatin-modifying characteristics as wildtype MLL. ENL comprises an N-terminal YEATS domain and a disordered C-terminal AHD (ANC1 homology domain) domain (Li and Song, 2021). The YEATS (Yaf9, ENL, AF9, Taf14, Sas5) domain mediates the protein's localization to acetylated lysines 9 and 27 of histone H3 followed by recruitment of additional transcriptional effectors such as the super elongation complex (SEC) regulating transcription via RNA polymerase II. While the YEATS domain is dispensable for the oncogenic character of the fusion protein, the C-terminal AHD domain is essential as it ensures interaction with the H3K79 methyltransferase DOT1L (Yokoyama et al., 2010). In this combinatorial setting with features of both MLL and ENL, MLL-target gene overexpression is initiated including *HOX* cluster genes (in particular *HOXA7 – HOXA10*) and the cofactor *MEIS1* associated with an enhanced proliferation and a concomitant differentiation block (Li et al., 2009) (Figure 4). During hematopoiesis, *HOX* genes as well as *MEIS1* are highly expressed in stem and early progenitor cells to sustain self-renewal properties whereas programmed differentiation of precursors along the hematopoietic hierarchy is associated with a downregulation. Thus, dysregulated and continuous expression of these genes decisively contribute to the stem-cell like character of MLL-ENL linked leukemias (Winters and Bernt, 2017). When exogenously overexpressed, e.g. via retroviral transduction, MLL-ENL contributes to the transformation of progenitor cells (Lavau et al., 1997). Of note, MLL-ENL can act as a sole driver of leukemogenesis without the need of cooperating co-mutations in mice (Okeyo-Owuor et al., 2019). Although associated with both lineages reflecting the presence of MLL-ENL in AML and ALL, enforced expression in murine hematopoietic stem and progenitor cells predominantly resulted in AML (Barabe et al., 2007). Irrespective of the initiating cell type (i.e., HSCs or multiple hematopoietic progenitor subsets with granulocytic and monocytic potential such as the common myeloid progenitor (CMP) and the granulocyte/monocyte progenitor (GMP)) the resulting MLL-ENL-transformed cells display immunophenotypes and gene expression profiles characteristic of late monocytic precursors (Cozzio et al., 2003, Somerville et

al., 2009). Similarly, analyses of various patient samples revealed a myelomonocytic AML M4/M5 subtype for MLL-ENL translocations (Pourrajab et al., 2020). By ectopically expressing MLL-ENL and MLL-related rearrangements in general, in myeloid progenitors their programmed differentiation towards granulocytes or macrophages *ex vivo* can be averted allowing for sustained proliferation and expansion. Of note, this is particularly due to maintained expression of HOXA9 eventually leading to immortalization (Krivtsov et al., 2006, Lavau et al., 1997).

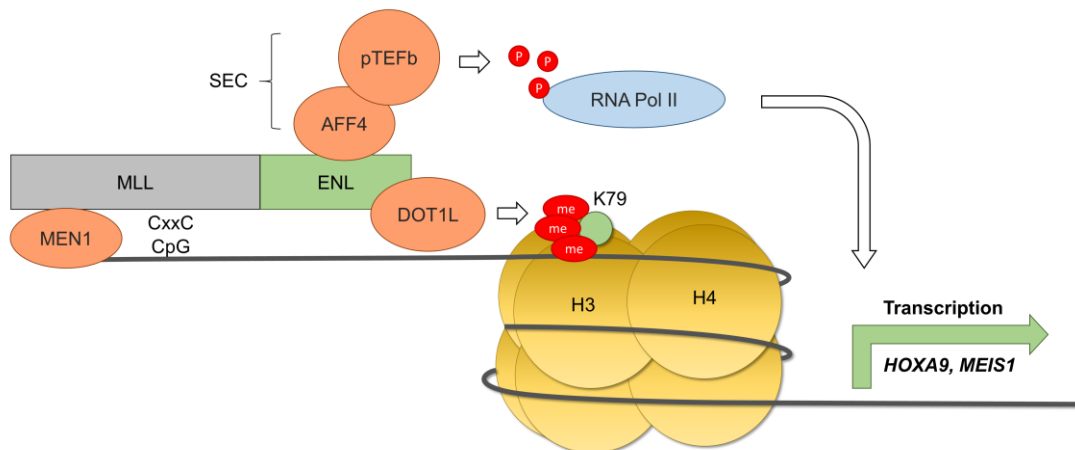


Figure 4: Mode of action of the fusion protein MLL-ENL. The N-terminal part of MLL recognizes and binds to DNA via the CxxC motif and interacts with menin. ENL mediates the protein's localization to acetylated lysines 9 and 27 of histone H3 followed by recruitment of additional transcriptional effectors such as AFF4 and pTEFb resulting in the phosphorylation of the RNA polymerase II. The C-terminus of ENL interacts with the methyltransferase DOT1L, which methylates the lysine residue 79 on H3. As a consequence transcription of HOXA9 and MEIS1 is initiated.

1.3 Macrophages

1.3.1 Ontogeny and Classification

Macrophages are highly plastic cells of the hematopoietic system and the first immune cells developing in the embryo. Present in all tissues, they are involved in governing a broad assortment of cellular processes such as development, homeostasis, tissue repair and immunity. Back in 1882, they were first identified by Elie Metchnikoff, a Russian and French zoologist, who observed cells trying to engulf a rose thorn which was implanted into a starfish. Suggesting a host immune defense and due to their devourer character, these cells were called macrophages, Greek for large eaters (Metchnikoff, 1921, Tauber, 2003). In human, these evolutionary conserved phagocytes were proposed to originate from circulating blood monocytes by Van Furth in the 1960s (van Furth and Cohn, 1968). Although evidence emerged that these tissue phagocytes developed independent of monocytes, the most successful classification remained the mononuclear phagocytic

system (MPS), comprising phagocytes as terminally differentiated end cells of the mononuclear lineage as well as their bone marrow progenitors, for several decades (Volkman et al., 1983). However, in recent years, several reports contradicted the theory of the circulation-dependent origin. The existence of non-monocyte-derived macrophages was demonstrated by sophisticated congenic parabiosis mouse models with mice sharing the same hematopoietic system but differ in a single locus leading to a mixed population of monocytes. Tracking and characterization of macrophages in the brain as well as in the skin verified that no mixture occurred even after more than a year of parabiosis (Ajami et al., 2007, Merad et al., 2002). Similarly, human suffering from severe monocytopenia do not exhibit a decreased number of macrophages in the epidermis (Bigley et al., 2011). These findings in addition to the fact that macrophages originate in the embryo before definitive hematopoiesis giving rise to monocytes is established, led to an adaption of the historical origin definition (Mizoguchi et al., 1992). Thus, lineage-tracing experiments in mice revealed that macrophages of the skin and of the central nervous system derived from yolk sac progenitors which are present before definitive hematopoiesis occurs (Ginhoux et al., 2010). As already outlined, the first definitive hematopoiesis occurs in the liver suggesting three different origins of the macrophages: yolk sac, liver, and bone marrow (Figure 5) (Williams et al., 2018).

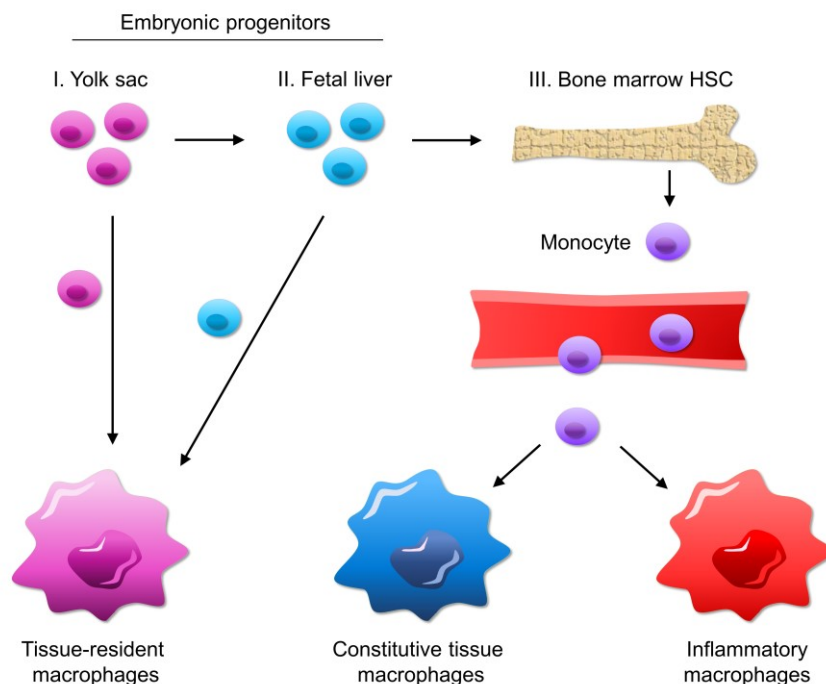


Figure 5: Graphical representation of the different origins of human macrophages. During embryogenesis macrophages originate from both yolk sac and fetal liver progenitor cells independent of monocytes. These macrophages persist into adulthood as tissue-resident macrophages. Adult-derived macrophages with bone marrow origin develop from circulating monocytes after extravasation and are primarily associated with inflammatory reactions. In addition, constitutive tissue macrophages can develop from monocytes as well. Based on Williams et al., 2018.

Although development of macrophages in the yolk sac as well as in the liver only takes place during embryogenesis, these originated macrophages persist into adulthood as long-lived tissue macrophages which orchestrate maintenance of homeostasis (Schulz et al., 2012). On the other hand, adult-derived macrophages emerge from the bone marrow origin as circulating monocytes infiltrating tissue (Jakubzick et al., 2013). These tissue macrophages possess a limited lifespan and are mainly associated with pathological inflammatory reactions (Parihar et al., 2010). Thus, at infection or injury sites, both steady-state macrophages and monocyte-derived macrophages co-exist. Based on the ontogeny these macrophages exert different functions with a highly plastic character which seems to be remodeled by tissue environment (Sreejit et al., 2020).

1.3.2 Phenotypes and Functions

During the earliest stages of development, embryonically derived macrophages exert various functions and contribute to patterning and remodeling in distinct tissues dependent on the microenvironment. As microglia, these macrophages mediate the shaping of the central nervous system vasculature and contribute to blood vessel regression in the eye development by interacting with adjacent cells (Fantin et al., 2010). This interaction allows macrophages to precisely mediate neuronal patterning in the developing brain by controlling both neuronal survival and cell death in a tightly regulated manner (Nayak et al., 2014). Another process facilitated by macrophages is the bone formation. Present on the bone surface, the macrophages, called osteoclasts, break down bone tissue, a critical process for the maintenance, repair, and remodeling (Kodama et al., 1991). Within the bone marrow niche, macrophages take over essential tasks as professional phagocytes by engulfing the erythrocyte nuclei, a critical process for healthy erythropoiesis as well as engulfing cells absent of the potent “don’t eat me” signal CD47, thereby tightly controlling egress from the bone marrow (Jaiswal et al., 2009). As tissue-resident macrophages are distributed throughout the body, additional pivotal functions include maintenance of metabolic homeostasis ensured by Kupffer cells in the liver and macrophages in the spleen, preservation of immunity and wound repair as Langerhans cells in the skin and immunosurveillance as intestinal and alveolar macrophages (Gordon et al., 2014). In each distinct tissue, macrophages adopt a specific identity which is governed by the physical scaffold and environmental cues that modify the macrophages’ functional character by inducing expression of a certain subset of transcription factors (Gautier et al., 2012).

Monocyte-derived macrophages and their monocytic progenitors are critical sentinels for the initiation and resolution of inflammatory processes via migrating to the inflammation

sites, performing phagocytosis, secreting inflammatory cytokines, producing reactive oxygen species (ROS) and activating the immune system (Auffray et al., 2009). Under physiological conditions, circulating monocytes survive for a short time before programmed cell death occurs. These monocytes display a heterogeneity and are therefore divided into “classical” and “non-classical” monocytes. The vast majority (over 90%) is categorized as classical monocytes with the expression of the lipopolysaccharide (LPS)-binding protein receptor CD14 accompanied by the absence of CD16a, the Fc γ receptor IIIa, whereas the “non-classical” monocytes do express CD16a (Gonzalez-Mejia and Doseff, 2009). Under inflammatory conditions, classical monocytes are abundantly recruited to the inflamed sites followed by extravasation and differentiation into macrophages. Critical factors for the recruitment are the CC-chemokine ligand 2 (CCL2) and CCL7 binding to the cognate receptor CCR2 on monocytes (Tsou et al., 2007). As soon as extravasation takes place, monocyte-derived macrophages develop in response to differentiation-inducing cytokines such as the granulocyte-macrophage colony-stimulating factor (GM-CSF) and macrophage colony-stimulating factor (M-CSF) (Ushach and Zlotnik, 2016). Within the tissue niche, additional cytokines affect macrophage physiology and functional character. Two extensively investigated cytokines that have a profound impact are interferon (IFN)- γ and interleukin 4 (IL-4) secreted by T helper (Th) 1 and Th2 cells, respectively. Dependent on the exposure to either cytokine, macrophages are categorized into M1 or M2 originated from *in vivo* observations in Th1 and Th2-type mouse strains (Mills et al., 2000). These two phenotypes possess different functional properties and gene expression pattern. Macrophages possess high-affinity receptors for IFN- γ that regulate numerous gene expression changes upon binding the respective ligand (Schroder et al., 2004). In addition to the cytokines, damage- and pathogen-associated molecular patterns (DAMPs and PAMPs) promote inflammation in response to receptor binding. While DAMPs are released from damaged and dying cells, PAMPs represent a group of conserved microbial molecular motifs (Tang et al., 2012). A prototype within the PAMP category is the bacterial LPS which is recognized by toll-like receptors (TLR) followed by an immune response with significant alterations in gene expression (Dalby et al., 2020). The combination of IFN- γ and LPS exposure is associated with the term “classically activated macrophages” (M1 macrophages) which feature an inflammatory and antimicrobial character. These M1 macrophages produce reactive oxygen species (ROS) contributing to pathogen killing and express specific surface markers such as CD80 and CD86, known as B7-1 and B7-2, modulating T cell immune functions via interaction with CD28 and CTLA-4 expressed on T cells (Canton et al., 2021). Based on functional properties production of IL-12 and IL-23 as well as secretion of pro-inflammatory cytokines such as

tumor necrosis factor (TNF) α or IL-6 is assigned to the M1 phenotype in addition to an enhanced antigen presentation capacity (Italiani and Boraschi, 2014). On the other hand, M2 macrophages manifest a profoundly different activation state with IL-4 being the major cue in combination with IL-13 resulting in the designation of “alternatively activated macrophages” (Stein et al., 1992). Linked with an anti-inflammatory character, these M2 macrophages are associated with an IL-12^{low}-IL-23^{low} profile and the production of the anti-inflammatory cytokines IL-10 and TGF- β . They typically express high levels of CD163, CD206 and CD209 and take part in dampening inflammation, tissue remodeling, angiogenesis and immunomodulation (Sica and Mantovani, 2012). In addition, a hallmark characteristic to discriminate between M1 and M2 macrophages is their way to metabolize arginine. There are two opposing pathways accredited to either subtype with the metabolism of arginine via nitric oxide synthase (NOS) to nitric oxide and citrulline or by the enzyme arginase 1 (ARG1) to ornithine and urea (Rath et al., 2014). Expression of NOS, specifically the inducible form (iNOS) relevant for immune responses, is a hallmark feature of M1 macrophages while M2 macrophages are linked to ARG1 expression (Salim et al., 2016). The category of M2 macrophages was later subdivided into M2a, M2b and M2c by Mantovani and colleagues according to their exposure to differing polarization inducers (M2a: IL-4 + IL-13; M2b: immune complex + TLR ligands; M2c: IL-10) as well as functional properties (Mantovani et al., 2004) (Figure 6).

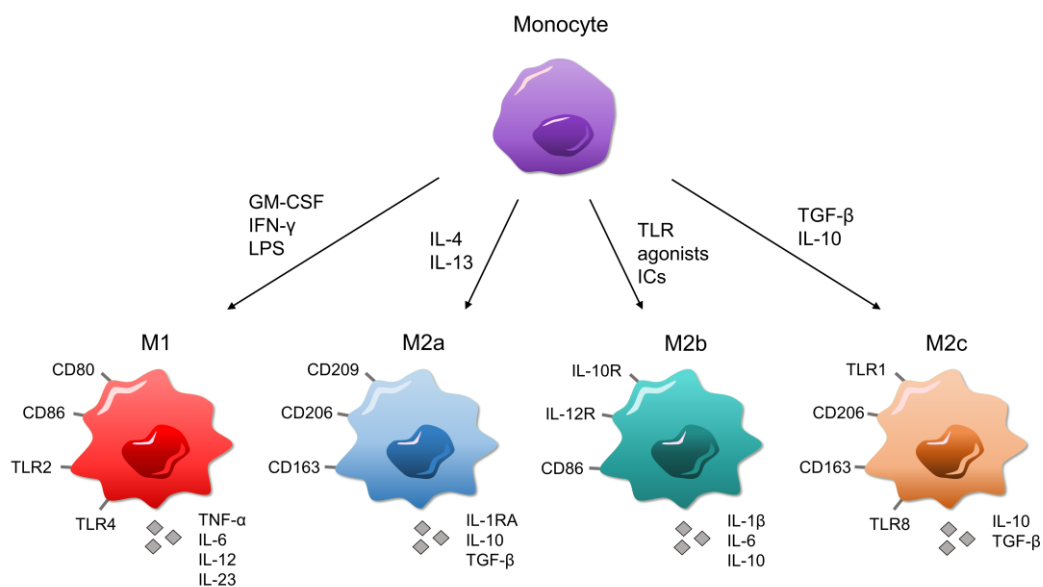


Figure 6: Schematic of M1 and M2 macrophage polarization. Classical monocytes are recruited to inflamed or damaged sites followed by extravasation and differentiation into macrophages. Dependent on environmental cues such as cytokines polarization towards either M1 or M2 subtypes occurs *in vitro*. Various stimuli were identified as main factors to drive polarization into either pro- or anti-inflammatory macrophages. M1 polarization is induced with GM-CSF, IFN- γ and LPS and associated with secretion of pro-inflammatory cytokines. M2 polarization is mainly mediated by IL-4, IL-13 and IL-10 and further categorized into M2a, M2b and M2c. M2 macrophages orchestrate tissue repair and secrete anti-inflammatory cytokines such as IL-10. Based on Mantovani et al., 2004.

Although this classification is based on well-studied stimuli and allows *in vitro* differentiation, it does not reflect the actual heterogeneity *in vivo* as macrophages are exposed to a vast assortment of signals in the complex tissue niche including auto- and paracrine signaling (Xue et al., 2014).

1.3.3 Macrophages in Cancer

Macrophages are a key component of cancers comprising up to 50% of the tumor mass (Poh and Ernst, 2018). For tumor initiation and promotion, chronic inflammation appears to be essential, which is assured by secretion of inflammatory cytokines by M1 macrophages within the tissue (Balkwill and Mantovani, 2012). Consequently, surrounding tissue macrophages infiltrate and accumulate in the tumor (Gabrusiewicz et al., 2011). As soon as the tumor grows and a vascular network is formed, monocyte-derived macrophages become the main source of infiltrating macrophages. Once established, the tumor microenvironment (TME) alters the macrophages' immunologically active state resulting in an anti-inflammatory phenotype elicited in response to various cues such as hypoxia, crosstalk with cancer cells and interaction with the extracellular matrix (Qian and Pollard, 2010). These tumor-associated macrophages (TAMs) resemble polarized M2 macrophages in terms of secretion of anti-inflammatory cytokines and exposure to mainly IL-4 and IL-13 within the TME (DeNardo et al., 2010). Due to their inherent character, TAMs exhibit a tumor-promoting phenotype by driving cell proliferation, angiogenesis, invasion and metastasis and immunosuppression (Pan et al., 2020). They are characterized by a significant downregulation of MHC class II molecules and secretion of the chemokines CCL17 and CCL22 thereby strongly contributing to immunosuppression by preventing T cell stimulation and recruitment of inhibitory regulatory T cells (Lewis and Pollard, 2006).

By abundantly populating tumors, macrophages became potential targets for current immunotherapy strategies such as suppressing secretion of CCL2 and M-CSF, both contributing to accumulation of TAMs within the tumor niche (Tang and Tsai, 2012, Zhu et al., 2014). The most frequently applied immunotherapy is the use of monoclonal antibodies. Monoclonal antibodies can disrupt various signaling pathways if addressed to block specific receptors and ligands on either tumor or immune cells. In this regard, the CD47-signal regulatory protein α (SIRP α) axis represents a promising target concerning modulation of macrophage-mediated phagocytosis (Chao et al., 2011). CD47, which is ubiquitously expressed in human cells, was found to be overexpressed in various tumor entities (Chao et al., 2012). Antibodies blocking the "Don't eat me" signal CD47 demonstrated efficient elimination of malignant cells, in particular when combined

with tumor-targeting therapeutic antibodies such as rituximab (Advani et al., 2018). A crucial mode of action of antibody-based immunotherapy is the induction of phagocytosis via antibody binding to an antigen on tumor cells and interacting with activating Fc receptors expressed on macrophages. In this context, application of rituximab to conventional treatment for lymphoma led to a more favorable outcome when macrophage infiltration was detected (Weiskopf and Weissman, 2015).

1.4 Cell-Based Immunotherapy

Cellular therapies, also known as cell transplantations or cytotherapies, refer to a therapy form in which viable autologous (taken from and applied to the same patient) or allogeneic (derived from a donor) cell-based material is transferred into patients to effectuate a medicinal effect which cannot be addressed adequately by existing pharmaceuticals. The origins of cell therapy can be traced back to the year 1889, when Charles-Édouard Brown-Séquard injected animal testicle extracts in an attempt to suppress the impact of aging (Lefrere and Berche, 2010). Since then, cell therapies progressively evolved as a burgeoning and intensive research field with a steadily increasing number of various approaches resulting in having a considerable medical impact nowadays. Hence, the global market size is estimated to increase from USD 9.5 billion in the year 2021 to USD 23.0 in 2028 (Research, 2021). In this regard, a remarkable rise in the number of ongoing cell therapy clinical trials were tracked with an increase of 78% in the year 2021 when compared to the trials reported in 2019 (Upadhaya et al., 2021). Collectively, cell therapeutic approaches cover various therapy types including stem cell- and non-stem cell-based unicellular as well as multicellular therapies and encompass diverse therapeutic areas such as regenerative medicine and, in particular, immunotherapy in the treatment of cancer. The various approaches range from transplantation of unmodified cells to *ex vivo* genetic engineering and modifications in formulation to enhance and ensure specific functional characteristics of the transplanted cells. The transplantation possibilities include topical administration, infusions and injectables as well as bioscaffold-associated and scaffold-free systems (De Pieri et al., 2021, Golchin and Farahany, 2019, Maeder and Gersbach, 2016, Mount et al., 2015). While most of the cellular therapies are still in the early stages of development, a few have been FDA-approved since 2010 as best practice for specific medical conditions. These approved therapies include transplantation of unmodified cord blood cells for the treatment of hematopoietic system disorders, transplantation of genetically modified or *ex vivo* activated immune cells for cancer treatment as well as use of chondrocytes, fibroblasts and keratinocytes for regenerative purposes (FDA, 2022). As

most of these approaches refer to immunotherapy and cancer treatment, their broad potential and variability is delineated in the following. Dependent on the cell type used for therapeutic purposes, these products are categorized in either stem cell-based or non-stem cell-based therapies.

1.4.1 Non-Stem Cell-Based Therapy

The use of non-stem cells for cell therapeutic approaches commonly includes somatic cells, which are isolated from the human body in an either autologous or allogeneic manner. Upon isolation, these cells are generally expanded, selected and can be genetically modified before administration to the patients (Golchin and Farahany, 2019). Apart from cells used for regenerative purposes and correction of metabolic errors such as fibroblasts, chondrocytes, keratinocytes or hepatocytes, the majority of cell types used comprises immune cells derived from the hematopoietic system such as T cells, dendritic cells, NK cells and macrophages (Mount et al., 2015, De Pieri et al., 2021). These cells can be individually isolated from the donor's or patient's peripheral blood according to their characteristic features such as the adhesion capacity of monocytes or the expression of distinct cell surface proteins that can be addressed with magnetic nanoparticles coated with the suitable antibodies allowing for magnetic-activated cell sorting (Jackson et al., 2020, Nielsen et al., 2020). Following isolation, these cells can be further manipulated by cultivation in the presence of certain cytokines mimicking *in vivo* cues such as the addition of GM-CSF and interleukin IL-4 to the isolated monocytes to obtain terminally differentiated dendritic cells (Niu et al., 2014). In addition, to enhance specific immunomodulatory functions and mount a directed reaction against cancer cells, genetic engineering can be performed *in vitro* to manufacture modified immune cells, which are subsequently used for an adoptive cell therapy (ACT) (Saudemont et al., 2018). ACT has become a promising option in the treatment of cancers refractory to standard therapy. It involves the intravenous transfer of either unmodified or genetically modified immune cells, particularly T cells (Morotti et al., 2021). The different types of T cells used for ACT include tumor-infiltrating lymphocytes (TILs), tumor-directed T-cell receptor (TCR)-engineered T cells as well as chimeric antigen receptor (CAR)-T cells (June et al., 2015, Zhao and Cao, 2019, Saudemont et al., 2018). The rationale of the usage of TILs for therapeutic purposes is based on the harvest of naturally occurring T cells which have already infiltrated the cancer in the patient followed by expansion and activation steps *in vitro* and reinfusion into the patient to effectively infiltrate the tumor again (Kumar et al., 2021). A way to engineer T cells for cancer treatment is the manipulation of the TCR. Isolated, patient-derived T cells can be equipped with a specific

TCR that targets a complementary tumor antigen presented by the major histocompatibility complex (MHC) on the cancer cells or antigen-presenting cells (Chandran and Klebanoff, 2019). These TCR-based ACTs have shown promising results in the treatment of melanoma and solid tumors (Robbins et al., 2015, Robbins et al., 2011), multiple myeloma (Stadtmauer et al., 2019) and acute myeloid leukemia (Chapuis et al., 2019). Similarly, T cells can be engineered to express a CAR which is able to bind to antigens naturally expressed on the surface of cancer cells rendering the engineered T cells independent of MHC interaction (June et al., 2018). Differing from the TCR, the CAR constructs typically encodes a single-chain variable fragment (scFv) of a monoclonal antibody for the recognition and binding of the tumor antigen, a CD3 ζ chain (the intracellular signaling domain of the TCR) and co-stimulatory domains, such as CD28 or 4-1BB (June et al., 2014, van der Stegen et al., 2015). First designed in 1989 in the Department of Chemical Immunology of the Weizmann Institute of Science, these CAR T cells were further modified and enhanced to become clinically effective during the last decades (Gross et al., 1989b, Gross et al., 1989a, Hartmann et al., 2017). The continuous development ultimately resulted in the design of a CAR ensuring improved antitumor activity, T cell proliferation, cytokine secretion and *in vivo* persistence (June et al., 2018). Promising *in vitro* and *in vivo* results finally led to the FDA approval of CD19-directed CAR T cells for the treatment of B-cell lymphoma and B-cell precursor acute lymphoblastic leukemia in 2017 (Braendstrup et al., 2020). Nowadays, six different CAR T cell therapy products are FDA-approved directed against either CD19 or the B-cell maturation antigen (BCMA) (FDA, 2022).

Apart from T cells promising cell therapy-relevant cell types include NK cells and macrophages. The flexible character of macrophages and their abundance in tumor tissue led to *ex vivo* modification for ACT approaches to actively target and eradicate tumor cells. Early studies starting in the 1990s focused on activating and modulating isolated monocytes towards an inflammatory macrophage phenotype by pretreatment with either IFN- γ or LPS. These pretreatments led to an enhanced cytotoxicity *in vitro* but did not hold a significant tumoricidal effect *in vivo*, although the adoptive transfer was well-tolerated (West et al., 1997, Andreesen et al., 1990). Recent approaches aimed for genetic engineering to overcome the immunosuppressive TME hurdle and pertain an inflammatory milieu associated with activation of bystander immune cells and efficient tumor clearance. A critical cytokine in this context is the pro-inflammatory IL-12. Thus, multiple groups genetically engineered macrophages and myeloid cells to recombinantly express IL-12 leading to an activation of the adaptive and innate immune system in preclinical models (Brempele et al., 2020, Kaczanowska et al., 2021). Likewise, additional strategies comprise modification of macrophages to deliver IFN- α and even

secrete bispecific T cell engagers or checkpoint inhibitors such as a full-length anti-CTLA-4 antibody at the tumor site (Escobar et al., 2014, Gardell et al., 2020). Bispecific T cell engagers comprise two scFv of different antibodies thereby binding to an antigen on a tumor cell and to T cells via the CD3 receptor. Anti-CTLA-4 antibodies block the inhibitory function of CTLA-4 resulting in enhanced T cell activation. Particularly in terms of addressing solid tumors remarkable progress concerning genetic engineering has been made with the example of developing CAR macrophages. As CAR T cells generally fail to penetrate the solid tumor niche and rapidly become exhausted in the immunosuppressive TME, the CAR technology was adopted for macrophages as cell type of interest to overcome these limitations (Abdin et al., 2021). Although macrophages are commonly unsusceptible for any kind of genetic manipulation due to their inherent property to react to foreign nucleic acid, Klichinsky and colleagues used a replication-incompetent chimeric adenoviral vector (Ad5f35) to efficiently deliver the CAR. This way, they were able to manufacture anti-HER2-CAR macrophages that showed promising *in vitro* results against HER2+ cell lines with similar results obtained *in vivo* in NOD-SCID mouse models (Klichinsky et al., 2020) which led to a first-in-human phase I clinical trial for the treatment of HER2-overexpressing solid tumors in 2021. Beside HER2 as an attractive target, another study focused on anti-CCR7-CAR macrophages to counteract tumor growth and metastasis to lymphoid organs (Niu et al., 2021). Again, auspicious results were generated as demonstrated by an anti-tumor immunity and prevention of metastasis *in vivo*. Apart from the intricacies regarding genetic engineering a major limitation represents the lacking expansion capacity leading to an insufficient number of manufactured macrophages (Wang et al., 2022). To address this issue, Zhang and his team utilized iPSCs as source allowing to expand followed by CAR delivery and terminal differentiation towards macrophages (Zhang et al., 2020). These findings in addition to the use of engineered macrophages for further applications where inflammation control is crucial, in conditions such as myocardial infarction or HIV-infection, led to the conclusion that macrophages represent an attractive cell type with high potential for cellular therapies (Yang et al., 2017, Taylor et al., 2018).

1.4.2 Stem Cell-Based Therapy

Stem cells represent a distinct cell population convenient for potential cell-based therapy approaches as they are able to differentiate into various type of cells accompanied by the ability to indefinitely proliferate *in vivo* (Jaenisch and Young, 2008). In general, various different types of stem cells exist with dissimilar cell potency. In a descending order from the highest to the lowest differentiation potential these include totipotent

(known as omnipotent, able to differentiate into any kind of cell), pluripotent (differentiation into cells derived from any of the three germ layers), multipotent (differentiation into cells closely related to the family of cells), oligopotent (differentiation into only a few cell types) and finally unipotent stem cells, which can produce only a single cell type (Zakrzewski et al., 2019, Singh et al., 2016). Of those, stem cells of two categories are of interest for cell therapeutic approaches: pluripotent stem cells (PSCs) and multi- or unipotent adult stem cells (ASCs). The major physiological PSC populations comprise embryonic stem cells (ESCs) derived from the inner blastocyst cell mass, epiblast-derived stem cells (EpiSCs) and embryonic germ cells (EGCs). Although these embryonic pluripotent cells offer auspicious advantages and several trials are under way particularly in the field of regenerative medicine such as the manufacture of cardiac cells, there have been ethical restrictions for the medical use of ESCs in therapy as most of the embryonic stem cells originate from eggs fertilized *in vitro* (Zakrzewski et al., 2019, Menasche, 2020). To overcome this concern as well as immune rejection after transplantation, multiple groups were trying to manufacture artificial human ESCs from the patient's somatic cells by dedifferentiation which ultimately led to the manufacture of induced pluripotent stem cells (iPSCs) by Yamanaka and Takahashi in 2006 (Takahashi and Yamanaka, 2006). By introducing the four identified reprogramming factors Myc, Oct3/4, Sox2 and Klf4, known as Yamanaka factors, into mouse fetal and adult fibroblasts, dedifferentiation was initiated resulting in pluripotency. A year later, the progression from mouse to human iPSCs was achieved (Takahashi et al., 2007, Yu et al., 2007). Although the clinical use of iPSCs lacks therapeutic evidence, several therapeutic approaches covering a broad spectrum of regenerative medicine and cancer immunotherapy have reached or are about to reach clinical trials (Yamanaka, 2020).

A different type of stem cell is represented by the ASCs featuring more limited self-renewal and differentiation capacity compared to the PSCs (Chagastelles and Nardi, 2011). Their main physiological function is the maintenance of cellular homeostasis by giving rise to progenitor cells which subsequently differentiate to mature cells able to replenish cells. ASCs span various cell types consisting of skin stem cells (SSCs), neural stem cells (NSCs), mesenchymal stem cells (MSCs) and hematopoietic stem cells (HSCs) (Gurusamy et al., 2018). Of these various types of ASCs, cell therapy approaches are mainly restricted to the use of MSCs and HSCs. MSCs are stromal cells found in various tissues including bone marrow (one of the essential sources of MSCs), adipose tissue, peripheral blood and human umbilical cord blood (Shammaa et al., 2020). Their pluripotent character in combination with the simple derivation from a variety of adult tissue and the absence of major ethical concerns render them a promising cell therapy candidate (Jiang and Xu, 2020). MSCs possess the ability to differentiate into

osteocytes, chondrocytes and adipocytes (Wei et al., 2013, Dominici et al., 2006) and are therefore mainly considered for regenerative medicine. Yet, MSCs also exhibit a profound therapeutic potential for the treatment of cancer and immune modulation (Lin et al., 2019, Jiang and Xu, 2020). Besides regulating immune responses by secreting both pro- and anti-inflammatory cytokines providing an equilibrium and interacting with immune cells such as monocytes and regulatory T cells, several preclinical trials suggest tumoricidal effects of MSCs due to the tropism property of MSCs to the sites of inflammation and tumor (Lin et al., 2019). Studies have shown that a beneficial suppression of cancer cell proliferation and apoptosis could be achieved (Yulyana et al., 2015, Lin et al., 2016).

As HSCs possess the ability to give rise to all blood constituents including cells of the innate and adaptive immune system and support lifelong homeostasis, they manifest a curative potential in the treatment of hematological disorders. Since their first clinical use in form of an allogeneic HSC transplantation (HSCT) in 1957, they have been used as standard therapeutic intervention for malignant and non-malignant hematological diseases, including leukemia and lymphoma (Thomas et al., 1957, Chabannon et al., 2018). The major advantage of an allogeneic HSC transplantation compared to an autologous setting is that the transplant is free of residual malignant cells. To avoid severe side effects such as a graft-versus-host disease (GvHD) and even rejection of the transplant, human leukocyte antigen (HLA) matching is required to ensure the highest possible similarity between donor and recipient (Petersdorf, 2004). Once transplanted and, in particular, engrafted in the patients as a single treatment, these HSCs replenish the hematopoiesis ensuring life-long supply of healthy and functional blood cells. Apart from treating cancer, HSCT is used to correct inborn defects leading to blood cell diseases such as severe combined immunodeficiency (SCID) or congenital neutropenia (Haddad and Hoenig, 2019, Connelly et al., 2012). In malignant disease settings, patients are treated with high-dose chemotherapy with or without radiotherapy prior to the transplantation to eradicate the tumor cell population. In addition, the recipient's bone marrow (myeloablative conditioning) gets ablated eliciting an immunosuppressive effect which prevents rejection of the transplant (Bazinet and Popradi, 2019). As chemotherapy mainly impact proliferating cells, normal as well as malignant quiescent stem cells remain unaffected. Consequently, relapse may occur originating from these malignant cells becoming proliferative again (Bhatia et al., 2003, Dean et al., 2005). Thus, transplantation of donor-derived healthy hematopoietic stem cells counteracts this issue by building up a renewed hematopoietic system including immunologically active cells provoking a graft-versus-leukemia effect (Bleakley and Riddell, 2004). Another, non-myeloablative approach uses reduced intensity conditioning

whereby the doses applied are too low to ablate all bone-marrow cells ultimately resulting in a chimerism following transplantation, where donor as well as recipient HSCs co-exist within the bone marrow niche (Bitan et al., 2014).

Mechanistically, HSCs can be isolated from three different sources: bone marrow, peripheral blood and umbilical cord blood (Huss, 2000). Extracting HSCs from their natural bone marrow niche using a needle represents the original isolation procedure. In recent years, HSC isolation from peripheral blood became the gold standard as the collection proved to be convenient accompanied by enhanced engraftment compared to bone marrow transplantation (Wu et al., 2015). This procedure relies on the usage of G-CSF, which can mobilize the HSCs by initiating the egress from the bone marrow as a consequence of the disruption of the SDF-1/CXCR-4 axis (Hopman and DiPersio, 2014). The third source represents the cord blood and the placenta, which both are rich in HSCs but limited in volume. These HSCs are isolated directly after birth and subsequently frozen for future applications primarily for children (Broxmeyer et al., 2020).

Once isolated, HSCs can be modified *ex vivo* in the course of a gene therapy to treat specific primary immune deficiencies such as the above-mentioned SCID or the X-linked chronic granulomatous disease (X-CGD), a genetic disorder caused by mutations in the CYBB gene resulting in impaired functions of phagocytes. Patients suffering from X-CGD are susceptible to life-threatening bacterial and fungal infections (Kohn et al., 2020). Thus, gene therapy-based correction of autologous HSCs presents a promising approach to treat such diseases. The transplantation of modified autologous HSCs showed clinical efficacy for patients with various genetic blood disorders including X-CGD (Sessa et al., 2016, De Ravin et al., 2016, Eichler et al., 2017). The correction itself is ensured by inserting a healthy copy of the abnormal gene into the host cell's genome by the use of retro- or lentiviral vectors. These vectors are used to produce infectious particles which are able to infect the target cells with subsequent incorporation of the desired transgene into the genome (Morgan et al., 2021).

1.4.3 Limitations and Challenges

Although promising *in vitro* and *in vivo* results have been achieved with various cell therapeutic strategies to address regenerative issues, reconstitute immune disorders and treat cancer that eventually led to FDA approval of 20 cellular products in total (as of May 2022) (FDA, 2022) there are several limitations and challenges restricting broader applications, primarily in targeting a large variety of cancer entities including solid tumors.

These challenges will be discussed in the following for the non-stem cell-based approaches and the stem cell therapies, respectively.

Although T cells can be engineered to virtually target any tumor-associated antigen, one of the major limitations for ACTs is the identification of such antigens. Within the category of tumors of the lymphoid tissue, the cell surface protein CD19 has been proven to present an attractive and convenient antigen to target B-cell-derived cancers (Kochenderfer et al., 2015, Kochenderfer et al., 2010) as well as BCMA for multiple myeloma. Beside those two well characterized antigens cell therapeutic approaches aim for targeting CD30 for the treatment of Hodgkin's lymphoma and CD33, CD123 and Flt3 expressed by acute myeloid leukemia (AML) cells (Schultz and Mackall, 2019). Yet, their clinical efficacy needs to be elucidated (ongoing clinical trials: NCT02917083, NCT04835519, NCT04014881, NCT05023707). Aside from blood cancer, solid tumors often impede therapy options due to their heterogeneity rendering it difficult to address a suitable target (Hanahan and Weinberg, 2011, Vogelstein et al., 2013). In addition, targeting a single tumor-associated antigen can result in antigen loss concomitant with an outgrowth of aggressive clones (Vyas et al., 2017). Concerning T cells as ACT another substantial drawback poses the poor infiltration into solid tumors (Galluzzi et al., 2018, Majzner and Mackall, 2019). Moreover, within the tumor microenvironment (TME) immune suppressive conditions provoked by the secretion of inhibitory and anti-inflammatory cytokines and metabolites by both regulatory T cells (Tregs) and tumor-associated macrophages (TAMs) impair full functionality of the cytotoxic T cells (Sharma et al., 2017, Anderson et al., 2017). Although TILs tend to adapt to the TME and consist of T cells with multiple TCR clones able to cover several tumor antigens, ACT with TILs remain a personalized treatment associated with laborious and time-consuming tissue collection and high costs (Kumar et al., 2021). Likewise, genetic engineering of T cells is linked with certain disadvantages. Manufactured TCR-engineered T cells often express both the introduced as well as the endogenous TCR which leads to mispairing of the respective TCR chains resulting in toxicity in mouse models (Bendle et al., 2010). In addition, avidity plays a crucial role as it has to be high enough to ensure adequate T cell activation as well as sustained T cell expansion (Tan et al., 2015, Zehn et al., 2009). Engineering T cell to express a CAR partly circumvents these issues. Nonetheless, the application of CAR T cells pose considerable limitations as well. Apart from the listed restrictions such as antigen escape, lacking infiltration propensity and the presence of immunosuppressive TME, additional challenges emerge with the occurrence of "on-target off-tumor" effects and CAR-T cell-linked toxicities. The "on-target off-tumor" effects describe the eradication of normal, healthy cells which also express the selected antigen against which the CAR is directed and fatal consequences thereof (Morgan et al., 2010,

Lamers et al., 2013). CAR-T cell toxicities arise as consequences of massive *in vivo* CAR-T cell expansion associated with severely augmented secretion of inflammatory cytokines such as IL-6, IFN- γ and TNF α , known as cytokine release syndrome (CRS) (Brudno and Kochenderfer, 2019). These elevated cytokine levels result in neurotoxicity and life-threatening conditions including organ dysfunction (Maude et al., 2018, Schuster et al., 2017). Ongoing approaches and trials aim to address these challenges by further engineering of T cells as well as manufacturing of CAR-NK cells or CAR macrophages that have the potential to cope with issues such as tumor escape mechanisms, graft-versus-host disease or limited infiltration into solid tumors (Simonetta et al., 2017, Klichinsky et al., 2020).

Similarly, stem cell-based therapies hold particular limitations. Despite their attractive pluripotency, ESCs and iPSCs display significant limitations that hamper their clinical usage. As already stated, two issues are linked to ESCs: ethical concerns about the usage of human embryos as well as immune rejection after transplantation (Zakrzewski et al., 2019). Despite bypassing these challenges, iPSCs' pluripotency displays a considerable drawback. The indefinite proliferation as well as the differentiation into any kind of body cell can become the downfall as tumors can develop with teratoma formation being the most frequent type displaying serious concerns (Robinton and Daley, 2012). These tumors either emerge from incomplete differentiation, residual activity of the reprogramming factors or accumulation of genetic mutations during *in vitro* expansion (International Stem Cell et al., 2011). In the category of ASCs, MSCs hold a variety of limitations concerning cell therapeutic application including cell source availability, administration technique, tissue localization and tissue persistence (Fitzsimmons et al., 2018, Le Blanc et al., 2008). Furthermore, although reports demonstrated a tumor suppressive function of MSCs, controversial results have been reported. Various studies observed tumor progression and metastasis associated with the presence of MSCs at the site of the tumor (Zhong et al., 2017, Wang et al., 2015).

Despite the success and clinical efficacy for HSCT, complications and limitations exist for both graft types, autologous or allogeneic. In terms of engraftment complications are divided into three categories including pre-engraftment, early post-engraftment and late post-engraftment (Jagasia et al., 2015). Pre-engraftment issues comprise cytopenia, infections and even organ failure elicited by chemo- and radiotherapy. After transplantation, acute GvHD can occur, an inflammatory immune system reaction upon receiving slightly HLA-mismatched HSCs with symptoms such as rash and fever. Moreover, in the early phase after transplantation, recipients are at higher risk of infections due to lacking cellular and humoral immunity. The GvHD can become established as chronic GvHD in the later post-engraftment period tremendously reducing

quality of life (Jagasia et al., 2015). In addition, during the post-transplantation period, relapse of the causal disease may arise (in particular for autologous HSCT containing residual tumor cells) as well as cardiovascular complications (Tichelli et al., 2007), reproductive dysfunction (Hammond et al., 2007) or secondary malignancies (Baker et al., 2003).

Beside these complications, two major limitations impede HSCT. Since HLA-matching proved to be essential to avoid fierce side effects and even rejection, the shortage of finding an appropriate donor poses the main limitation. Only for around one third of all patients in the need of allogeneic HSCT matched donors are available (Ballen et al., 2012). Another crucial drawback poses the limited quantities of HSCs isolated from either patients or donors dependent on graft type (Notta et al., 2011, Sun et al., 2014, Wilson and Trumpp, 2006). *In vitro* expansion of HSCs prior to transplantation would counteract this limitation. Yet, HSCs undergo spontaneous differentiation once detached from their bone marrow niche due to lacking signals thereby strongly restricting *in vitro* expansion. For this reason, various different attempts have been made in the last decades in order to mimic niche characteristics *ex vivo* and to maintain self-renewal property. As growth factors play a major role in influencing proliferation, activation and differentiation, combinations of different cytokines were used to robustly accomplish *in vitro* expansion of HSCs (Buza-Vidas et al., 2006). A commonly used combination to support HSC survival and maintenance of immaturity consists of IL-3, IL-6, SCF, Flt3 and TPO (Metcalf, 2008). However, in this setting survival and proliferation seems to be only short-term as demonstrated by Knapp et al. (Knapp et al., 2017) which emphasizes the need for additional factors to ensure prolonged proliferation. In recent years a broad variety of molecules were analyzed via high-throughput screening regarding HSC expansion. Three molecules were found to boost expansion of CD34+ HSCs *in vitro*, which include Prostaglandin E2 (PGE2), StemRegenin1 (SR1) and UM171 (Boitano et al., 2010, Wagner et al., 2016, Fares et al., 2014). In clinical trials PGE2 did not result in a beneficial effect on *ex vivo* proliferation although enhancing lentiviral gene transfer efficiency eventually becoming a promising feature for genetically modified HSCT (Heffner et al., 2018). SR1, an aryl hydrocarbon receptor antagonist, was the first identified molecule that favorably impacts the expansion of HSCs in combination with the above-mentioned cytokine cocktail (Boitano et al., 2010). In addition, a phase 1/2 trial demonstrated a 330-fold expansion of umbilical cord blood with successful engraftment and rapid neutrophil and platelet recovery (Wagner et al., 2016). On the other hand, *in vitro* culturing of HSCs with SR1 results in an increase of multipotent progenitors with erythroid/megakaryocytic potential but suppressed granulocytic/monocytic gene profile (Psatha et al., 2017). Similarly, the small molecule UM171, a pyrimidoindole derivate, represents a promising

candidate for *ex vivo* expansion of HSCs. Fares et al. demonstrated a favorable effect on the proliferation of HSCs although it was recently shown that UM171 impairs erythroid and megakaryocytic differentiation as well as inhibits expression of inflammatory chemokines (Fares et al., 2014, Wen et al., 2020). Although these molecules facilitate HSC expansion *in vitro* to a certain extent, they exhibit limitations with the lack of long-term and large-scale expansion being the major unmet need. Therefore, additional robust and reliable expansion techniques are required to assure high numbers of HSCs for an unlimited time span rectifying shortage. Moreover, these *in vitro* expanded stem as well as progenitor cells can be differentiated into functional immune cells *ex vivo* followed by cell therapeutic approaches to address specific issues. With genetic engineering coming to the fore in the last decades, various approaches make use of the proliferation-favoring capacity of leukemia-associated genes, which have been considered to fulfill the unmet need regarding expansion. Such recent advances employed chimeric fusion genes originated from chromosomal translocations. Besides the described fusion gene MLL-ENL these include RUNX1-ETO, NUP98-HOX fusions and other MLL fusions (Lavau et al., 1997, Mulloy et al., 2003, Mulloy et al., 2002, Abdul-Nabi et al., 2010, Faridi et al., 2013, Sloma et al., 2013, Chung et al., 2006, Abramovich et al., 2005).

1.4.4 Aims and Objectives

The *ex vivo* expansion of human HSPCs has been a longstanding challenge due to rapid terminal differentiation in the absence of supportive bone marrow niche cues. This issue hinders the large-scale *ex vivo* manufacture of several mature blood cells, such as macrophages, in numbers suitable for cell therapeutic approaches. A promising way to prevent differentiation and ensure expansion of hematopoietic progenitor cells is the use of leukemia-associated fusion proteins. Several studies revealed that leukemia-associated fusion proteins, such as MLL-ENL, confer extensive self-renewal and proliferation of immature hematopoietic cells *in vitro*. With the notion to exploit the fusion protein MLL-ENL for the generation of functional macrophages on a large scale, two aims were set: First, to analyze the impact of continuous MLL-ENL activity on large-scale and long term *ex vivo* expansion of HSPCs; Second, to investigate whether shutdown of the fusion protein results in loss of immaturity and allows differentiation into fully functional macrophages.

In the first part of this work, the focus was set on the characterization of MLL-ENL expressing progenitor cells and determination of the long term and large-scale expansion capacity. For this purpose, a controllable MLL-ENL construct should be introduced into

healthy human HSPCs via retroviral transduction to ensure stable expression. By utilizing a destabilization domain protein tag fused to the N-terminus of MLL-ENL, the dependency of continuous MLL-ENL activity on sustained *in vitro* proliferation and colony-forming ability in the presence of the stabilizing small molecule Shield-1 should be investigated. As the leukemia-associated fusion protein MLL-ENL should be used as expansion factor thorough characterization of the expanded cells should be performed. In this context, the cells' phenotype should be identified by morphological analysis via cytochemical stains and immunophenotyping. Furthermore, to rule out chromosomal alterations and the occurrence of additional proliferation-promoting mutations, karyotyping and whole exome sequencing should be performed.

In the second part of this work, the expanded MLL-ENL expressing progenitor cells should be analyzed for their ability to differentiate into functional macrophages upon MLL-ENL degradation. For this purpose, the MLL-ENL cells should be cultivated in the absence of Shield-1 in media containing GM-CSF, LPS and IFN- γ , which promote differentiation into M1 macrophages. Successful differentiation into macrophages should be evaluated by determination of cell morphology, analysis of macrophage-associated cell surface protein expression and investigation of the mRNA expression levels of myeloid innate immunity-related genes. Moreover, functional assays should be carried out covering properties characteristic of macrophages. These should address adhesion under shear stress, migration towards a chemoattractant and phagocytosis features. The latter should include co-incubation assays with bacterial particles and dead human cells as well as antibody-dependent cellular phagocytosis of malignant cells. For comparison and to attest the manufactured MLL-ENL macrophages' full functionality, macrophages derived from both peripheral blood of healthy donors and unmodified HSPCs should be included.

2. Materials and Methods

2.1 Materials

2.1.1 Chemicals

Table 2: Overview of chemicals

Chemical	Manufacturer
Acrylamide / bisacrylamide (37,5:1) 30%	Carl Roth GmbH, Karlsruhe, Germany
Agarose Standard	Carl Roth GmbH, Karlsruhe, Germany
Albumin Standard	Thermo Fisher Scientific, Waltham, MA, USA
Ammonium persulfate (APS)	Sigma-Aldrich, St. Louis, MO, USA
Ampicillin sodium salt	Sigma-Aldrich, St. Louis, MO, USA
autoMACS® Rinsing Solution	Miltenyi Biotec, Bergisch Gladbach, Germany
Bovine Serum Albumin solution 30% (BSA)	Sigma-Aldrich, St. Louis, MO, USA
Cell Lysis Buffer (10x CLB)	Cell Signaling Technologies, Danvers, MA, USA
cOmplete Mini protease inhibitor tablets	Roche Diagnostics GmbH, Mannheim, Germany
Coomassie Plus Protein Assay Reagent	Thermo Fisher Scientific, Waltham, MA, USA
CryoSure-DMSO	WAK-Chemie Medical GmbH, Steinbach, Germany
Double-distilled water (ddH ₂ O)	Thermo Fisher Scientific, Waltham, MA, USA
Dulbecco's phosphate-buffered saline (10X) (10x PBS)	Thermo Fisher Scientific, Waltham, MA, USA
Dulbecco's phosphate-buffered saline (1X) (PBS)	Sigma-Aldrich, St. Louis, MO, USA
Dynabeads M-280 Streptavidin	Thermo Fisher Scientific, Waltham, MA, USA
EDTA	Carl Roth GmbH, Karlsruhe, Germany
Ethanol ≥99.8%	Carl Roth GmbH, Karlsruhe, Germany
Ficoll® Paque Plus	Cytiva, Uppsala, Sweden
Gamunex® 10% 100 mg/ml	Grifols, Barcelona, Spain
Glycine	Carl Roth GmbH, Karlsruhe, Germany

Glycogen (20 µg/µl)	Roche Diagnostics GmbH, Mannheim, Germany
Hank's Balanced Salt Solution (HBSS), calcium, magnesium, no phenol red	Thermo Fisher Scientific, Waltham, MA, USA
Hydrochloric acid (HCl)	Carl Roth GmbH, Karlsruhe, Germany
Immobilon™ Western Chemiluminescent HRP Substrate	Millipore Corporation, Billerica, MA, USA
Isopropyl alcohol	Sigma-Aldrich, St. Louis, MO, USA
LB (lysogeny broth) Agar (Lennox)	Carl Roth GmbH, Karlsruhe, Germany
LB (lysogeny broth) Broth (Lennox)	Carl Roth GmbH, Karlsruhe, Germany
Magnesium chloride (MgCl ₂)	Carl Roth GmbH, Karlsruhe, Germany
Methanol ≥ 99.9% (MeOH)	Carl Roth GmbH, Karlsruhe, Germany
PageRuler™ Plus Prestained Protein Ladder	Thermo Fisher Scientific, Waltham, MA, USA
Powdered milk	Carl Roth GmbH, Karlsruhe, Germany
Propidium Iodide Solution (PI)	BioLegend, San Diego, CA, USA
S.O.C. media	Thermo Fisher Scientific, Waltham, MA, USA
SDS sample buffer, 4x	Merck Millipore, Burlington, MA, USA
Sodium acetate buffer, pH 5.2 ± 0.1	Sigma-Aldrich, St. Louis, MO, USA
sodium dodecyl sulfate (SDS)	Carl Roth GmbH, Karlsruhe, Germany
SYBR™ Safe DNA Gel Stain	Thermo Fisher Scientific, Waltham, MA, USA
TAE buffer (50X)	Carl Roth GmbH, Karlsruhe, Germany
Tetramethylenediamine (TEMED)	Carl Roth GmbH, Karlsruhe, Germany
TRIS	Carl Roth GmbH, Karlsruhe, Germany
TRIS-hydrochlorid (TRIS-HCl)	Carl Roth GmbH, Karlsruhe, Germany
TWEEN® 20 (Tween)	Carl Roth GmbH, Karlsruhe, Germany
X-β-Gal	Carl Roth GmbH, Karlsruhe, Germany

2.1.2 Kits

Table 3: Overview of kits

Kit	Manufacturer
APC Annexin V Apoptosis Detection Kit	BioLegend, San Diego, CA, USA
Classical Monocyte Isolation Kit, human	Miltenyi Biotec, Bergisch Gladbach, Germany
First Strand cDNA Synthesis Kit	Thermo Fisher Scientific, Waltham, MA, USA
Inside Stain Kit	Miltenyi Biotec, Bergisch Gladbach, Germany
nCounter® Myeloid Innate Immunity Panel	Nanostring Technologies, Seattle, WA, USA
NucleoBond® Xtra Maxi EF	Macherey-Nagel, Dueren, Germany
NucleoSpin® Gel and PCR Clean-up	Macherey-Nagel, Dueren, Germany
NucleoSpin® Plasmid EasyPure	Macherey-Nagel, Dueren, Germany
pHrodo® Cell Labeling Kit for Incucyte® Phagocytosis Assays	Sartorius, Goettingen, Germany
pHrodo™ Red <i>E. coli</i> BioParticles™ Phagocytosis Kit	Thermo Fisher Scientific, Waltham, MA, USA
PureLink™ Genomic DNA Mini Kit	Thermo Fisher Scientific, Waltham, MA, USA
QIAquick Gel Extraction Kit	Qiagen, Hilden, Germany
Quick Ligation Kit	New England Biolabs, Ipswich, MA, USA
RNeasy Mini Kit	Qiagen, Hilden, Germany
TOPO™ TA Cloning™ Kit for Subcloning	Thermo Fisher Scientific, Waltham, MA, USA
Zero Blunt™ TOPO™ PCR Cloning Kit for Sequencing	Thermo Fisher Scientific, Waltham, MA, USA

2.1.3 Buffers and Solutions

Table 4: Overview of buffers and solutions

Buffer / Solution / Media	Composition	Concentration
10x SDS running buffer	Tris Glycin SDS	0.25 M 1.92 M 1 % (m/v)
2x bead wash (BW) buffer	Tris-HCl pH 7.5 EDTA NaCl	10 mM 1 mM 2.0 M
5x annealing buffer (polylinker)	Tris-HCl pH 7.4 MgCl ₂	0.5 M 0.35 M

2 Materials and Methods

Blocking solution	PBS	
	Powdered milk	5 % (m/v)
Cell lysis buffer (1x)	10x CLB	10 % (v/v)
	H ₂ O	90 % (v/v)
	cOmplete Mini protease inhibitor tablets	1 per 10 ml volume
EST reaction solution	4% pararosaniline	3% (v/v)
	4% sodium nitrite	3% (v/v)
	0.1 M phosphate buffer	89% (v/v)
	Ethylene glycol monomethyl ether	5% (v/v)
	1-naphthyl acetate	5.3 mM
Esterase stock solution, pH 6.6	H ₂ O	
	Na ₂ HPO ₄	4.7 mM
	KH ₂ PO ₄	24.5 mM
Fixation solution (EST-FIX)	Esterase stock solution	30% (v/v)
	Aceton	45% (v/v)
	37% formaldehyde	25% (v/v)
Fixation solution (POX-FIX)	MeOH	90% (v/v)
	37% formaldehyde	10 % (v/v)
Flow chamber buffer	HBSS	
	BSA	1 % (v/v)
Flow cytometry (FACS) buffer	PBS	
	BSA	0.5 %
Giemsa Staining Solution	Giemsa solution	7.5% (v/v)
	Weise Buffer	92.5% (v/v)
MACS buffer	autoMACS [®] Rinsing Solution	
	BSA	0.5 % (v/v)
	EDTA	2 mM
PBST	PBS	
	Tween 20	0.1 % (v/v)
POX reaction solution	0.05 M Tris-HCl	
	3,3'-Diaminobenzidine	33.3% (m/v)
	1% H ₂ O ₂	0.16% (v/v)
SDS-PAGE separating gel	H ₂ O	40 % (v/v)
	Acrylamide 30%	33 % (v/v)
	1.5 M Tris (pH 8.8)	25 % (v/v)
	SDS (10 % (w/v))	1 % (v/v)
	APS (10 % (w/v))	1 % (v/v)
	TEMED	0.04 % (v/v)
SDS-PAGE stacking gel	H ₂ O	70 % (v/v)
	Acrylamide 30%	16.6 % (v/v)
	1.0 M Tris (pH 6.8)	12.6 % (v/v)
	SDS (10 % (w/v))	1 % (v/v)
	APS (10 % (w/v))	1 % (v/v)
	TEMED	0.1 % (v/v)
Weise buffer, pH 6.8	H ₂ O	
	Buffer tablet, pH 6.8	1 per liter

2.1.4 DNA Oligonucleotides

Table 5: Overview of primers

Primer	Sequence
qPCR	
IL-6 fwd	AAG AGT AAC ATG TGT GAA AG
IL-6 rev	CTA CTC TCA AAT CTG TTC TG
CCL2 fwd	AGT CTC TGC CGC CCT TCT
CCL2 rev	GTGACTGGGGCATTGATTG
CCL22 fwd	CCC CTG ACC CCT CTA ACC
CCL22 rev	GGG AAC AGG ACC CTC TGA CT
CCL17 fwd	GGG AGA GCT GAA TTC AAA AC
CCL17 rev	GGC CAG CAT CTT CAG TGG
Actin fwd	AGA GCT ACG AGC TGC CTC AC
Actin rev	CGT GGA TGC CAC AGG ACT
IL-10 fwd	ATG AAG GAT CAG CTG CAC AA
IL-10 rev	GCA ACC CAG GTA ACC CTT AA
TNF fwd	AGC CCA TGT TGT AGC AAA CC
TNF rev	TCT CAG CTC CAC GCC ATT
INOS fwd	CAA CGT GGA ATT CAC TCA GC
INOS rev	ATC GAA GCG GCC GTA CTT
AGR1 fwd	CAA GGT GGC AGA AGT CAA GA
ARG1 rev	GCT TCC AAT TGC CAA ACT GT
Amplification	
HOXA9 fwd	ACC GGA ATT CGC CAC CAT GGC CAC CAC TGG GGC CCT G
HOXA9 rev	ACC GGG ATC CCT ACT CGT CTT TTG CTC GGT C
Sequencing	
MSCV fwd	TCG ATC CTC CCT TTA TCC AG
IRES end fwd	AAC CAC GGG GAC GTG GTT TT
M13 forward (-20)	GTA AAA CGA CGG CCA G
LM-PCR	
Biotin-rvLTR 1	Biotin – CTG GGG ACC ATC TGT TCT TGG CCC T
Linker-Oligo 1	GAC CCG GGA GAT CTG AAT TCA GTG GCA CAG CAG TTA GG
Linker-Oligo 2	CCT AAC TGC TGT GCC ACT GAA TTC AGA TCT CCC G
OC 1	GAC CCG GGA GAT CTG AAT TC
OC 2	AGT GGC ACA GCA GTT AGG

rvLTR 2	AAC CTT GAT CTG AAC TTC TC
rvLTR 3	CCA TGC CTT GCA AAA TGG C
Seq LM-PCR	CTT GCA AAA TGG CGT TAC

2.1.5 Cell Lines

Table 6: Overview of cell lines

Cell Line	Cell Type	Source
HEK 293T	Human embryonal kidney	DSMZ ACC 635
Jurkat	T cell leukemia	DSMZ ACC 282
Raji	Burkitt lymphoma	DSMZ ACC 319
Daudi	Burkitt lymphoma	DSMZ ACC 78
Carnaval	Diffuse large B cell lymphoma	DSMZ ACC 724

2.1.6 Primary Cells

Table 7: Overview of primary cells

Cell Type	Source	Reference
Peripheral blood mononuclear cells (PBMCs)	Leukocyte reduction system chamber of plateletpheresis	Division of Transfusion Medicine, Cell Therapeutics and Haemostaseology, University Hospital, LMU Munich
CD34+ hematopoietic stem cells	Bone marrow of healthy donors	Lonza Group, Basel, Switzerland
Mantle cell lymphoma cells (MCL)	Peripheral blood of patients	Prof. Dr. Oliver Weigert Department of Medicine III, University Hospital, LMU Munich
Chronic lymphocytic leukemia cells (CLL)	Peripheral blood of patients	Prof. Dr. Tobias Herold Department of Medicine III, University Hospital, LMU Munich

2.1.7 Cell Culture Media, Supplements and Reagents

Table 8: Overview of cell culture media, supplements and reagents

Media, Supplement, Reagent	Manufacturer
CellBrite™ Orange Cytoplasmic Membrane Labeling Dye	Biotium, Inc., Fremont, CA, USA

Carboxyfluorescein succinimidyl ester (CFSE) Cell Division Tracker	BioLegend, San Diego, CA, USA
Cytochalasin D from <i>Zygosporium mansonii</i>	Sigma-Aldrich, St. Louis, MO, USA
Dulbecco's Modified Eagle's Medium (DMEM) (1x), + 4.5 g/L D-Glucose, L-Glutamine	Thermo Fisher Scientific, Waltham, MA, USA
Fetal calf serum (FCS) Standard, South America	PAN-Biotech GmbH, Aidenbach, Germany
Hank's Balanced Salt Solution (HBSS) (1x), + CaCl ₂ , MgCl ₂	Thermo Fisher Scientific, Waltham, MA, USA
Iscove's Modified Dulbecco's Medium (IMDM), w stable Glutamine, 25 mM HEPES, 3.024 g/L NaHCO ₃	PAN-Biotech GmbH, Aidenbach, Germany
L-Glutamine 200 mM	Bio & Sell GmbH, Feucht, Germany
Lipopolysaccharide (LPS) from <i>E. coli</i> O127:B8, BioXtra, γ -irradiated	Sigma-Aldrich, St. Louis, MO, USA
Methyl cellulose, MethoCult GF H8444	Stemcell Technologies, Vancouver, Canada
Monocyte Attachment Medium	PromoCell GmbH, Heidelberg, Germany
Penicillin (10,000 U/ml)-Streptomycin (10 mg/ml)	PAN-Biotech GmbH, Aidenbach, Germany
pHrodo [®] Cell Labeling Kit for Incucyte [®] Phagocytosis Assays	Sartorius, Goettingen, Germany
Polyethylenimin, branched 20 mM	Sigma-Aldrich, St. Louis, MO, USA
Recombinant human Flt3-L	PeptoTech, Rocky Hill, CA, USA
Recombinant human GM-CSF	PeptoTech, Rocky Hill, CA, USA
Recombinant human IFN γ	PeptoTech, Rocky Hill, CA, USA
Recombinant human IL-3	PeptoTech, Rocky Hill, CA, USA
Recombinant human IL-6	PeptoTech, Rocky Hill, CA, USA
Recombinant human M-CSF	PeptoTech, Rocky Hill, CA, USA
Recombinant human SCF	PeptoTech, Rocky Hill, CA, USA
Recombinant human TPO	PeptoTech, Rocky Hill, CA, USA
RetroNectin reagent	Takara Bio Inc., Kusatsu, Japan
Roswell Park Memorial Institute (RPMI) 1640 (1x), + L-Glutamine	Thermo Fisher Scientific, Waltham, MA, USA
Shield-1	Aobious Inc., Gloucester, MA, USA
Staurosporine AM-2282	Selleck Chemicals LLC, Houston, TX, USA

TheraPEAK™ X-VIVO™-15 Serum-free Hematopoietic Cell Medium	Lonza Group, Basel, Switzerland
Trypan blue solution	Sigma-Aldrich, St. Louis, MO, USA
Trypsin-EDTA (1x) 0.05%	Thermo Fisher Scientific, Waltham, MA, USA
VCAM-1	R&D systems, Minneapolis, MN, USA

2.1.8 Antibodies

Table 9: Overview of antibodies

Antibody	Structure	Manufacturer
Anti-HOXA9	Rabbit monoclonal IgG	Abcam, Cambridge, UK
Anti-β-Actin	Mouse monoclonal IgG1k	Santa Cruz Biotechnology, Dallas, TX, USA
APC AffiniPure F(ab') ₂ Fragment Goat Anti-Mouse IgG	Goat F(ab') ₂ Fragment anti-Human IgG, Fcγ fragment specific, polyclonal	Jackson ImmunoResearch, Europe Ltd., Ely, United Kingdom
CD117-APC	Mouse IgG1k clone YB5.B8	Becton Dickinson, Franklin Lakes, NJ, USA
CD11b-PE	Human IgG1 clone REA713	Miltenyi Biotec, Bergisch Gladbach, Germany
CD123-PE	Human IgG1 clone REA918	Miltenyi Biotec, Bergisch Gladbach, Germany
CD135-PE	Human IgG1 clone REA786	Miltenyi Biotec, Bergisch Gladbach, Germany
CD14-PE	Human IgG1 clone REA599	Miltenyi Biotec, Bergisch Gladbach, Germany
CD163-PE	Human IgG1 clone REA812	Miltenyi Biotec, Bergisch Gladbach, Germany
CD16-PE	Human IgG1 clone REA423	Miltenyi Biotec, Bergisch Gladbach, Germany
CD32 A	Mouse IgG2b clone IV.3	Bio X Cell, Lebanon, NH, USA
CD32 B/C	Mouse IgG1k clone S18005H	BioLegend, San Diego, CA, USA
CD32-PE	Human IgG1 clone REA997	Miltenyi Biotec, Bergisch Gladbach, Germany
CD33-APC	Human IgG1 clone REA775	Miltenyi Biotec, Bergisch Gladbach, Germany
CD34-PE	Human IgG1 clone REA1164	Miltenyi Biotec, Bergisch Gladbach, Germany

CD47-IgG σ	Human Fc silent IgG2 σ variant of Hu5F9	C. Kellner (unpublished)
CD64-PE	Human IgG1 clone REA978	Miltenyi Biotec, Bergisch Gladbach, Germany
CD80-PE	Human IgG1 clone REA661	Miltenyi Biotec, Bergisch Gladbach, Germany
CD86-PE	Human IgG1 clone REA968	Miltenyi Biotec, Bergisch Gladbach, Germany
Daratumumab (Darzalex [®])	Human monoclonal anti-CD38 IgG1	Janssen-Cilag GmbH, Neuss, Germany
DD monoclonal antibody	Mouse IgG	Takara Bio Inc., Kusatsu, Japan
FcR Blocking Reagent, human	-	Miltenyi Biotec, Bergisch Gladbach, Germany
Goat Anti-Rabbit IgG H&L (HRP)	Goat IgG	Abcam, Cambridge, UK
HER2-IgG σ	Human Fc silent IgG2 σ variant of trastuzumab	C. Kellner (unpublished)
HLA-ABC-APC	Mouse IgG2a clone W6/32	BioLegend, San Diego, CA, USA
HLA-DP, DQ, DR-APC	Mouse IgG2a clone Tü39	BioLegend, San Diego, CA, USA
IgG1 Isotype Control	Mouse, monoclonal IgG clone 11711	R&D Systems, Minneapolis, MN, USA
Mouse-IgGk BP-HRP	Binding protein for mouse IgGk	Santa Cruz Biotechnology, Dallas, TX, USA
REA Control (S)-PE	Human IgG1 clone REA293	Miltenyi Biotec, Bergisch Gladbach, Germany
REA Control-APC	Human IgG1 clone REA293	Miltenyi Biotec, Bergisch Gladbach, Germany
Rituximab (MabThera [®])	Chimeric, monoclonal anti-CD20 IgG1	Hoffmann-La Roche, Basel, Switzerland
R-PE AffiniPure F(ab') ₂ Fragment Goat Anti-Human IgG	Goat F(ab') ₂ Fragment anti-Human IgG, Fc γ fragment specific polyclonal	Jackson ImmunoResearch, Europe Ltd., Ely, United Kingdom
Trastuzumab (Herceptin [®])	Humanized, monoclonal anti-HER2 IgG1	Hoffmann-La Roche, Basel, Switzerland

2.1.9 Enzymes

All restriction enzymes with the respective buffers were purchased from New England Biolabs (Ipswich, MA, USA). In addition, the enzymes depicted in Table 10 were used.

Table 10: Overview of enzymes

Enzyme	Manufacturer
BioTherm™ Taq DNA polymerase	GeneCraft, Manchester, UK
DreamTaq™ Hot Start Green PCR Master Mix	Thermo Fisher Scientific, Waltham, MA, USA
<i>Pfu</i> DNA polymerase	Promega, Madison, WI, USA
Phusion® green hot start II high-fidelity PCR master mix	Thermo Fisher Scientific, Waltham, MA, USA
T4 DNA ligase	New England Biolabs, Ipswich, MA, USA

2.1.10 Consumables

Table 11: Overview of consumables

Consumables	Manufacturer
µ-Slide Chemotaxis, uncoated	Ibidi GmbH, Graefelfing, Germany
µ-Slides 8 Well ibiTreat	Ibidi GmbH, Graefelfing, Germany
µ-Slides VI 0.4 6 channel, uncoated	Ibidi GmbH, Graefelfing, Germany
24 Well Cell Culture Plates	Greiner Bio-One GmbH, Frickenhausen, Germany
24 Well Flat Bottom Not Treated Cell Culture Plates	Corning, NY, USA
48 Well Cell Culture Plates	Greiner Bio-One GmbH, Frickenhausen, Germany
Biosphere® Filter Tips 10 colourless (10 µl / 20 µl / 100 µl / 200 µl / 1000 µl)	Sarstedt, Nuembrecht, Germany
Cell Scraper (Size M)	Sarstedt, Nuembrecht, Germany
Cellstar® 6 Well Cell Culture Plate	Greiner Bio-One GmbH, Frickenhausen, Germany
Cellstar® 96 Well Cell Culture Plate (F-bottom)	Greiner Bio-One GmbH, Frickenhausen, Germany
Cellstar® Cell Culture Dishes	Greiner Bio-One GmbH, Frickenhausen, Germany
Cellstar® Cell Culture Flasks (25 cm ² / 75 cm ² / 175 cm ²)	Greiner Bio-One GmbH, Frickenhausen, Germany
Cellstar® Screw cap tubes (50 ml)	Greiner Bio-One GmbH, Frickenhausen, Germany
Cryo.s™ vials	Greiner Bio-One GmbH, Frickenhausen, Germany
Millex-GP Syringe filter unit, 0.22 µm	Merck Millipore, Burlington, MA, USA
MS Columns	Miltenyi Biotec, Bergisch Gladbach, Germany

Nunc™ EasYFlask™ Cell Culture Flasks (25 cm ² / 75 cm ²)	Thermo Fisher Scientific, Waltham, MA, USA
PCR reaction tube 0.2 ml	Eppendorf SE, Hamburg, Germany
PS-Tube (5 ml, for flow cytometry)	Greiner Bio-One GmbH, Frickenhausen, Germany
Round bottom tubes (14 ml)	Thermo Fisher Scientific, Waltham, MA, USA
SafeSeal reaction tube (0,5 ml / 1,5 ml / 2 ml)	Sarstedt, Nuembrecht, Germany
Screw cap tubes (15 ml)	Sarstedt, Nuembrecht, Germany
Serological pipettes (2 ml / 5 ml / 10 ml)	Sarstedt, Nuembrecht, Germany
Serological pipettes (25 ml / 50 ml)	Greiner Bio-One GmbH, Frickenhausen, Germany
SmartDish 6-well plate	Stemcell Technologies, Vancouver, Canada
Syringe, 10 ml	Becton Dickinson, Franklin Lakes, NJ, USA
UV-cuvettes, semi-micro	BRAND GMBH + CO KG, Mannheim, Germany

2.1.11 Devices

Table 12: Overview of devices

Device	Manufacturer
Apollo 150 nitrogen tank	Cryotherm GmbH, Kirchen/Sieg, Germany
Avanti J-26 XP ultra-centrifuge	Beckman Coulter, Pasadena, CA, USA
Axio Observer D1 fluorescence microscope	Carl Zeiss, Jena, Germany
AxioCam MRm camera	Carl Zeiss, Jena, Germany
Biosafe Chronos 120 cryotank	Cryotherm GmbH, Kirchen/Sieg, Germany
C1000 Touch Thermal Cycler	Bio-Rad Laboratories, Inc., Hercules, CA, USA
EnviroFALK water purification plant	EnviroFALK GmbH, Haimhausen, Germany
Eppendorf centrifuge 5424	Eppendorf SE, Hamburg, Germany
Eppendorf centrifuge 5804R	Eppendorf SE, Hamburg, Germany
Eppendorf centrifuge 5810R	Eppendorf SE, Hamburg, Germany
Eppendorf Research® Plus pipette (10 µl; 20 µl; 100 µl; 200 µl; 1000 µl)	Eppendorf SE, Hamburg, Germany
ETG MBT 250 heat block	ETG GmbH, Ilmenau, Germany

FACScalibur flow cytometer	Becton Dickinson, Franklin Lakes, NJ, USA
Fusion SL imaging system	Vilber Lourmat, Eberhardzell, Germany
HBO 100 (microscope illuminator)	Carl Zeiss, Jena, Germany
Heraeus Fresco 21 benchtop centrifuge	Thermo Fisher Scientific, Waltham, MA, USA
HERAfreeze Basic (-80 °C)	Thermo Fisher Scientific, Waltham, MA, USA
HERAsafe KS-12 biological safety cabinet	Thermo Fisher Scientific, Waltham, MA, USA
HERAtherm oven	Thermo Fisher Scientific, Waltham, MA, USA
IKA RH basic 2 magnetic stirrer	IKA GmbH, Staufen, Germany
IncuCyte [®] S3 Live-Cell Analysis System	Sartorius, Goettingen, Germany
Julabo MP-5 water bath	JULABO GmbH, Seelbach, Germany
Kendro Megafuge 1.0 R centrifuge	Thermo Fisher Scientific, Waltham, MA, USA
KF85 flake ice maker	Ice line Migel, Milan, Italy
Legato 100 Syringe Pump	KD Scientific Inc.
LKB GPS 200/400 electrophoresis power supply	Cytiva, Marlborough, MA, USA
MACS MultiStand	Miltenyi Biotec, Bergisch Gladbach, Germany
Magnetic Separation Rack	Cell Signaling Technologies, Danvers, MA, USA
Mini-PROTEAN [®] Tetra Cell	Bio-Rad Laboratories, Inc., Hercules, CA, USA
Multistep [®] HandStep [®] S	BRAND GMBH + CO KG, Mannheim, Germany
Nanodrop 2000c spectrophotometer	Thermo Fisher Scientific, Waltham, MA, USA
nCounter Pro Analysis System	Nanostring Technologies, Seattle, WA, USA
neoVortex shaker	neoLab Migge GmbH, Heidelberg, Germany
Neubauer counting chamber 0.1 mm	Paul Marienfeld GmbH, Lauda-Königshofen, Germany
New Brunswick [™] Galaxy [®] 170S incubator	Eppendorf SE, Hamburg, Germany
New Brunswick [™] Innova 42 shaker	Eppendorf SE, Hamburg, Germany
Orbital shaker GFL 0815	LAUDA-GFL GmbH, Burgwedel, Germany
pH meter inoLab [®] pH 7110	Xylem Analytics GmbH, Weilheim, Germany

PowerPac™ 300 power supply	Bio-Rad Laboratories, Inc., Hercules, CA, USA
Safe Imager™ 2.0 blue light transilluminator	Thermo Fisher Scientific, Waltham, MA, USA
Sartorius Quintix precision scales	Sartorius, Goettingen, Germany
Sharp R-5975 microwave	Sharp, Sakai, Japan
Systec VX-150 autoclave	Systec GmbH, Linden, Germany
Trans-Blot®-Turbo™ transfer system	Bio-Rad Laboratories, Inc., Hercules, CA, USA
Zeiss Primovert inverted microscope	Carl Zeiss, Jena, Germany

2.1.12 Bacterial strains

Table 13: Overview of bacterial strains

Strain	Genotype	Reference
<i>E. coli</i> One Shot Top10 (chemically competent)	F- <i>mcrA</i> Δ (<i>mrr-hsdRMS-mcrBC</i>) Φ 80 <i>lacZ</i> Δ M15 Δ <i>lacX74 recA1 araD139 Δ(<i>araleu</i>)7697 <i>galU galK rpsL</i> (StrR) <i>endA1 nupG</i></i>	Thermo Fisher Scientific, Waltham, MA, USA
<i>E. coli</i> DH5 α Subcloning Efficiency (chemically competent)	F- Φ 80 <i>lacZ</i> Δ M15 Δ (<i>lacZYA-argF</i>) U169 <i>recA1 endA1 hsdR17</i> (r_k^- , m_k^+) <i>phoA supE44 thi-1 gyrA96 relA1</i> λ^-	Thermo Fisher Scientific, Waltham, MA, USA

2.1.13 Plasmids

Table 14: Overview of the vectors

Vector	Reference
pMizi-MLL-ENL-i-GFP	Prof. Dr. Rolf Marschalek (University Frankfurt)
pMizi-DD-MLL-ENL-i-GFP	Synthesized by Geneart (Thermo Fisher Scientific, Waltham, MA, USA)
pMizi-HOXA9-i-GFP	Based on Addgene #97041
MSCV-HOXB8-i-GFP	Synthesized by Geneart (Thermo Fisher Scientific, Waltham, MA, USA)
FMEV-HOXB4-i-GFP	PD Dr. Hannes Klump (University Hospital Essen)
Packaging plasmid M634 (GALV)	PlasmidFactory GmbH & Co. KG, Bielefeld, Germany
Packaging plasmid M620 (Gag, Pol)	PlasmidFactory GmbH & Co. KG, Bielefeld, Germany

2.1.14 Software

Table 15: Overview of software

Software	Manufacturer
AxioVs 40 v 4.8.20	Carl Zeiss, Jena, Germany
Basic Local Alignment Search Tool (BLAST)	National Center for Biotechnology Information, Bethesda, MD, USA
CellQuest Pro v 6.0	Becton Dickinson, Franklin Lakes, NJ, USA
DNASTAR Lasergene v 7.1.0	DNASTAR, Madison, WI, USA
FlowJo v10.6.2	Becton Dickinson, Franklin Lakes, NJ, USA
FusionCapt Advance 16.01	Vilber Lourmat, Eberhardzell, Germany
GraphPad Prism 8.0.2	GraphPad Software, La Jolla, CA, USA
IncuCyte 2020B	Sartorius, Goettingen, Germany
Microsoft Office Professional Plus 2016	Microsoft Corporation, Redmond, WA, USA
Nanodrop 2000c v 1.6.198	Thermo Fisher Scientific, Waltham, MA, USA
nSolver 4.0.70	Nanostring Technologies, Seattle, WA, USA
R i386 3.3.2	The Comprehensive R Archive Network
ROSALIND	Nanostring Technologies, Seattle, WA, USA

2.2 Methods

2.2.1 Molecular Biology Techniques

2.2.1.1 Polymerase Chain Reaction (PCR)

The polymerase chain reaction technique (PCR) was used for various purposes. In addition to classical amplification of specific target genes (conventional PCR), PCR was performed to quantitatively detect the cDNA of defined genes obtained from mRNA by reverse transcription (qPCR) on the one hand, and to identify the integration sites of foreign DNA incorporated into the genome on the other. The latter refers to a special form of PCR known as ligation-mediated PCR (LM-PCR).

2.2.1.1.1 Conventional PCR

For the amplification of the *HOXA9* gene used for cloning purposes, a PCR reaction was set up with the components contained in Table 16. The oligonucleotides, shown in Table 5, were used as the corresponding primer pair (forward primer + reverse primer). The vector pInducer-21-HOXA9, acquired from Addgene (#97041, PubMed 28514439), was utilized as DNA template for amplification.

Table 16: Components for conventional PCR reactions

Component	Volume
Template DNA	300 ng
10x BioTherm Taq reaction buffer	5 μ l
dNTPs (25 mM)	1 μ l
Forward primer	1 μ l
Reverse primer	1 μ l
BioTherm Taq DNA polymerase	1 μ l
ddH ₂ O	ad 50 μ l

The PCR reaction was performed in a 0.2 ml reaction tube in the C1000 Touch thermal cycler (Bio-Rad Laboratories, Hercules, CA, USA) using the PCR cycling conditions listed in Table 17. The annealing temperature and the elongation time were calculated according to the primer set used and the amplicon size. In general, the annealing temperature was set to 5 degrees below the lower T_m of the primer set while the elongation time was set to 1 min/kb with 1 minute minimum.

Table 17: Cycling conditions for *HOXA9* amplification.

Step	Temperature	Duration	Cycles
Initial denaturation	94 °C	5 min	
Denaturation	94 °C	30 s	
Primer annealing	61 °C	45 s	25-30
Elongation	72 °C	2 min	
Final elongation	72 °C	5 min	

2.2.1.1.2 Real-time Quantitative PCR (qPCR)

The qPCR represents a method to quantitatively measure gene expression. It monitors the target gene's amplification during the PCR reaction, i.e., in real time, and was performed in cooperation with Dr. Adrian Hoffmann and Prof. Dr. Jürgen Bernhagen at the Institute for Stroke and Dementia Research (University Hospital, LMU Munich). To start with, total RNA was isolated from the target cells using RNeasy Mini Kit (Qiagen) according to the manufacture's protocol. RNA was transcribed into cDNA using the First Strand cDNA Synthesis Kit (Thermo Fisher Scientific) according to the manufacture's protocol. Quantitative RT-PCR samples contained cDNA, ORA™ SEE qPCR Green ROX L Mix, 2X (highQu) and specific primer pairs for the genes of interest (see Table 5). Quantitative RT-PCR was performed using the Rotor-Gene Q thermocycler (Qiagen). Data were evaluated using the $2^{-\Delta\Delta C_t}$ method.

2.2.1.1.3 Ligation-Mediated PCR (LM-PCR)

Ligation-mediated PCR is a method for the investigation of retroviral vector integration sites (RVIs) in the genome of transduced cells (Schmidt et al., 2003). By gene transfer using retroviral vectors, the gene segment located between the 5' long terminal repeat (LTR) and 3' LTR is inserted into the genome semi-randomly (see 2.2.2.3). Thus, the insertion site can be different in each cell, resulting in a whole range of different clones. As vector integration may disrupt open reading frames of genes, unfavorable insertion can lead to activation of proto-oncogenes on the one hand or to deactivation of tumor suppressors on the other, which can result in a proliferation advantage. This so-called transactivation or deactivation can result in clonal dominance, progressing over time accompanying with environmental cues. Via the LM-PCR method, the different, primarily dominant insertion sites can be analyzed within a defined cell population, allowing to determine whether mono-, oligo- or polyclonal growth occurred. The different genes

involved can then be sequenced to investigate whether they potentially have an impact on enhanced proliferation and self-renewal.

The LM-PCR was performed as described by Kustikova and colleagues (Kustikova et al., 2008) with minor modifications (listed in the following passage). In principle, the LM-PCR is classified into the following succeeding steps:

1. Genomic DNA isolation
2. Choice of restriction enzyme
3. Preparation of an asymmetric polylinker cassette
4. Restriction digest of the genomic DNA
5. Primer extension
6. Target DNA enrichment
7. Linker cassette ligation
8. First and nested PCR
9. Analysis by gel-electrophoresis
10. Purification and sequencing of visualized bands
11. Database search for identification

Genomic DNA was isolated from transduced DD-MLL-ENL expressing progenitor cells at different time points as delineated in subheading 2.2.1.7. Given the sequence of the inserted DNA (between 5'LTR and 3'LTR) a 4 bp type II restriction enzyme (frequent recognition site) was determined meeting the criteria of preserving the amplification-related part of the LTR plus providing an internal control in a range between 100 and 500 bp. Hence, the restriction enzyme CviQI (NEB) was selected fulfilling these requirements.

For each LM-PCR reaction 0.5 µg DNA were initially used for enzymatic digestion (2.2.1.9). For the steps 3-9 the protocol was strictly followed using the enzymes and reagents listed in Table 4 and Table 10. The minor modifications of the protocol include the use of a Pfu DNA polymerase from a different supplier (Promega), the use of the 2x Phusion Green HSII Hi-fidelity PCR master mix and the DreamTaq™ Hot Start Green PCR Master Mix instead of the Extensor Hi-fidelity PCR master mix (both Thermo Fisher) and changes in the primer design matching the LTR sequence of the retroviral vector used (Table 5). The first and nested PCR was either performed with the 2x Phusion Green HSII Hi-fidelity or the DreamTaq™ Hot Start Green PCR Master Mix eventually generating 3' A-overhangs or blunt ends applicable for subsequent TOPO cloning (see 2.2.1.2).

Upon visualization of the insertion pattern by gel-electrophoresis, the bands were excised and purified as described in 2.2.1.11. The purified DNA was then either directly

sequenced (2.2.1.12) using the LM-PCR sequencing primer listed in Table 5 or subcloned via TOPO cloning (2.2.1.2).

The sequencing results were ultimately analyzed regarding the respective integration sites by aligning the nucleotide sequence adjacent to the 3' LTR with the human genome library using the bioinformatic tool BLAST (National Center for Biotechnology Information). This way, the particular genes, where the insertion took place, could be verified.

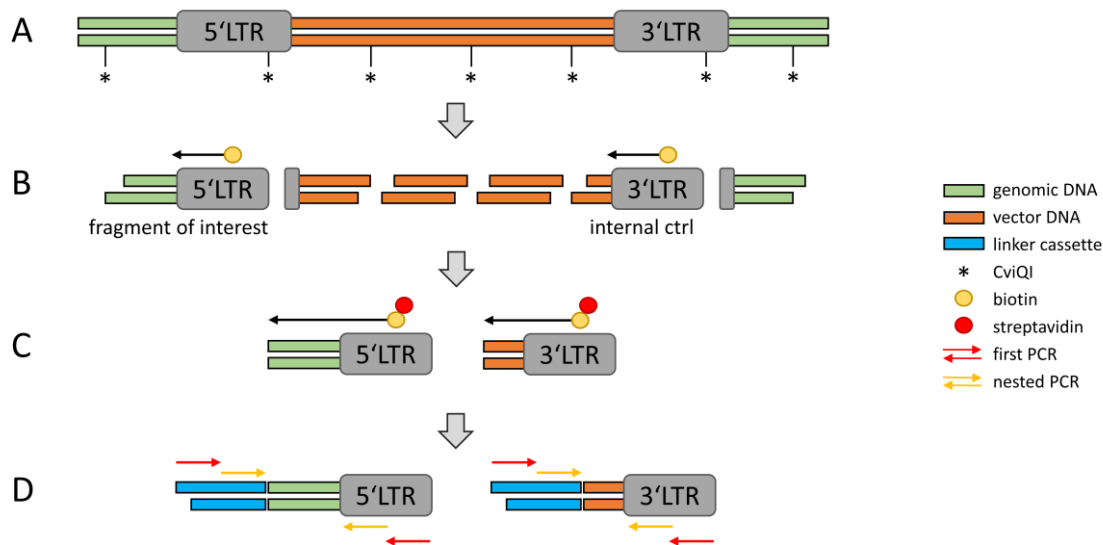


Figure 7. Graphical abstract illustrating the different steps during an LM-PCR.

(A) Isolated genomic DNA is restricted using the 4 bp type II enzyme CviQI. **(B)** Primer extension with a biotinylated primer annealed to the LTR sequence generating 5' blunt ends. **(C)** Target DNA enrichment via streptavidin coated dynabeads (Thermo Fisher). **(D)** Blunt-end ligation of the asymmetric linker cassette providing a unique sequence as a template for the first and nested PCR.

2.2.1.2 TOPO Cloning

TOPO cloning is a molecular biology technique to integrate specific DNA fragments into a linear vector in a ligase-free manner. The vector itself harbors the enzyme topoisomerase (topoisomerase I from *Vaccinia* virus) covalently attached to both of its 3' ends via a phospho-tyrosyl bond between the DNA and the enzyme. This bond can be attacked by the 5' hydroxyl group of PCR fragments leading to efficient ligation and release of the topoisomerase (Shuman, 1991, Shuman, 1994). The addition of a salt solution (200 mM NaCl, 10 mM MgCl₂) further increases efficacy.

TA cloning

The “sticky end” TOPO TA vector features 3' thymine residues (T) able to hybridize with DNA fragments possessing 3' adenine (A) overhangs. This process strictly depends on the A' overhangs which are generated performing a PCR with the *Taq* polymerase, a polymerase lacking proof-reading capacity. The analysis of transformants with the TA cloning kit relies on a blue-white screening with the substrate X-gal. The blue-white screening depends on the expression of the β -galactosidase enzyme which is able to hydrolyze the substrate X-gal to form 5-bromo-4-chloro-indoxyl, which subsequently dimerizes resulting in an insoluble blue pigment called 5,5' dibromo-4,4'-dichloro-indigo. Most *E. coli* strains including the TOP10, contain *LacZ* Δ M15, a deletion mutation of the *lacZ* gene coding for the β -galactosidase. As soon as transformation takes place and the pCRTM2.1-TOPO vector carrying a short segment of the *lacZ* gene, is taken up by the cells, a functional β -galactosidase is produced due to a process called α -complementation. Given the fact that the pCRTM2.1-TOPO vector contains a multiple cloning site within the *lacZ* sequence, inserting foreign DNA result in disruption of the open reading frame. Consequently, the *E. coli* which have taken up plasmids including inserts are not able to produce functional β -galactosidase resulting in white colonies. On the other hand, colonies formed by non-recombinant cells comprising an empty, religated pCRTM2.1-TOPO vector appear blue.

Blunt end cloning

Contrary to the TA cloning, the blunt end cloning relies on PCR fragments without overhangs generated by polymerases exhibiting proof-reading capacity (e.g., Phusion DNA polymerase). The pCRTMII-Blunt-TOPO vector contains the lethal *E. coli* gene, *ccdB* fused to the C-terminus of the *LacZ* α gene. When a PCR fragment is inserted, disruption of the *ccdB* gene takes place allowing direct selection of transformants independently of a blue-white screening. *E. coli* that have taken up empty, religated vector are not able to grow due to the expression of the toxic protein CcdB.

All TOPO cloning reactions were set up in a 0.2 ml PCR tube as described in Table 18 using either the TOPO TA cloning Kit (Thermo Fisher) for PCR products possessing A overhangs (DreamTaq) or the Zero BluntTM TOPOTM PCR Cloning Kit (Thermo Fisher) for PCR products with blunt end (Phusion DNA polymerase).

Table 18: Components for TOPO cloning

Component	volume
PCR product (A overhang or blunt)	2 μ l
Salt solution	1 μ l
pCR TM 2.1-TOPO/pCR TM II-Blunt-TOPO	1 μ l
H ₂ O	2 μ l

After an incubation time of 20 minutes at room temperature, 1.5 μ l of the reaction mix was transferred into chemically competent *E. coli* One Shot TOP10 (Thermo Fisher Scientific) via heat shock transformation (2.2.1.3). For each sample 50 μ l of the bacteria suspension was spread on LB agar plates containing 100 μ g/ml ampicillin. Beforehand, the plates were soaked with 40 μ l of 40 mg/ml X-gal each for TA cloning samples. The desired colonies (white for TA cloning, any for blunt end cloning) can be subsequently picked and cultivated for DNA preparation (2.2.1.5).

2.2.1.3 Heat Shock Transformation of *E. coli*

Heat shock transformation was performed to introduce foreign DNA into chemically competent *E. coli* (One Shot Top10). To do so, 1.5 μ l of the ligation or TOPO cloning reaction mix, respectively, was used for transformation according to the manufacturer's specifications (Thermo Fisher Scientific). A vial of thawed *E. coli* One Shot Top10 (50 μ l) served for up to two samples. Lastly, 150 μ l of each sample was spread on individual LB agar plates containing 100 μ g/ml ampicillin which were incubated at 37 °C overnight.

2.2.1.4 Culture and Storage of *E. coli*

LB agar plates containing *E. coli* colonies were either stored at 4 °C for short term or directly used for suspension cultures. For suspension cultures sterile LB medium with 100 μ g/ml ampicillin was prepared and transferred to 14 ml round-bottom tubes with 3 ml each. Every tube was inoculated with a single colony using sterile pipette tips and subsequently incubated at 37 °C overnight with continuous shaking at 180 rpm.

2.2.1.5 Isolation of Plasmid DNA from *E. coli*

To obtain plasmid DNA, a suspension culture was prepared as described in 2.2.1.4. Isolation and purification of plasmid DNA was performed using the NucleoSpin Plasmid

Kit (Macherey-Nagel, Düren, Germany) according to the manufacturer's instructions. The final elution of the DNA was performed with 30 μ l of ddH₂O each. The purified plasmids were then commissioned for sequencing (2.2.1.12) and stored at -20 °C until further use.

To isolate large plasmid DNA amounts, 250 ml of LB medium was supplemented with ampicillin, inoculated with the appropriate bacterial clone, and cultivated at 37 °C and 180 rpm overnight. On the following day, the plasmid DNA was isolated using the endotoxin-free NucleoBond Xtra Maxi EF kit (Macherey-Nagel) according to the manufacturer's instructions, and eluted in 300 μ l TE-EF buffer. The final plasmid was used for transfection purposes and stored at 4 °C short term and at -20 °C long term.

2.2.1.6 Isolation of RNA from Mammalian Cells

Total RNA was isolated from mammalian cells using the RNeasy Mini Kit (QIAGEN) according to the manufacturer's recommendations. For each sample 3×10^5 cells were harvested in RNase-free reaction tubes and used for disruption with the buffer RLT and homogenization by vortexing. To elute the RNA, 30 μ l of RNase-free ddH₂O were added to the spin column in the last step. The isolated RNA was subsequently stored at -80 °C or directly used for gene expression analysis (2.2.1.14 and 2.2.1.1.2).

2.2.1.7 Isolation of Genomic DNA from Mammalian Cells

Genomic DNA (gDNA) was isolated from mammalian cells using the PureLink™ Genomic DNA Mini Kit (Thermo Fisher) according to the manufacturer's protocol. For each sample $2-3 \times 10^6$ cells were harvested and used for gDNA isolation. For elution of the gDNA 150 μ l of the PureLink® Genomic Elution Buffer was added to the column in the last step. The isolated gDNA was stored at -20 °C until further use for either whole exome sequencing (2.2.1.13) or LM-PCR (2.2.1.1.3).

2.2.1.8 Photometric Analysis of Nucleic Acids

To determine both the concentration and the purity of isolated DNA and RNA, spectrophotometric analysis was performed using a NanoDrop™ 2000c Spectrophotometer (Thermo Fisher) at 260 nm and 280 nm wavelength. The purity was determined by calculating the extinction quotient $E_{260\text{nm}}/E_{280\text{nm}}$. DNA samples with a value of at least 1.8 and RNA samples with a quotient of 2.0 were considered as pure. As a reference the respective solutions used for eluting the nucleic acid were used (ddH₂O and TE-EF buffer for DNA, RNase-free ddH₂O for RNA).

2.2.1.9 Enzymatic Restriction Digestion

The restriction digest of DNA was performed using 10 units (U) per μg DNA of the respective restriction enzyme in a total volume of 50 μl . All enzymes were used according to the manufacturer's recommendations. The reactions were incubated in a heat block or a thermal cycler with lid at the given temperature for at least one hour.

2.2.1.10 Ligation of DNA Fragments

The ligation of DNA fragments was conducted using either the Quick Ligation Kit or the T4 DNA ligase (both NEB) according to the manufacturer's protocol. The Quick Ligation Kit was used for the ligation of cohesive ends within 15 minutes at room temperature. This way DNA fragments generated via PCR and/or restriction digest could be ligated into suitable vector backbones. For cloning a molar ratio of 1:3 vector to insert was employed in a total volume of 20 μl . The T4 DNA ligase was applied for blunt end ligation (e.g., LM-PCR) running over night at 16 °C in a thermocycler with lid (C1000 Touch Thermal Cycler). Finally, the ligated DNA was used for heat shock transformation into *E. coli* bacteria (2.2.1.3).

2.2.1.11 Agarose Gel Electrophoresis

For electrophoretic separation, a 1% or 2% agarose gel (m/v) was prepared depending on the expected DNA fragment sizes. After the samples were mixed with 6x Gel loading dye (NEB) and applied to the gel pockets, separation was performed in a TAE buffer system at 120 V for 45 (for 1% gels) or 75 minutes (for 2% gels). As a molecular weight reference, the 1 kb Plus DNA ladder (NEB) was utilized. After the separation step, the gel was incubated in 1x TAE buffer containing SYBRTM Safe (Thermo Fisher) at a 1:10,000 dilution (5 μl to 50 ml 1x TAE) for 30-45 minutes on an orbital shaker at 50 rpm. SYBRTM Safe intercalates into the DNA allowing for visualization using either a blue light transilluminator (Thermo Fisher) or the Fusion gel documentation imaging chamber (Vilber Lourmat). Extraction of DNA was performed on the blue light transilluminator to avoid damage resulting from UV exposure. The suitable bands were excised and either stored at -20 °C or purified using the QIAquick Gel Extraction Kit (QIAGEN) according to the manufacturer's protocol. For the elution of the DNA 30 μl of ddH₂O was added to the column before the final centrifugation step. The purified DNA was subsequently used for cloning or sequencing purposes.

2.2.1.12 Sanger Sequencing of DNA

To verify the sequence of generated DNA samples, e.g., after isolation of plasmid DNA (2.2.1.5) or gel extraction (2.2.1.11) Sanger sequencing was performed. For this purpose, a total of 100-300 ng in a volume of 5 μ l of the respective DNA sample was mixed with 5 μ l of a 5 μ M solution of a suitable sequencing primer (see Table 5) in a 1.5 ml reaction tube. The following sequencing was performed by Eurofins Genomics (Ebersberg, Germany) using LightRun tubes. The results were checked for quality and sequences were analyzed with the DNASTAR Lasergene v 7.1.0 software (DNASTAR, Madison, USA).

2.2.1.13 Whole Exome Sequencing

Whole exome sequencing (WES) was performed in cooperation with Prof. Dr. Philipp Greif and Dr. Sebastian Vosberg from the Department of Medicine III (University Hospital, LMU Munich) and with Dr. Helmut Blum and Dr. Stefan Krebs from the Gene Center Munich (LMU Munich). The goal of this approach is to analyze the protein coding regions within the genomic DNA of both untransduced HSPCs (UTD) and outgrown, DD-MLL-ENL expressing cells (referred to as >90% GFP+) and compare them with each other. This way copy number alterations and genetic variants can be identified.

To start with, gDNA of the respective cells was isolated providing the starting material for the WES (2.2.1.13). WES was conducted utilizing the HiSeq 1500 and NextSeq 2000 systems (Illumina, San Diego, CA, USA) with 2x150 bp read length. The raw sequences were cropped based on base calling quality (minimum 13) at both ends and reads comprising "N" bases plus reads less than 50 nucleotides upon trimming were discarded. Reads were plotted to the hg19 Human reference genome using Burrows-Wheeler Aligner BWA-aln version 0.7.10 with default settings. Reads that did not map to annotated protein coding regions were excluded while reads arising from PCR duplicates were deleted using Samtools rmdup. Local realignment around insertions and deletions without downsampling was performed with GATK Indel Realigner. Single nucleotide variants, insertions, and deletions were detected via samtools mpileup and VarScan 2.3.7 within the coding region of genes in comprehensive cancer gene lists as targeted by the TruSightOncology 500 Assay (illumine) and the IonTorrent OncoPrint Comprehensive Assay Plus (Thermo Fisher Scientific) based on a minimum variant allele frequency (VAF) of 20% the samples, a minimum coverage of 30x and a base calling quality of 20. Synonymous variants which do not result in an amino acid change, variants annotated as SNPs (minor allele frequency \geq 1% in the dbSNP database) and variants

in blacklisted regions (i.e., `hiSeqDepth`, `wgEncodeDukeMapabilityRegionsExcludable`, `wgEncodeCrgMapabilityAlign-100merNonUniqueExome`) were excluded. Copy number alterations (CNAs) were analyzed based on the *optimalCaptureSegmentation* R package (Rigaill et al., 2012) as described by Vosberg and colleagues (Vosberg et al., 2016). The size of CNAs on a genome wide scale was set to 5 Mb, with 2 exons minimum per segment, allowing up to 10 segments per chromosome. The minimum size of CNAs on a chromosome scale was 10kb, with 1 exon minimum per segment and up to 10 segments per chromosome. The minimum size of segments within a single gene was set to 100bp (1 exon minimum, up to 10 segments).

2.2.1.14 Gene expression profiling

The nCounter[®] Analysis system (NanoString Technologies, Seattle, USA) was used to quantitatively analyze mRNA expression using total RNA. This system displays a technology utilizing digital detection and molecular barcoding of target molecules where a unique probe pair is utilized for each gene of interest. The probe pair (referred to as CodeSet) consists of a target-specific reporter probe (color-coded) and a capture probe which directly hybridize to a target of interest. The reporter probe holds six positions with each being one of four different colors leading to a specified code for each target (Figure 8). After the manual hybridization step, the samples are transferred to the nCounter Prep Station, a multi-channel pipetting robot, where excess probe pairs are automatically washed away by a two-step purification process using magnetic beads. First, magnetic beads harboring a nucleic acid sequence complementary to the capture probe are applied. This way, unbound reporter probes and non-target mRNA transcripts are removed. Subsequently, beads binding the reporter probes are added allowing the removal of excess capture probes. Eventually, the purified complexes containing the transcript of interest are eluted, immobilized on the sample cartridge surface, and aligned for data collection. Data collection is conducted via epifluorescence microscopy and charge-coupled device (CCD) capture technology creating thousands of target molecule counts depicted in a digital image. The nCounter system processes the digital images leading to a rendering of the detected counts into a comma separated value format (CSV). This tabulated format can subsequently be analyzed using either Nanostring's free nSolver[™] Analysis Software or the ROSALIND software. The nCounter Analysis system was kindly provided by Prof. Dr. Oliver Weigert from the Department of Medicine III (University Hospital, LMU Munich).

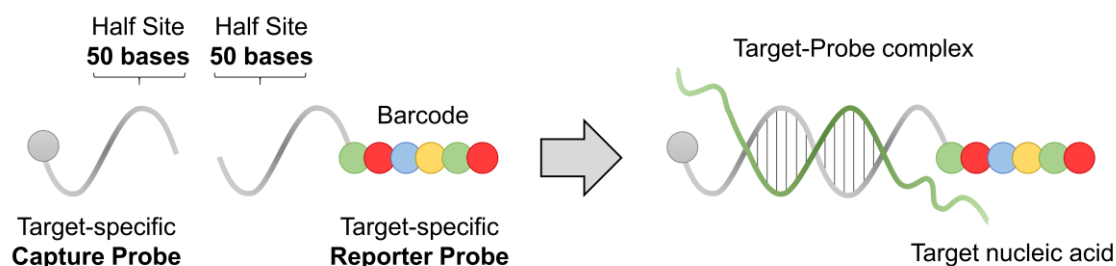


Figure 8: Nanostring's CodeSet chemistry enabling specific target mRNA detection.

During an overnight hybridization step with the isolated mRNA, the specific Capture and Reporter Probes hybridize directly to the single-stranded RNA forming a target-probe complex. The specified color code allows for quantification of the respective target.

This method was used to compare mRNA expression levels between different cell types regarding innate immunity-related genes. To start with, total RNA from untransduced hematopoietic CD34+ cells, PBMC-derived CD14+ cells, proliferating DD-MLL-ENL + Shield-1 cells and differentiated DD-MLL-ENL cells was isolated with the RNeasy Plus Mini Kit (Qiagen, Hilden, Germany) according to the manufacturer's specifications. RNA concentrations were spectrophotometrically determined (Nanodrop 2000c, Thermo Scientific). As a gene set of interest regarding macrophage differentiation the NanoString Human Myeloid Innate Immunity v2 panel (NanoString, Seattle, WA) was used covering a total of 730 genes involved in immune signaling and 40 internal reference controls. The panel itself provides 12 slots for individual mRNA samples. For each above-mentioned cell type three biological replicates from different donors were used with DD-MLL-ENL + Shield-1 and the resulting differentiated DD-MLL-ENL cells originating from the same respective donors. Before RNA isolation, the untransduced CD34+ cells were cultivated in CD34+ complete medium for three days after thawing to induce cell division. All RNA samples were diluted at a concentration of 20 ng/ μ l using RNase-free ddH₂O. For each sample, 100 ng were transferred into provided 12-strip tubes. To set up the hybridization reaction 5 μ l of hybridization buffer and 3 μ l of the reporter probe were added before mixing the tubes by inverting and flicking. Lastly, 2 μ l of the capture probes were added to a total volume of 15 μ l to each tube before immediately placing the strip at 65 °C in a thermocycler for at least 16 hours. The following day, after hybridization the reactions were ramped down to 4 °C before proceeding to sample processing on the nCounter Prep Station. Prior to use the provided nCounter Prep Plates, the Prep Pack as well as the nCounter cartridge were loaded. After placing the hybridized sample strip on the deck of the Prep Station a run was initiated with high sensitivity settings to purify and immobilize the samples in the cartridge. As soon as the run was finished the cartridge holding the immobilized samples was positioned in the correct slot in the nCounter Digital Analyzer for data collection selecting the highest resolution.

For analysis of the generated data, the Reporter Code Count files, and the Reporter Library File, specific for the CodeSet, were imported into the nSolver 4.0 software. Default quality control parameters were selected, and annotations were assigned according to the cell type (PBMC-derived CD14⁺ monocytes, DD +Shield-1, DD macrophages and CD34⁺ cells). For normalization of the raw gene expression data, a two-step process was performed: a positive control normalization as well as a CodeSet content normalization. The geometric means of the six positive controls and the 40 housekeeping genes were used to compute the normalization factor. To determine fold change, the “all pairwise ratios” and “partitioning by CD34” method was used to obtain ratios between the given annotations (monocytes, DD +Shield-1, DD macrophages and CD34⁺). The software module *Advanced Analysis* was used for deeper data insights following normalization.

2.2.1.15 Cell Lysate Preparation

Total cell lysates were prepared to extract cellular contents enabling subsequent detection and analysis of intracellular proteins. First, the cells to be lysed were counted and washed with ice-cold 1x PBS (1500 rpm, 5 minutes, 4 °C). Adherent cells were detached using a cell scraper. After a second wash step, the supernatant was discarded, and the cell pellet was detached by tapping. For the subsequent lysis, 100 µl of cell lysis buffer per 1x10⁶ cells were added and the cell pellet was dissolved by pipetting. After 30 minutes incubation on ice, the cell components were centrifuged (5000 rpm, 20 min, 4 °C). The supernatant containing the lysate, was transferred to a fresh 1.5 ml reaction tube, and stored at -80 °C until further use.

2.2.1.16 Protein Quantification via Bradford assay

The Bradford assay is a colorimetric, spectrophotometer-based method to analyze protein concentrations within a defined solution, e.g., cell lysates (2.2.1.15) (Bradford, 1976). Protein quantification relies on the absorbance shift from the initially brown to a blue color of the specific dye Coomassie brilliant blue G-250 (Thermo Fisher) elicited by protein binding. The optimal wavelength for detection is given with 595 nm representing the greatest difference between the two dye forms. A calibration curve has to be generated to allow determination of samples with unknown concentrations.

To generate the calibration curve, standard albumin dilutions (from 0-2000 µg/µl) were prepared in a 10 mm cuvette (Table 19).

Table 19: BSA dilutions for the Bradford assay calibration curve.

$\mu\text{g}/\mu\text{l}$	0	125	250	500	750	1000	1500	2000
BSA Stock	0	0.625	1.25	2.5	3.75	5	7.5	10
H ₂ O	10	9.4	8.75	7.5	6.25	5	2.5	0

The samples were prepared by diluting 2 μl of protein lysate with 8 μl ddH₂O and transferring into 10 mm cuvettes. To start the reaction, 500 μl of the Coomassie dye were added to each cuvette followed by an incubation time of 10 minutes at room temperature. Afterwards, the calibration curve was generated by measuring the albumin dilutions at 595 nm in the spectrophotometer (Nanodrop 2000c). By this curve, the protein concentration of the samples can be verified when measured at 595 nm as well.

2.2.1.17 Sodium Dodecyl Sulfate Polyacrylamide Gel Electrophoresis

For the separation of proteins with a molecular mass between 5 and 250 kDa, sodium dodecyl sulfate polyacrylamide gel electrophoresis (SDS-PAGE) was performed (Laemmli, 1970). This is an analytical method in which a discontinuous polyacrylamide-based gel consisting of a separating and stacking gel, is used in an electric field, resulting in the separation of proteins according to their molecular weight. SDS is utilized as the anionic detergent to mask the intrinsic charge of the proteins resulting in the migration of the proteins towards the anode.

For comparability, the concentration of all protein samples used for the SDS-PAGE was first determined (2.2.1.16). For each sample 30 μg of total protein were prepared by adding a suitable amount of 4x SDS sample buffer (Merck KGaA) according to the protein solutions' volume, and denaturated for 5 minutes at 95 °C. After denaturation the samples were loaded on the gel. The separation of the proteins in the samples was performed on a 10% polyacrylamide gel at 120 V for 60-80 minutes. The PageRuler™ Plus Prestained Protein Ladder (Thermo Fisher) was used as a molecular weight standard. After the SDS-PAGE detection of specified proteins was carried out using the western blot technique.

2.2.1.18 Western Blot Experiment

To specifically verify single proteins within a sample, western blotting was performed. This method consists of the protein transfer from the SDS-PAGE gel to a solid support and the subsequent detection of a protein of interest using a primary and secondary

antibody for visualization (Burnette, 1981). Using the Trans-Blot® Turbo™ Transfer Pack, including buffer and membrane, the proteins in the gel were transferred in the Trans-Blot® Turbo™ transfer system (Bio-Rad Laboratories, Inc.) at 1.0 A and 25 V for 30 minutes. To saturate free unspecific binding sites on the immobilized proteins, the membrane was incubated in blocking solution at 4 °C overnight. The next day, the membrane was incubated with a recommended dilution of primary antibody in blocking buffer for 1 hour at room temperature under gentle rotation. The membrane was then washed three times with 1x PBST for 10 minutes each. A secondary HRP-conjugated antibody with suitable species reactivity was added in blocking solution at the recommended dilution. After an incubation time of 1 hour the membrane was washed again three times for 10 minutes with 1x PBST. For visualization of the protein band by chemiluminescence, Immobilon™ Western Chemiluminescent HRP Substrate (Millipore Corporation) was added at a 1:1 ratio. Thereafter, a digital image of the membrane was produced using the Fusion SL imaging system (Vilber Lourmat).

2.2.2 Cell Biology Techniques

2.2.2.1 Cell Culture

Eukaryotic cells (Table 6) were cultivated in a CO₂ incubator with 37 °C and 5% CO₂ using tissue culture flasks (Greiner Bio-One GmbH) sized between 25 cm² and 125 cm². Suspension cell lines (Jurkat, Daudi, Raji, Carnaval) were kept RPMI-1640 Medium supplemented with 10% FCS, 100 U/ml Penicillin, 100 µg/ml Streptomycin and 2 mM L-Glutamine at a density between 0.5 and 1.5 x 10⁶ cells per ml. The adherent cell line HEK 293T was cultured in Dulbecco's Modified Eagle Medium (DMEM) containing 10% FCS, 100 U/ml Penicillin, 100 µg/ml Streptomycin and 2 mM L-Glutamine (DMEM complete). Dependent on the confluency, the HEK 293T were passaged up to three times per week by detaching and transferring the cells into a fresh cell culture flask. Detachment was performed by removing the supernatant, rinsing with 1x PBS, adding Trypsin-EDTA (1x) 0.05% and incubating for one minute at 37 °C.

Primary human CD34+ hematopoietic stem/progenitor cells were stored in liquid nitrogen until used for transduction purposes. For thawing, the frozen vial was incubated in a 37 °C water bath for two minutes, washed with 1x PBS once (1100 rpm, 8 minutes) and subsequently cultivated in Iscove's Modified Dulbecco's Medium (IMDM) supplemented with 20% FCS, 100 U/ml Penicillin, 100 µg/ml Streptomycin and 2 mM L-Glutamine on a 48-well cell culture plate (Greiner Bio-One). In addition, the following cytokines were added at the given concentrations: IL-3 (10 ng/ml), IL-6 (20 ng/ml), SCF (20 ng/ml), TPO

(20 ng/ml), FLT3-L (20 ng/ml) and GM-CSF (20 ng/ml) (modified from (Mulloy et al., 2003) and referred to as CD34+ complete medium). After the transduction (2.2.2.3), the cells were transferred to a fresh 24-well tissue-treated cell culture plate and kept at a density between 0.5 and 2.5×10^6 cells per ml. For hematopoietic stem cells transduced with a vector expressing destabilization domain (DD) fusion proteins the small molecule Shield-1 was added every other day at a final concentration of 500 nM.

The DD-Shield-1 interplay represents a single ligand-single domain ProteoTuner system (Takara) which allows for controllable activity of a protein of interest after its expression. The DD domain is an engineered 12 kDa mutant of the FK506 binding protein 12 (FKBP12) designed to be rapidly degraded after expression in mammalian cells. The here utilized DD domain harbors three amino acid substitutions (E31G-R71G-K105E) which were demonstrated to ensure the most efficient protein turnover (Chu et al., 2008). Fusing the DD domain to a protein of interest, in this case MLL-ENL, results in the fast proteasomal degradation. This instability is reversed by binding of the ligand Shield-1, a non-toxic, membrane permeable small molecule (750 Da), thereby preventing degradation (Figure 9). Thus, the activity of MLL-ENL can be tightly regulated in a fast and non-toxic manner as this system provides reversibility by washout of the Shield-1 ligand. This way, the protein can be either switched on or off at an arbitrary time point (Banaszynski et al., 2006).

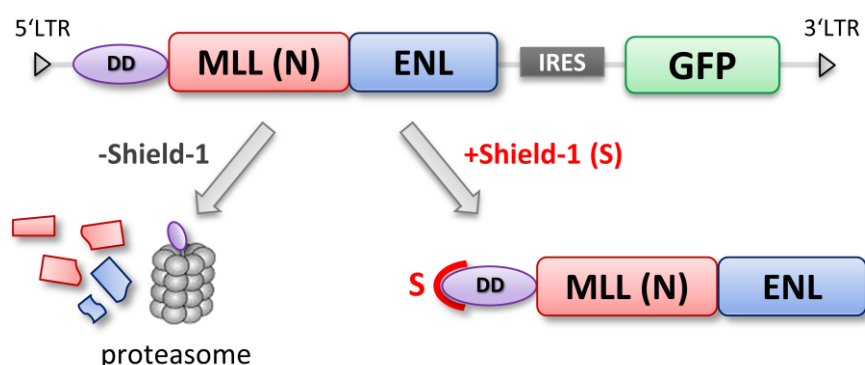


Figure 9: Graphical depiction of the regulable DD-Shield-1 interplay with MLL-ENL as protein of interest.

The DD domain, an FKBP12 mutant, is rapidly degraded after expression in mammalian cells. When fused in-frame to MLL-ENL, the full protein is constitutively degraded via the proteasome rendering MLL-ENL inactive. As soon as the small, membrane permeable DD-ligand Shield-1 is added, degradation is prevented allowing for activity of MLL-ENL. LTR, long terminal repeat; DD, destabilization domain.

2.2.2.2 Mammalian Cell Transfection with Polyethylenimine

To produce viral particles for transduction purposes, HEK 293T were transfected using the polyethylenimine (PEI) transfection reagent. The method is based on the condensation of the present DNA into positively charged complexes caused by the PEI, binding to the naturally positively charged cell membrane due to the electrostatic interaction and are taken up by the cell via the process of endocytosis (Boussif et al., 1995). The producer cell line HEK 293T represents a specified variant of the HEK 293 cells additionally expressing the SV40 large T antigen allowing replication of plasmids harboring the SV40 origin of replication. This way, the amount of generated retroviral particles can efficiently be increased due to the high copy number of the transfected plasmids. For the assembly of the retroviral particles, expression of certain viral proteins is essential. Beside the plasmid carrying the gene of interest, so called packaging plasmids (M634 and M620) have to be included. These plasmids harbor genes encoding the envelope proteins responsible for the infection of the target cell, structural proteins including the matrix, capsid and nucleocapsid components and the enzymes reverse transcriptase and integrase for efficient genomic integration of the target DNA. As an envelope protein the Gibbon ape leukemia virus (GALV) glycoprotein with broad tropism is expressed on one of the packaging plasmids (M620). The other plasmid (M634) drives the expression of the group-specific antigens (Gag) consisting of the structural proteins and the enzymes (Pol) under the control of the CMV promoter. As these genes are provided in trans all three plasmids are necessary for producing infectious replication-incompetent viral particles. These viral particles incorporate the genetic element of interest located between the 5' LTR and the 3' LTR.

The day before transfection $2.5 - 3.0 \times 10^6$ HEK 293T cells were plated on 10 cm culture dishes in 10 ml DMEM. For each construct, two plates were prepared to generate a sufficient amount of retroviral particles. The following day, the plates were checked for sub-confluency (around 70%). For each plate the following transfection solutions were prepared in 15 ml tubes separately:

Table 20: Composition of the PEI transfection solutions

Component	Solution A	Solution B
DMEM empty (w/o FCS, Penicillin-Streptomycin and L-Glutamine)	586 μ l	1000 μ l
MSCV vector (w gene of interest), 2 μ g/ μ l	12 μ g	-
M634 packaging plasmid, 2 μ g/ μ l	7.5 μ g	-
M620 packaging plasmid, 2 μ g/ μ l	2.5 μ g	-
Polyethylenimine 20 mM	-	70 μ l (Shi et al., 2003)

Upon brief vortexing both solutions, solution B was added dropwise to solution A while vortexing followed by an incubation time of 20 minutes at room temperature. Thereafter, the supernatant of the HEK 293T containing plate was discarded, 5 ml of DMEM empty is mixed with the combined solutions and slowly pipetted onto the plated HEK 293T cells. As metabolites in supplemented medium would inhibit the transfection it is crucial to use DMEM empty. After an incubation time of 4-5 hours at 37 °C and 5% CO₂ the transfection mix is discarded, the plates were supplied with DMEM complete and further incubated overnight. The next day, fluorescence microscopy of the cells was performed to check transfection efficacy if a gene encoding a fluorescent protein was included between the LTRs. Thereafter, the supernatant containing retroviral particles was harvested for transduction purposes.

2.2.2.3 Retroviral Transduction of Hematopoietic Stem Cells

Retroviral transduction represents the retrovirus-mediated process of introducing foreign DNA into a host cell's genome. Retroviral particles are spherical enveloped particles able to invade dividing target cells. Upon cell entry the single stranded RNA is reverse transcribed via the viral enzyme reverse transcriptase and eventually incorporated into the host cell's genome by an integrase enzyme. These particles produced by transfected HEK 293T cells are replication-defective rendering them unable to reproduce after delivering. Thus, genes of interest can be stably integrated into the genome of dividing cells, such as proliferation competent CD34⁺ hematopoietic stem cells.

For transduction of human CD34⁺ cells, a pre-stimulation is necessary for inducing robust cell proliferation. To maximize the transduction efficiency four rounds of transduction were performed on two consecutive days. The same day the HEK 293T cells were seeded for the transfection, a frozen vial containing 1 x 10⁵ human bone marrow derived CD34⁺ cells (Lonza Group) was thawed, transferred to a 48 well plate in CD34⁺ complete medium and incubated for two days at 37 °C and 5% CO₂. The day before the transduction, i.e., the day of the transfection, two 24 well untreated plates were coated with 500 µl of a 50 µg/ml RetroNectin solution (Takara Bio Inc.) per well and incubated at 4 °C for at least 6 hours or overnight. RetroNectin is a 63 kDa fragment of recombinant human fibronectin comprising three functional domains: the cell binding domain (C-domain), the heparin-binding domain (H-domain) and the CS1-site. Binding of the viral particles is assured by the H-domain while the target cells bind to both the C-domain and the CS1-site via the surface integrin receptor VLA-5 and VLA-4, respectively. This way, RetroNectin greatly enhances the transduction efficiency by directing both components into spatial proximity thereby facilitating the infection process. The

requirement is the expression of both VLA-5 and VLA-4 present on hematopoietic stem cells. The next day (the day of the transduction) RetroNectin was removed and unspecific binding was blocked by adding 1 ml of a 2% BSA solution per well and incubating for 30 minutes at room temperature. BSA was discarded and each well was rinsed once with HBSS and once with 1x PBS. Viral supernatant was harvested from the transfected HEK 293T containing plates (2.2.2.2) by filtration using 0.22 μm filters and added to the respective RetroNectin-coated wells (1 ml per well). Both plates (for the first and second transduction) were loaded individually and centrifuged at 3,700 rpm and 4 °C for 60 minutes. This step was repeated two more times with fresh viral supernatant each time. Meanwhile, the HEK 293T plates were supplied with DMEM complete and further incubated at 37 °C and 5 % CO₂ for continuous virus production. After the third centrifugation one plate was stored at 4 °C, while the other plate was immediately used for the first round of transduction. Thus, supernatant was discarded and the pre-stimulated CD34+ cells were transferred to the respective wells in a volume of at least 800 μl per well. The plate was incubated at 37 °C and 5 % CO₂ for at least 8 hours allowing the target cells to divide. For the second transduction, the supernatant from the other plate was removed and the cells were transferred from the first plate to the respective virus-coated wells. The plate was then incubated at 37 °C overnight. The next day, the described steps were repeated for the third and fourth transductions. The day after the fourth transduction the target cells were transferred to a fresh 24-well cell culture plate for further cultivation.

2.2.2.4 Differentiation of DD-MLL-ENL Expressing Monocytic Precursor Cells

As expression of the MLL-ENL fusion gene remarkably enhances proliferation of immature cells with a concomitant differentiation block, transduced CD34+ HSPCs exhibit a growth advantage leading to a pure MLL-ENL expressing population after approximately 30-40 days. Utilizing a DD-MLL-ENL construct allows for targeted degradation of the MLL-ENL protein by deprivation of the Shield-1 ligand. As soon as a pure GFP+ population of DD-MLL-ENL expressing cells was obtained in the presence of Shield-1, the cells were counted and washed three times with 1x PBS (1,500 rpm, 5 minutes) to get rid of residual Shield-1 ligand. The cells were resuspended in IMDM medium supplemented with 10% FCS, 100 U/ml Penicillin, 100 $\mu\text{g}/\text{ml}$ Streptomycin, 2 mM L-Glutamine, GM-CSF (20 ng/ml), IFN- γ (20 ng/ml) and LPS (100 ng/ml) (referred to as differentiation medium) at a concentration of 1×10^6 per ml, transferred to either a 25 cm² or 75 cm² cell culture flask and further incubated at 37 °C and 5% CO₂. After 7 days, cells were checked for adherence under the microscope. Non-adherent cells were

discarded by removing the supernatant and changing the medium. After 14 days, the differentiated cells were harvested by trypsinization, and detaching using a cell scraper. The obtained macrophages were further used for analyses and functional assays.

2.2.2.5 Cytospin Technique

The cytospin technique is a method to produce one-cell-thick-monolayer preparations used for determination of the cellular morphology and subsequent hematological staining (Martinazzi et al., 1972). First, cells within a liquid culture are concentrated onto a microscope slide via centrifugation in a suitable cytocentrifuge. The slide is attached to a centrifugation-compatible slide clip, covered with a filter card and connected to a cytofunnel. The cytofunnel contains the cell suspension to be analyzed, which will be pushed through the funnel's opening by centrifugal force whereby the cells become concentrated in a small area on the slide. Excess fluid is absorbed by the filter card.

This technique was performed in cooperation with Dr. Stephanie Schneider from the Laboratory for Leukemia Diagnostic (University Hospital, LMU Munich). Up to 1×10^6 in a volume of 100-500 μl were transferred into the cytofunnel. The assembly was then centrifuged at 800 rpm for 10 minutes following an incubation time of 30 minutes at room temperature allowing drying of the microscope slide. The dried slides were then used for fixation and staining.

POX reaction

To detect myeloperoxidase (POX) reaction in leukocytes, a cytochemical reagent consisting of a POX-FIX and a POX reaction solution was used (Table 4) (Herzog and Fahimi, 1973). The dried microscope slide containing the cells was first fixated for 30 seconds in the POX-FIX solution. After a subsequent rinsing step with ddH₂O, the slide was dried and incubated in the POX reaction solution for 25 minutes. For staining of the cell nucleus, the slide was incubated in hematoxylin for 3 minutes before washing in tap water for 5 minutes and final drying at room temperature.

Nonspecific esterase staining

To detect enzymatic activity of the alpha-naphthyl acetate esterase (nonspecific esterase staining), indicating monocytic phenotype, staining of the microscope slide was performed (Yam et al., 1971). On the lines of the POX staining, the nonspecific esterase staining was performed using the EST-FIX and the esterase reaction solutions.

When leukemic cells are used for the above-mentioned staining, the individual leukemia subtype, e.g., of myeloid leukemia, can be verified via the combined percentages of POX and EST positive cells according to the French-American-British (FAB) classification.

Pappenheim staining

The panoptic and panchromatic Pappenheim staining represents a combination of the May-Grünwald staining and Giemsa staining enabling discrimination between cell types by staining basophilic, neutrophilic, and eosinophilic structures as well as cell nuclei (Tverdynin et al., 1980). To conduct the staining, the dried microscope slide was incubated in May-Grünwald staining solution (Merck KGaA) for 6 minutes. After two wash steps with Weise Buffer for 10 seconds each, the second staining took place with the Giemsa staining solution for 35 minutes followed by another, final wash step.

2.2.2.6 Flow Cytometry

All cell samples were analyzed using the BD FACSCalibur™ platform (Becton Dickinson), a dual-laser design providing both the flexibility and sensitivity for multicolor analysis. This way, cells exhibiting a fluorescence signal either due to the presence of a fluorescent cellular component or by staining of individual cell surface proteins using fluorescently labelled antibodies can be detected. Additionally, the cells' immaturity could be verified by investigating the cell size and granularity depicted by the forward and side scatter (FSC, SSC). For the antibody-based immunostaining, cells were first counted and distributed to 5 ml PS-tubes with 1×10^5 cells each if not otherwise stated. Adherent cells were detached by trypsinization and the use of a cells scraper before counting. Cells were washed with 3 ml FACS buffer for 5 minutes at 1,500 rpm. Thereafter cell pellets were resuspended in 200 μ l FACS buffer. To avoid binding of the used antibodies to the Fc receptors of human Fc receptor-expressing cells, FcR blocking reagent (Miltenyi Biotec) was used according to the manufacturer's protocol (10 minutes at 4 °C). To stain specific cell surface proteins the antibodies shown in Table 9 were added to the respective tubes at the recommended dilution. After an incubation time of 30 minutes at 4 °C the cells were washed again with buffer to remove excess antibody and analyzed by flow cytometry.

2.2.2.7 Karyotyping

Karyotyping represents a conventional method to identify chromosomal abnormalities and rearrangements in single cells (Teerenhovi et al., 1984). Through staining of condensed chromosomes during the metaphase all chromosomes become visible. For this purpose, growing cell cultures must be used. This technique was performed in cooperation with Dr. Stephanie Schneider from the Laboratory for Leukemia Diagnostic (University Hospital, LMU Munich). A minimum of 2×10^6 dividing cells were cultivated on a 12 well plate in suitable medium allowing proliferation. DD-MLL-ENL cells from different transductions and at various time points were used. To fixate chromosomes in the metaphase, colchicine (10 μ l/ml), an inhibitor of microtubule formation, was added to the cell suspension preventing the progression to the anaphase during mitosis. The cells were incubated at 37 °C for 2 hours before centrifugation at 1,200 rpm for 10 minutes in a 50 ml conical tube. The supernatant was discarded, and the cell pellet was resuspended. A 0.0375 M KCl solution was added dropwise to the cells to a volume of 10 ml and then filled up to 40 ml. After further incubation at 37 °C for 20 minutes, the cells were centrifuged at 1,200 rpm for 10 minutes. The same way the KCl solution was applied, Carnoy's Fixative (3:1 ratio of methanol:glacial acetic acid) was added to the resuspended cells. The suspension was then dropwise transferred to a microscope slide and stained using the Giemsa staining solution. Giemsa darkly stains heterochromatic regions resulting in specific bands in the chromosome structure which allows identification and grouping of the chromosomes. The chromosomes were examined by high-resolution microscopy.

2.2.2.8 Colony-Forming Unit Assay

The colony-forming unit (CFU) assay displays a technique to investigate the proliferation and differentiation capacity of individual progenitor cells in semi-solid media supplemented with cytokines (methylcellulose) (Kronstein-Wiedemann and Tonn, 2019). The CFU assay is designed to promote proliferation and differentiation of single CFUs leading to the formation of characteristic and discrete cell clusters or colonies consisting of identifiable descendants. This way various cell types can be analyzed regarding their potency, proliferation capability and lineage commitment. Under optimal conditions, a single colony is derived from one progenitor cell allowing to determine cell fate frequencies within a defined cell culture.

For the procedure a vial of methylcellulose (MethoCult GF H84444) was thawed at room temperature. Meanwhile, 3×10^5 of the cells of interest were harvested and washed with 1x PBS. The cell pellet was resuspended in 1 ml of IMDM supplemented with 2% FCS, 1000 U/ml Penicillin and 1 mg/ml Streptomycin. To mix the cells with the thawed methylcellulose, 300 μ l of the cell suspension was transferred into the methylcellulose vial (10^4 cells/ml plating concentration) and mixed by vortexing. After an incubation time of 10 minutes to allow the bubbles to disperse, the cell-methylcellulose mix was taken up with a syringe and homogeneously dispensed into two wells of a SmartDish 6-well plate (Stemcell Technologies) with 1 ml per well for duplicates. The empty wells were filled with 1x PBS to maintain humidity which is crucial for the assay. The plates were incubated at 37 °C and 5% CO₂ for 14 days. After 14 days, colonies were quantified using a high-quality inverted microscope. According to Stemcell Technology's specification colonies were discriminated between the various types including CFU-E (erythroid), CFU-GM (granulocyte, macrophage), CFU-GEMM (granulocyte, erythrocyte, macrophage, megakaryocyte) and CFU-Mk (megakaryocyte).

2.2.2.9 Flow Chamber Adhesion Assay

The flow chamber assay was performed to investigate the cells' adhesion characteristics in an *in vitro* environment with fluid shear stress mimicking the *in vivo* environment of a blood vessel (Bianchi et al., 2013). Using suitable slides coated with purified adhesion ligands allows assessment of cell binding under increasing shear stress. In this study, the vascular cell adhesion molecule 1 (VCAM-1, R&D systems) was used as ligand. To prepare the assay, a starvation step was included the day before to get rid of FCS and cytokines. For this purpose, 1×10^6 differentiated DD-MLL-ENL cells were detached by trypsinization, washed with 1x PBS (1,500 rpm, 5 minutes), resuspended in IMDM supplemented with 1% Penicillin-Streptomycin and 2% L-Glutamine at a concentration of 1×10^6 /ml and incubated overnight at 37 °C and 5% CO₂ on a 12-well tissue culture plate. The day of the flow chamber assay, HBSS medium was supplemented with 1% BSA (HBSS+) and warmed in a 37 °C water bath. Meanwhile, an uncoated μ -slide VI 0.4 (Ibidi GmbH) was coated by loading 30 μ l VCAM-1 (2 μ g/ml) into a channel and tilting the slide to spread the ligand equally. To ensure efficient coating the slide was incubated at room temperature for 30 minutes. As a control an uncoated slide was deployed as well. The starved cells were then arranged by washing with 1x PBS and resuspending 1×10^5 cells in 100 μ l HBSS+. After coating a blocking step was conducted by transferring 50 μ l of 1x PBS + 2% BSA to the VCAM-1 coated channel and incubating for 10 minutes at room temperature. Afterwards, the slide was fixed under the microscope (Axio

Observer D1) and set up by removing 50 μl of the volume inside the channel and subsequently adding 100 μl of the particular cell suspension. To allow binding of the cells to VCAM-1, the slides were incubated for 5 minutes at room temperature. During the incubation time the slide was connected to the flow chamber system, consisting of a glass syringe (filled with warm HBSS+) and the Legato 100 syringe pump, via flexible tubes. One flexible tube connects the glass syringe with one end of the channel (inlet well) while the other tube is stuck to the second well (outlet well) for collection of the pumped medium. The microscope was focused on the center of the channel where the cells settled and an image was taken (AxioCam MRm) before the flow was initiated by starting the pump. The shear stress was increased continuously as shown in Table 21.

Table 21: Shear stress settings for the flow chamber adhesion assay

Flow speed [l/min]	Shear stress [dynes/cm ²]	Duration [s]
0.17	0.35	30
1.14	2	30
2.81	5	30
4.53	8	30
8.1	15	30

Every 30 seconds an image was taken with the camera to analyze the number of cells which are still adherent at the given flow speed. For analysis, the cells were counted on each image to determine the percentage of adherent cells.

2.2.2.10 Cell Migration Assay (Chemotaxis)

The migration properties of DD-MLL-ENL cells and thereof derived macrophages were investigated using a matrix-based three-dimensional (3D) chemotaxis assay. These experiments were performed in cooperation with Dr. Adrian Hoffmann and Prof. Dr. Jürgen Bernhagen from the Institute for Stroke and Dementia Research (University Hospital, LMU Munich). For this purpose, chemotaxis-related μ -slides (Ibitreat, Ibiti GmbH) were used consisting of chambers which contain two large reservoirs for building up a chemokine gradient connected by a narrow observation canal. For each sample 2×10^6 cells were washed with 1x PBS (1,500 rpm, 5 minutes), resuspended in 50 μl of “empty” RPMI (without FCS) and mixed with 250 μl of a rat tail collagen type I solution (1 mg/ml final collagen I concentration) fabricated as shown in Table 22.

Table 22: Composition of the rat tail collagen I solution

Component	Volume
10x DMEM	20 μ l
NaOH, 1 M	5 μ l
ddH ₂ O	112 μ l
NaHCO ₃ , 7.5%	3 μ l
1x DMEM	50 μ l
Collagen I, 5 mg/ml	60 μ l

The observation canal of the μ -slide was filled with the collagen-cell mix according to the manufacturer's protocol (Ibidi GmbH) and then incubated at 37 °C for 30 minutes. Following the protocol, the reservoirs were filled with empty RPMI following the addition of a chemokine (C-C motif) ligand 2 (CCL2) solution to one reservoir at an end concentration of 300 ng/ml generating a gradient. The cell motility towards the chemoattractant was then monitored with time-lapse imaging every 1.5 minutes at 37 °C for 2 hours using an inverted microscope (Leica DMI8) with the appropriate live cell-cell imaging software (Leica Microsystems, Wetzlar, Germany). The generated images were imported as stacks to the ImageJ software for analysis of the cell migration with the use of the manual tracking plugin as well as the chemotaxis and migration tool (Ibidi GmbH).

2.2.2.11 *E. coli* BioParticles™ Uptake Assay

To verify the DD-MLL-ENL originated macrophages' phagocytosis ability, *E. coli* BioParticles (pHrodo™ Red *E. coli* BioParticles™ Phagocytosis Kit for Flow Cytometry, Thermo Fisher Scientific) were used. These BioParticles are non- or only weakly-fluorogenic in neutral or basic solutions, i.e., when attached to the cell membrane of the cells. However upon internalization, they exhibit a strong fluorescence in the acidic environment of the phagosome. The particles were prepared following the manufacturer's protocol. The day before, 2×10^4 differentiated DD-MLL-ENL cells (2.2.2.4) were detached from the culture flasks, seeded in 300 μ l differentiation medium on μ -Slides (8 Well ibiTreat, Ibidi GmbH) per well and further incubated at 37 °C and 5% CO₂ overnight. In total, four wells were prepared. The next day, cytochalasin D (Sigma-Aldrich), a potent inhibitor of actin polymerization, thus phagocytosis, was added to two of the wells at a concentration of 10 μ M. The solvent, DMSO in this case, was added to the other wells in the same volume. After an incubation time of 20 minutes at 37 °C, 10 μ l of the BioParticles solution were added to the respective wells yielding a > 20:1 particle:cell ratio. The slide was incubated for 2 hours at 37 °C allowing uptake via

phagocytosis. Finally, supernatant was removed completely and replaced with 1x PBS before analyzing via fluorescence microscopy.

2.2.2.12 Efferocytosis Assay

Similar to the pHrodo BioParticles phagocytosis assay, the DD-MLL-ENL macrophages were investigated regarding their efferocytosis capacity. Efferocytosis is the phagocytosis of apoptotic cells elicited by specific “eat me” signals, such as the presence of phosphatidylserine on the outer surface of the cell membrane (Li, 2012). Accordingly, 2×10^4 differentiated DD-MLL-ENL cells were seeded on μ -slides in four wells for technical duplicates. In this assay the Jurkat cell line was used as target cells and cultivated on two wells of a 24 well plate with a concentration of 1×10^6 cells/ml. To induce apoptosis, staurosporine (Selleck Chemicals LLC), a potent ATP-competitive kinase inhibitor, was added to one of the wells at a final concentration of $1 \mu\text{M}$. The same volume of DMSO, the correspondent solvent, was added to the other well for comparison. The plate was then incubated at 37°C and $5\%\text{CO}_2$ for 4 hours. After the incubation both cell suspensions were fluorescently labeled using the CFSE Cell Division Tracker Kit (Biolegend) according to the manufacturer's protocol. The labeled target cells were added to the differentiated DD-MLL-ENL cells at an E:T ratio of 1:2, resulting in 40,000 target cells per well (2x apoptotic cells, 2x healthy cells). To induce efferocytosis, the slide was incubated at 37°C and $5\%\text{CO}_2$ for 2 hours. Finally, the supernatant was removed and replaced with 1x PBS before fluorescence microscopy. For each well 50 macrophages were counted and analyzed for uptake of fluorescent cells determining efferocytosis. Efferocytosis was displayed as percentage of counted macrophages positive for engulfment of target cells (alive or dead).

2.2.2.13 Isolation of Mononuclear Cells from Peripheral Blood

The here used method for isolation of peripheral blood mononuclear cells (PBMCs) relies on density gradient centrifugation. The blood components have different densities and can therefore be separated by centrifugation. Residual blood from healthy donors present in leukocyte reduction system (LRS) chambers during plateletpheresis (Division of Transfusion Medicine, Cell Therapeutics and Haemostaseology, University Hospital, LMU Munich) was used as a source of PBMCs. The LRS chamber was opened using a sterile scissor. The dripping blood was collected in a 50 ml conical tube and mixed with four equivalents of 1x PBS. Density gradient centrifugation was prepared by transferring 20 ml of a Ficoll solution (Ficoll-Paque™, Cytiva) into fresh 50 ml conical tubes. The

blood-PBS mix was piled up onto the Ficoll solution by carefully pipetting 10 ml to avoid any intermixture. The tubes were then centrifuged at 2,500 rpm for 20 minutes with the brake turned off. The characteristic mononuclear cell layer was then transferred into a fresh conical tube and washed two times with 50 ml 1x PBS (1,500 rpm, 5 minutes). To induce erythrocyte lysis after the wash steps the pellet was resuspended with 45 ml of ice-cold water and inverted for 30 seconds. To stop the reaction 5 ml of 10x PBS were added. The cells were centrifuged two more times with 1x PBS and finally resuspended in a total volume of 50 ml 1x PBS. Prior to use for subsequent differentiation into macrophages (2.2.2.14) the cell number was determined using a hemocytometer.

2.2.2.14 Generation of M0 and M1 Macrophages

In vitro differentiation of peripheral blood monocytes into macrophages was conducted with isolated PBMCs. By utilizing different cytokines in combination with inflammatory stimuli either unpolarized M0 or polarized M1 macrophages were obtained. Starting with the isolated PBMCs, consisting of lymphocytes and monocytes, 6×10^7 cells were incubated for 10 minutes at 37 °C in 5 ml of Monocyte-Attachment Medium (PromoCell GmbH) in a 75 cm² Nunc™ EasYFlask™ Cell Culture Flasks (Thermo Fisher Scientific). Non-attached lymphocytes were subsequently eliminated by rinsing the flask with 10 ml 1x PBS three times. These wash steps were repeated two more times before adding 10 ml of X-VIVO™-15 serum-free Hematopoietic Cell Medium (Lonza Group) supplemented with 0.5% Penicillin-Streptomycin. The flasks were then further incubated at 37 °C and 5% CO₂ overnight. The next day, the washing steps were repeated before adding 10 ml of fresh X-VIVO™-15 medium with either 10 ng/ml M-CSF (M0) or 10 ng/ml GM-CSF (M1). Thereafter the flasks were incubated at 37 °C and 5% CO₂ for further six days to induce efficient differentiation. For classical activation of M1 macrophages, LPS (100 ng/ml) and IFN- γ (20 ng/ml) was supplemented at day six for 24 hours.

2.2.2.15 Fc γ R Binding Assay

Functional Fc receptors (FcR) provide the basis for inducing phagocytosis of antibody-opsonized pathogens and cells by recognizing and binding the Fc (fragment crystallizable) region of the antibody. The Fc γ R family able to bind immunoglobulin G (IgG) antibodies represent the most important Fc receptors in terms of phagocytosis. This assay aims to verify the Fc γ R functionality expressed on differentiated DD-MLL-ENL cells concerning binding capacity. For this purpose, differentiated DD-MLL-ENL cells were harvested, washed with 1x PBS and incubated with Gamunex® 10%, a sterile

solution of unmodified human IgGs at various concentrations (4, 20, 100, 500 µg/ml). For each sample, 1×10^5 cells were used in a total volume of 50 µl 1x PBS + 1% BSA in a 5 ml PS-tube. After IgG addition, the tubes were incubated at 4 °C for 2 hours. Thereafter, the samples were washed with 1x PBS (1,500 rpm, 5 minutes) followed by staining with a secondary PE-conjugated Fcγ fragment specific antibody (Jackson ImmunoResearch) at the recommended dilution in a volume of 50 µl 1x PBS + 1% BSA. After an incubation time of 45 minutes at 4 °C, the cells were washed again with 1x PBS (1,500 rpm, 5 minutes) before analyzing via flow cytometry.

2.2.2.16 Antibody-Dependent Cellular Phagocytosis

To investigate the DD-MLL-ENL derived phagocytes' ability to engulf alive, antibody-opsionized target cells, an antibody-dependent cellular phagocytosis assay (ADCP) was performed. ADCP was conducted and analyzed in two different ways: determination of phagocytosis percentage by counting via fluorescence microscopy as well as phagocytosis time courses via real-time live cell imaging (IncuCyte® S3 Live-Cell Analysis System). ADCP of the DD-MLL-ENL derived phagocytes was compared to PBMC-derived M0 and M1 macrophages (2.2.2.14) as well as untransduced HSPC-derived macrophages differentiated in the same way as DD-MLL-ENL cells described in 2.2.2.4.

2.2.2.16.1 Analysis by Fluorescence Microscopy

The differentiated cells were seeded on µ-Slides (8 Well ibiTreat, Ibidi GmbH) as described in 2.2.2.11 the day before. The following day, up to 5×10^6 target leukemia/lymphoma cells were labeled using the fluorescent CFSE dye (Biolegend) according to the manufacturer's recommendations. Daudi and Raji cells were used as targets as well as patient-derived MCL and CLL cells which were isolated from peripheral blood and stored at -80 °C until use for the phagocytosis assay. Hence, for thawing MCL and CLL cells vials were incubated at 37 °C in the water bath before labelling. The CFSE labeled cells were counted and diluted to a concentration of 4×10^5 cells/ml in RPMI with 10% FCS. For each well on the µ-slides, 100 µl of the supernatant were carefully discarded allowing the addition of 100 µl of the labeled target cell suspension (4×10^4 cells) to ensure an E:T ratio of 1:2 in a total volume of 300 µl. To initiate ADCP, the therapeutic IgG antibodies rituximab (anti-CD20) and daratumumab (anti-CD38) were added separately at a final concentration of 10 µg/ml. As a control the IgG antibody trastuzumab (anti-HER2, absent on the target cells) was used in addition to the control

reaction without any antibody. To further augment the phagocytosis rate, the potent “don’t eat me” signal CD47 was blocked by the use of a IgG2 σ variant of the CD47 antibody hu5F9-G4 (magrolimab) with depleted C1q and Fc γ R binding (CD47 σ) (Kellner, unpublished) in combination with rituximab. As an additional control a respective variant of trastuzumab was used (HER2 σ) (Kellner, unpublished). All samples were prepared in duplicates. The slides were incubated for 2-3 hours at 37 °C and 5% CO₂. Ultimately, the supernatant containing residual non-phagocytized target cells was removed completely and replaced with RPMI + 10% FCS before analyzing via fluorescence microscopy (1000x magnification, immersion oil). In sum, 50 macrophages were counted and analyzed for engulfed fluorescent cells. The number of macrophages which engulfed at least one target cell was related to the total amount of counted macrophages to calculate the phagocytosis percentage.

2.2.2.16.2 Analysis by Live Cell Imaging

For live cell imaging differentiated cells were harvested, washed with 1x PBS and seeded on a 96 well flat bottom cell culture plate (Greiner Bio-One GmbH) with 4×10^4 cells per well in 50 μ l differentiation medium (2.2.2.4 and 2.2.2.14) followed by further incubation at 37 °C and 5% CO₂ overnight. The next day, target cells (Carnaval) were labeled with pHrodo[®] Cell Labeling Dye (Sartorius) according to the manufacturer’s specifications. According to 2.2.2.16.1 antibodies were added to the wells at a final concentration of 10 μ g/ml. The labeled target cells were diluted to 1.6×10^6 /ml to use 50 μ l, i.e. 8×10^4 cells, for co-incubation generating an E:T ratio of 1:2 in 100 μ l final volume. Immediately after, the plate was installed in the IncuCyte S3 live-cell analysis system. Real-time measurements (red fluorescence + phase contrast) were initiated via the software IncuCyte 2020B with a scan duration of 8 hours in a 30 minute interval generating 4 images per well each scan. Subsequent analysis was performed by determination of the red object counts reflecting the phagocytized target cells for each individual well in a time-dependent manner.

2.2.2.17 Statistical Analysis

Statistically significant differences were analyzed using GraphPad Prism 8.0 with two-tailed paired t tests, multiple t tests, two-tailed Mann-Whitney *U* tests, one-way and two-way ANOVA with multiple comparisons. The used method for *P* value correction is displayed for each analysis individually. For all analysis, ns indicates not significant, **P* < 0.05, ***P* < 0.01, ****P* < 0.001, *****P* < 0.0001.

3. Results

The leukemia-associated transcription factor MLL-ENL resulting from the chromosomal translocation t(11;19) encodes a fusion protein able to single-handedly initiate leukemic transformation associated with both AML and ALL. Since MLL-ENL is known to require no to little concomitant co-mutations to confer remarkable *ex vivo* proliferation capacity entailing a myeloid-lineage-associated, homogeneous immature progenitor cell population, it can be regarded as a promising candidate for expanding myeloid progenitor cells with subsequent terminal differentiation when rendered adjustable (Okeyo-Owuor et al., 2019, Basilico et al., 2020). Thus, in this thesis, the expansion capacity of MLL-ENL was investigated in human bone marrow-derived hematopoietic stem cells. Subsequent phenotypic, chromosomal and genetic analyses were performed with these resulting progenitor cells. By rendering the fusion protein's activity regulable using the DD domain (Figure 9), the cells' ability to terminally differentiate into functional macrophages upon MLL-ENL degradation was examined. The resulting, differentiated cells were finally deeply surveyed concerning morphological, genetic as well as functional properties.

3.1 HSPC Expansion via Stable Expression of DD-MLL-ENL

3.1.1 Analysis of Shield-1 Dependent Proliferation Advantage

DD-MLL-ENL was stably integrated into the HSPCs' genome by retroviral transduction using the MSCV-based vector pMizi-DD-MLL-ENL-IRES-GFP to ensure sustained expression (2.1.13, 2.2.2.3). The transduced cells were cultivated in CD34+ complete medium containing IL-3, IL-6, SCF, TPO, Flt3-L and GM-CSF. To avoid degradation of the fusion protein, the ligand Shield-1 was supplemented every other day following retroviral transduction. Additionally, to rule out leakiness of the DD-Shield-1 interplay, a fraction of the cell population was cultivated in the absence of Shield-1 as control. As the reporter gene GFP is concomitantly expressed, cells could be analyzed by flow cytometry regarding the transduction efficacy and the tracking of the outgrowth of the DD-MLL-ENL expressing progenitors.

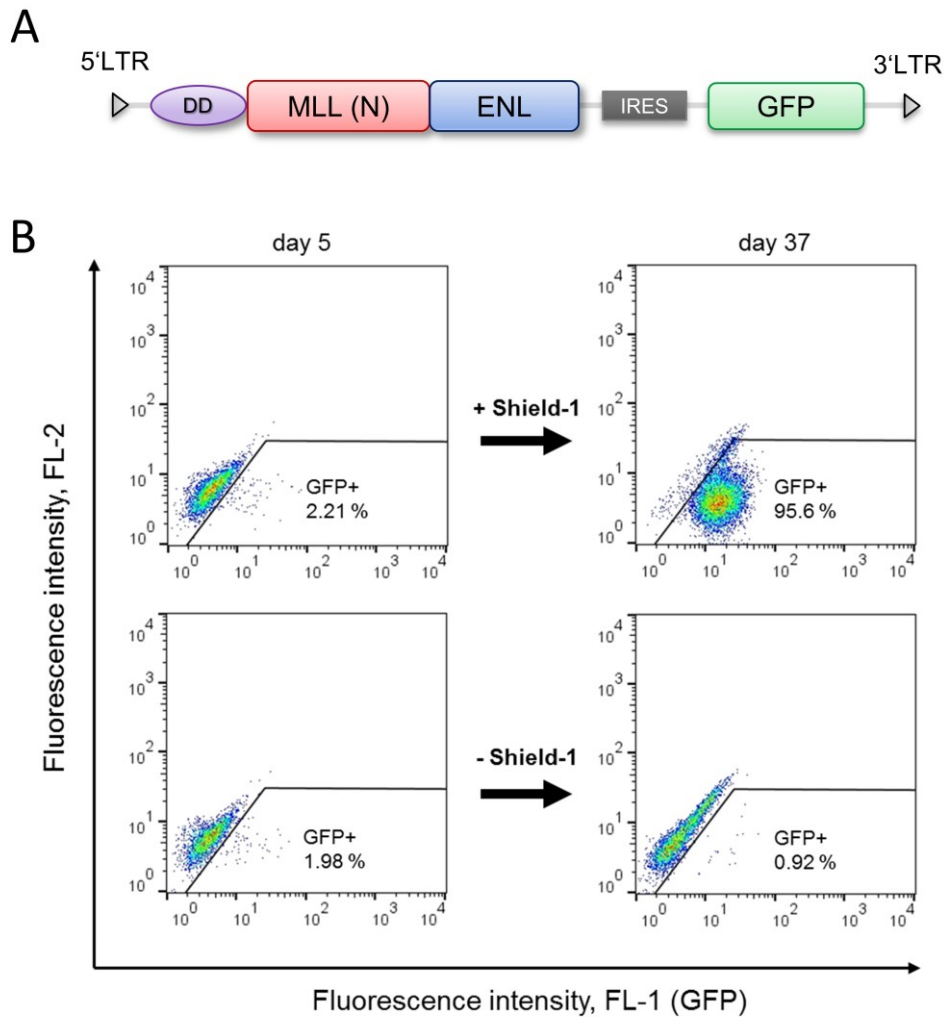


Figure 10: Tracking of DD-MLL-ENL transduced, GFP+ cells in the presence or absence of Shield-1.

(A) Scheme of the expression cassette between the 5' and 3' LTR of the MSCV-based vector pMizi-DD-MLL-ENL-IRES-GFP. (B) Upon retroviral transduction of bone marrow-derived CD34+ hematopoietic stem cells with the DD-MLL-ENL-IRES-GFP construct, cells were split into two subpopulations cultivated with or without Shield-1 (500 nM). Both populations were analyzed at regular intervals by flow cytometry. Depicted are flow cytometry dot plots of measurements with both subpopulations at day 5 and day 37 after transduction revealing the percentage of GFP+ cells. These plots are representative for one of three independent experiments with CD34+ cells from different donors.

As shown in Figure 10B, it can be clearly asserted that the cells transduced with the expression construct had a growth advantage over the untransduced CD34+ cells in the presence of Shield-1. This growth advantage resulted in an almost pure population of GFP+ cells within 37 days even with an initially transduction rate of 2.21%. In contrast, cultivation in the absence of Shield-1 did not lead to an augmented division rate of transduced cells compared to untransduced cells, as reflected by the ratio of GFP+ to GFP- cells. Thus, it was concluded that in the same period (up to 37 days) no increase in the GFP+ fraction, but a slight decrease from 1.98% to 0.92% was detected, which indicated a tight regulatory DD-Shield-1 interplay system. Of note, microscopy analyses

3.1.2 Comparison with *HOX* Gene Overexpression in HSPCs

Reports by others state that overexpression of different *HOX* genes including *HOXB4*, *HOXB8* and *HOXA9*, a direct target of MLL-ENL, is sufficient for *in vitro* expansion of murine bone marrow-derived progenitor cells (Zhang et al., 2007, Rosas et al., 2011, Calvo et al., 2000). Hence, these transcription factors, which act as principal regulator of embryogenesis by governing proliferation, were investigated for enabling the *in vitro* expansion of human bone marrow-derived HSPCs in this setting.

For this purpose, *HOX* gene expression vectors were acquired either via cloning or received from a cooperation partner. A retroviral *HOXB4* expression vector, named FMEV-HOXB4-IRES-GFP was kindly provided by PD Dr. Hannes Klump (University Hospital, Essen). This vector exhibits an FMEV backbone combining the LTR-related enhancer and promoter region of Friend Mink cell focus-forming viruses (FMCF) with the 5' untranslated leader of the murine embryonic stem cell virus (MESV) allowing robust transgene expression in hematopoietic cells (Hildinger et al., 1998). For the construction of the *HOXB8* and *HOXA9* expression vectors, the pMizi-DD-MLL-ENL-IRES-GFP backbone was used. The sequence for *HOXB8* (UniProtKB - P17481) was cloned into the MSCV-empty backbone via the restriction sites *XhoI* and *EcoRI*. To obtain an expression vector for human *HOXA9*, the *HOXA9* sequence was PCR-amplified using an Addgene vector (#97041) as template with the primers depicted in 2.1.4. The PCR fragment was gel-extracted and subcloned into the pMizi-DD-MLL-ENL-IRES-GFP backbone via *EcoRI* and *BamHI* restriction sites to substitute the DD-MLL-ENL fragment. These three expression vectors were used for retroviral transduction of CD34+ HSPCs. The percentages of GFP+ cells were determined every 3-4 days and compared to HSPCs transduced with the DD-MLL-ENL construct in the presence of the small molecule Shield-1.

As a result, retroviral overexpression of the homeobox genes *HOXB4*, *HOXB8* and *HOXA9* in human HSPCs was not sufficient to outcompete untransduced cells as assessed by steady or decreasing GFP+ percentage within the cell population. Both untransduced and transduced cells stopped proliferating in the course of time. In comparison, MLL-ENL expressing cells exhibited a growth advantage outcompeting untransduced cells, although the initial transduction rate was substantially lower. Hence, a pure GFP+ population was obtained within 30 days (Figure 12).

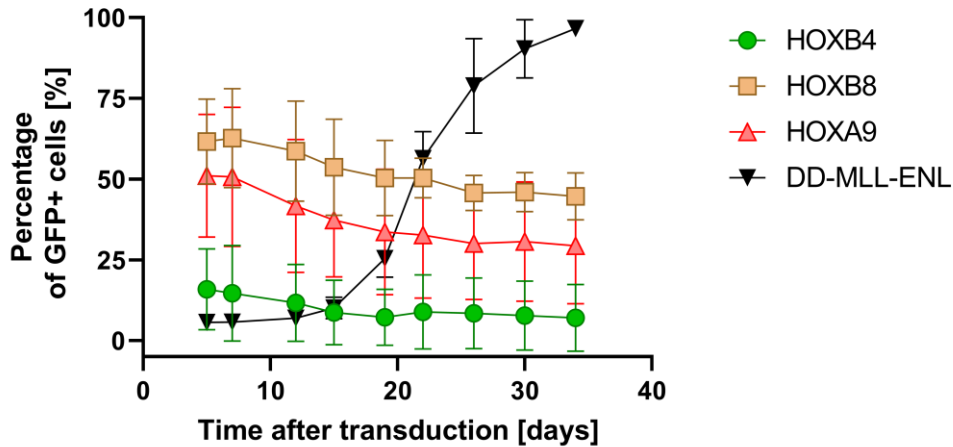


Figure 12: Tracking of HOXB4, HOXB8 and HOXA9 transduced, GFP+ cells.

For each individual transduction, bone marrow-derived CD34+ hematopoietic stem cells were transduced with either FMEV-HOXB4-IRES-GFP, MSCV-HOXB8-IRES-GFP, MSCV-HOXA9-IRES-GFP or MSCV-DD-MLL-ENL-IRES-GFP and continuously analyzed for GFP expression via flow cytometry. DD-MLL-ENL cells were cultivated in the presence of Shield-1. Data points represent the means \pm SD of three independent experiments.

3.2 Characterization of DD-MLL-ENL Expressing Progenitor Cells

Shield-1 leads to an outgrowth of DD-MLL-ENL expressing cells. These immature cells were characterized by analyzing their long-term proliferation capacity associated with Shield-1 dependency, determining the cell type and revealing chromosomal and genetic abnormalities.

3.2.1 Analysis of Sustained Proliferative Ability

The continuously active fusion protein MLL-ENL in the presence of Shield-1 is linked to preserving immature cell state accompanied by a differentiation block. Hence, proliferation assays were conducted either in the presence or in the absence of Shield-1 at various time points after transduction to analyze long-term proliferation and Shield-1 dependency. Additionally, the mean doubling time and the potential limitless expansion were determined in large-scale expansion experiments.

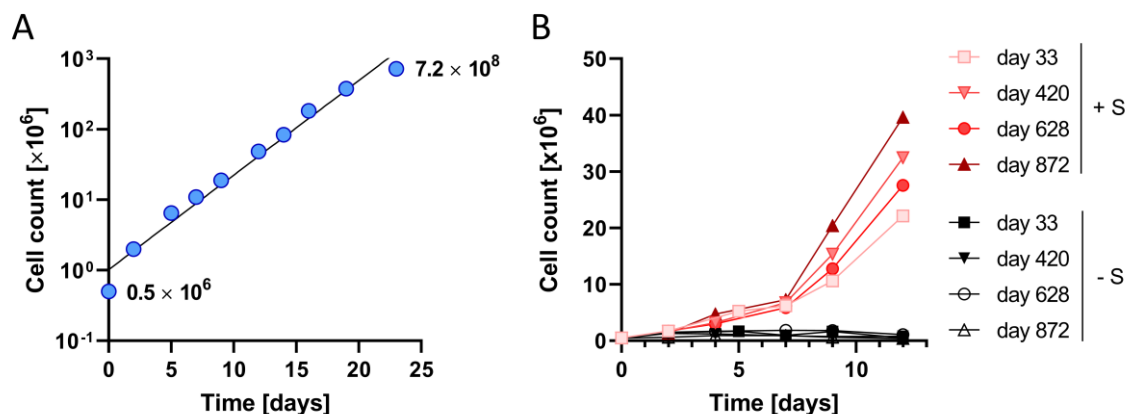


Figure 13: Long-term and large-scale proliferation capacity of DD-MLL-ENL expressing progenitor cells in the presence of Shield-1.

(A) For the large-scale proliferation assay, 0.5×10^6 outgrown DD-MLL-ENL cells were cultivated in CD34+ complete medium supplemented with Shield-1. Cells were counted every 2-3 days using a hemocytometer. Illustrated is the growth curve of DD-MLL-ENL cells from a single transduction with cell count given as decadic logarithm. Data points were analyzed using simple linear regression and are representative of two independent experiments. $R^2 = 0.9784$. (B) For the long-term proliferation assay, outgrown DD-MLL-ENL cells were harvested at different time points after the transduction, washed three times with 1x PBS and cultivated in CD34+ complete medium with and without Shield-1 (S). Cells were counted every 2-3 days with continuous Shield-1 supplementation in one of the wells. All data were generated with DD-MLL-ENL cells from the same transduction. S, Shield-1.

The large-scale proliferation illustrates the exceeding expansion capacity of DD-MLL-ENL with a total cell count increase from 0.5×10^6 to 7.2×10^8 cells within 23 days (Figure 13A). This corresponds to a calculated 1440-fold expansion and a 2.2 days doubling time. The linear regression indicated continuous growth without signs of exhaustion suggesting a limitless expansion. When investigating the proliferation of DD-MLL-ENL cells from a single transduction at different time points, an ongoing proliferation up to almost three years (day 872) was observed in the presence of Shield-1. By contrast, Shield-1 deprived cells stopped proliferating independent of the deprivation time point (Figure 13B). From this data it was concluded that the regulatory system is steadily reliable.

3.2.2 Phenotypical Characterization of DD-MLL-ENL Expressing Progenitor Cells

As proven by the proliferation assays, DD-MLL-ENL expressing cells featured an immature phenotype in media containing myeloid-linked cytokines. Hence, these progenitor cells were investigated further regarding their morphological and immunophenotypical characteristics.

3.2.2.1 Morphologic Classification by Cytochemical Stains

For the morphologic classification and lineage determination of the DD-MLL-ENL cells cytochemical stains were used according to the FAB classification systems. In general, the FAB classification can be conducted to determine the leukemia subtype regarding lineage and differentiation level (Bennett et al., 1976). DD-MLL-ENL cells were harvested after outgrowth and prepared by the cytopspin technique and subsequently stained for myeloperoxidase (POX) and non-specific esterase (EST) activity. In addition, a Pappenheim staining was conducted to analyze the morphology and the cellular components.

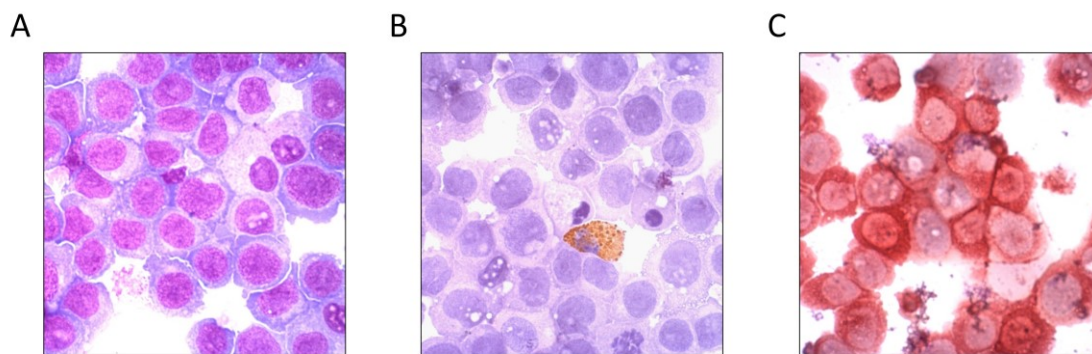


Figure 14: Cytochemical staining of DD-MLL-ENL progenitor cells.

DD-MLL-ENL cells were harvested at day 43 after the transduction, centrifuged, fixed on a microscope slide via cytopspin technique and subsequently stained with different cytochemical stains. **(A)** Panchromatic Pappenheim staining revealing intracellular structures which allows to discriminate between different hematopoietic cells. **(B)** Myeloperoxidase (POX) staining of the DD-MLL-ENL cells. Active peroxidase forms insoluble brown derivatives at the site of the activity. **(C)** Non-specific esterase staining (EST) of the DD-MLL-ENL cells. Esterase-positive cells exhibit a reddish, brown staining pattern. The images are representative for three biological replicates. All staining were performed in cooperation with Dr. Stephanie Schneider from the Laboratory for Leukemia Diagnostic (University Hospital, LMU Munich).

The Pappenheim staining revealed the cells' morphology as well as nucleus to cytoplasm ratio. The round cells possessed a large nucleus and a small cytoplasm indicating immaturity. A distinct homogeneity was observed with the lack of other cell types including erythrocytes or granulocytes (Figure 14A). According to the FAB classification, the percentage as well as the intensity of both the POX and the EST staining provide information about the respective subtype. Accordingly, the slightly positive POX staining in combination with a strong positive EST staining designated an AML M4, M5 subtype considered a type of acute monoblastic/monocytic leukemia (Figure 14B and C). Consequently, it can be assumed that the DD-MLL-ENL cells represent myelomonocytic progenitor cells presumably evoked by the cytokine setting.

3.2.2.2 Immunophenotyping

To further characterize the myeloid progenitor cells, immunophenotyping was performed by staining of characteristic HSPC- and myeloid-lineage-associated markers. For this purpose, specific fluorochrome-conjugated antibodies directed against the cell surface antigens were used.

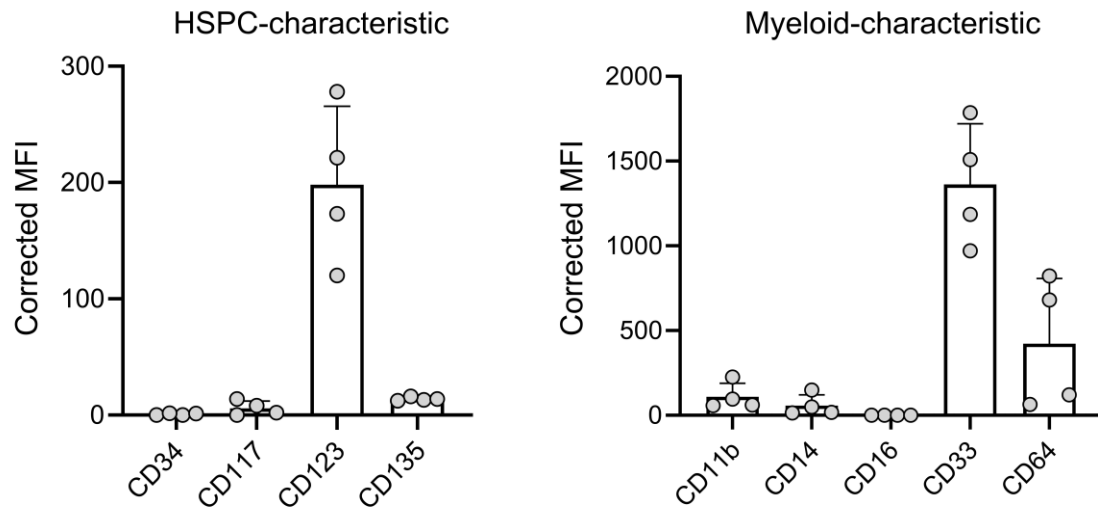


Figure 15: Immunophenotype of DD-MLL-ENL cells cultivated in the presence of Shield-1. DD-MLL-ENL expressing progenitor cells were harvested and washed with 1x PBS at 1,500 rpm for 5 minutes. For each sample, 1×10^5 cells were resuspended in 200 μ l of 1x PBS with 0.5% BSA and incubated with FcR blocking reagent and the respective antibody (diluted as recommended by the manufacturer) for 45 minutes. Excess antibody was removed by washing with 1x PBS. The cells were resuspended in 200 μ l PBS with 0.5% BSA and analyzed by flow cytometry. For each antibody, a sample with the respective isotype control was prepared. Depicted is the corrected mean fluorescent intensity (MFI) \pm SD for each sample using antibodies directed against either HSPC-characteristic (CD34, CD117, CD123, CD135) or myeloid-characteristic surface markers (CD11b, CD14, CD16, CD33, CD64) after background subtraction of the isotype control. In total, DD-MLL-ENL expressing cells of four different transductions were analyzed. All antibodies were PE-conjugated apart from CD117 and CD33 (APC-conjugated).

Immunophenotyping confirmed the DD-MLL-ENL cells' myeloid progenitor character. Although a complete loss of the HSPC-associated marker CD34 was detected, the cells expressed the SCF receptor c-KIT/CD117, and CD135 (FLT3) to a minor degree accompanied by a high expression of the IL-3 receptor CD123. For the selected myeloid markers, the cells were negative for CD16, weakly positive for CD11b and CD14 and showed a pronounced signal for both CD64 and CD33. In particular, CD33 was highly expressed as assessed by a mean MFI of approximately 1300 (Figure 15). Moreover, the DD-MLL-ENL progenitor cells did not express any T or B cell-associated surface markers such as CD3, CD8, CD10 and CD20 (data not shown).

3.2.3 Investigation of Chromosome Number and Structure

For the aim of expanding progenitor cells with inducible differentiation into functional immune cells, the number and integrity of chromosomes was analyzed. Karyotyping of the expanded DD-MLL-ENL progenitor cells was performed to detect possible chromosomal aberrations. Twenty metaphases from three different transductions were analyzed per sample. The individual chromosomes were counted, paired, and scrutinized for discrepancies, e.g., translocations.

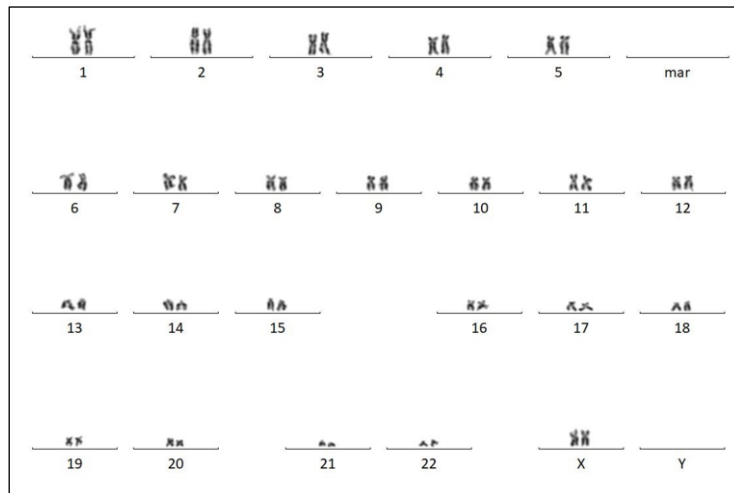


Figure 16: Representative karyogram of a DD-MLL-ENL progenitor cell sample at day 72 of expansion derived from a female HSC donor.

DD-MLL-ENL progenitor cells were prepared with colchicine (10 µg/ml) and transferred to a microscope slide followed by Giemsa-staining. An image of each chromosome was taken and paired with the concordant match. In total, 20 metaphases were analyzed for the number and structure of the chromosome pairs in DD-MLL-ENL cells from three independent transductions. Karyotyping was performed in cooperation with Dr. Stephanie Schneider and Dr. Luise Hartmann from the Laboratory for Leukemia Diagnostic (University Hospital, LMU Munich).

The representative karyogram showed a normal karyotype with a set of 23 chromosome pairs. Expansion of DD-MLL-ENL cells for 72 days did not reveal signs of abnormalities regarding deletions of chromosomal parts or changes in chromosome count. Moreover, no anomalies in shape and banding of the metaphase chromosomes were observed (Figure 16). The other two karyograms of DD-MLL-ENL progenitor cells from different transductions were similar with no aberrations detected.

3.2.4 Genome Integrity of DD-MLL-ENL Expanded Monocytic Progenitors

Besides karyotyping, genome integrity was analyzed in DD-MLL-ENL cells to exclude copy number alterations (CNAs) and genetic variants that arose during outgrowth. CNAs, which originate from deletions, duplication or amplification of chromosomal regions are often associated with disease-initiating events in leukemia (Beroukhim et al., 2010). For investigation, a whole exome sequencing of both outgrown DD-MLL-ENL cells and their

untransduced counterpart as a reference was performed and compared with each other on genome wide and chromosome wide scale.

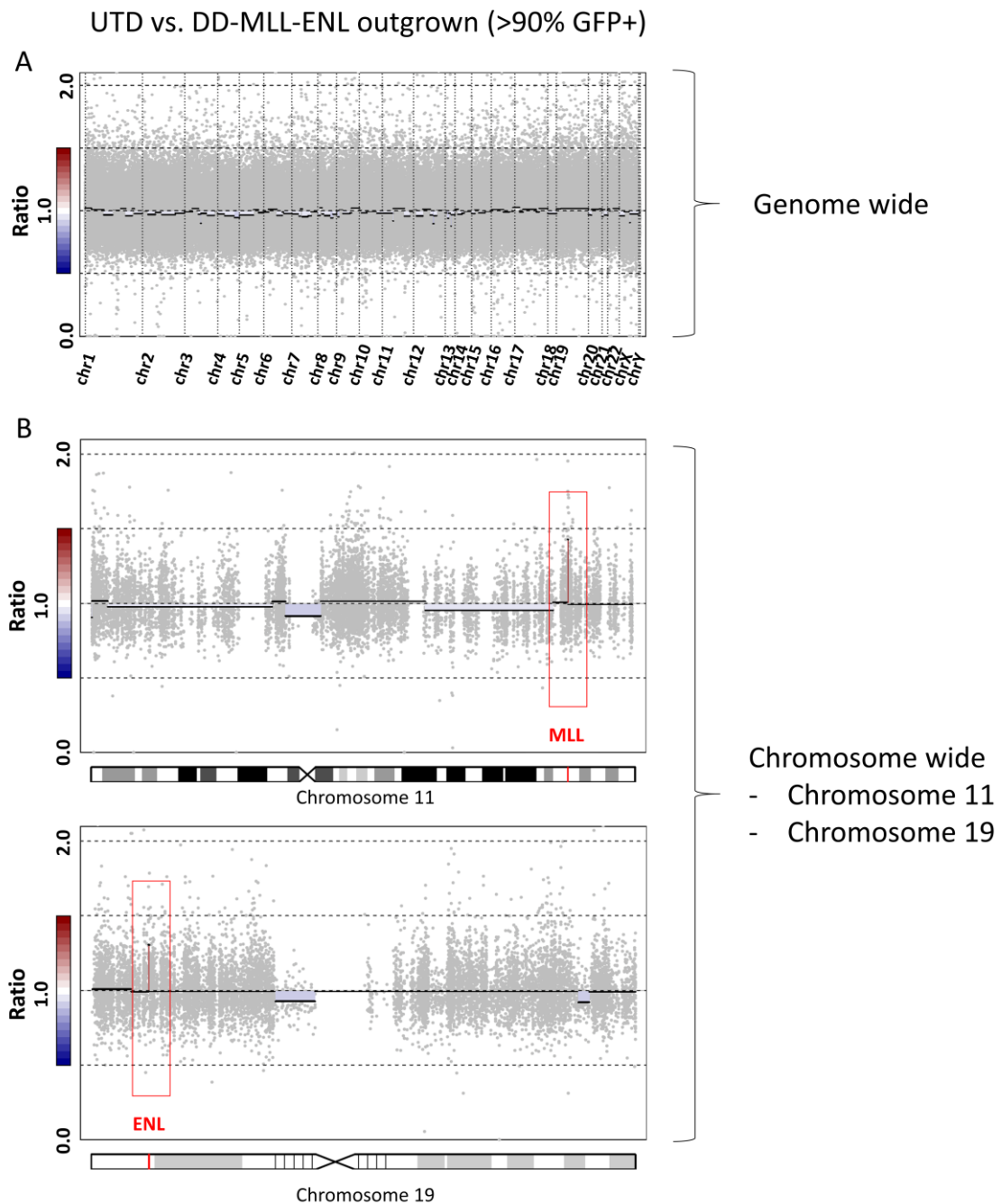


Figure 17: CNA comparison of outgrown DD-MLL-ENL progenitor cells with donor-matched untransduced HSCs.

Genomic DNA was isolated from untransduced hematopoietic stem cells (UTD) and from transduced DD-MLL-ENL cells upon outgrowth at day 40. Whole exome sequencing was performed to compare the copy number segments of both samples to identify alterations. Each grey dot indicates the ratio of an individual exon. The black horizontal lines represent segments of exons with equal copy number at the level of the corresponding ratio while red and blue lines show deviations from normal copy number status. **(A)** Genome wide CNA plot pinpointing copy number segments within each chromosome. **(B)** Chromosome wide CNA plot. Depicted are the chromosomes 11 and 19 where the genes MLL and ENL are located. Whole exome sequencing was performed in cooperation with Prof. Dr. Philipp Greif and Dr. Sebastian Vosberg from the Department of Medicine III (University Hospital, LMU Munich) and with Dr. Helmut Blum and Dr. Stefan Krebs from the Gene Center Munich (LMU Munich).

Consistent with the karyotyping results, on a genome wide scale no copy number segment changes provoked by chromosomal deletions or deviation from diploidy was observed (Figure 17A). This way an outgrowth of a subclone harboring specific alterations contributing to the proliferation was ruled out, as the whole exome sequencing was performed with already outgrown cells. When inspecting exomes of individual chromosomes, no significant changes in the copy numbers were observed. Overall, only two variances could be detected. These were found on chromosome 11 and 19 where both single genes of the fusion gene MLL-ENL are located. Highlighted with a red square, an increased ratio of the respective exon segments of MLL and ENL was detected attributed to the genomic integration of the fusion gene (Figure 17B). Whole exome sequencing was performed two times with different donors, yielding the same result.

Apart from copy number determination, the WES was mainly performed to identify genetic variants that occurred during outgrowth compared to the reference. All reads of both samples (before transduction and after outgrowth) were mapped to the human reference genome. This way, possible mutations in exons of putative driver genes could be investigated, which might contribute to enhanced proliferation. Dependent on the affected gene, it is manifested by a significant gain or loss of variant allele frequency (VAF). To narrow down the genes of interest, two comprehensive cancer gene lists covering 709 genes were used to investigate mutations within these cancer-associated genes. The detected variants were analyzed for their VAF before and after outgrowth to determine significant in- or decrease in VAF.

A total of 77 variants of 709 analyzed genes were detected, which are displayed in Figure 18. Variants being in the range of 50% or 100% refer to heterozygous and homozygous germline alleles as neither a significant increase nor a decrease of VAF was observed after outgrowth as illustrated by the proximity to the linear slope. Of note, merely a single variant was considered to hold an unambiguous gain from 0% to 20%. This variant was detected in the *KMT2A* gene encoding MLL (Figure 18). It originated from the retroviral vector integrating the N-terminal *KMT2A* sequence into the genome containing a divergent single nucleotide resulting in a lysine instead of a glutamic acid (E1282K). Thus, beside the expected MLL variant, no additional mutations in cancer-related genes were observed.

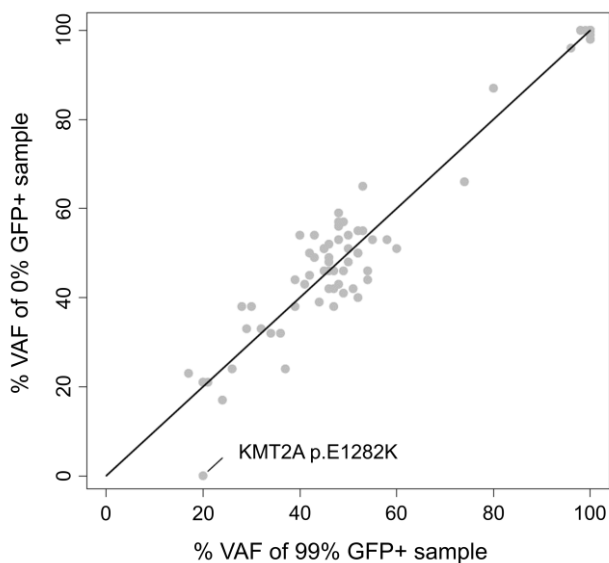


Figure 18: Allele frequency of cancer-related genetic variants prior to transduction and after complete outgrowth of DD-MLL-ENL cells.

WES reads of untransduced cells (0% GFP+), and outgrown DD-MLL-ENL-expressing cells (99% GFP+) were mapped to the hg19 human reference genome with default parameters. Sequence variants were detected within the coding region of genes included in the comprehensive cancer gene lists as targeted by either the TruSightOncology 500 Assay or the IonTorrent OncoPrint Comprehensive Assay Plus based on a VAF of 20% in any sample, a minimum coverage of 30x, and a minimum base calling quality of 20. All detected variants were analyzed for their allele frequency in both samples and plotted against each other to visualize significant gain or loss of VAF after outgrowth. Each grey dot represents an individual variant of a gene within the list.

3.2.5 Retroviral Integration Site Analysis

Genomic integration site analysis has to be performed when working with retroviral vectors able to transactivate neighboring genes. The retroviral construct is integrated into the host's genome in a semi-random manner and thereby irrevocably marks individual cells and their progeny (Kustikova et al., 2008). Integration may lead to disruption of genes impacting the clonal fitness of the transduced genes. Consequently, clonal imbalance can be evoked by insertional activation of proto-oncogenes or disruption of tumor suppressor genes. Thus, oligo- or even monoclonal outgrowth can occur over time. Identification of the genomic integration sites represents a fundamental approach to analyze the cells' clonality within a defined cell population over a course of time. For that reason, the aim was to investigate the influence of retroviral integration on the outgrowth of the transduced cells. In total, three distinct genomic DNA samples of DD-MLL-ENL cells from different transductions were analyzed after complete outgrowth at various time points via LM-PCR followed by gel electrophoresis. The LM-PCR products from genomic DNA of three freshly outgrown cells (ranging from 30 to 43 days after transduction) exposed a pattern with several dominant and minor bands indicating oligo- to polyclonality (Figure 19). No reduction to monoclonality, which could indicate growth enhancement through insertional mutagenesis was observed.

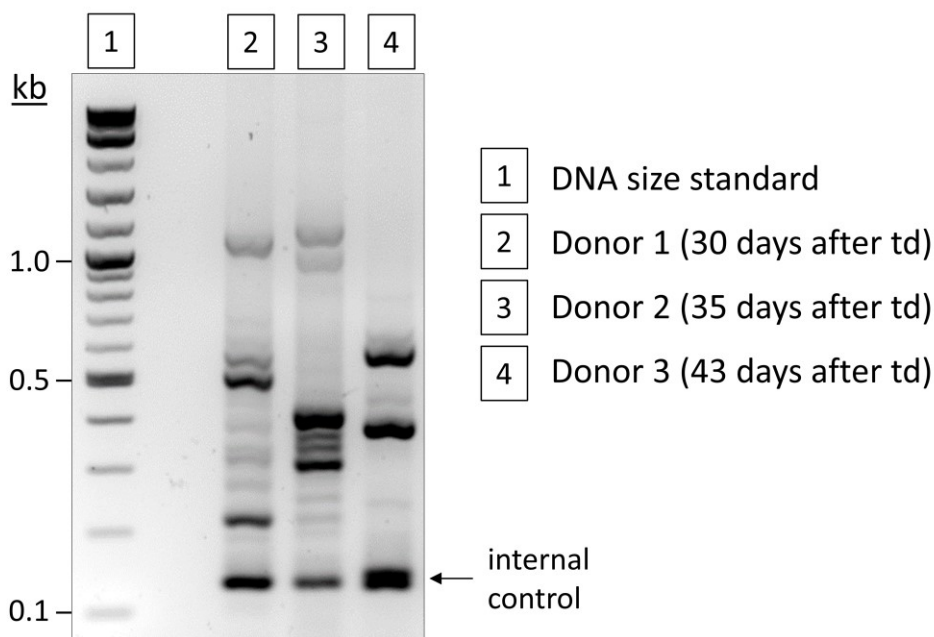


Figure 19: Agarose gel electrophoresis of amplified LM-PCR products from genomic DNA of DD-MLL-ENL cells.

Genomic DNA was isolated from DD-MLL-ENL progenitor cells after complete outgrowth and digested with the type II restriction endonuclease CviQI. After purification of the LTR-containing fragments two consecutive PCRs were performed with primers allowing amplification upstream of the 5' LTR (into the genomic DNA) as well as upstream of the 3' LTR (into the sequence of DD-MLL-ENL-IRES-GFP referred to as internal control). The amplified fragments were subsequently size-separated by agarose gel electrophoresis (2%). Each line represents a separate transduction with the given culture time while each individual band indicates a distinct integration site. The number of bands allows determination of clonality. The internal control refers to the CviQI site within the DD-MLL-ENL-IRES-GFP sequence resulting in a fragment with a size of 120 bp. In total, outgrown DD-MLL-ENL progenitor cells from three individual transductions with different CD34+ cell donors were analyzed. td, transduction.

The dominant as well as the faint bands were excised, subcloned via TOPO cloning and sequenced. The sequencing results were analyzed using the web-based BLAST basic local alignment search tool with the human genome as reference. The identified affected genes within the various insertion sites for each separate transduction are summarized in Table 23 as HUGO Gene Nomenclature Committee (HGNC) symbols.

The identification of the affected genes via sequencing confirmed the oligo- to polyclonal pattern revealed by gel electrophoresis. Collectively, nine, three and five different integration sites were determined for the three samples. For each integration site, one or two neighboring genes were found. Of note, every integration site was unique without reoccurrence in various transduction samples (Table 23). These results demonstrated the oligoclonal outgrowth of the DD-MLL-ENL expressing cells when investigating genomic DNA of outgrown cells at early time points. Accordingly, none of the detected integrations provoked clonal imbalance resulting in monoclonality.

Table 23: LM-PCR-based identification of genes affected by retroviral integration.

Independent retroviral transductions with DD-MLL-ENL			
	Donor 1	Donor 2	Donor 3
Culture time	30 days	35 days	43 days
Identified genes as HGNC symbols	<i>TRAPPC10</i> <i>LOC102724334</i>	<i>SERPINB9</i> <i>SERPINB6</i>	<i>GATM</i> <i>SPATA5L1</i>
	<i>PCBP2</i>	<i>SMG6</i>	<i>ARPIN</i> <i>ZNF710</i>
	<i>AAK1</i> <i>ANXA4</i>	<i>TMEM212</i> <i>FNDC3B</i>	<i>PALD1</i> <i>PRF1</i>
	<i>NARS1</i> <i>ATP8B1</i>	<i>LEPROTL1</i>	<i>MPPE1</i> <i>IMPA2</i>
	<i>ABCC1</i>		<i>PTGR2</i> <i>ZNF410</i>
	<i>BCAT1</i>		
	<i>GRIND1</i>		
	<i>PRDM2</i>		
	<i>RNF24</i> <i>SMOX</i>		

Excised dominant and faint bands originated from LM-PCR were subcloned into the pCR™2.1-TOPO and the pCR™II-Blunt-TOPO vector which were used for sequencing with the primer shown 2.1.4. Sequencing results were analyzed via BLAST for identification of integration sites by investigating the sequence adjacent to the 5' LTR. This way, for each integration site, separated by dashed lines, one or two genes were identified.

3.3 Differentiation of DD-MLL-ENL Myeloid Progenitor Cells

The objective of the thesis was to generate functional macrophages in an efficient way as well as in relevant numbers to be considered for cell therapy approaches. Thus, it was investigated whether the DD-MLL-ENL expanded progenitor cells are able to differentiate along the hematopoietic hierarchical paradigm in the same way as physiological monocytic precursors resulting in functional macrophages. The fundamental premise for this approach is the continuous degradation of MLL-ENL upon Shield-1 deprivation. In this context, strategies to initiate efficient terminal differentiation towards macrophages were explored. The resulting cells were characterized for their lacking proliferation capacity, their morphology, and gene expression pattern as well as functional properties including adhesion, migration and phagocytosis. Altogether, this approach constitutes a two-step procedure consisting of expansion and subsequent differentiation (Figure 20).

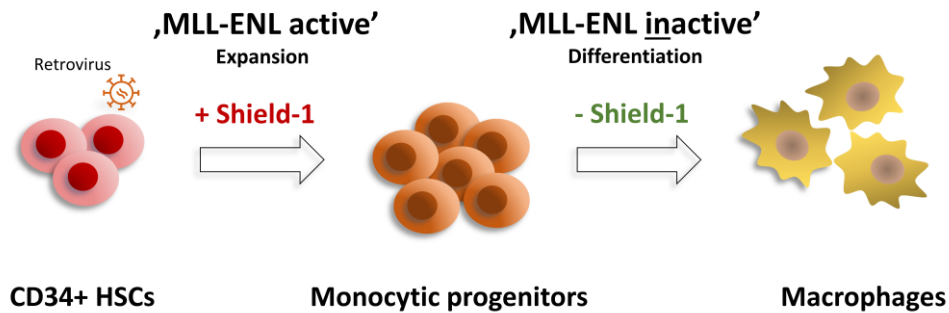


Figure 20: Graphical scheme illustrating the hypothetical two-step procedure for large-scale manufacture of human macrophages.

Retroviral transduction of hematopoietic CD34+ cells with a vector containing the DD-MLL-ENL construct allows for expansion of immature monocytic progenitor cells in the presence of the ligand Shield-1. After deprivation of the ligand, MLL-ENL gets degraded resulting in the loss of immaturity associated with monocytic differentiation.

3.3.1 Differentiation upon Shield-1 Deprivation

To initiate monocytic differentiation DD-MLL-ENL progenitor cells were cultivated in the absence of Shield-1 for up to six days and compared with cells cultivated in the presence of Shield-1. Flow cytometry analyses allowed for discrimination of cells by size and complexity via forward and side scatter. For the analysis of DD-MLL-ENL cells cultivated in the presence of Shield-1, an analysis gate was created closely encircling the major cell population with a low FSC/SSC profile that represents the cells exhibiting immature cell state. Differentiated cells featured increased cell size and granularity. In addition, to verify degradation of the protein and consequences thereof, intracellular staining against the DD domain was performed as well as a western blot of the direct MLL-ENL target *HOXA9*.

After withdrawal of Shield-1, flow cytometry analysis revealed a shift in size and granularity at day six indicating initiated differentiation. In comparison, DD-MLL-ENL cells cultivated in the presence of Shield-1 display a low FSC/SSC profile (Figure 21A). Upon Shield-1 depletion, MLL-ENL got degraded as demonstrated by the significant decrease in the fluorescence signal upon intracellular staining against the DD domain (Figure 21B). Accordingly, as MLL-ENL was not able to exert its function due to the rapid degradation, the direct target *HOXA9* was considerably downregulated on the protein level (Figure 21C). Yet, the majority of the cell population exhibited features similar to the progenitor cells cultivated with Shield-1.

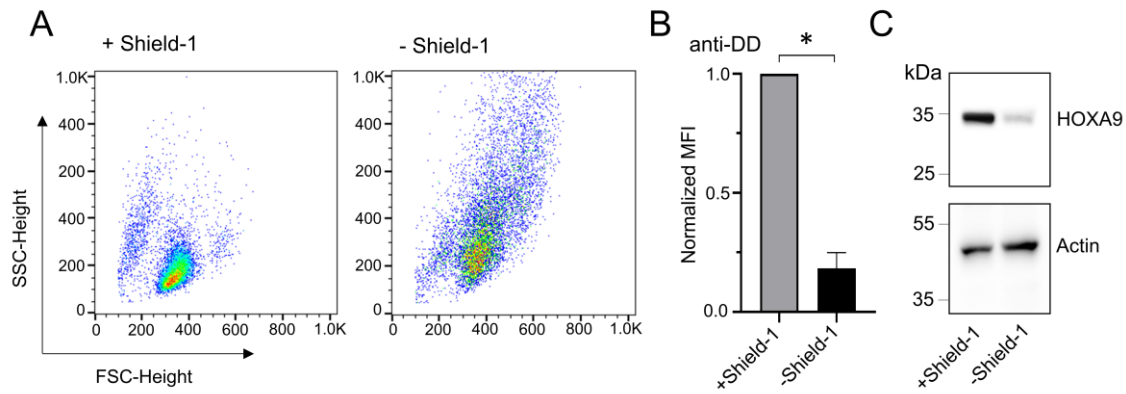


Figure 21: Flow cytometry and western blot after Shield-1 deprivation.

(A) 5×10^5 DD-MLL-ENL cells were harvested, washed with 1x PBS three times, and cultivated in CD34+ complete medium in the absence of Shield-1 for six days. A control with Shield-1 supplementation was included for comparison. At day six, both cell populations were analyzed by flow cytometry. (B) Similar to (A) two cell populations were prepared for intracellular staining. 5×10^5 cells per sample were fixed and permeabilized using the Inside Stain Kit (Miltenyi) and subsequently stained with a murine DD monoclonal antibody according to the manufacturer's recommendations. To detect the binding, a secondary anti-mouse APC-conjugated antibody was used. As a control reaction the secondary antibody was applied alone. Depicted is the mean fluorescent intensity (MFI) normalized to the +Shield-1 control. Statistical significance was calculated with a two-tailed paired t test. * $P < 0.05$. (C) Cell lysates of 2×10^6 DD-MLL-ENL cells cultivated with and without Shield-1 were prepared for western blotting. A total of 30 μ g of whole cell lysate was used for SDS-PAGE. Subsequent western blot analysis of HOXA9 and beta-actin expression was performed.

Due to proliferation-favoring cytokines (SCF, TPO, Flt3-L) in the medium, alteration of the cytokine setting was necessary to facilitate efficient and most importantly directed differentiation. IL-3 and GM-CSF among others represent cytokines associated with myeloid differentiation and are therefore examined in various differentiation compositions. In this thesis, the main focus was set on the manufacture of the pro-inflammatory macrophage M1 subtype. Correspondingly, various differentiation compositions lacking proliferation-associated cytokines but containing combinations of IL-3, GM-CSF, LPS and IFN- γ were set up and analyzed for initiating differentiation. Upon withdrawal of Shield-1, the cells were cultivated in these different media and time-dependently analyzed by flow cytometry. At each indicated time point the percentages of dead cells/debris, immature cells as well as differentiated cells were analyzed via forward and side scatter analysis.

Upon Shield-1 withdrawal, the differentiation medium containing GM-CSF in combination with LPS and IFN- γ provided the most effective differentiation with the lowest percentage of dead cells both at day 3 and day 5 and a mean percentage of > 80% of cells with shifted forward and side scatter profiles referred to as "differentiated" (Figure 22). Hence, this medium was subsequently used for the generation of differentiated cells which were characterized for macrophage-associated properties.

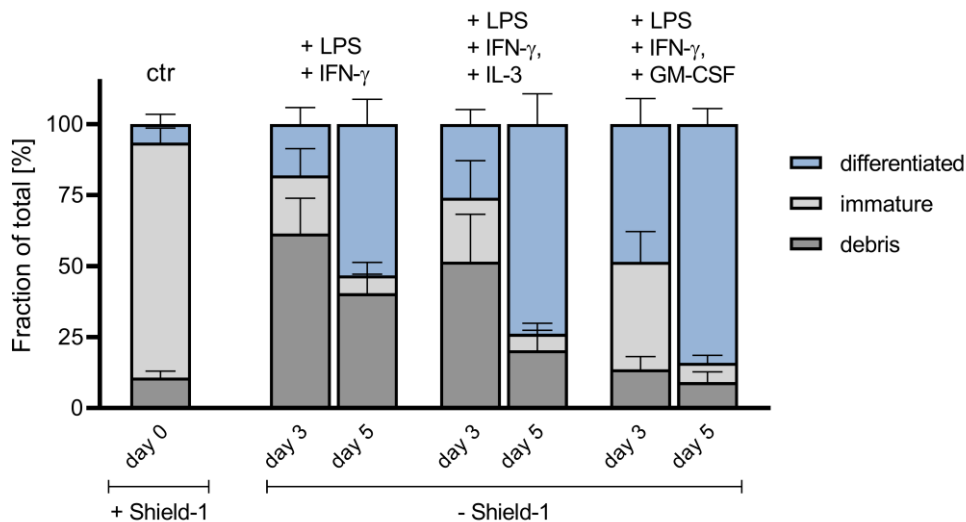


Figure 22: Flow cytometry analyses of DD-MLL-ENL cells after withdrawal of Shield-1 in different cytokine settings.

Outgrown DD-MLL-ENL progenitor cells cultivated in CD34+ complete medium (ctr) were harvested at an arbitrary time point after expansion, washed three times with 1x PBS (1,500 rpm, 5 min) and resuspended in IMDM supplemented with 10% FCS, 100 U/ml Penicillin, 100 μ g/ml Streptomycin, 2 mM L-Glutamine containing either IFN- γ (20 ng/ml) and LPS (100 ng/ml) alone or in combination with IL-3 (20 ng/ml) or GM-CSF (20 ng/ml). The cells were analyzed by flow cytometry at day 3 and 5 to determine the percentages of differentiated, immature as well as dead cells indicated by forward and side scatter profile. Depicted is a stacked bar graph with the mean percentages \pm SD of three independent transductions.

3.3.2 Macrophage Differentiation Mediated by GM-CSF, LPS and IFN- γ

Both undifferentiated cells and cells differentiated for six days in medium containing GM-CSF, LPS and IFN- γ were analyzed via flow cytometry and Pappenheim staining to determine the morphology.

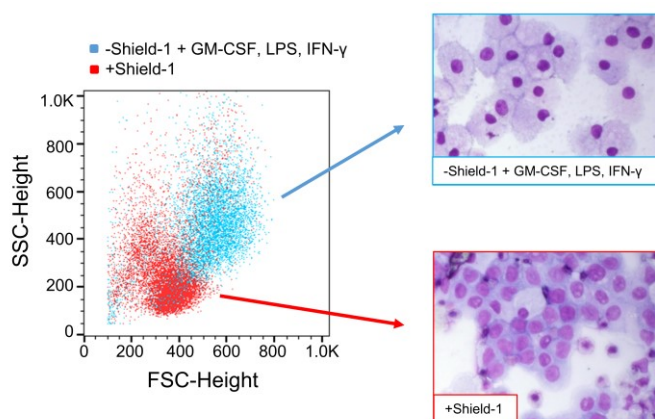


Figure 23: Morphology of DD-MLL-ENL cells prior and after a six-day differentiation.

DD-MLL-ENL progenitor cells were washed three times with 1x PBS, resuspended in differentiation medium containing GM-CSF (20 ng/ml), LPS (100 ng/ml) and IFN- γ (20 ng/ml) and cultivated on a 24-well plate at a concentration of $0.5-1.0 \times 10^6$ cells/ml for six days in the absence of Shield-1 followed by flow cytometry analysis. Depicted is an overlay of both the cell population cultivated in the presence of Shield-1 and the cells differentiated for six days. The forward (FSC) and side (SSC) scatter indicate cell size and granularity. The distinct populations were additionally analyzed for their morphology via cytospin in combination with the Pappenheim stain.

The flow cytometry analysis showed a clear separation between both populations in the FSC/SSC profile indicating efficient differentiation, which was proven by morphological analysis via microscopy. The Pappenheim staining revealed a pronounced shift in the nucleus to cytoplasm ratio, which demonstrated loss of immaturity (Turgeon, 2005). As comparison the DD-MLL-ENL cells cultivated in the presence of Shield-1 featured large nuclei with a small cell size resembling progenitor morphology (Figure 23). Additionally, differentiation duration was increased to gradually analyze further morphological changes. For this purpose, differentiation was extended to 14 days with a medium change at day seven. To verify morphological changes, the cells were analyzed by microscopy at different time points.

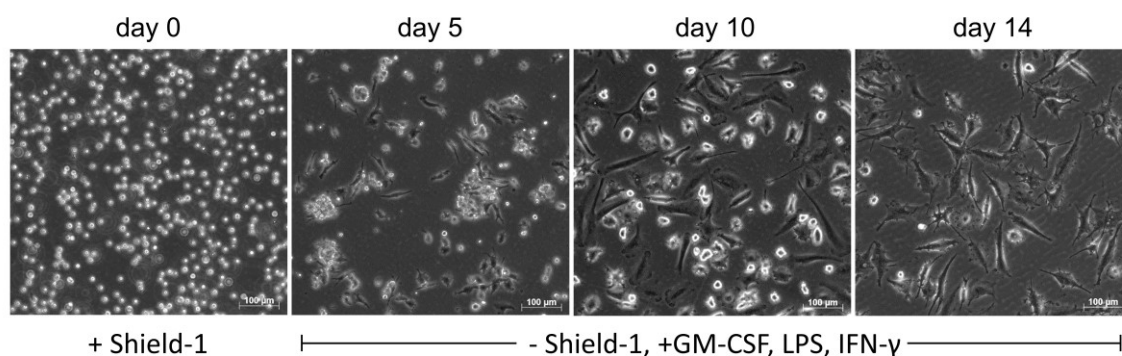


Figure 24: Differentiation progress of DD-MLL-ENL progenitor cells upon Shield-1 withdrawal and stimulation with GM-CSF, LPS and IFN- γ .

DD-MLL-ENL progenitor cells were harvested, washed three times with 1x PBS, resuspended in differentiation medium containing GM-CSF (20 ng/ml), LPS (100 ng/ml) and IFN- γ (20 ng/ml) and cultivated in cell culture flasks at a concentration of $0.5-1.0 \times 10^6$ cells/ml for 14 days. After seven days fresh medium was added. Cells' morphology was analyzed by light microscopy at day 0, 5, 10 and 14 (200x magnification).

During cultivation in medium containing GM-CSF, LPS and IFN- γ , the DD-MLL-ENL cells acquired an elongated phenotype, became adherent and increased in cell size. At day 5 initiation of differentiation was observed with formed cell clusters and scattered attached cells becoming more pronounced at day 10. At day 14, a pure population of elongated, adherent cells could be detected indicating complete differentiation towards a macrophage-like phenotype (Figure 24). Thus, for subsequent differentiation of DD-MLL-ENL progenitor cells the differentiation period was set to 14 days.

3.3.3 Analysis of Colony-Forming Capacity

To determine the colony-forming ability of Shield-1-deprived and differentiated DD-MLL-ENL cells CFU assays were performed allowing measurement of the proliferation of individual cells. Collectively, DD-MLL-ENL cells were analyzed in the presence and

absence of Shield-1 in either CD34+ complete or differentiation medium. To further scale up the possibility to obtain an infrequent clone able to sustain proliferative characteristics, larger input numbers of cells cultivated in differentiation medium in the absence of Shield-1 were investigated.

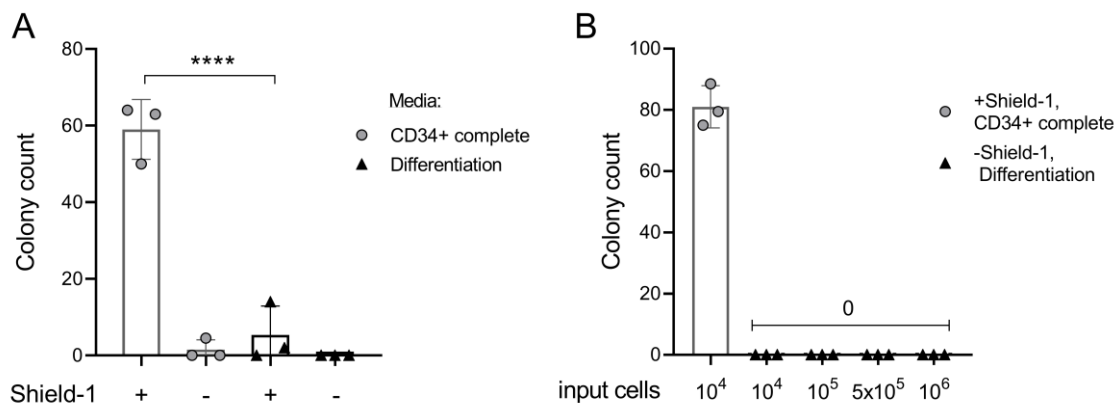


Figure 25: Colony-forming capacity of DD-MLL-ENL cells prior and upon Shield-1 deprivation and differentiation.

(A) DD-MLL-ENL were cultivated in either CD34+ complete or differentiation medium (GM-CSF, LPS, IFN- γ) \pm Shield-1 for seven days. For each sample, 1×10^4 cells were mixed with methylcellulose and transferred to a SmartDish 6-well plate followed by an incubation period of 14 days at 37 °C and 5% CO₂. Samples were analyzed for colony formation by microscopy. Data represent the mean of $n = 3$ biological replicates. Statistical significance was calculated with a two-way ANOVA with Tukey's multiple comparisons. **(B)** DD-MLL-ENL cells were deprived of Shield-1 and cultivated in differentiation medium for 14 days. Samples were prepared with different input cell numbers up to 1×10^6 cells per ml of methylcellulose. As a control DD-MLL-ENL cells + Shield-1 were included with the standard input cell number of 10^4 . Data represent the mean of $n = 3$ biological replicates. **** $P < 0.0001$.

The ability to form colonies reflects the progenitors' replicative and self-renewal character. When cultivated in the presence of Shield-1, a colony count ranging between 60 and 80 colonies per 10,000 cells could be observed. In contrast, when deprived of Shield-1 resulting in rapid degradation of MLL-ENL, cells considerably lost colony-forming abilities although cultivated in CD34+ complete medium. Of note, when cultivating the cells in differentiation medium accompanied by the removal of proliferation-favoring cytokines such as SCF or FLT3-L similar results were obtained, even in the presence of Shield-1. However, few colonies were counted in the presence of Shield-1 indicating incomplete terminal differentiation. The same applies for the sample cultivated in the absence of Shield-1 but in CD34+ complete medium (Figure 25A). Solely for cells in differentiation medium in the absence of Shield-1 not a single colony was counted, even when the initial input cell number was significantly increased up to 1×10^6 (Figure 25B). These results suggest complete terminal differentiation upon Shield-1 withdrawal and cultivation in differentiation-stimulating media.

3.4 Characterization of Differentiated DD-MLL-ENL Derived Macrophages

The obtained DD-MLL-ENL derived macrophages were deeply characterized to verify the functionality and comparability with macrophages derived from physiological monocytes. The following passages include immunophenotyping and gene expression profiling as well as functional analysis covering adhesion and migration properties and the ability to remove apoptotic cells and engulf bacterial-derived particles. Finally, the cells' capability to mediate ADCP of human lymphoma cells was evaluated.

3.4.1 Immunophenotyping

Differentiated hematopoietic cells such as macrophages display a unique expression pattern of cell surface proteins. To verify the immunophenotype, the DD-MLL-ENL differentiated cells were characterized for the expression of macrophage-, primarily M1 macrophage-associated surface proteins. The selected markers include CD11b, also known as macrophage-1 antigen (Mac-1), the pattern recognition receptor CD14, the M1 macrophage-related B7 molecules CD80 and CD86, both interacting with CD28 to modulate T cell immune function, and the M2-associated scavenger receptor CD163.

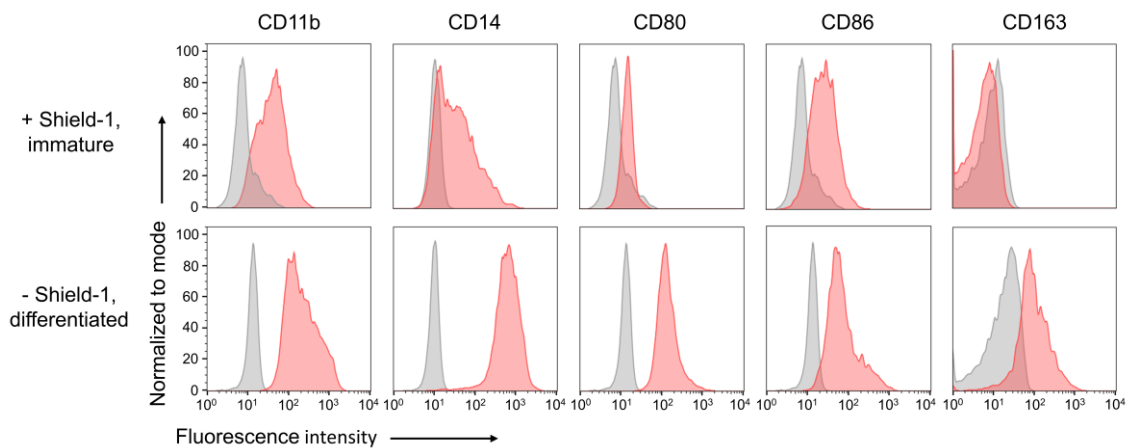


Figure 26: Immunophenotypical characterization of DD-MLL-ENL derived macrophages.

Differentiated DD-MLL-ENL derived macrophages as well as their undifferentiated counterparts were harvested and washed with 1x PBS. For each staining, 1×10^5 cells were incubated with FcR blocking reagent and the respective antibody for 45 minutes. Excess antibody was removed by washing with 1x PBS. The cells were resuspended in 1x PBS with 0.5% BSA and analyzed by flow cytometry. For each antibody, a sample with the respective isotype control was prepared. The histograms depict the fluorescence signal for each individual CD marker (red) indicating the expression in comparison with the isotype control (gray). The illustrated analysis is representative of three independent experiments.

When compared to their immature counterparts, macrophages upregulated individual cell surface markers. Both common macrophage-associated markers CD11b and CD14 showed an increased expression by the differentiated DD-MLL-ENL cells. When investigating the expression of M1 macrophage-associated markers, strong upregulation of CD80 could be assessed while only a slight shift was observed for CD86 expression. Additionally, the differentiated macrophages upregulated the M2 macrophage-associated marker CD163 completely absent on undifferentiated cells (Figure 26). Thus, the expression pattern revealed a mixed M1/M2 immunophenotype for the differentiated DD-MLL-ENL derived macrophages. Furthermore, according to the progenitors' immunophenotype the differentiated cells were absent for markers characteristic of T and B cells (data not shown).

Beside the depicted macrophage markers, further analysis of immune response-associated surface proteins was conducted. Expression of major histocompatibility complex (MHC) class I and II antigens, in human also known as human leukocyte antigen (HLA) system, was determined. These genes comprise classical HLA-A, -B, -C (MHC class I complex) and HLA-DP, -DQ, -DR (MHC class II complex) molecules. Additionally, expression of Fcγ receptor (FcγR) family members crucial for orchestrating phagocytosis of opsonized microbes and cells was determined on the differentiated macrophages. These include FcγRI (CD64), FcγRII (CD32) and FcγRIII (CD16). Specifically, for CD32, involved in cellular response regulation such as phagocytosis or induction of cytokine secretion (Anania et al., 2019), particular expression of the isoform CD32A (activating) and CD32B (inhibitory) was investigated .

The staining analyses revealed expression of CD16, CD32 and CD64 on the differentiated macrophages. CD32 displayed the most pronounced expression within the FcγR family followed by CD64. For CD16 only a minor shift in the fluorescence signal intensity reflecting low protein expression was observed (Figure 27A). Scrutinizing the CD32 isoform expression disclosed a significant difference between the isoform CD32A and the isoforms CD32B/C. Although the antibody was not able to discriminate between CD32B and CD32C, a strong and distinct expression of the activating CD32A was determined (Figure 27A). Additionally, surface expression of HLA-A, -B, -C corresponding to MHC class I as well as HLA- DP, -DQ, -DR (MHC class II) was significantly upregulated upon macrophage differentiation. In particular, upregulation of the MHC class II antigens, mainly expressed on professional APCs, was more pronounced with a mean MFI of over 8000 in comparison to 1100 prior to differentiation (Figure 27B).

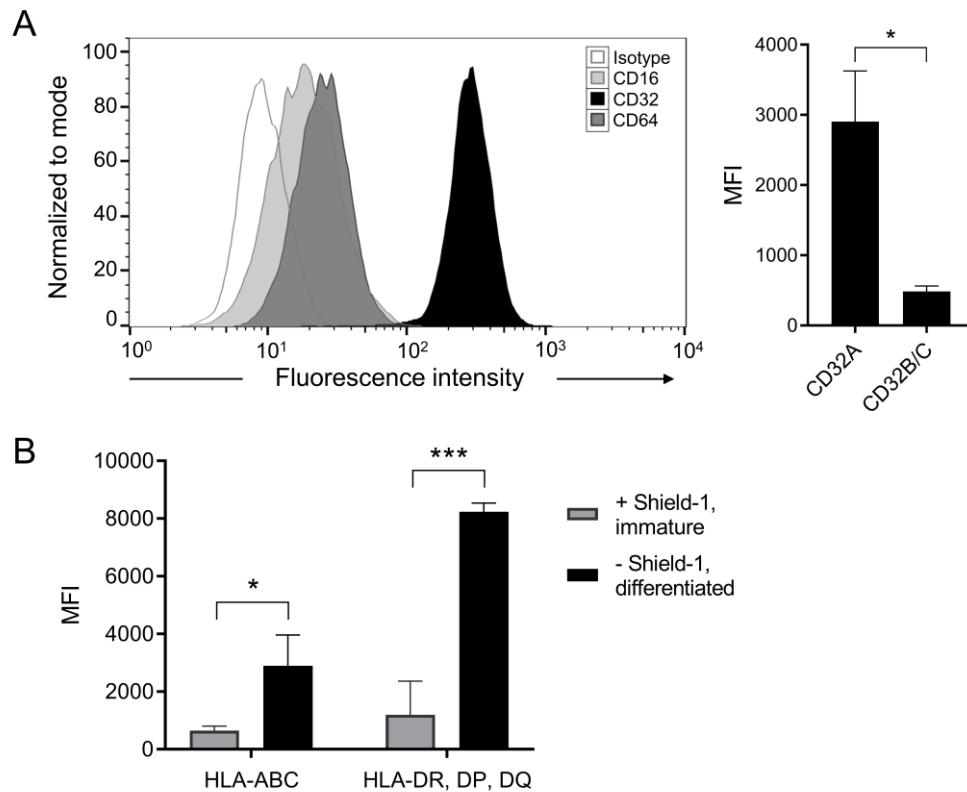


Figure 27: Analysis of Fc γ receptor and MHC class I and II surface expression on DD-MLL-ENL derived macrophages.

(A) For each CD marker staining, 1×10^5 differentiated DD-MLL-ENL derived macrophages were resuspended in 1x PBS with 0.5% BSA and incubated with FcR blocking reagent and the respective antibody for 45 minutes. Excess antibody was removed by washing with 1x PBS. The cells were resuspended in 1x PBS with 0.5% BSA and analyzed by flow cytometry. A sample with the respective isotype control was included. The histogram represents the fluorescence intensity for each Fc γ receptor. Fc γ receptor II (CD32) was further analyzed for its respective isoform expression. Statistical significance was calculated with a two-tailed paired t test and data represent the mean MFI \pm SD of $n = 3$ biological replicates. **(B)** According to (A) DD-MLL-ENL derived macrophages and their undifferentiated counterparts were prepared for staining. Statistical significance was calculated with multiple t tests and data represent the mean MFI \pm SD of $n = 3$ biological replicates after background subtraction of the isotype control. P values were corrected with the false discovery approach by Benjamini, Krieger and Yekutieli. For all panels, $*P < 0.05$; $***P < 0.001$.

3.4.2 Gene Expression Profiling

Beside the analysis of surface protein expression, gene expression profiling on mRNA level was conducted to gain insights into differences between the progenitor cells and the differentiated macrophages. Furthermore, similarities between the DD-MLL-ENL derived macrophages and unmodified monocytes from peripheral blood of healthy donors were scrutinized. As macrophages were the cell type of interest, the focus was set on immunity-associated genes. Hence, inflammatory genes as well as myeloid innate immunity-related genes were investigated.

3.4.2.1 Expression of Inflammatory Genes

In a first approach inflammatory genes classified as either M1 or M2 macrophage signatures were analyzed by qPCR. As cell surface antigen expression analysis revealed the presence of M1 as well as M2 markers, inflammatory genes connected to both subtypes were investigated. These include the pro-inflammatory, M1 subtype-associated TNF α and IL-6, and the anti-inflammatory, M2 subtype-associated IL-10. Additionally, expression of CCL2, CCL17 and CCL22, members of the CC chemokine ligand subgroup, were analyzed. Moreover, expression of iNOS and ARG1 was investigated to discriminate between M1 and M2 subtype. These distinct genes were analyzed in DD-MLL-ENL progenitor cells and differentiated macrophages.

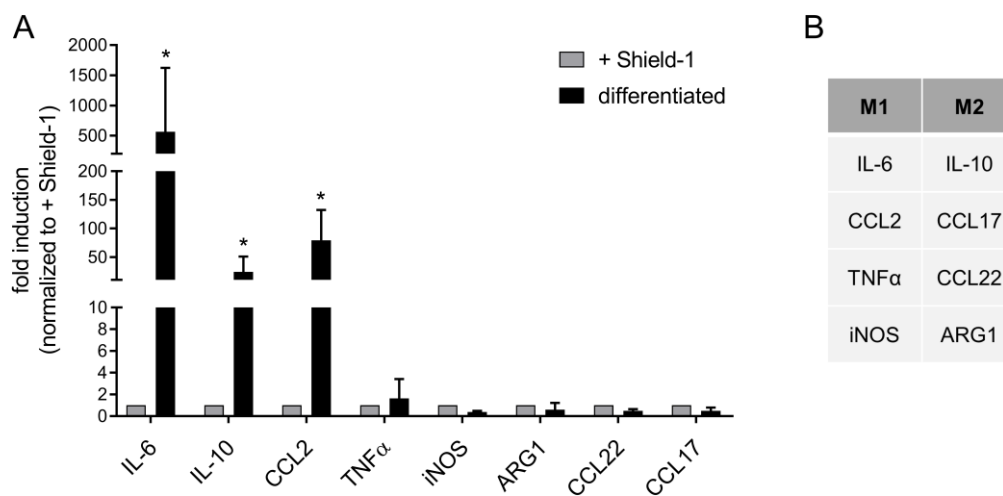


Figure 28: qPCR analysis for mRNA expression of inflammatory genes.

(A) Differentiated DD-MLL-ENL cells were harvested for RNA isolation together with the cognate undifferentiated counterparts (+ Shield-1). qPCR was performed according with the primers listed in 2.1.4. Fold induction in reference to the undifferentiated DD-MLL-ENL control group was calculated by the $2^{-\Delta\Delta C_t}$ method with Actin as reference gene. Data are represented as means \pm SD of three independent experiments using cells from different transductions. Statistical significance was calculated with a two-tailed Mann-Whitney U test. $*P < 0.05$. **(B)** Tabular overview of the investigated genes assigned to either M1 or M2 macrophage subtype. The qPCR analysis was performed in cooperation with Dr. Adrian Hoffmann and Prof. Dr. Jürgen Bernhagen at the Institute for Stroke and Dementia Research (University Hospital, LMU Munich).

The most prominent upregulation upon differentiation and polarization using LPS and IFN- γ was observed for the pro-inflammatory IL-6 with a massive 500-fold increase with respect to the undifferentiated DD-MLL-ENL + Shield-1 control. Expression of IL-10 and CCL2 was significantly upregulated as well as demonstrated by a 24- and 80-fold increase, respectively. In contrast, no significant changes in expression were determined for TNF α , iNOS, ARG1, CCL22 and CCL17 (Figure 28A). In respect to the delineated macrophage subtypes, the expression analysis revealed M1 and M2 features for the DD-MLL-ENL derived macrophages with pro- as well as anti-inflammatory cytokine expression (Figure 28B).

3.4.2.2 Expression of Innate Immunity-Related Genes

As macrophages represent a myeloid cell population, which is part of the innate immune system and coordinates immune defense mechanisms, an in-depth expression analysis of myeloid innate immunity-related genes was accomplished. For this purpose, the nCounter® platform (NanoString Technologies, WA, USA) was employed enabling multiplex analysis of up to 800 targets. As a pre-defined target set, the nCounter® Myeloid Innate Immunity Panel covering a total of 730 innate immune response genes was utilized. Along the lines of the qPCR analysis, mRNA was used to determine the individual expression levels. To characterize both the DD-MLL-ENL progenitor cells and the differentiated macrophages via gene expression profiling suitable control cell types were included. Hence, untransduced CD34+ HSPCs and PBMC-derived CD14+ monocytes were included. The untransduced CD34+ HSPCs were pre-stimulated in CD34+ complete medium for three days after thawing to induce cell division. Three biological replicates from different donors were used for each group. For robust comparability prior and after differentiation, each differentiated macrophage sample originated from the DD-MLL-ENL progenitor sample included in this analysis. After obtaining the raw expression levels of every single gene for each sample, a two-step normalization consisting of housekeeping genes and positive controls was performed for comparison. The following passage details the analyses including comparison of all four cell types as well as discrete comparison of two selected cell types in terms of proliferation, migration and immunity-related gene subsets involving macrophage-associated gene clusters.

First, normalized expression of all genes was analyzed for each sample to overview differences as well as similarities between the given cell types in an exploratory manner. For this purpose, a heatmap was generated, which illustrates the expression level of each gene for each sample as log₂ normalized expression.

Plotting the normalized expression levels on a heatmap revealed obvious differences and similarities between the different sample groups. Both DD + Shield-1 and CD34+ HSPCs held a discernibly alike signature with only a couple of clusters differing. On the other side, comparison of CD14+ monocytes with the DD macrophages unveiled both similar and diverse gene clusters likewise. Of note, expression levels of the majority of the analyzed 730 innate immunity-related genes were considerably higher in the mature CD14+ monocytes and DD macrophages compared to both undifferentiated cell types. Overall, within each sample group only minor deviation between the three biological replicates were identified (Figure 29).

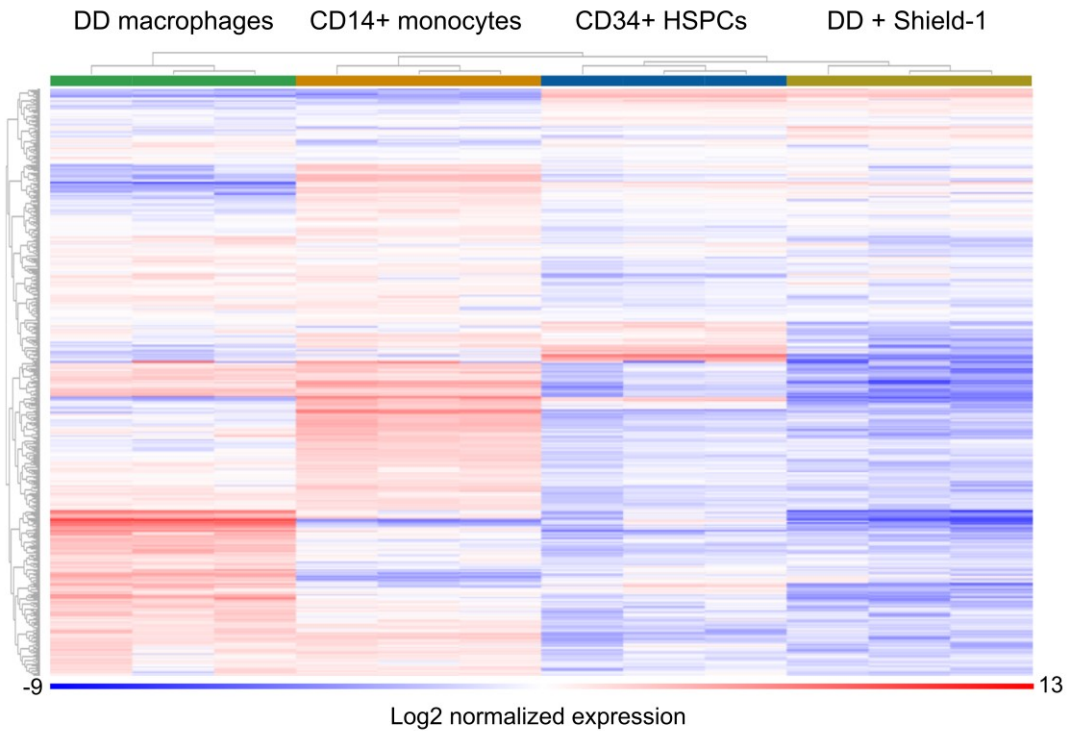


Figure 29: mRNA expression levels of 730 innate immunity-related genes in the four different cell types.

mRNA was isolated from untransduced CD34+ hematopoietic stem and progenitor cells (CD34+ HSPCs), DD-MLL-ENL progenitor cells (DD + Shield-1), thereof derived macrophages (DD macrophages) and PBMC-derived CD14+ monocytes (CD14+ monocytes) from three different donors per group. After the nCounter multiplex analysis, raw expression levels were normalized to housekeeping genes and positive controls and subsequently displayed as log₂ values in a heatmap format using ROSALIND software (ROSALIND, Inc., San Diego, CA, USA).

Next, these differences in gene expression were scrutinized in detail. To start with, advanced analysis using the cell type profiling module was performed via the nCounter® Advanced Analysis Software tool. This software allows to determine the abundance of diverse cell populations by clustering specific marker genes which serve as reference and are stably expressed in the respective cell type. The closer the expression of these signature genes in the given samples are to the reference, the higher the calculated score. This method was described by Danaher and colleagues (Danaher et al., 2017). Accordingly, the abundance scores were calculated. As cell type of interest “macrophages” was selected.

The DD-MLL-ENL macrophages displayed the highest macrophage abundance score with approximately 13.5 implying most similar gene expression to the predefined macrophage cell type reference. The second highest score was determined for the CD14+ monocytes, which naturally differentiate into macrophages. In contrast, the undifferentiated DD-MLL-ENL progenitor cells represent the group with the lowest score (Figure 30). This result provided evidence of actually manufacturing macrophages

derived from DD-MLL-ENL progenitor cells. The differentiated cells' macrophage-like character had to be further scrutinized in terms of analysis of gene subsets as well as discovery of significant differences on individual gene scale upon differentiation.

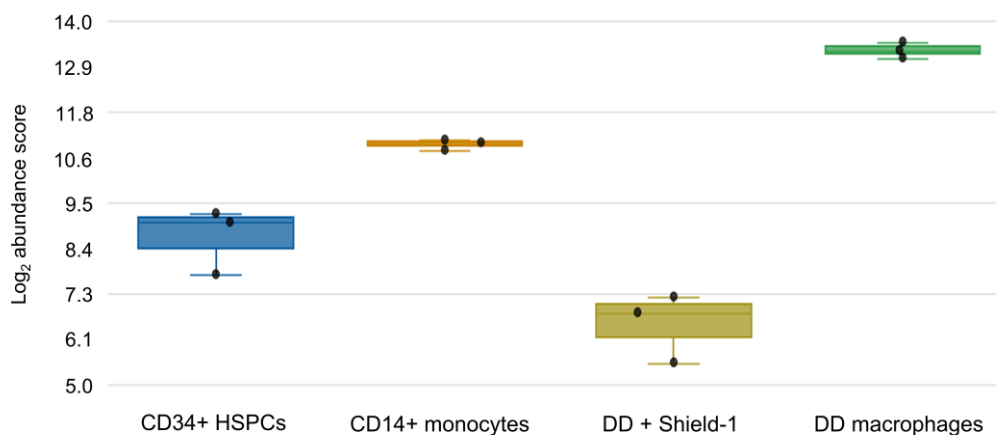


Figure 30: Analysis of the macrophage abundance score by cell type profiling based on specific gene expression.

Via analyzing the expression levels of the 730 analyzed genes, a gene subset specific for the macrophage cell type was selected by default and referred to reference values representing the ideal cell type. Filtering was performed to include result with p-values ≥ 0.05 with a p-value adjustment using the Benjamini-Hochberg method of estimating false discovery rates. Depicted is a box plot for each analyzed sample group with values portrayed as \log_2 generated using the ROSALIND software (ROSALIND, Inc., San Diego, CA, USA).

To determine which genes are expressed at different levels between the annotated cell types, differential expression analysis was performed. This method compares the expression levels between two chosen sample groups. Thus, an overview of specific targets that exhibit significantly in- or decreased expression in response to the selected covariate can be obtained. For visualization a volcano plot for each selected pair was generated depicting each target gene's $-\log_{10}$ (p-value) and \log_2 fold change compared to the chosen covariate.

The volcano plots depicted in Figure 31 identified genes, which displayed significantly increased or decreased expression in response to the selected covariate. Highly statistically significant targets are located at the top of the plot while highly differentially expressed genes fall to either side depending on up- or downregulation. When compared to CD34+ HSPCs expression, both significant up- and downregulation of individual genes could be spotted for DD + Shield-1, DD macrophages as well as for CD14+ monocytes. The DD + Shield-1 sample group shared the most similarity to the CD34+ HSPCs with a total of 121 genes differentially expressed genes whereof merely 29 genes were significantly upregulated. Both differentiated cell types consisting of DD macrophages and CD14+ monocytes exhibit more explicit differences in terms of expression levels when compared with the CD34+ HSPCs. The DD macrophage sample

group held 216 differentially expressed genes with the majority of 142 genes being upregulated. These results were even more pronounced for the CD14+ monocyte group with an overall count of 274 genes exhibiting a statistically significant difference in expression whereof 220 genes are upregulated. Moreover, comparable to the CD34+ HSPCs covariate, DD macrophages showed a similar differential expression profile when the DD + Shield-1 sample group was selected as a reference with 273 genes being differentially expressed (201 genes upregulated, 72 genes downregulated). Moreover, DD macrophages and the CD14+ monocytes displayed a similar profile when compared to CD34+ HSPCs (Figure 31). As these findings revealed both similarities and significant differences of individual gene expression between the given samples subsequent in-depth analysis was performed regarding the affected genes and their immunity-associated function.

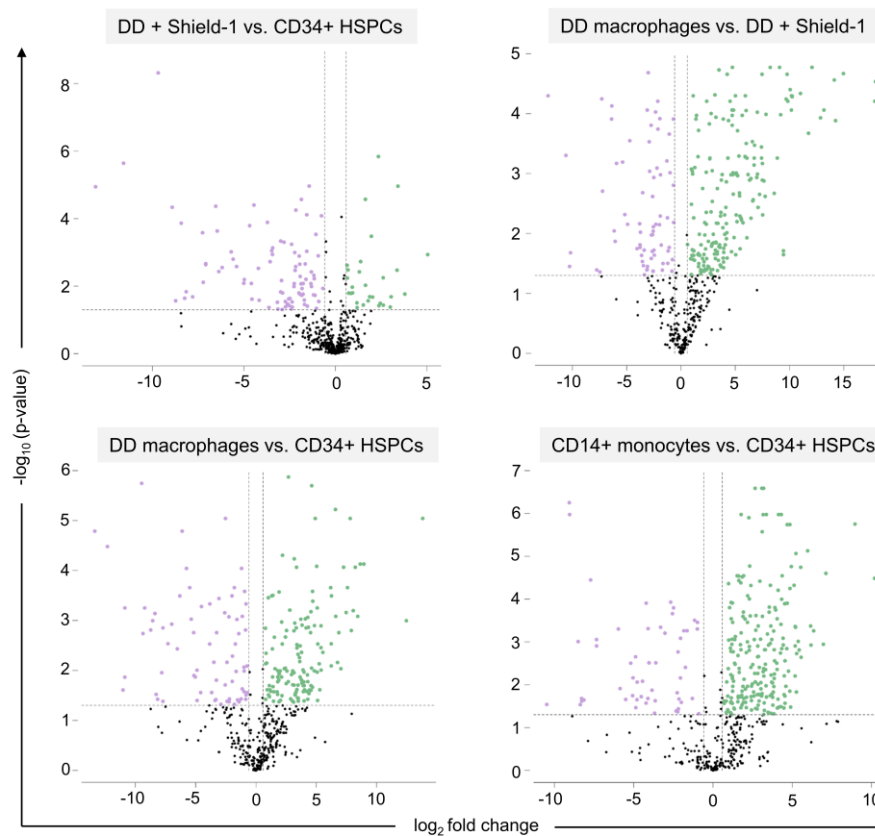


Figure 31. Gene expression volcano plots of sample groups versus annotated reference. Differential gene expression was analyzed by comparing two sample groups with each other based on normalized expression levels of each gene. Each sample group (DD + Shield-1, DD macrophages and CD14+ monocytes) were plotted against CD34+ HSPC expression levels with an additional plot comparing DD macrophages with the undifferentiated counterpart (DD + Shield-1). The volcano plots display the significance in form of $-\log_{10}(\text{p-value})$ on the y axis while differentially expressed genes fall along the x axis as \log_2 fold change dependent on upregulation (positive values) or downregulation (negative values). The plots were generated using the ROSALIND software with the criteria for differentially expressed genes set at a $\geq 1.5 \log_2$ fold change threshold for upregulation and $\leq -1.5 \log_2$ fold change for downregulation with an adjusted p-value of ≤ 0.05 . Green dots represent significant differentially upregulated genes in respect to the given reference, while purple dots are associated with downregulation likewise.

Operating various immunity-related signaling pathways like Fc receptor signaling, antigen presentation or chemokine and cytokine signaling is a crucial hallmark of functional macrophages. To detect changes in the regulation within each defined pathway and group, the differentially expressed genes were clustered and analyzed for up- or downregulation in each cell type. This way, the sample sets DD + Shield-1, DD macrophages and CD14+ monocytes were compared with each other relative to baseline expression in untransduced CD34+ HSPCs resulting in a directed global significance score heatmap. The data generated by differential expression analysis shown in Figure 31 was used for this gene set analysis.

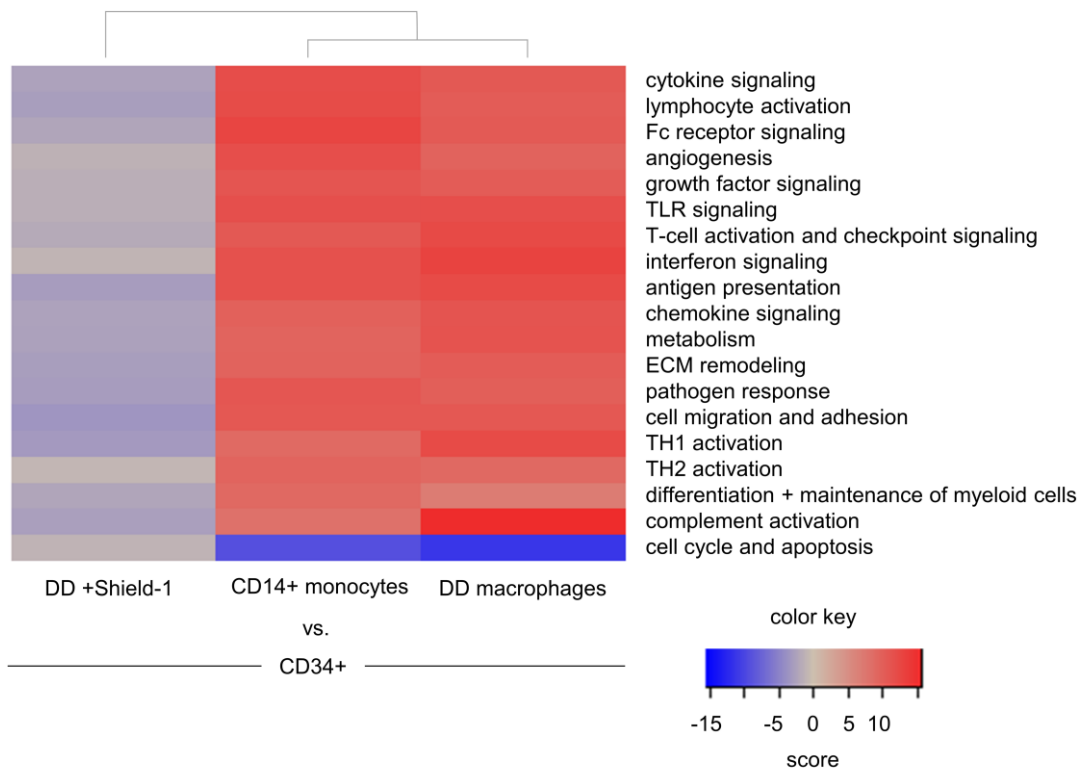


Figure 32: Directed global significance score of innate immunity-related gene subsets in the analyzed sample groups.

The 730 analyzed genes were categorized into immunity-related subsets. Differential expression analysis calculated a t-statistic for each individual gene against the covariate (CD34+ cells). The directed global significance score was determined as the square root of the mean squared t-statistics of the genes while taking the sign of the t-statistics into account. Depicted is a heatmap with the individual scores for each gene cluster generated by the nCounter advanced analysis 2.0 software. The scores illustrate the tendency to have over- or underexpressed genes within the given subset relative to the baseline expression in CD34+ HSPCs. Positive values represent overexpression, negative values represent downregulation. TLR, toll-like receptor; ECM, extracellular matrix; TH, T helper cell.

When compared to CD34+ baseline expression, a clear upregulation of innate immunity-associated gene subsets in DD macrophages as highlighted by a high directed global significance score could be detected similar to the expression pattern in CD14+ monocyte with the exception of the cell cycle and apoptosis category. Genes of these

two categories were strongly downregulated in CD14+ monocytes and DD macrophages. By contrast, DD + Shield-1 samples displayed an expression pattern similar to the CD34+ control as indicated by a score ranging close to zero with only a slight downregulation in some subsets (Figure 32). In conclusion, the DD macrophages upregulate innate immunity related genes crucial for various pathways characteristic of macrophages.

The above-mentioned gene subsets were further analyzed at single gene level to accentuate differences in expression levels of central targets between the annotated cell types. To start with, four highly induced cell cycle-associated genes in DD + Shield-1 cells were selected as core proliferation genes and analyzed regarding pronounced downregulation after differentiation into DD macrophages. These genes included *BIRC5* (Survivin), *TOP2A*, *CCNB2* and *MYC*.

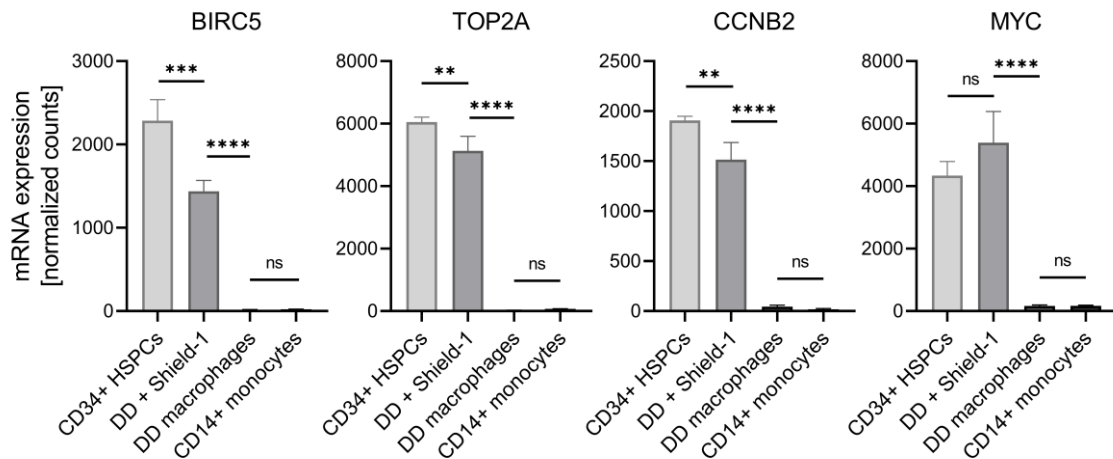


Figure 33: mRNA expression levels of core proliferation genes.

Four highly induced cell cycle-associated genes in DD + Shield-1 cells were selected and analyzed for their expression in all sample groups. The counts represent the mean mRNA level \pm SD after normalization with housekeeping genes as well as positive and negative control genes. Statistical significance was calculated with a one-way ANOVA with Tukey's multiple comparison tests. Ns, not significant; ** $P < 0.01$; **** $P < 0.0001$.

All four analyzed core proliferation genes (*BIRC5*, *TOP2A*, *CCNB2* and *MYC*) were considerably downregulated after differentiation. For each gene, both DD macrophages and CD14+ monocytes showed a similarly low count reflecting absent to little expression. In contrast, investigation of the CD34+ HSPCs and DD + Shield-1 samples revealed high counts. In particular, *TOP2A* and *MYC* were highly expressed with counts ranging between 4000 and 6000 (Figure 33). Hence, absence of these proliferation-associated genes in the DD macrophages samples further suggests terminal differentiation with a complete loss of proliferation capacity.

Additionally, upregulated innate immunity-related key pathways in macrophages were investigated at the single gene level. These pathways include chemokine signaling, Fc receptor signaling, antigen presentation and toll-like receptor signaling.

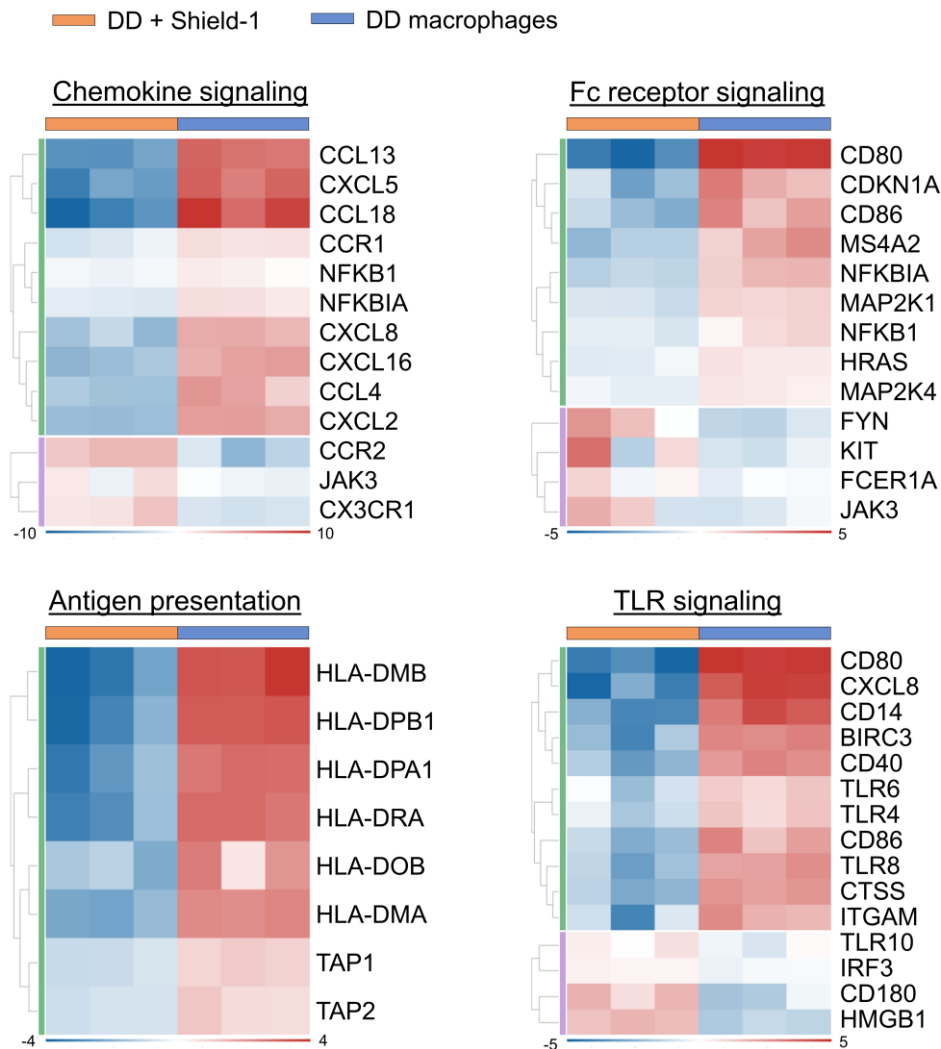


Figure 34: Heatmaps of differentially expressed genes involved in selected immunity-related pathways.

Differential expression analysis between the DD + Shield-1 sample group and the DD macrophage group was performed using ROSALIND software based on the normalized gene expression. Selected genes which are differentially expressed between those two groups were clustered into immunity-related pathways. The individual genes of overall four selected pathways consisting of chemokine signaling, Fc receptor signaling, antigen presentation and TLR signaling are shown in separate heatmaps. Average log₂ normalized expression of all six samples was calculated for each gene individually to allow deviation thereof. Expression differences compared to the average are illustrated by positive values marked in red while lower expression is shown in blue (negative values).

When comparing DD + Shield-1 samples with the DD macrophages concerning differentially expressed genes within selected immunity-related pathways, a significant upregulation of the corresponding genes was observed consistent with the clustered overview depicted in Figure 32. A pronounced expression of C-C and C-X-C motif

chemokines such as CCL4, CCL13, CXCL5 and CXCL8 was determined for DD macrophages. In addition, as illustrated, one of the chemokine receptors, CCR1, was upregulated upon differentiation.

Apart from the demonstrated surface expression of Fc γ receptors (Figure 27), differential expression analysis revealed upregulation of Fc receptor signaling-associated genes. These include members of the mitogen-activated protein kinase family, such as MAP2K1 and MAP2K4 involved in downstream signaling resulting in the orchestration of immune response-related functions including antibody-dependent cellular cytotoxicity and phagocytosis (Rosales, 2017, Ben Mkaddem et al., 2019). Moreover, cellular activation by Fc γ receptor signaling is linked with an upregulation of costimulatory molecules like CD80 and CD86 (Junker et al., 2020). Accordingly, both genes were found upregulated in the DD macrophage samples.

HLA class II proteins mediate antigen presentation of peptides derived from extracellular proteins thereby initiating immune responses. Gene expression analysis revealed upregulation of members of the HLA class II family in concordance with the immunophenotyping depicted in Figure 27. Furthermore, transporter associated with antigen processing 1 (TAP1) as well as antigen peptide transporter 2 (TAP2) critical for engaging translocation of cytosolic peptides to the endoplasmic reticulum to be bound to MHC molecules were significantly higher expressed in the differentiated cells (Seyffer and Tampe, 2015).

As toll-like receptors (TLR) play a pivotal role for macrophage-mediated innate immune responses against microbial pathogens as well as instructing adaptive immune responses these signaling pathways were investigated (Barton and Medzhitov, 2003). Differential expression analysis pointed out upregulation of various TLRs such as TLR4, TLR6 and TLR8 while solely TLR10 seemed to be downregulated following differentiation. Of note, in accordance with the Fc receptor signaling heatmap CD80 was found to be strongly upregulated within the TLR signaling pathway upon differentiation (Figure 34).

These findings suggest that the DD-MLL-ENL derived macrophages are able to orchestrate common innate immunity-related immune responses. Hence, functional assays verifying adhesion and migration properties towards a chemokine gradient were conducted. Moreover, phagocytosis approaches including uptake of bacterial particles mediated by TLRs and antibody-dependent cellular phagocytosis of lymphoma and leukemia target cells were performed as described in the following parts.

3.4.3 Functional Characteristics of Differentiated DD-MLL-ENL Macrophages

After verifying a macrophage-associated immunophenotype and demonstrating expression of innate immunity-related genes, *in vitro* assays were performed to prove functionality of the manufactured DD-MLL-ENL derived macrophages. Thus, adhesion and migration properties were scrutinized in addition to phagocytic capacities. The latter include uptake of *E. coli* derived particles, clearance of apoptotic and dead cells and engulfment of opsonized lymphoma cell lines as well as patient-derived mantle cell lymphoma (MCL) and chronic lymphocytic leukemia (CLL) cells.

3.4.3.1 Adhesion under Shear Stress

A decisive feature of monocyte-derived macrophages is their ability to adhere to endothelial cells initiating trafficking (Geissmann et al., 2010). The cell-cell interaction is primarily provided by binding of Integrin $A_4\beta_1$, known as very late antigen-4 (VLA4) expressed on monocytes to vascular cell adhesion molecule 1 (VCAM-1) on the endothelial cells under shear stress elicited by blood flow. This so-called endothelial wall shear stress ranges between 10 – 20 dynes/cm² correlating with 1-2 Pa (Roux et al., 2020). To evaluate the capacity of the DD-MLL-ENL derived macrophages to adhere to VCAM-1 under shear stress a flow chamber assay mimicking the *in vivo* blood flow was performed. This way binding to VCAM-1 could be determined at different, increasing flow speeds.

Analysis of adhesion properties using the flow chamber assay revealed effective binding to VCAM-1 even under a shear stress of physiological 15 dynes/cm². As verified by microscopy, approximately one third of the initially adherent macrophages retained bound upon applying the maximum flow speed when using slides coated with VCAM-1. In contrast, on uncoated slides almost all macrophages are rapidly washed away under minimal shear stress of 2 dynes/cm² not being able to adhere to the untreated plastic surface within the given incubation time (Figure 35B). At the highest shear stress of 15 dynes/cm² no adherent macrophage was detected as verified by microscopy (Figure 35A). These results demonstrate specific and intense binding of the DD-MLL-ENL macrophages to VCAM-1 defying blood flow equivalent shear stress.

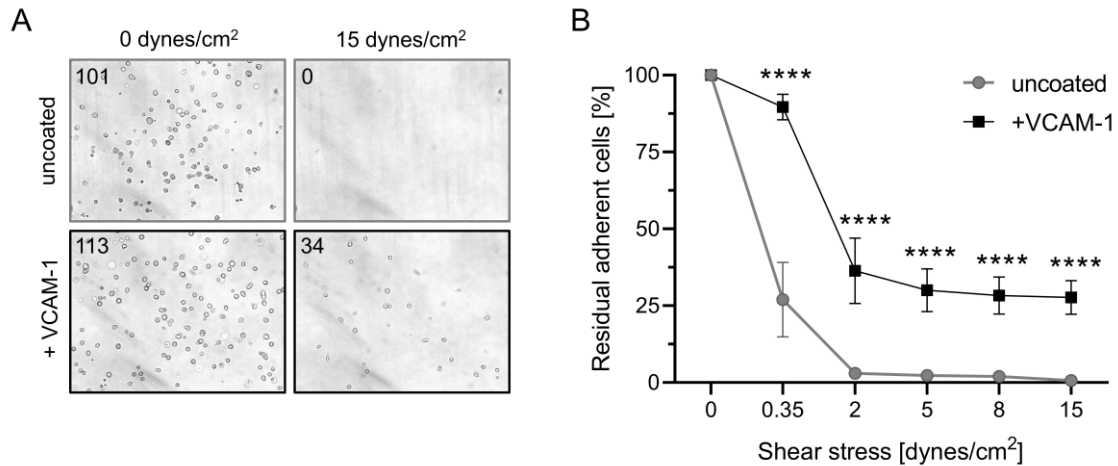


Figure 35: Adhesion properties of DD-MLL-ENL derived macrophages under shear stress. (A) FCS and cytokine overnight-starved DD-MLL-ENL derived macrophages were harvested and resuspended in HBSS + 1% BSA. A μ -slide VI 0.4 was either coated with VCAM-1 (2 μ g/ml) for 30 minutes or left uncoated as control. The cell suspension was transferred to the slide and allowed to adhere by incubating at room temperature for 5 minutes. Increasing flow speeds were applied pumping HBSS buffer through the channel. Images were taken after 30 seconds of each flow speed to analyze the number of adherent cells. The images before applying shear stress (0 dynes/cm²) and after the highest flow speed (15 dynes/cm²) are shown including the number of adherent cells displayed at the upper left corner. (B) Percentages of initially adherent cells were calculated by determining the number of cells after each flow speed. Statistical significance was calculated with a two-way ANOVA with Sidak's multiple comparison tests. Data represent the mean \pm SD of $n = 3$ biological replicates. **** $P < 0.0001$.

3.4.3.2 Chemokine-Guided Migration

Recruitment of macrophages to the site of inflammation or damaged tissue is mediated by chemoattractant cytokines, known as chemokines. This so-called chemotaxis is a critical prerequisite for efficient homing of the macrophages to mediate immune response-related functions (Xuan et al., 2015). Among these chemokines the monocyte chemoattractant protein-1 (MCP-1/CCL2) is a prominent member known for its capacity to trigger chemotaxis during inflammation (Gschwandtner et al., 2019). To elucidate the ability of the DD-MLL-ENL macrophages to direct their movement towards a chemokine gradient, a 3D chemotaxis assay with CCL2 as chemoattractant was performed. Via live cell microscopy directional movements of single cells within a gel matrix were investigated.

In the absence of a chemokine gradient, the tracking of the immature DD-MLL-ENL + Shield-1 cells and the differentiated macrophages showed only minor nonspecific movements with centering in the middle of the gel matrix. However, upon application of a CCL2 gradient, distinct directional movements towards the chemokine could be observed for both cell populations. In this context, the macrophages' migration towards CCL2 was more distinctive as verified by a higher number of single cell routes and a

prominently shifted center of the mass (Figure 36A). Analyses revealed a significantly higher accumulated distance and velocity for the macrophages compared to the undifferentiated progenitors when a CCL2 gradient was applied. In contrast, when undifferentiated DD-MLL-ENL cells were used on slides with a CCL2 gradient the calculated accumulated distance and velocity did not differ from uncoated slides although single directional movements were observed (Figure 36B). These results point out that the DD-MLL-ENL derived macrophages exhibit a pronounced migratory capacity towards CCL2, even though the cognate receptor CCR2 is downregulated after differentiation as demonstrated by gene expression profiling (Figure 34).

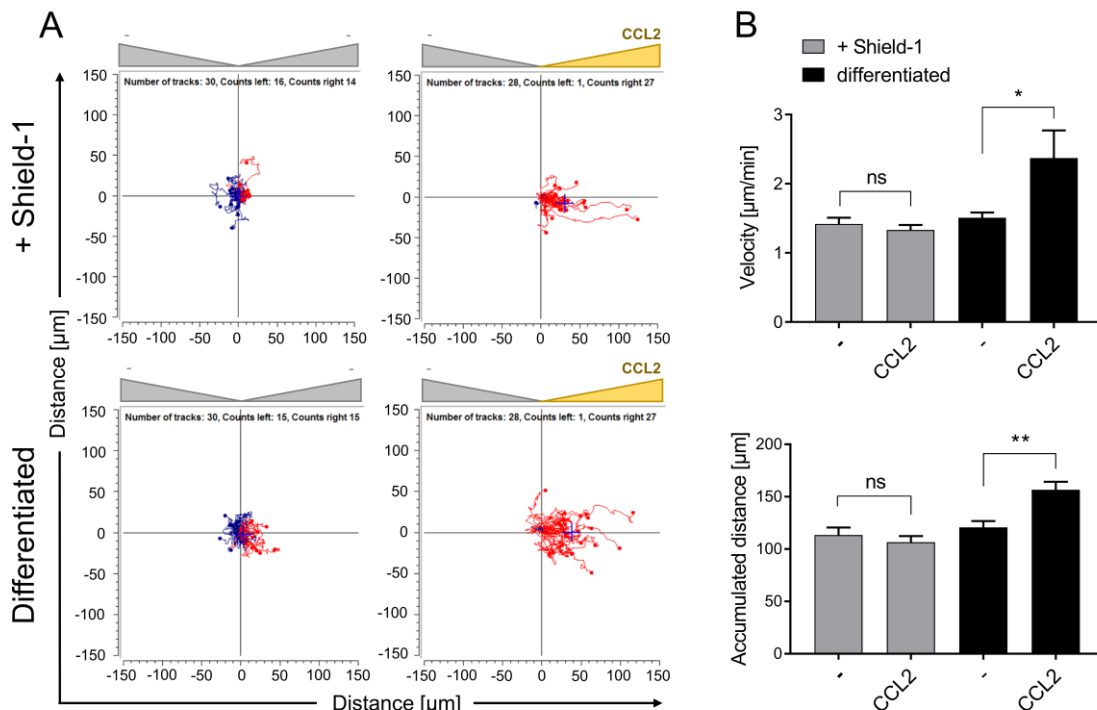


Figure 36: Chemotaxis of DD-MLL-ENL macrophages towards the chemoattractant CCL2. (A) 2×10^6 DD-MLL-ENL + Shield-1 cells and DD-MLL-ENL macrophages were harvested and mixed with a rat tail collagen type I solution. The observation canal of chemotaxis μ -slides was filled with the collagen-cell mix followed by incubation at 37 °C for 30 minutes. A CCL2 solution (300 ng/ml) was added to one reservoir. The cell motility towards the chemoattractant was then monitored with time-lapse imaging every 1.5 minutes at 37 °C for 2 hours via microscopy. Depicted are the final images generated with the chemotaxis and migration tool after 2 hours incubation for each sample with and without a CCL2 gradient. Each route represents the movement of a single cell. Red color indicates migration towards CCL2. Starting point was centered to $x=y=0$. The blue cross displays the center of the mass. (B) Velocity as well as accumulated distance were determined by evaluating the data generated in (A). Statistical significance was calculated with a two-way ANOVA with Tukey's multiple comparison tests and data represent the mean \pm SD of $n = 3$ biological replicates. * $P < 0.05$; ** $P < 0.01$. The chemotaxis assay was performed in cooperation with Dr. Adrian Hoffmann and Prof. Dr. Jürgen Bernhagen at the Institute for Stroke and Dementia Research (University Hospital, LMU Munich).

3.4.3.3 Phagocytic Properties

Macrophages are professional phagocytes highly specialized in phagocytosis of pathogens and clearance of apoptotic and antibody-opsonized cells. Various phagocytosis assays were conducted to analyze the DD-MLL-ENL macrophages' ability to mediate the above-mentioned functions.

3.4.3.3.1 Phagocytosis of Bacterial Particles

For the assessment of bacterial-derived pathogen uptake, *E. coli* BioParticles™ were used. These particles are conjugated to a rhodamine-based pHrodo™ Red dye that is non-fluorescent at neutral pH but turns bright red following acidification within the phagosome. Co-incubation with the macrophages allowed to determine the phagocytic capacity in the presence or absence of cytochalasin D, an inhibitor of actin polymerization and phagocytosis. After co-incubation cells were analyzed by fluorescence microscopy. Bright fluorescence signal indicated phagocytosis of the bacterial particles in a qualitative manner.

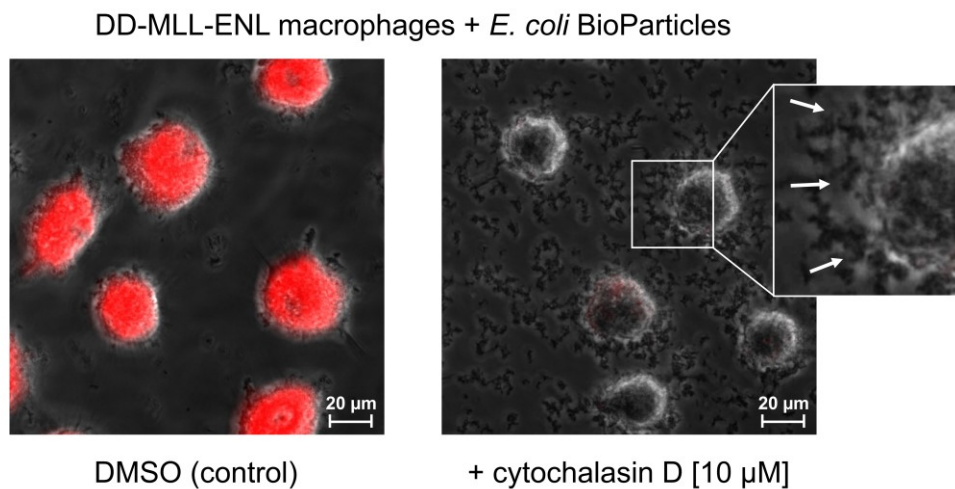


Figure 37: Proof of phagocytosis of bacterial particles by DD-MLL-ENL macrophages.

For verify phagocytosis of bacterial particles 2×10^5 DD-MLL-ENL macrophages were seeded on an ibidi slide and treated with either a cytochalasin D solution (10 μM) or DMSO for 20 minutes at 37 °C. A pHrodo™ Red *E. coli* BioParticles™ solution was added to obtain a 20:1 particle:cell ratio followed by incubation for 2 hours at 37 °C. Phagocytosis was verified via fluorescence microscopy. The images are representative for both samples and depict an overlay of phase contrast and the fluorescence channel. White arrows indicate *E. coli* BioParticles attached to the cell surface.

The microscopy images portrayed an explicit difference in bacterial particle uptake as assessed by the fluorescent signals inside the cells. The macrophages treated with DMSO exhibited a bright fluorescent emission indicating efficient uptake of the pH-sensitive bacterial particles in the acidic phagosome. In contrast, when pretreated with

cytochalasin D the macrophages were not able to engulf the particles as assessed by lacking fluorescent signal. Of note, the particles clearly surrounded the cells without being taken up leading to the suggestion that specific receptors such as TLR recognize these particles as pathogens leading to effective binding (Figure 37). Summing up, the DD-MLL-ENL derived phagocytes were able to recognize and engulf bacterial particles, which constitutes an essential feature of macrophages.

3.4.3.3.2 Efferocytosis

To determine the DD-MLL-ENL macrophages' ability to engage in the removal of apoptotic cells, a process called efferocytosis, co-incubation with apoptotic target cells was set up. For this purpose, Jurkat cells were used as target cells. Apoptosis was induced with the protein kinase inhibitor staurosporine. Efficient cell death induction was validated by Annexin V staining determining surface presence of the prominent eat-me signal phosphatidylserine, which is exposed on the outer leaflet of the plasma membrane of apoptotic cells (Lemke, 2019, Doran et al., 2020).

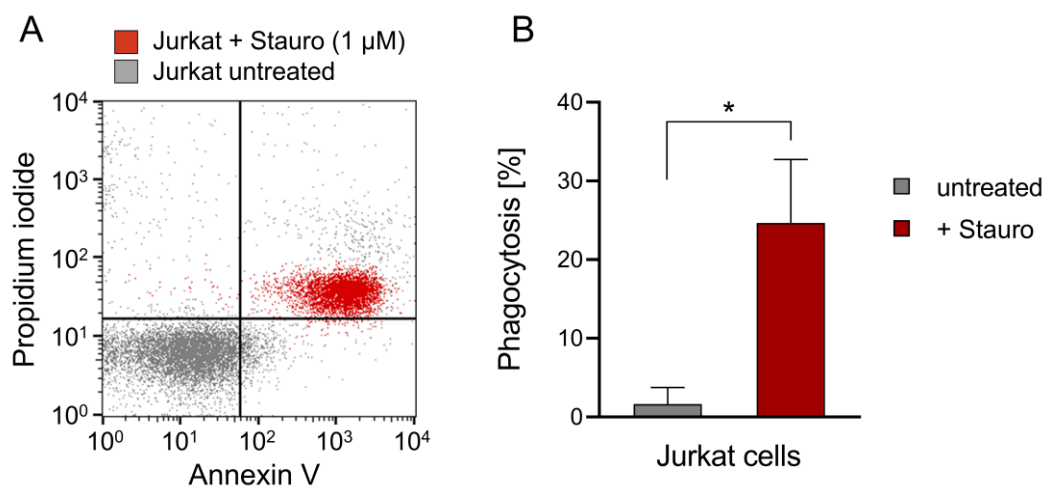


Figure 38: Efferocytosis of apoptotic Jurkat cells mediated by DD-MLL-ENL macrophages. (A) Jurkat cells were incubated at a concentration of $1 \times 10^6/\text{ml}$ in the presence of $1 \mu\text{M}$ staurosporine (Stauro) for 4 hours at 37°C to induce apoptosis. Cell death was measured by Annexin V and propidium iodide staining. As a control, staining was performed with live Jurkat cells. The plot shows both samples (untreated and staurosporine-treated) as an overlay analyzed by flow cytometry. (B) DD-MLL-ENL macrophages were harvested at day 14 and seeded on 8-well ibidi slides. To initiate efferocytosis, staurosporine-treated and untreated CFSE-labeled Jurkat cells were co-incubated with the macrophages at an E:T ratio of 1:2 for 2 hours at 37°C . Efferocytosis was determined by analyzing macrophages for uptake of labeled cells via fluorescence microscopy. Statistical significance was calculated with a two-tailed paired t test and data represent the mean \pm SD of $n = 3$ biological replicates. ** $P < 0.01$.

Flow cytometry analyses revealed that staurosporine-treated Jurkat cells were positive for Annexin V and propidium iodide staining, which is characteristic of a late apoptotic or

necrotic state. In contrast, untreated cells did not exhibit a fluorescent signal for either staining as shown in gray (Figure 38). Co-incubation with the DD-MLL-ENL macrophages resulted in efficient engulfment of the late apoptotic/necrotic cells with a mean phagocytosis rate of 25%. No significant phagocytosis with a mean value of 1.6 % was observed when using untreated Jurkat cells as a control. These findings demonstrated the macrophages' ability to clear dead cells.

3.4.3.3.3 Antibody-Dependent Cellular Phagocytosis (ADCP)

Following verification of efferocytosis and uptake of bacterial particles, engulfment of opsonized target cells in an antibody-dependent manner was investigated. As all currently approved therapeutic monoclonal antibodies are IgGs (as of 2022) the DD-MLL-ENL macrophages' ability to bind the Fc region of IgG via the expressed FcγR was scrutinized. Hence, increasing concentrations of a sterile solution of unaltered IgGs (Gamunex) were added to the macrophages to allow binding.

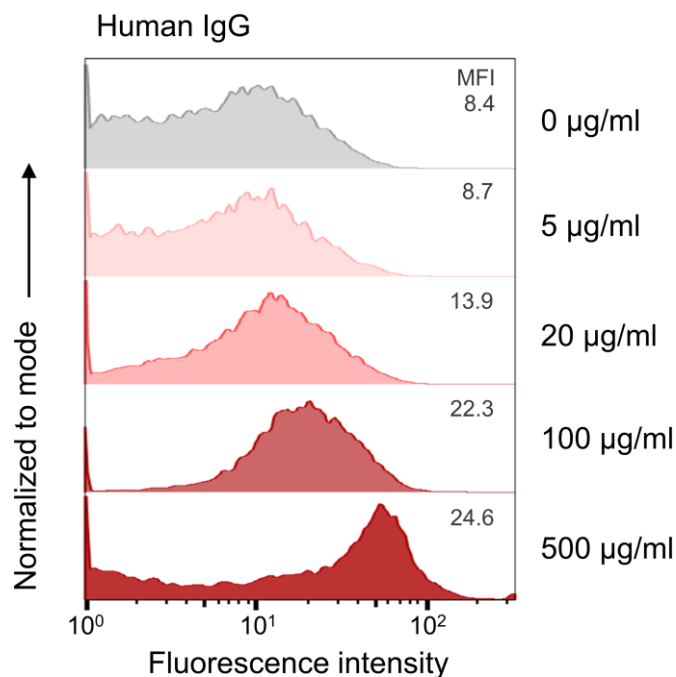


Figure 39: Binding of IgGs by FcγR expressed on DD-MLL-ENL macrophages.

DD-MLL-ENL macrophages were harvested at day 14 and washed with 1x PBS. For each reaction, 1×10^5 cells were incubated in the presence of various IgG concentrations (0, 5, 20, 100, 500 µg/ml) at 4 °C for 2 hours. The samples were washed with 1x PBS followed by staining with a secondary PE-conjugated Fcγ fragment specific F(ab')₂ fragment. Fluorescence intensity was measured for each sample and portrayed as histogram. For each histogram the mean fluorescence intensity (MFI) is depicted.

Flow cytometry analyses following incubation of the DD-MLL-ENL macrophages in the presence of various concentrations of IgG revealed effective binding of IgGs to the cells.

A distinct shift in the fluorescence intensity was observed when high concentrations of IgG were applied. In the presence of 500 µg/ml of IgG a considerably shifted peak associated with an MFI of 24.6 was detected in comparison to the background MFI of 8.4 in the absence of IgGs (Figure 39).

Consequently, the macrophages' competence to perform ADCP was studied. For this purpose, various therapeutic IgG antibodies were used. The target cells to be opsonized constituted both cell-line- and patient-derived lymphoma cells. First, the DD-MLL-ENL macrophages' capacity to phagocytose the Burkitt lymphoma cell lines Daudi and Raji as well as patient-derived mantle cell lymphoma cells (MCL) was analyzed. As therapeutic antibodies rituximab and daratumumab binding the target cells' antigens CD20 and CD38, respectively, were used. As a negative control trastuzumab was applied, which binds the receptor HER2 that is absent on lymphoma cells. Additionally, for detailed comparison with macrophages derived from unmodified cells, ADCP was performed with macrophages originated from untransduced CD34+ cells as well as PBMC-derived M0 and M1 macrophages with Daudi cells as target.

Efficient engulfment of opsonized lymphoma cells was observed revealing the DD-MLL-ENL macrophages' proficiency to perform ADCP. The highest percentage of macrophages positive for engulfed target cells was achieved with Daudi cells with a mean phagocytosis of approximately 50% in the presence of rituximab implying that half of the counted macrophages phagocytosed at least one target cell. Similarly, when co-incubating with Raji and MCL cells mean phagocytosis rates of 30% and 20% were observed. The second therapeutic antibody daratumumab also entailed significant phagocytosis of both Burkitt lymphoma cell lines Daudi (mean of 38%) and Raji (mean of 22%) but not of MCL cells. Surface staining of the three MCL samples revealed the absence of CD38 in two samples and only minor expression on cells of the third sample (data not shown). In the presence of the control antibody trastuzumab only background phagocytosis similar to the control without antibody was observed (Figure 40A). Importantly, macrophages originated from untransduced CD34+ cells as well as PBMC-derived M0 or polarized M1 macrophages featured similar phagocytosis rates in the presence of rituximab and daratumumab with Daudi target cells (Figure 40B). Thus, phagocytosis rates of DD-MLL-ENL macrophages were comparable to macrophages derived from unmodified monocytes from peripheral blood indicating full phagocytic functionality.

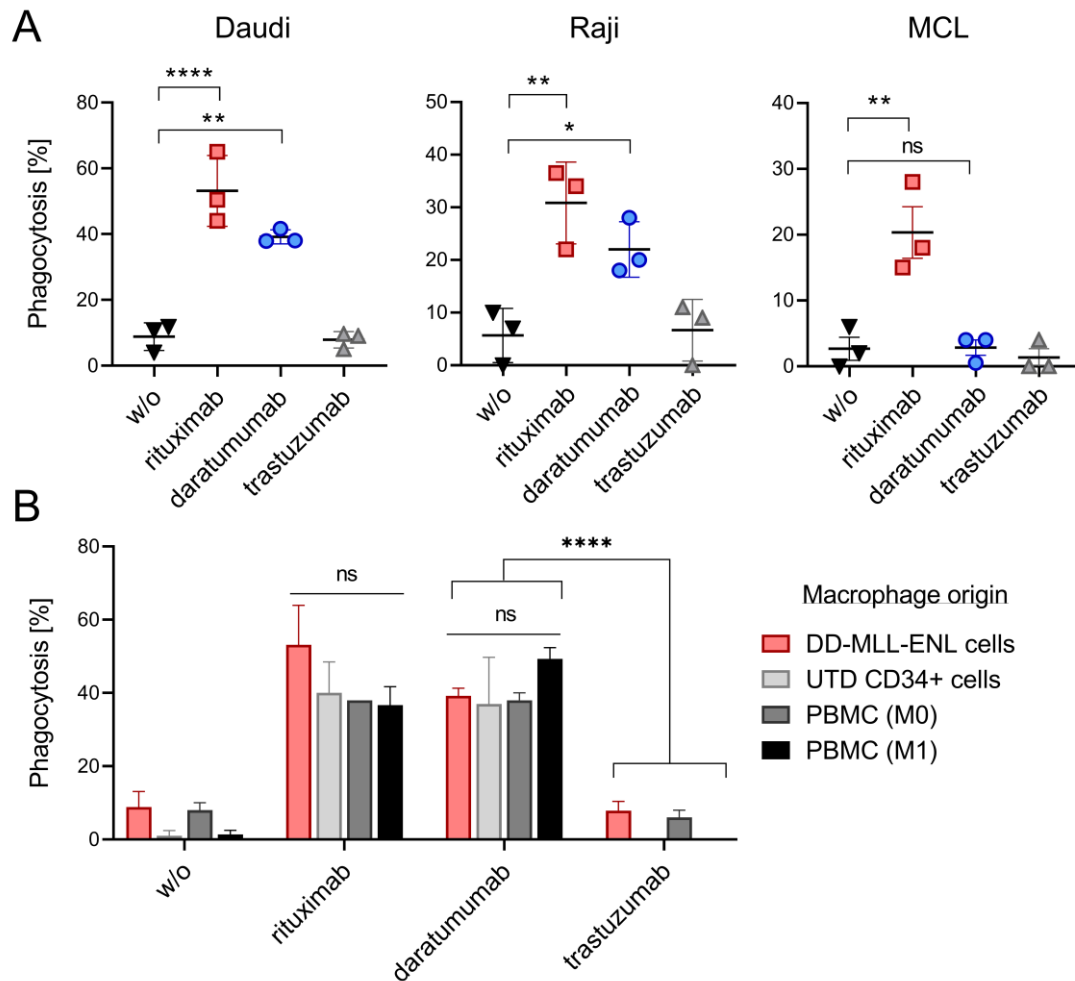


Figure 40: ADCP of lymphoma cells by DD-MLL-ENL macrophages.

(A) DD-MLL-ENL macrophages were harvested at day 14 and seeded on 8-well ibidi slides with 20.000 cells per well. CFSE-labeled Daudi, Raji or patient-derived MCL cells were added at an E:T ratio of 1:2 and co-incubated in the absence (w/o) or presence of either rituximab, daratumumab or trastuzumab at a final concentration of 10 $\mu\text{g/ml}$ for 2 hours at 37 $^{\circ}\text{C}$. Percentage of phagocytosis was determined by counting 50 macrophages and analyzing for engulfment of fluorescently labeled cells via fluorescence microscopy. Statistical significance was calculated with a one-way ANOVA with Sidak's multiple comparison tests and data represent the mean \pm SD of $n = 3$ biological replicates (Daudi and Raji: $n=3$ for DD-MLL-ENL macrophages, MCL: $n=3$ for patient-derived MCL cells). (B) ADCP of Daudi cells was performed with either DD-MLL-ENL macrophages, macrophages originated from untransduced (UTD) CD34+ or PBMC-derived M0 and M1 macrophages. To obtain the different macrophages, UTD CD34+ were differentiated the same way as DD-MLL-ENL cells via a 14-day stimulation with GM-CSF (20 ng/ml), IFN- γ (20 ng/ml) and LPS (100 ng/ml). M0 macrophages were generated by differentiating PBMC-originated monocytes in the presence of M-CSF (10 ng/ml) for seven days while M1 macrophages were stimulated with GM-CSF (20 ng/ml) for six days followed by a classical activation with IFN- γ (20 ng/ml) and LPS (100 ng/ml) for 24 hours. Statistical significance was calculated with a two-way ANOVA with Sidak's multiple comparison tests and data represent the mean \pm SD of $n = 3$ biological replicates. For all panels, ns indicates not significant, * $P < 0.05$, ** $P < 0.01$, **** $P < 0.0001$.

Next, phagocytosis was additionally tracked over time via live-cell imaging (IncuCyte[®] S3 Live-Cell Analysis System) allowing the survey of phagocytic frequency as well as peak phagocytosis within the observation period. For this approach, Carnival cells, a diffuse large B cell lymphoma cell line, was used as a target cell line. The cells were

labeled with the pH-sensitive pHrodo™ Red dye. In the acidic phagosome labeled cells become brightly fluorescent which allows to track phagocytosis as red object counts. The phagocytosis rate of DD-MLL-ENL macrophages and PBMC-derived M0 and M1 macrophages was monitored for five hours.

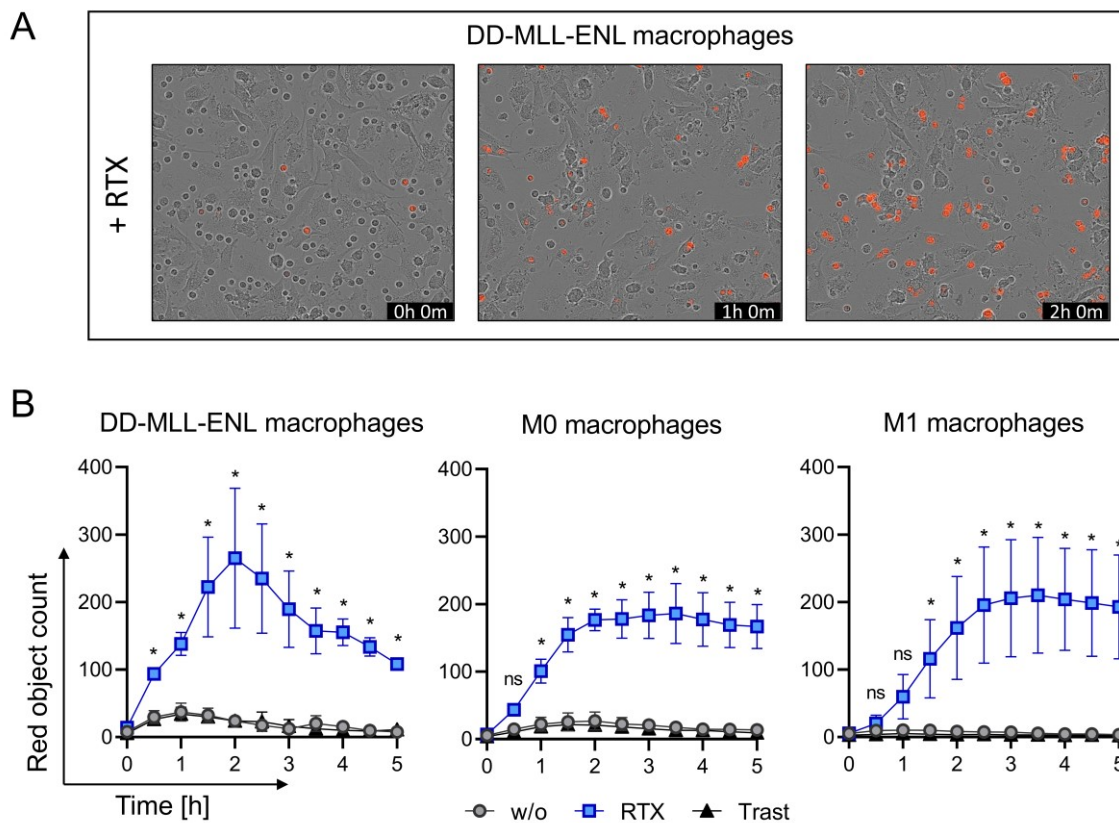


Figure 41: ADCP progression of DD-MLL-ENL and PBMC-derived M0 and M1 macrophages. To determine time-dependent ADCP progression, 4×10^4 macrophages per well were seeded on a 96-well plate overnight. Daudi cells were labeled with the pHrodo Red dye and added to the macrophages at an E:T ratio of 1:2 in the presence or absence of rituximab and trastuzumab (10 $\mu\text{g}/\text{ml}$ each). Upon co-incubation, ADCP was tracked in a 30-minute interval via Incucyte Live-Cell Analysis Systems for five hours. To determine red object counts, threshold of the fluorescence intensity detection limit was adjusted to the start point (0h 0m). **(A)** Images of DD-MLL-ENL macrophages were taken after one and two hours of co-incubation with pHrodo-labeled Daudi cells in the presence of rituximab (10 $\mu\text{g}/\text{ml}$). **(B)** Time-dependent ADCP courses were generated as graphs highlighting the measured red object counts. Data represent the means \pm SD of $n = 3$ biological replicates and statistical significance was calculated with a two-way ANOVA with Tukey's multiple comparison tests. RTX, rituximab; Trast, trastuzumab; ns, not significant; $*P < 0.05$.

Phagocytosis was rapidly initiated with first detectable counts after 30 minutes of co-incubation in the presence of rituximab (Figure 41). The DD-MLL-ENL macrophages displayed significant phagocytosis compared to the trastuzumab control with a red object count of approximately 100 in the presence of rituximab. This difference after 30 minutes was not significant when M0 and M1 macrophages were used. However, phagocytosis by the three different macrophage populations peaked after two to three hours with red object counts ranging between 200 and 300. Of note, a perceptible trend towards a

prompt flattening of the DD-MLL-ENL macrophage graph was observed presumably indicating degradation of the target cells. In contrast, M0 and M1 macrophages displayed a rather steady plateau following peak phagocytosis within the observation time (Figure 41B). Taken both the ADCP progression as well as phagocytic rates into account, the DD-MLL-ENL derived macrophages operate in a similar manner as M0 and M1 macrophages originated from peripheral blood of healthy donors.

As phagocytosis is governed by “eat me” and “don’t eat me” signals, the influence of the prominent “don’t eat me” signal CD47 interacting with SIRP α expressed on macrophages was scrutinized. For this, a CD47 σ antibody with depleted complement component 1q and Fc γ R binding (C. Kellner, unpublished) was applied to abrogate the inhibitory CD47-SIRP α axis. A similarly designed IgG2 σ antibody derived from trastuzumab (HER2 σ) was employed as control antibody.

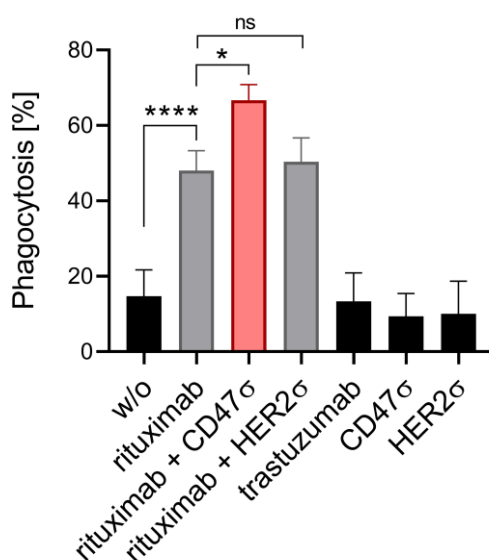


Figure 42: Influence of CD47 blockade on ADCP of Daudi cells by DD-MLL-ENL macrophages.

DD-MLL-ENL macrophages were harvested at day 14 and seeded on 8-well ibidi slides. CFSE-labeled Daudi cells were added at an E:T ratio of 1:2 and co-incubated in the absence (w/o) or presence of rituximab, CD47 σ , HER2 σ or trastuzumab and combinations thereof at a final concentration of 10 μ g/ml for 2 hours at 37 $^{\circ}$ C. Percentage of phagocytosis was determined by counting 50 macrophages and analyzing for engulfment of fluorescently labeled cells via fluorescence microscopy. Statistical significance was calculated with a one-way ANOVA with Sidak’s multiple comparison tests and data represent the mean \pm SD of $n = 3$ biological replicates. Ns, not significant; * $P < 0.05$; **** $P < 0.0001$.

In the presence of rituximab an ADCP percentage of approximately 50% was determined. This phagocytosis rate could be significantly increased by the addition of the blocking antibody CD47 σ resulting in a mean percentage of 66%. When the control antibody HER2 σ was used in combination with rituximab no significant increase in phagocytosis was observed. Of note, CD47 σ alone did not induce phagocytosis. Thus, merely background phagocytosis of roughly 10% was determined in line with the

additional controls including HER2 σ alone, trastuzumab and the co-incubation in the absence of antibodies (Figure 42). These results imply a functional CD47-SIRP α axis in the DD-MLL-ENL derived macrophages, which can be blocked to further boost phagocytosis.

Finally, the DD-MLL-ENL macrophages' ability to engulf patient-derived chronic lymphocytic leukemia (CLL) cells was investigated. For this purpose, CLL cells isolated from peripheral blood of three patients were co-incubated with the DD-MLL-ENL macrophages to determine phagocytosis in the presence of rituximab with or without concomitant CD47 blockade.

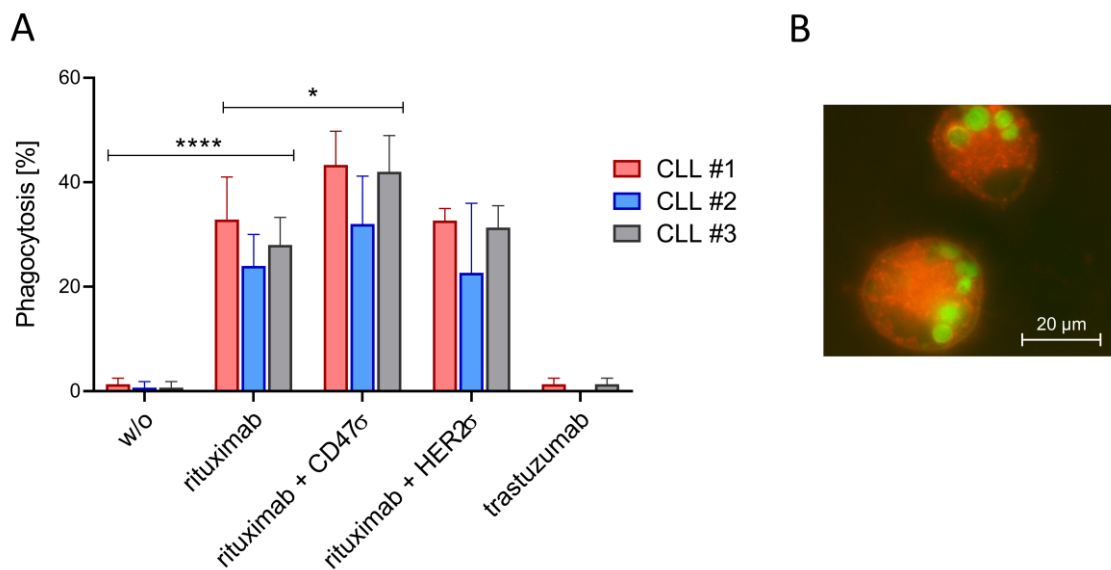


Figure 43: ADCP of patient-derived CLL cells by DD-MLL-ENL macrophages.

(A) DD-MLL-ENL macrophages were harvested at day 14 and seeded on 8-well ibidi slides. CFSE-labeled CLL cells were added at an E:T ratio of 1:2 and co-incubated in the absence (w/o) or presence of rituximab, CD47 σ , HER2 σ or trastuzumab and combinations thereof at a final concentration of 10 μ g/ml for 2 hours at 37 $^{\circ}$ C and 5% CO₂. Percentage of phagocytosis was determined by counting 50 macrophages and analyzing in terms of engulfment of fluorescently labeled cells via fluorescence microscopy. Statistical significance was calculated with a two-way ANOVA with Sidak's multiple comparison tests and data represent the mean \pm SD of $n = 3$ biological replicates, i.e., DD-MLL-ENL macrophages from three different transductions. **(B)** Visualization of engulfed CFSE-labeled CLL cells (green) inside macrophages, which were stained with the cytoplasmic membrane dye CellBrite Orange (Biotium Inc., Fremont, CA, USA) after co-incubation. * $P < 0.05$, **** $P < 0.0001$.

Comparable to the results obtained with Burkitt lymphoma cell lines as well as primary MCL cells, co-incubation with patient-derived CLL cells entailed a pronounced phagocytosis with a mean value of approximately 30% in the presence of rituximab. Furthermore, similar to the preceding assay with the Daudi cells, CD47 blockade significantly augmented the phagocytosis resulting in a percentage of nearly 40%. This increase was observed for each individual CLL sample. Of note, DD-MLL-ENL macrophages were able to engulf multiple target cells (Figure 43B). Combining rituximab

with the HER2 σ control antibody did not increase phagocytosis rate compared to rituximab alone. No significant phagocytosis was detected in the presence of trastuzumab comparable to the control without antibody (Figure 43A).

In summary, these phagocytosis assays unambiguously demonstrate the DD-MLL-ENL macrophages' ability to engulf lymphoma cell lines and patient-derived primary MCL and CLL cells in an antibody-dependent manner. The DD-MLL-ENL macrophages exhibit a similar phagocytic capacity as M0 and M1 macrophages derived from peripheral blood of healthy donors both quantitatively and qualitatively.

4. Discussion

HSCs exhibit self-renewing capacity and give rise to all blood components (Seita and Weissman, 2010). Hence, they represent a promising cell type for *ex vivo* expansion in order to obtain a sufficient number for cell therapeutic purposes or *in vitro* differentiation into functional blood cells. The major limitation hindering *ex vivo* expansion of HSCs is their propensity to differentiate along the hematopoietic hierarchy as soon as they are detached from their bone marrow niche (Kumar and Geiger, 2017). Since decades, several approaches have been made to prevent differentiation and sustain a proliferative immature phenotype *ex vivo*. Yet, long-term and large-scale expansion could not be achieved calling for effective alternatives. Consequently, focus was set on genetic engineering to overexpress specific genes such as HOX genes associated with perpetuating self-renewal (Abramovich et al., 2005). Although ectopically expressing a single gene resulted in solid expansion of murine HSCs, it has not been shown for human HSCs so far (Zhang et al., 2007, Rosas et al., 2011, Calvo et al., 2000). This led to the strategy to exploit the proliferative nature of leukemic fusion genes with unique features resulted from chromosomal translocation. Chimeric genes used in such approaches include RUNX1-ETO, NUP98-HOX fusions and MLL fusions as these serve as “single hit” implying that no secondary mutations are required to confer *ex vivo* expansion (Lavau et al., 1997, Mulloy et al., 2002, Sloma et al., 2013, Chung et al., 2006).

In this thesis, a two-step cell culture system was established comprising *ex vivo* large-scale and long-term progenitor cell expansion and the subsequent arbitrary differentiation into immune cells. The focus was set on the manufacture of macrophages as immune cell type of interest. To enable such a two-step system a retroviral vector containing the fusion gene DD-MLL-ENL was used to transduce human HSCs from healthy donors. In the presence of the small molecule Shield-1, which prevents degradation of the DD-MLL-ENL protein, complete outgrowth and expansion of the transduced cells was demonstrated. These MLL-ENL expanded progenitor cells displayed a myeloid phenotype, devoid of chromosomal abnormalities, putative driver mutations and copy number alterations. After withdrawal of Shield-1 and in the presence of GM-CSF, IFN- γ and LPS, the progenitor cells lost proliferation potential and differentiated into macrophages. These macrophages expressed characteristic surface proteins as well as innate immunity-related genes and were shown to be fully functional. As this two-step cell culture system necessitates the use of a leukemia-associated fusion protein, the following passages discuss the characteristics of the DD-MLL-ENL myeloid progenitors, the integrity of the thereof derived macrophages, potential safety concerns and advantages of the DD-MLL-ENL expansion system.

4.1 Characteristics of DD-MLL-ENL Expanded Progenitor Cells

The use of leukemia-associated fusion proteins, such as MLL-ENL, as expansion factors raises the question to what extent the transduced and *ex vivo* expanded cells disclose progenitor attributes. These include the cells' behavior in the presence of proliferation-favoring as well as lineage-associated hematopoietic cytokines, their sustained self-renewal potential, their immunophenotype and their ability to differentiate into functional mature blood cells. These features are discussed in the following for the DD-MLL-ENL expanded myeloid progenitor cells.

Hematopoietic cytokines tightly orchestrate differentiation of HSPCs along the hematopoietic hierarchy and have a pivotal influence on the maintenance of self-renewal potential and lineage choice (Asada et al., 2017a). Once detached from the hematopoietic stem cell niche HSPCs differentiated due to the lack of supportive cell-cell contacts and cytokines. Hence, since decades approaches aimed for elucidation of the optimal cytokine settings to mediate HSPC expansion *ex vivo* mimicking the bone marrow niche. Although an ideal reflection of the niche could not be achieved by the sole addition of cytokines *ex vivo*, short-term expansion of HSPCs has been accomplished by combining various combinations of the cytokines Flt-3L, IL-3, IL-6, SCF, and TPO (Branco et al., 2020). Furthermore, the addition of growth factor such as G-CSF and GM-CSF results in the expansion of committed progenitor cells. A crucial parameter is the optimal concentration of each cytokine as inadequate concentrations may negatively impact self-renewal potential (Audet et al., 2002). These supportive cytokine settings were also used when expansion of HSPCs was induced by using leukemia-associated fusion genes, such as RUNX1-ETO as demonstrated by Mulloy and colleagues (Mulloy et al., 2003, Mulloy et al., 2002). In this thesis, the given concentrations for each cytokine, apart from EPO, were used to cultivate the HSPCs. For proper retroviral integration of the vector coding for the gene of interest, in this case DD-MLL-ENL, proliferation of HSPCs is required. The low transduction rates (below 10%) are attributed to the large construct used between the 5' LTR and the 3' LTR with a total size of 8.6 kb whereas the maximum packaging capacity of retroviruses is generally suggested to be around 9 kb (Chen et al., 2018). Large fragments are packaged less efficiently resulting in a lower viral titer. Thus, regarding the low transduction rate it can be expected that more than one integration per cell is highly unlikely. The DD-MLL-ENL construct was stably integrated into the target cells' genome indicated by sustained GFP expression of transduced cells. The continuous expression and in particular the activity of MLL-ENL in the presence of the small molecule Shield-1 led to a proliferation advantage of transduced cells ultimately outcompeting untransduced cells as these exhaust their self-renewal potential *ex vivo* as delineated before. As myeloid cytokines were present in the

media, analysis of the outgrown DD-MLL-ENL cells revealed a late monocytic progenitor phenotype as determined by FAB classification and immunophenotyping. Notably, IL-3 and GM-CSF considerably impact lineage choice towards myeloid commitment and feature a proliferative effect (Maciejewski et al., 1991). Thus, the resulting homogeneous DD-MLL-ENL expressing cell population displays a myelomonocytic phenotype, proposed to be directly downstream of GMP with the potential to differentiate into the granulocytic and monocytic lineage (Cozzio et al., 2003, Sun et al., 2018, Yokoyama, 2017). These findings come along with results obtained by other groups ectopically expressing MLL-ENL in HSPCs (Horton et al., 2005, Cozzio et al., 2003, Zeisig et al., 2004, Schreiner et al., 2001). Interestingly, MLL-ENL induced AML seems to originate from hematopoietic progenitors and not HSC, which were vastly resistant to transformation as demonstrated by Ugale and colleagues in a conditional, inducible mouse model (Ugale et al., 2014). Consistently, the outgrown DD-MLL-ENL expressing cells in this study lost the HSPC marker CD34. In general, CD34 is present on stem and progenitor cells but gets gradually lost the more differentiated the cells become (Sidney et al., 2014). As late monocytic progenitors the cells are explicitly committed whereby the absence of CD34 can be explained. However, immunophenotyping of DD-MLL-ENL expressing progenitor cells revealed high expression of CD123, the IL-3 receptor and low to mediocre expression of CD117, the SCF receptor c-KIT and CD135, known as Flt3. Of note, upon complete outgrowth, IL-3 and Flt3-L were sufficient for continuous expansion without any decrease in proliferation compared to complete medium containing the above-mentioned cytokines (data not shown). Such a cytokine reduction significantly lowers costs for possible large-scale applications. Apart from cytochemical staining, analyses of myeloid-specific surface markers indicate a myelomonocytic phenotype strongly positive for CD33 and CD64 in combination with low expression of CD11b and CD14. As only a single genetic element was integrated into the genome leading to overexpression of a leukemia-associated fusion gene, the resulting cells cannot be regarded as fully leukemic cells. Leukemic cells are shaped by the tumor microenvironment and often harbor several accumulated mutations. The DD-MLL-ENL cells are rather described as expanded progenitors due to the MLL-ENL's features in blocking differentiation and enabling proliferation via the key targets *HOXA9* and *Meis1* (Zeisig et al., 2004). In contrast, modeling *bona fide* chromosomal translocation via CRISPR-Cas9 *in vitro* mimicking the natural formation of the fusion gene MLL-ENL resulted in only transient growth advantage lacking a full transformation (Reimer et al., 2017). These findings suggest that environmental cues and additional mutations are necessary to advance MLL-ENL induced leukemias *in vivo*. Hence, supraphysiological expression of MLL-ENL seems to be essential to drive sustained proliferation of

progenitor cell *in vitro* without the need for co-mutations. The results in this thesis underline this issue by demonstrating a maintained proliferation of the transduced cells for more than 2.5 years without losing their self-renewal potential. By establishing the regulable DD-Shield-1 system it was confirmed that MLL-ENL is required to keep up the immature phenotype as upon Shield-1 withdrawal and the resulting degradation of the fusion protein, self-renewal exhausted accompanied by proliferation stop and loss of immaturity. This is in accordance with experiments performed with a doxycycline-inducible transgenic mouse model by Stavropoulou and colleagues (Stavropoulou et al., 2018). In the absence of Shield-1, the MLL-ENL fusion protein got degraded resulting in a cellular change in size and granularity after a couple of days accompanied by the downregulation of HOXA9. As HOXA9 expression is normally restricted to HSCs, CMP and GMP subsets and was demonstrated to be essential for maintenance of MLL-ENL-driven transformation, downregulation is linked to differentiation (Ayton and Cleary, 2003). Accordingly, loss of immaturity is accompanied by initiated differentiation along the hematopoietic hierarchy. Hence, the DD-MLL-ENL cells, which exhibit a myelomonocytic phenotype could be successfully differentiated into functional macrophages. This finding points out that the phenotype of the MLL-ENL expanded progenitor cells is not irreversibly changed.

To rule out genomic abnormalities in MLL-ENL expanded progenitor cells, genome-wide analyses were performed including karyotyping, whole exome sequencing as well as verification of retroviral integration sites. The absence of chromosomal abnormalities and mutations in cancer-related genes verified an unaltered genome integrity in the expanded cells. These results suggest MLL-ENL as sole, potent driver that is able to expand human hematopoietic progenitor cells without promoting chromosomal instability or acquisition of driver mutations. Retroviral integration sites were determined to investigate the influence of vector insertion on outgrowth of transduced cells. For the samples analyzed after outgrowth an oligo- to polyclonal pattern was identified similar to the pattern described for MLL-AF9 *ex vivo* expanded human primary CD34+ progenitor cells (Wei et al., 2008). Retroviral integration did not result in single cell outgrowth as indicated by multiple LM-PCR products. The identified neighboring genes of each integration site were confirmed in an MLV/Moloney retroviral integration site database (Shao et al., 2016). Of note, no integration in EVI1, PRDM16 and MDS, which have been repeatedly shown to enhance leukemic growth *in vivo*, was observed (Modlich et al., 2008, Stein et al., 2010). These results do not provide explicit information to distinguish if the observed integration patterns originate from outgrowth of transduced cells by gene activation, are the result of open chromatin regions allowing permanent vector expression, or reflect clonal fluctuation. However, as monoclonal outgrowth was not

detected in the analyzed samples it can be assumed that the retroviral integration did not favorably affect the cells' proliferation capacity.

4.2 How Natural Are DD-MLL-ENL Derived Macrophages?

The *in vitro* manufactured macrophages derive from myeloid progenitors, which were massively expanded via stable overexpression of the MLL-ENL oncogene. Therefore, the question arises how similar these engineered macrophages are to *in vitro* differentiated macrophages originated from unmodified monocytes from healthy donors. In the following, several points regarding differentiation process, polarization towards a pro-inflammatory phenotype, gene expression profile and functional properties are discussed.

The unipotent character of the expanded MLL-ENL expressing myelomonocytic progenitor cells allows differentiation into either mature granulocytes or macrophages (Cozzio et al., 2003). To facilitate terminal differentiation into activated pro-inflammatory macrophages GM-CSF, IFN- γ and LPS was used, which entailed the most efficient differentiation within 14 days as assessed by microscopy and flow cytometry. Although GM-CSF regulates various cellular processes including survival and proliferation, it also mediates differentiation and activation by stimulating the production of pro-inflammatory cytokines, particularly in the absence of other proliferation-promoting cytokines such as SCF or Flt3-L (Hamilton, 2019). IFN- γ is described to initiate a pro-inflammatory M1 macrophage polarization reflecting exposure to CD4⁺ T_h1 cells *in vivo* and is therefore used in combination with the TLR agonist LPS to stimulate macrophages *in vitro* (Murray, 2017). Although IFN- γ and LPS are commonly used for 24 to 48 hours for efficient activation of M1 macrophages, both molecules were included in the differentiation medium for the complete 14 day differentiation period as this setting resulted in the most robust macrophage differentiation. Accordingly, within 14 days the complete cell population lost immaturity and self-renewal capacity as assessed by microscopy and CFU assays. As the DD-Shield-1 regulatory mechanism acts at the protein level, LTR-driven MLL-ENL expression continues in the absence of Shield-1 but the resulting protein is rapidly degraded, which may lead to minimal activity for a short period. Yet, this potential activity is evidently not enough to have an impact on proliferation. Similar findings were reported for the fusion gene MLL-AF9 where the dosage plays a critical role in initiation as well as maintenance of the transformation (Chen et al., 2008). Of note, reapplying Shield-1 in cultures of terminally differentiated DD-MLL-ENL cells did not result in anew proliferation or reversion of the phenotype (data not shown).

The obtained differentiated macrophages expressed the co-stimulatory molecules CD80 and CD86 and strongly upregulated CD14 and MHC class II (HLA-DP, -DQ, -DR), which is described for the polarized M1 macrophage phenotype *in vitro* (Chavez-Galan et al., 2015). Thus, the MLL-ENL expanded progenitor cells were shown to be responsive to the stimuli IFN- γ and LPS. IFN- γ orchestrates upregulation of interferon-stimulated genes including MHC II, CD80 and CD86 via the JAK-STAT pathway while LPS regulates the upregulation of its own receptor CD14 (Landmann et al., 1996, Ambarus et al., 2012). Additionally, expression of the Fc γ R family members CD16, CD32 and CD64 was demonstrated with the highest expression for CD32, a surface glycoprotein involved in cellular response regulation such as phagocytosis or induction of cytokine secretion (Anania et al., 2019). In particular, the activating isoform CD32A was prominently expressed which may be enhanced in the presence of IFN- γ (van Schie et al., 1992). Consequently, the DD-MLL-ENL macrophages share considerable similarities with *in vitro* polarized M1 macrophages derived from healthy donors as described by literature with the exception of CD163 expression, which is frequently associated with M2 macrophage polarization.

High expression of the pro-inflammatory cytokine IL-6 was observed strongly related to the polarized M1 subtype (Italiani and Boraschi, 2014). In addition, the differentiated cells displayed a significant upregulation of CCL2, another pro-inflammatory cytokine contributing to immune cell extravasation and described to be upregulated by IFN- γ and LPS (Sierra-Filardi et al., 2014). Conversely, only a minor upregulation of the regulatory M1-associated cytokine TNF α was observed, although termed to be strongly upregulated via LPS stimulation (Salim et al., 2016). On the other hand, regarding M2-related anti-inflammatory gene signatures significant upregulation of IL-10 was determined. This upregulation might be the consequence of continuous LPS stimulation as TLR signaling is associated with IL-10 expression in form of a feedback mechanism to restrain inflammation (Iyer et al., 2010). IL-10 itself acts as a potent anti-inflammatory molecule and mediates inhibition of TNF α production via suppression of NF κ B activation therefore potentially explaining the marginal upregulation (Dhingra et al., 2009). Thus, in accordance with the immunophenotype the cytokine expression profile highlighted the cells' pro-inflammatory character although some features are rather attributed to the anti-inflammatory M2 subtype. Interestingly, neither iNOS nor ARG1, two hallmark characteristics for M1 and M2, respectively, involved in opposing pathways to metabolize arginine, were upregulated following differentiation (Rath et al., 2014).

To take a deeper look into gene expression profiles in both undifferentiated and differentiated DD-MLL-ENL cells, mainly focused on innate immunity with macrophages as cell type of interest, in-depth expression analysis covering 730 genes was performed.

For this purpose, untransduced CD34+ cells were included as an “immature cell type control” for the expanded DD-MLL-ENL expressing cells. In addition, the expression pattern of PBMC-derived CD14+ monocytes from healthy donors were compared to differentiated DD-MLL-ENL macrophages. Overview of gene expression signatures unveiled considerable similarity between the CD34+ cells and the expanded DD-MLL-ENL monocytic progenitors. As a myeloid innate immunity panel was used, which is designed to address innate immune responses of myeloid-derived cells overall low expression profiles for both immature cell types were expected. In the subcategories “cell cycle and apoptosis” as well as “differentiation and maintenance of myeloid cells” few gene clusters were highly expressed in both cell types likewise. Within this group, the most prominent cell cycle- and proliferation-associated genes include *BIRC5* (Survivin), *TOP2A*, *CCNB2* and *MYC*, which were all shown to be completely downregulated in the mature cell types when comparing the normalized counts on single gene level. In particular, the expression of *MYC* plays a crucial role in orchestrating differentiation as it has been shown to block myelomonocytic differentiation at an intermediate stage during the progression from immature blast cells to mature macrophages (Liebermann and Hoffman, 1994). *MYC* and its transcriptional program substantially impact *MLL*-rearranged leukemia progression. *MLL* fusion proteins bind to *MYC* promoter regions leading to H3K4 and H3K79 methylation. In particular, in *MLL*-AF9 and *MLL*-ENL expressing cells high *MYC* protein levels as well as enrichment of *MYC* target genes were detected, which were associated with an aggressive proliferation and a shorter disease latency in mice (Chen et al., 2016). Accordingly, *MLL*-ENL requires *MYC* expression to maintain a differentiation blockade and ensure proliferation (Schreiner et al., 2001). Accordingly, significant downregulation of *MYC* is accompanied by differentiation.

As expected, differentiated DD-MLL-ENL macrophages and CD14+ monocytes strikingly differed in their gene expression profile when compared to the immature cell type signature. The majority of analyzed genes is characterized by high expression for both sample types indicating innate immunity context. Although similar in the directed global significance score represented by a significant upregulation of all clustered innate immunity-related subcategories except cell cycle and apoptosis in comparison to baseline CD34+ expression, distinct differences between the DD-MLL-ENL macrophages and monocyte samples existed at the single gene level. Highlighted as log2 normalized expression several genes, which were upregulated in DD-MLL-ENL macrophages, were downregulated in the monocytes or vice versa. These differences are most likely due to cytokine-driven stimulation. *In vivo*, monocytes are able to differentiate into macrophages following tissue infiltration in the presence of various

environmental cues such as GM-CSF (Ushach and Zlotnik, 2016). Mimicking the stimulation *in vitro* by differentiating isolated monocytes with GM-CSF triggers drastic changes in gene expression profiles as previously demonstrated by Lehtonen and colleagues (Lehtonen et al., 2007). In addition, it was shown that polarization towards the M1 phenotype with IFN- γ and LPS *in vitro* fundamentally altered the expression pattern particularly in gene subsets related to chemotaxis and cell migration function in accordance with the profile of the DD-MLL-ENL macrophages (Orecchioni et al., 2020). LPS is described to activate the canonical NF κ B pathway via binding to the cognate receptor TLR4 subsequently resulting in the induction of pro-inflammatory chemokine expression such as CCL4, CXCL8 and CXCL16 (Liu et al., 2017, Mantovani et al., 2004). These molecules play a pivotal role in mediating recruitment of immune cells as well as sustaining inflammatory milieu and were found upregulated in the DD-MLL-ENL macrophages again proving their identity as pro-inflammatory macrophages with a functional NF κ B signaling pathway. Overall, it must be taken into account that *in vitro* stimulated macrophages do not reflect the *in vivo* gene expression signature as demonstrated in murine cells (Orecchioni et al., 2020). This was the reason why unmodified CD14⁺ monocytes from healthy donors were used as comparison. Although their expression profile naturally differs from those of the DD-MLL-ENL macrophages, both groups express innate immunity-related gene subsets thereby identifying themselves as myeloid immune cells. Moreover, including polarized M1 macrophages originated from CD14⁺ monocytes might provide additional valuable information. Despite this lacking information the DD-MLL-ENL derived macrophages were shown to be reactive to various cues resulting in a gene expression alteration characteristic for *in vitro* simulated M1 macrophages as described in the literature (Mantovani et al., 2004).

Macrophages exert their hallmark functions in tissue. During inflammation, a critical requirement for the resolution is the successful recruitment of monocytes, which differentiate into macrophages upon extravasation. Chemotaxis and trafficking are two pivotal steps to ensure this accumulation at diseased sites (Gerhardt and Ley, 2015). A key molecule driving blood monocyte attraction is CCL2 (Gschwandtner et al., 2019). The here presented results revealed a significant chemotaxis of both undifferentiated DD-MLL-ENL derived monocytic progenitors and macrophages towards the chemoattractant CCL2. Although macrophages naturally originate following tissue penetration, this migratory property is of utmost importance to address inflamed or damaged sites when applied in form of a cell therapeutic product. Klichinsky and colleagues demonstrated successful homing of genetically engineered macrophages by analyzing the biodistribution of CAR-macrophages after systemic administration in mice in a tumor xenograft model. These CAR-macrophages were able to migrate and traffic

to established solid tumors (Klichinsky et al., 2020). Trafficking to inflammatory sites includes arrest on the vascular endothelium, migration through the ECM and retention within the site. It depends on the monocyte/macrophage adhesion to molecules, such as VCAM-1, expressed on endothelial cells (Hart and Greaves, 2010). The exertion of this crucial first step, i.e., the adhesion to VCAM-1 under shear stress, was demonstrated for the DD-MLL-ENL macrophages suggesting the ability to initiate trafficking.

Within damaged or inflamed sites, macrophages are established for their characteristic functions in immunoregulation. These include clearance of pathogens and cellular debris, modulating inflammation and impacting cancer development. Dependent on the polarized state of the highly plastic macrophages, they are either associated with an anti-tumor (M1) or pro-tumor phenotype (M2). Anti-tumor M1 macrophages can perform phagocytosis and subsequent antigen presentation, critical features for T cell activation and efficient elimination of cancer cells. Phagocytosis of tumor cells was demonstrated *in vitro* for the DD-MLL-ENL derived macrophages in an antibody-dependent manner. The phagocytic capacity of the DD-MLL-ENL macrophages was comparable to M0 (M-CSF) and polarized M1 (GM-CSF + LPS + IFN- γ) macrophages, which were derived from PBMCs of healthy donors. Thus, it can be stated that the genetically engineered DD-MLL-ENL macrophages feature unimpaired ADCP property essential for tumor cell clearance. In addition, ADCP was demonstrated to be highly specific, as the DD-MLL-ENL derived macrophages did not engulf non-opsonized target cells most likely due to interaction with “Don’t eat me” signals such as CD47 (Morrissey et al., 2020). When CD47 was blocked on the target cells, increased ADCP was detected in the presence of the therapeutic antibody rituximab. These results are consistent with findings by Chao and colleagues who observed a significantly improved elimination of lymphoma cells in human NHL xenotransplant models when an anti-CD47 blocking antibody was used together with rituximab (Chao et al., 2010). In addition, Müller and colleagues demonstrated enhanced phagocytosis of T-ALL cell lines as well as T-ALL patient derived xenograft samples when an Fc-silent CD47 antibody was used in combination with the monoclonal antibody daratumumab (Muller et al., 2022). Within the tumor, most macrophages present a pro-tumor M2-like phenotype orchestrated by tumor-secreting cytokines. Therefore, various methods have been developed to shift the M1/M2 ratio towards the M1 side by reprogramming M2 macrophages. These include the use of small molecule inhibitors, neutralizing antibodies against the M-CSF/M-CSFR axis or the application of nanocarriers delivering M1-polarizing transcription factors such as interferon regulatory factor 5 (Zhang et al., 2019, Bart et al., 2021). As the DD-MLL-ENL macrophages derive from genetically engineered progenitor cells, the genes for such small molecules and transcription factors can be additionally inserted between the LTRs

of the DD-MLL-ENL retroviral vector. Furthermore, it needs to be elucidated, if the DD-MLL-ENL macrophages themselves are capable to induce a repolarization of the M2-like TAMs as it was demonstrated with anti-HER2 CAR macrophages by Klichinsky and colleagues. These anti-HER2 CAR macrophages were capable of remodeling the tumor microenvironment to acquire a pro-inflammatory status as illustrated by the enrichment of pro-inflammatory genes at single-cell resolution (Klichinsky et al., 2020).

4.3 Risk Assessment of Oncogenes as Expansion Factors

The usage of oncogenes for blood cell expansion purposes harbors safety concerns. First, MLL-ENL is a potent leukemia-associated fusion gene, which is strongly linked to both AML and ALL with dismal prognosis (Fu et al., 2007). For stable expression, integration into the host cells' genome was performed via retroviral transduction. Thus, although a regulable system was included (i.e., Shield-1-dependent degradation), continuous expression of the fusion gene in hematopoietic progenitor cells occurs. This sustained expression is considered a drawback even though terminally differentiated cells without residual proliferation capacity were manufactured and reapplying Shield-1 after differentiation did not result in outgrowth again. With a single domain controlling the degradation, mutational changes might render MLL-ENL independent of Shield-1 resulting in uncontrolled proliferation of DD-MLL-ENL progenitors. Thus, when the differentiated macrophages are applied for cell therapy purposes single residual undifferentiated cells within the cell population harboring such mutations might lead to uncontrolled cell growth. However, during a prolonged cultivation time of almost 2.5 years the proliferation of the DD-MLL-ENL progenitor cells strictly remained Shield-1 dependent *in vitro* at any time suggesting a fully functional destabilization domain. The destabilization domain is an FKBP12 mutant, which is unstructured and therefore targeted for proteasomal degradation (de Azevedo et al., 2012). Hence, an escape scenario is highly unlikely as several mutations must accumulate within the destabilization domain to retain the protein's structure preventing degradation. Up to date, no reports exist claiming such a loss of functionality due to mutational changes. Nevertheless, there are ways to further enhance the safety in this context. Beside the DD-Shield-1 system, the similar estrogen receptor-based gene regulation was proven a tightly controllable system as well. Redecke and colleagues were able to immortalize murine hematopoietic progenitor cells with defined subsequent differentiation when the hormone binding domain of the estrogen receptor was fused to HOXB8. Proteins fused to a hormone binding domain remained inactive in the absence of the ligand as the domain formed an inhibitory complex with a variety of proteins such as Hsp90. Following

ligand binding, the complex dissipated and the fused protein became functional (Whitfield et al., 2015). Consequently, in the presence of the ligand estrogen active HOXB8 induced expansion of immature myeloid cells while estrogen removal was associated with inactivation and subsequent differentiation of the expanded progenitors (Redecke et al., 2013). Another regulatory system represents the inducible gene expression via the tetracycline-controlled transcriptional activation (Gossen et al., 1995). By adapting such an element to MLL-ENL, Stavropoulou and colleagues were able to induce aberrant proliferation of HSPCs in the presence of doxycycline. As soon as doxycycline was removed, transcription was abrogated resulting in differentiation mainly towards macrophages (Stavropoulou et al., 2018). Combining an inducible system at the DNA level with the DD-Shield-1 protein turnover system might further strengthen the reliability and safety of using oncogenes for expansion of blood progenitor cells. To ultimately investigate residual leukemic transforming potential suitable *in vivo* models are required. For this purpose, Shield-1-depleted DD-MLL-ENL expressing progenitors could be injected into sub-lethally irradiated mice followed by monitoring of leukemia initiation. This issue is further delineated under 4.5.

A second concern is the use of γ -retroviral vectors, which are frequently employed to ensure stable expression of genes of interest. Due to efficient transduction of dividing cells and a long-term and stable transgene expression γ -retroviral vectors are commonly used for genetic engineering of various cell types (Maetzig et al., 2011). Indeed, two FDA-approved CAR T cell products, i.e., axicabtagene ciloleucel (Yescarta) and brexucabtagene autoleucel (Tecartus), are manufactured by the use of γ -retroviral vectors highlighting their convenience (Albinger et al., 2021). However, genetic modification via retroviral vectors can lead to unwanted so-called insertional mutagenesis, which can occur as a consequence of the virus' capacity to integrate the reverse transcribed cDNA into the host cell's genome. Dependent on the genomic locus, insertion might disrupt genes or repressor and enhancer regions leading to over- or underexpression of neighboring genes. This way, proto-oncogenes can be switched on ultimately resulting in oncogene activation (Irving et al., 2021). Such an aberrantly induced expression of the LMO2 proto-oncogene was identified in SCID-X1 patients, who received autologous CD34+ bone marrow cells, retrovirally engineered to express a healthy copy of the affected gene (Cavazza et al., 2013, Hacein-Bey-Abina et al., 2003). This overexpression led to an uncontrolled proliferation of mature T cells and leukemia in two patients. Such an oncogenic event, which is associated with outgrowth of single cells was not observed in the DD-MLL-ENL expansion system as verified by LM-PCR. Retroviral integration site analyses revealed an oligo- to polyclonal pattern without any reduction to monoclonality. In addition, the here detected neighboring genes

have not been described as either proto-oncogenes or tumor suppressor genes. However, the potential concern of inducing insertional mutagenesis can be addressed by altering the gene transfer method. Sticking to γ -retroviral vectors, strategies exist to retarget integration to genomic regions where integration is less likely to have an impact on gene dysregulation. Within the cell's nucleus the host bromodomain and extraterminal (BET) proteins play a crucial role in directing the retroviral integrase complex to the chromatin bearing transcriptionally active sites thereby defining integration. Hence, deleting or replacing the integrase peptide responsible for the interaction with the BET proteins allows alteration of the integration distribution. Consequently, the risk for insertional mutagenesis is reduced for the deletion variant and the variant where the peptide was replaced with a CBX1 chromodomain to bypass integration in gene regulatory elements (Loyola et al., 2019, El Ashkar et al., 2017). Another option to reduce the risk for integration-associated oncogene activation is the use of lentiviral vectors. In general, in comparison to retroviruses, which display an integration preference near promoter regions, lentiviruses integrate across the complete transcribed gene region including introns. In particular, promoter-proximal integration raises the risk of oncogenesis (Sinn et al., 2005).

Furthermore, non-integrating lentiviruses were developed to completely abrogate integration via introducing specific point mutations in the integrase or the recognition DNA sequence. Accordingly, the transgene is expressed transiently. This also applies to other non-integrating viruses such as adenoviruses, adeno-associated viruses or sendai viruses, which are used for the manufacture of iPSCs (Macarthur et al., 2012). Apart from the viral overexpression systems, two additional strategies allow stable transgene expression via integration into the genome. These comprise the sleeping beauty transposon system and the CRISPR-Cas9 system. The sleeping beauty system relies on the use of transposable elements, also known as jumping genes, in combination with a transposase (Ivics et al., 1997). The transposase recognizes and cuts out the transposable element, i.e. the gene of interest with characteristic repeats at both ends, and mediates integration into defined sites within the genome. As these sites represent TA dinucleotides, the system is linked with a random integration profile with 200 million sites (Kebriaei et al., 2017). The CRISPR-Cas9 system can be designed to efficiently lead to a knock-in at desired chromosomal sites. This was demonstrated by Kelly and colleagues by integrating three reporter genes at a so-called safe harbor locus which is not linked to alterations of the host genome or occurrence of oncogenic activation (Kelly et al., 2021). Thus, it remains to be demonstrated if such a strategy can be used for efficient transfer and incorporation of the DD-MLL-ENL construct at secure sites in the genome of HSPCs to ensure high and long-term expression.

A third safety concern is the potential occurrence of additional mutations during the expansion phase favoring uncontrolled, MLL-ENL independent proliferation. Rapidly proliferating cells are prone to acquisition of somatic mutations due to their high doubling rate. While it was shown that cells acquire approximately 1.14 mutations per division during healthy hematopoiesis *in vivo*, the mutation rate is considerably higher in *in vitro* expanded cells due to oxidative stress (Werner et al., 2020, Kuijk et al., 2020). This was demonstrated by *in vitro* cultivation of adult stem cells over a longer period, which led to a 40 times higher mutation rate compared to their *in vivo* counterpart. Interestingly, the mutation rate in MLL-AF9 transduced CD34+ cells *in vitro* was confirmed to be relatively low although the fusion protein strongly enhanced proliferation (Araten et al., 2013). This is in line with a mutation screening of various leukemia subtypes with different translocations where leukemia cells harboring an MLL fusion carry an exceedingly low number of additional mutations (Mullighan et al., 2007). Accordingly, the whole exome sequencing in this study did not reveal the occurrence of variants associated with oncogenesis during the outgrowth. It is worth mentioning that expansion for a long duration is not intended as a significant 1440-fold expansion, which was achieved within 23 days, is in principle sufficient for cell therapeutic approaches. Consequently, acquisition of additional mutations is highly unlikely.

Moreover, such oncogene-driven expansion models can be utilized for the large-scale manufacture of functional blood cells lacking a cell nucleus, such as erythrocytes and thrombocytes. This would further rule out safety concerns as the retrovirally integrated oncogene and the associated risk potential is eliminated with the loss of the nucleus. The principle of *in vitro* generated functional red blood cells was demonstrated with expanded iPSCs, which were first differentiated towards HSCs. Yet, manufacture of mature erythrocytes from iPSCs remains an inefficient process and is accompanied by high costs (Ebrahimi et al., 2020). Exploiting single oncogenes might therefore represent a promising alternative.

4.4 Comparison with Established Expansion Methods

The *in vitro* expansion of HSPCs remains a challenge (Ghafouri-Fard et al., 2021). During the last decades, significant efforts have been made to ensure sustained HSPCs proliferation *in vitro* without losing self-renewal properties. Within the bone marrow niche, a multifaceted interplay of extrinsic factors such as cell-cell contacts and auto- and paracrine secretion of cytokines regulates both HSC quiescence and self-renewal. Thus, approaches to mediate *ex vivo* expansion aimed for generating an *in vitro* microenvironment, which induces HSC symmetric cell division. Therefore, various

cytokines, which were identified to be secreted by niche cells and facilitate self-renewal *in vivo*, were investigated for their *in vitro* potential to ensure expansion. Combinations of SCF, Flt3-L, TPO, G-CSF, IL-3, IL-6 were shown to have a beneficial impact on the maintenance of HSC self-renewal. In particular, SCF in combination with TPO and Flt3-L provided increased proliferation of murine stem and progenitor cells *in vitro* (Yonemura et al., 1997, Sitnicka et al., 1996). However, such culture conditions generally ensured only moderate human HSPC expansion of up to 10-fold for a maximum of two weeks (Wilkinson et al., 2020, Bhatia et al., 1997). These findings emphasize that both the optimal combination of growth factors has not yet been determined and that additional environmental cues are necessary for replicating the bone marrow niche. Therefore, numerous studies focused on mimicking the bone marrow niche besides the soluble growth factors. Such niche factors include the ECM, other bone marrow residing cells and the characteristic 3D architecture (Kumar and Geiger, 2017). Biomaterial reflecting the ECM structure such as polyethylene terephthalate, tissue culture polystyrene and polyether sulfone failed to promote HSPC expansion *in vitro* (Laluppa et al., 1997). Yet, when polyethylene terephthalate was coated with fibronectin elevated numbers of HSPCs were obtained (Feng et al., 2006). Similar results were obtained when HSPCs were co-incubated with stromal cells, including endothelial and bone marrow derived MSCs, providing a supportive microenvironment *in vitro* (Wilkinson et al., 2020). The expression and secretion of Notch ligands by endothelial cells stimulated proliferation of murine HSCs and hampered exhaustion (Butler et al., 2010). MSCs were shown to provide a supportive microenvironment for HSCs in the bone marrow niche partially mediated by secretion of extracellular vesicles (Crippa and Bernardo, 2018). Accordingly, co-incubation studies demonstrated enhanced expansion of human cord blood hematopoietic progenitor cells (Robinson et al., 2006). Furthermore, the establishment of a 3D culture matrix using a degradable zwitterionic hydrogel promoted considerable expansion of CD34+ cord blood and bone marrow HSPCs. This was presumably due to the 3D structure as well as the hydrogel's characteristics to prevent the accumulation of reactive oxygen species (Bai et al., 2019). Although these approaches identified ways to keep up proliferation and self-renewal ability of human HSPCs *in vitro*, they either require complex 3D architecture or cumbersome co-culture and lack long-term expansion potential. In contrast, the potent fusion protein MLL-ENL, which ensures sustained proliferation and self-renewal, allows for convenient and efficient expansion of myeloid progenitor cells. This way, within 23 days a 1440-fold expansion could be achieved generating 7.2×10^8 cells with a calculated doubling time of 2.2 days. As the proliferation characteristic did not change over time, hypothetical

unlimited proliferation of immature cells can be accomplished with a theoretical cell count of 7.2×10^{130} within 2.5 years, starting with 0.5×10^6 cells.

Apart from mimicking the stem cell niche, several small molecule agonists of HSPC self-renewal were identified which led to substantial expansion. In particular, StemRegenin1 (SR1) and UM171 yielded promising results. SR1 acts as an aryl hydrocarbon receptor (AhR) antagonist thereby promoting expansion and preventing differentiation of human HSCs (Boitano et al., 2010). The AhR is expressed on HSPCs and regulates both differentiation and expansion dependent on its modulation (Smith et al., 2013). Antagonists, such as SR1, mitigate AhR signaling thereby facilitating symmetrical divisions of HSCs (Zhu et al., 2021). In the presence of SR1 and specific cytokines, a considerable 330-fold increase in CD34+ umbilical cord blood cells was achieved *in vitro*. In a phase I/II trial, infusion of these expanded cells was well tolerated while the cells retained multi-lineage potential and accelerated neutrophil and platelet recovery (Wagner et al., 2016). The second identified molecule UM171 is a pyrimidoindole derivate boosting *ex vivo* expansion of HSPCs by two different modes of actions. First, it orchestrates re-establishment of the H3K4me2 and H3K27ac epigenetic marks via CULLIN3-E3 ubiquitin ligase-mediated degradation of the CoREST demethylase/deacetylase complex. These two epigenetic marks are crucial for maintenance of self-renewal potential and generally decrease in *ex vivo* culture (Chagraoui et al., 2021). The second mechanisms is the induction of an inflammatory response resulting in the detoxification of reactive oxygen species (Chagraoui et al., 2019). Fares and colleagues demonstrated an up to 100-fold expansion of CD34+ cells after a 7-day culture in the presence of UM171 *in vitro* (Fares et al., 2014). Additionally, in phase I/II studies, transplantation of UM171-expanded CD34+ cord blood cells led to successful rapid engraftment of neutrophils and platelet recovery without signs of graft failure (Cohen et al., 2020). Although SR1- and UM171-mediated expansion of human CD34+ was proven to be feasible and safe for hematopoietic stem cell transplantation, the expansion time *in vitro* was limited. This limited expansion time might be not sufficient to manufacture immune cells *in vitro* in quantities relevant for cell therapeutic approaches. Such a restriction can be overcome with the use of MLL-ENL as expansion factor.

Another promising strategy to manufacture human cells in large-scale is the iPSC-based technology. The iPSC method relies on the dedifferentiation of somatic cells via reprogramming using the four Yamanaka factors. The resulting pluripotent stem cell-like cells can be expanded and subsequently differentiated into virtually any kind of cell type including hematopoietic cells such as macrophages. Although several groups already demonstrated efficient manufacture of macrophages, which display similar

morphological and functional features in comparison to their primary unmodified counterparts, the iPSC technology holds drawbacks (Gutbier et al., 2020, Monkley et al., 2020, Ackermann et al., 2022). Manufacture of iPSCs by reprogramming constitutes a time-consuming, costly and elaborate technique. The first critical step is the selection of the donor cell type, typically fibroblast, keratinocytes or T cells, which might impact the eventual differential potential of the originated iPSCs. Various groups have demonstrated that the somatic cells, which are used as starting material exhibit residual epigenetic memory thereby restricting full pluripotency (Bar-Nur et al., 2011, Boland et al., 2014). Once established by transducing four factors in comparison to the single genetic element DD-MLL-ENL in this study, iPSC populations often exhibit a critical heterogeneity. This results in a lack of maturity when specified differentiation protocols are applied accompanied by the risk of potential tumorigenicity. Thus, residual undifferentiated iPSCs can induce malignant tumors including neuroblastoma, carcinoma as well as teratoma formation (Okita et al., 2007). Additionally, genetic instability is a concern associated with iPSC manufacture. Apart from the use of somatic cells such as fibroblast, which might already carry mutations and chromosomal abnormalities because of UV exposure and elevated turnover rates, genetic instability is often observed in combination with *in vitro* expansion of iPSCs (Kim et al., 2017). Currently, directed differentiation of iPSCs into hematopoietic cells remains inefficient with relatively low numbers of reprogrammed HSPCs, which would require expansion for therapeutic approaches (Haase et al., 2019). Although restricted to the granulocytic-monocytic lineage compared to the pluripotency of iPSCs, all of these described limitations can be circumvented by the use of the DD-MLL-ENL expansion system. With a single transduction step and subsequent liquid culture expansion without the need for laborious characterization and isolation of single clones, the here presented method represents an unsophisticated, cost-effective and strictly controlled method to obtain highly homogeneous, terminally differentiated, and fully functional macrophages.

A further important advantage of the here described DD-MLL-ENL expansion method is the convenient vector inclusion of additional genetic elements such as genes encoding pro-inflammatory cytokines or CARs directed against tumor cells to orchestrate efficient phagocytosis. Macrophages feature an inherent insensitive nature to genetic manipulation rendering gene transfer into macrophages a longstanding challenge (Zhang et al., 2009). As transduction takes place at the progenitor cell level in this system, this complex and often ineffective genetic engineering can be avoided. Although transduction of macrophages was demonstrated by Klichinsky and colleagues by using a replication-incompetent chimeric adenoviral vector (Ad5f35) in order to manufacture CAR macrophages, transduction of progenitors shows several advantages including

easy handling, higher vector flexibility and large retro- and lentiviral vector sizes (Klichinsky et al., 2020). In addition, no selection or isolation steps are required as the transduced cells exhibit a proliferation advantage leading to complete outgrowth linked with the expression of the genetic element of choice. This way, CAR macrophages may be easily manufactured by further upgrading the DD-MLL-ENL vector to comprise the necessary CAR cDNA elements in an all-in-one plasmid.

4.5 Consideration for Clinical Application: What Follow-Up Steps Are Required?

The controllable exploitation of the leukemia-associated transcription factor MLL-ENL described in this thesis represents a promising method for the large-scale manufacture of functional human macrophages. This system might become relevant for cell therapeutic approaches as it displays an unsophisticated and rapid way to generate high numbers of immune cells *in vitro* thereby fulfilling an unmet need. A premise for clinical application is the manufacture of the cell product according to Good Manufacturing Practice (GMP) guidelines to ensure high quality and consistency from batch to batch (Bedford et al., 2018). In this context, DD-MLL-ENL macrophages must be generated in GMP compliant serum-free culture media containing GMP grade cytokines and other supplements. In general, the development of cell-based medicinal products relies on data obtained from *in vitro* studies as well as from testing in animals and ultimately in patients (McBlane et al., 2018). In the first step, primary toxicity and pharmacology studies are required to demonstrate the cellular product's safety and activity and constitute that the use of this product could provide a benefit for a specified medical condition. In this thesis, these steps were already validated *in vitro* for the DD-MLL-ENL macrophages. As an oncogene is exploited for the manufacture of the macrophages, verification of the product's safety *in vivo* is of paramount importance. For this purpose, DD-MLL-ENL macrophages and even expanded, Shield-1 depleted DD-MLL-ENL progenitor cells can be injected into sub-lethally irradiated NSG mice to evaluate the toxicity and malignancy. A similar approach was outlined by Stavropoulou and colleagues who investigated AML initiation and maintenance in transgenic mice with doxycycline-inducible MLL-AF9 expression (Stavropoulou et al., 2016). They demonstrated that a continuous exposure to doxycycline doses above a certain threshold leading to MLL-AF9 expression is required to initiate and maintain leukemia in mice. In the absence of doxycycline, the mice did not develop AML. In addition, doxycycline removal induced differentiation of the cells and enabled long-term survival of the mice,

which were previously exposed to doxycycline. Such a toxicity study provides the base for subsequent activity and benefit studies in a certain disease background, e.g., cancer.

To target the DD-MLL-ENL macrophages to tumor sites, and therefore address a specified medical condition as required, these macrophages can be further modified by genetic engineering. This could be easily achieved by inserting an additional expression cassette between the LTRs of the original retroviral vector containing DD-MLL-ENL without the need to elaborately transduce the manufactured macrophages. For this purpose, various genetic elements together with a promoter of choice can be introduced to further enhance the macrophages' efficacy. Such elements include the pro-inflammatory cytokines IL-12 and IFN- α , checkpoint inhibitors such as an anti-CTLA-4 antibody or CAR constructs. As these modifications tend to boost efficient tumor clearance and ensure a pro-inflammatory environment, particularly in solid tumors, suitable *in vitro* approaches have to be designed. In particular, CAR macrophages can be directed against tumor antigens expressed on cancer cells in tumors of the hematopoietic system (e.g. CD19 for B-lineage ALL or lymphomas) and solid tumors (e.g. HER2 for breast, colorectal or lung cancer). Therefore, the macrophages produced can be genetically engineered to express a CD19- or HER2-CAR and examined for their ability to phagocytose cancer cells *in vitro*. Until 2022, two clinical trials with CAR macrophages received FDA-approval. These include anti-HER2 CAR macrophages developed by CARISMA Therapeutics (Philadelphia, PA, USA) and mesothelin-targeting CAR macrophages developed by MaxCyte (Gaithersburg, MD, USA). Especially the anti-HER2 CAR macrophages demonstrated improved overall survival in a preclinical model of HER2-positive cancer and were therefore granted a fast track designation by the FDA (Chen et al., 2021). As soon as successful genetic engineering of the DD-MLL-ENL macrophages is verified and *in vitro* proof of principle studies are conducted, such preclinical *in vivo* studies would be the next step. For these *in vivo* studies animal models replicating the target disease are used. With the example of CAR macrophages directed against either CD19 or HER2, standardized immunocompromised NSG mouse tumor models with xeno-transplanted human primary material, such as CD19+ leukemia samples or cell line-derived cells (HER2+ SKOV3) can be used. This way, the activity of the engineered macrophages can be characterized including evaluation of the biodistribution, persistence and toxicity (McBlane et al., 2018).

Apart from addressing cancer, these large-scale manufactured macrophages could potentially be applied for other diseases, e.g., chronic granulomatous disease, where macrophages play a pivotal role. Chronic granulomatous disease is a primary immunodeficiency disorder causing malfunction of phagocytes, which results in accumulation of bacterial and fungi infections (Roos, 2019). Substitution of *ex vivo*

produced functional monocytes co-expressing a functional $gp91^{phox}$ gene, which is mutated in most of the cases, represents a further rational perspective. Accordingly, suitable *in vitro* and *in vivo* assays must be performed to demonstrate a benefit in treatment of this particular disease and ensure a safe therapy.

In conclusion, exploiting the regulable leukemia-associated transcription factor DD-MLL-ENL enables large-scale and long-term expansion of myeloid progenitor cells *in vitro*, which is not alternatively feasible due to rapid differentiation. These progenitors can be differentiated into functional macrophages at an arbitrary time point. The utilized retroviral vector can be additionally modified to facilitate continuous expression of various proteins, such as cytokines or receptors, boosting activity and enhancing specificity. Such promising expansion and engineering systems might become relevant for cell therapy approaches as they counteract current limitations, such as the restricted macrophage cell count and the challenge to genetically modify macrophages (Figure 44).

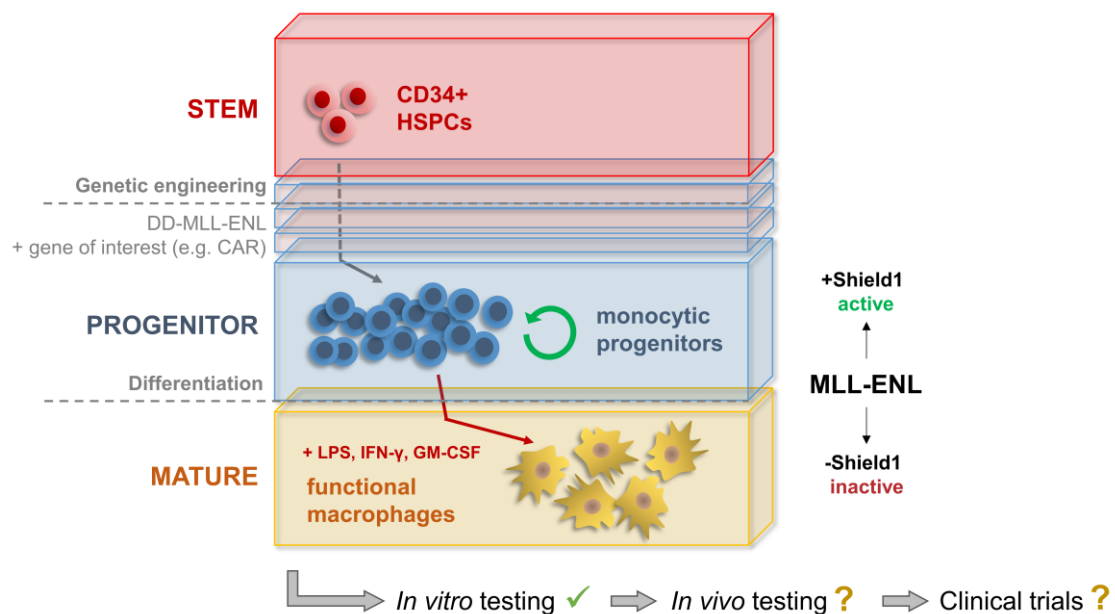


Figure 44: Graphical scheme of the macrophage manufacturing process for potential cell therapeutic approaches.

Isolated CD34+ HSPCs from healthy donors are transduced with a retroviral vector containing the regulable DD-MLL-ENL and additional genes of interest such as a CAR construct directed against tumor antigens. In medium containing myeloid-associated cytokines, monocytic progenitors can be massively expanded in the presence of Shield-1. At an arbitrary time point, Shield-1 can be withdrawn resulting in the rapid degradation of MLL-ENL and differentiation into macrophages in the presence of GM-CSF, IFN- γ and LPS. These macrophages are fully functional in *in vitro* assays and lack residual proliferation capacity. To be considered for clinical trials, these genetically engineered macrophages must be thoroughly characterized *in vivo* for their biodistribution, persistence and activity using suitable animal models.

List of References

- Abdul-Nabi, A. M., Yassin, E. R., Varghese, N., Deshmukh, H. & Yaseen, N. R. 2010. In vitro transformation of primary human CD34+ cells by AML fusion oncogenes: early gene expression profiling reveals possible drug target in AML. *PLoS One*, 5, e12464.
- Abramovich, C., Pineault, N., Ohta, H. & Humphries, R. K. 2005. Hox genes: from leukemia to hematopoietic stem cell expansion. *Ann N Y Acad Sci*, 1044, 109-16.
- Ackermann, M., Rafiei Hashtchin, A., Manstein, F., Carvalho Oliveira, M., Kempf, H., Zweigerdt, R. & Lachmann, N. 2022. Continuous human iPSC-macrophage mass production by suspension culture in stirred tank bioreactors. *Nat Protoc*, 17, 513-539.
- Adolfsson, J., Mansson, R., Buza-Vidas, N., Hultquist, A., Liuba, K., Jensen, C. T., Bryder, D., Yang, L., Borge, O. J., Thoren, L. A., Anderson, K., Sitnicka, E., Sasaki, Y., Sigvardsson, M. & Jacobsen, S. E. 2005. Identification of Flt3+ lympho-myeloid stem cells lacking erythro-megakaryocytic potential a revised road map for adult blood lineage commitment. *Cell*, 121, 295-306.
- Advani, R., Flinn, I., Popplewell, L., Forero, A., Bartlett, N. L., Ghosh, N., Kline, J., Roschewski, M., LaCasce, A., Collins, G. P., Tran, T., Lynn, J., Chen, J. Y., Volkmer, J. P., Agoram, B., Huang, J., Majeti, R., Weissman, I. L., Takimoto, C. H., Chao, M. P. & Smith, S. M. 2018. CD47 Blockade by Hu5F9-G4 and Rituximab in Non-Hodgkin's Lymphoma. *N Engl J Med*, 379, 1711-1721.
- Ajami, B., Bennett, J. L., Krieger, C., Tetzlaff, W. & Rossi, F. M. 2007. Local self-renewal can sustain CNS microglia maintenance and function throughout adult life. *Nat Neurosci*, 10, 1538-43.
- Akashi, K., Traver, D., Miyamoto, T. & Weissman, I. L. 2000. A clonogenic common myeloid progenitor that gives rise to all myeloid lineages. *Nature*, 404, 193-7.
- Albinger, N., Hartmann, J. & Ullrich, E. 2021. Current status and perspective of CAR-T and CAR-NK cell therapy trials in Germany. *Gene Ther*, 28, 513-527.
- Ambarus, C. A., Krausz, S., van Eijk, M., Hamann, J., Radstake, T. R., Reedquist, K. A., Tak, P. P. & Baeten, D. L. 2012. Systematic validation of specific phenotypic markers for in vitro polarized human macrophages. *J Immunol Methods*, 375, 196-206.
- Anania, J. C., Chenoweth, A. M., Wines, B. D. & Hogarth, P. M. 2019. The Human FcγRIIb (CD32) Family of Leukocyte FcR in Health and Disease. *Front Immunol*, 10, 464.
- Anderson, K. G., Stromnes, I. M. & Greenberg, P. D. 2017. Obstacles Posed by the Tumor Microenvironment to T cell Activity: A Case for Synergistic Therapies. *Cancer Cell*, 31, 311-325.
- Araten, D. J., Krejci, O., Ditata, K., Wunderlich, M., Sanders, K. J., Zamechek, L. & Mulloy, J. C. 2013. The rate of spontaneous mutations in human myeloid cells. *Mutat Res*, 749, 49-57.
- Arber, D. A., Orazi, A., Hasserjian, R., Thiele, J., Borowitz, M. J., Le Beau, M. M., Bloomfield, C. D., Cazzola, M. & Vardiman, J. W. 2016. The 2016 revision to the World Health Organization classification of myeloid neoplasms and acute leukemia. *Blood*, 127, 2391-405.
- Asada, N., Kunisaki, Y., Pierce, H., Wang, Z., Fernandez, N. F., Birbrair, A., Ma'ayan, A. & Frenette, P. S. 2017a. Differential cytokine contributions of perivascular haematopoietic stem cell niches. *Nat Cell Biol*, 19, 214-223.
- Asada, N., Takeishi, S. & Frenette, P. S. 2017b. Complexity of bone marrow hematopoietic stem cell niche. *Int J Hematol*, 106, 45-54.
- Audet, J., Miller, C. L., Eaves, C. J. & Piret, J. M. 2002. Common and distinct features of cytokine effects on hematopoietic stem and progenitor cells revealed by dose-response surface analysis. *Biotechnol Bioeng*, 80, 393-404.
- Auffray, C., Sieweke, M. H. & Geissmann, F. 2009. Blood monocytes: development, heterogeneity, and relationship with dendritic cells. *Annu Rev Immunol*, 27, 669-92.

- Ayton, P. M. & Cleary, M. L. 2003. Transformation of myeloid progenitors by MLL oncoproteins is dependent on Hoxa7 and Hoxa9. *Genes Dev*, 17, 2298-307.
- Bai, T., Li, J., Sinclair, A., Imren, S., Merriam, F., Sun, F., O'Kelly, M. B., Nourigat, C., Jain, P., Delrow, J. J., Basom, R. S., Hung, H. C., Zhang, P., Li, B., Heimfeld, S., Jiang, S. & Delaney, C. 2019. Expansion of primitive human hematopoietic stem cells by culture in a zwitterionic hydrogel. *Nat Med*, 25, 1566-1575.
- Baker, K. S., DeFor, T. E., Burns, L. J., Ramsay, N. K., Neglia, J. P. & Robison, L. L. 2003. New malignancies after blood or marrow stem-cell transplantation in children and adults: incidence and risk factors. *J Clin Oncol*, 21, 1352-8.
- Baldrige, M. T., King, K. Y., Boles, N. C., Weksberg, D. C. & Goodell, M. A. 2010. Quiescent haematopoietic stem cells are activated by IFN-gamma in response to chronic infection. *Nature*, 465, 793-7.
- Balkwill, F. R. & Mantovani, A. 2012. Cancer-related inflammation: common themes and therapeutic opportunities. *Semin Cancer Biol*, 22, 33-40.
- Ballabio, E. & Milne, T. A. 2014. Epigenetic control of gene expression in leukemogenesis: Cooperation between wild type MLL and MLL fusion proteins. *Mol Cell Oncol*, 1, e955330.
- Ballen, K. K., Koreth, J., Chen, Y. B., Dey, B. R. & Spitzer, T. R. 2012. Selection of optimal alternative graft source: mismatched unrelated donor, umbilical cord blood, or haploidentical transplant. *Blood*, 119, 1972-80.
- Banaszynski, L. A., Chen, L. C., Maynard-Smith, L. A., Ooi, A. G. & Wandless, T. J. 2006. A rapid, reversible, and tunable method to regulate protein function in living cells using synthetic small molecules. *Cell*, 126, 995-1004.
- Bar-Nur, O., Russ, H. A., Efrat, S. & Benvenisty, N. 2011. Epigenetic memory and preferential lineage-specific differentiation in induced pluripotent stem cells derived from human pancreatic islet beta cells. *Cell Stem Cell*, 9, 17-23.
- Barabe, F., Kennedy, J. A., Hope, K. J. & Dick, J. E. 2007. Modeling the initiation and progression of human acute leukemia in mice. *Science*, 316, 600-4.
- Bart, V. M. T., Pickering, R. J., Taylor, P. R. & Ipseiz, N. 2021. Macrophage reprogramming for therapy. *Immunology*, 163, 128-144.
- Barton, G. M. & Medzhitov, R. 2003. Toll-like receptor signaling pathways. *Science*, 300, 1524-5.
- Basilico, S., Wang, X., Kennedy, A., Tzelepis, K., Giotopoulos, G., Kinston, S. J., Quiros, P. M., Wong, K., Adams, D. J., Carnevalli, L. S., Huntly, B. J. P., Vassiliou, G. S., Calero-Nieto, F. J. & Gottgens, B. 2020. Dissecting the early steps of MLL induced leukaemogenic transformation using a mouse model of AML. *Nat Commun*, 11, 1407.
- Bazinet, A. & Popradi, G. 2019. A general practitioner's guide to hematopoietic stem-cell transplantation. *Curr Oncol*, 26, 187-191.
- Becker, A. J., Mc, C. E. & Till, J. E. 1963. Cytological demonstration of the clonal nature of spleen colonies derived from transplanted mouse marrow cells. *Nature*, 197, 452-4.
- Bedford, P., Jy, J., Collins, L. & Keizer, S. 2018. Considering Cell Therapy Product "Good Manufacturing Practice" Status. *Front Med (Lausanne)*, 5, 118.
- Ben Mkaddem, S., Benhamou, M. & Monteiro, R. C. 2019. Understanding Fc Receptor Involvement in Inflammatory Diseases: From Mechanisms to New Therapeutic Tools. *Front Immunol*, 10, 811.
- Bendle, G. M., Linnemann, C., Hooijkaas, A. I., Bies, L., de Witte, M. A., Jorritsma, A., Kaiser, A. D., Pouw, N., Debets, R., Kieback, E., Uckert, W., Song, J. Y., Haanen, J. B. & Schumacher, T. N. 2010. Lethal graft-versus-host disease in mouse models of T cell receptor gene therapy. *Nat Med*, 16, 565-70, 1p following 570.
- Bennett, J. M., Catovsky, D., Daniel, M. T., Flandrin, G., Galton, D. A., Gralnick, H. R. & Sultan, C. 1976. Proposals for the classification of the acute leukaemias. French-American-British (FAB) co-operative group. *Br J Haematol*, 33, 451-8.

- Beroukhim, R., Mermel, C. H., Porter, D., Wei, G., Raychaudhuri, S., Donovan, J., Barretina, J., Boehm, J. S., Dobson, J., Urashima, M., Mc Henry, K. T., Pinchback, R. M., Ligon, A. H., Cho, Y. J., Haery, L., Greulich, H., Reich, M., Winckler, W., Lawrence, M. S., Weir, B. A., Tanaka, K. E., Chiang, D. Y., Bass, A. J., Loo, A., Hoffman, C., Prensner, J., Liefeld, T., Gao, Q., Yecies, D., Signoretti, S., Maher, E., Kaye, F. J., Sasaki, H., Tepper, J. E., Fletcher, J. A., Taberero, J., Baselga, J., Tsao, M. S., Demichelis, F., Rubin, M. A., Janne, P. A., Daly, M. J., Nucera, C., Levine, R. L., Ebert, B. L., Gabriel, S., Rustgi, A. K., Antonescu, C. R., Ladanyi, M., Letai, A., Garraway, L. A., Loda, M., Beer, D. G., True, L. D., Okamoto, A., Pomeroy, S. L., Singer, S., Golub, T. R., Lander, E. S., Getz, G., Sellers, W. R. & Meyerson, M. 2010. The landscape of somatic copy-number alteration across human cancers. *Nature*, 463, 899-905.
- Betermier, M., Bertrand, P. & Lopez, B. S. 2014. Is non-homologous end-joining really an inherently error-prone process? *PLoS Genet*, 10, e1004086.
- Bhatia, M., Bonnet, D., Kapp, U., Wang, J. C., Murdoch, B. & Dick, J. E. 1997. Quantitative analysis reveals expansion of human hematopoietic repopulating cells after short-term ex vivo culture. *J Exp Med*, 186, 619-24.
- Bhatia, R., Holtz, M., Niu, N., Gray, R., Snyder, D. S., Sawyers, C. L., Arber, D. A., Slovak, M. L. & Forman, S. J. 2003. Persistence of malignant hematopoietic progenitors in chronic myelogenous leukemia patients in complete cytogenetic remission following imatinib mesylate treatment. *Blood*, 101, 4701-7.
- Bianchi, E., Molteni, R., Pardi, R. & Dubini, G. 2013. Microfluidics for in vitro biomimetic shear stress-dependent leukocyte adhesion assays. *J Biomech*, 46, 276-83.
- Bigley, V., Haniffa, M., Doulatov, S., Wang, X. N., Dickinson, R., McGovern, N., Jardine, L., Pagan, S., Dimmick, I., Chua, I., Wallis, J., Lordan, J., Morgan, C., Kumararatne, D. S., Doffinger, R., van der Burg, M., van Dongen, J., Cant, A., Dick, J. E., Hambleton, S. & Collin, M. 2011. The human syndrome of dendritic cell, monocyte, B and NK lymphoid deficiency. *J Exp Med*, 208, 227-34.
- Bitan, M., He, W., Zhang, M. J., Abdel-Azim, H., Ayas, M. F., Bielorai, B., Carpenter, P. A., Cairo, M. S., Diaz, M. A., Horan, J. T., Jodele, S., Kitko, C. L., Schultz, K. R., Kletzel, M., Kasow, K. A., Lehmann, L. E., Mehta, P. A., Shah, N., Pulsipher, M. A., Prestidge, T., Seber, A., Shenoy, S., Woolfrey, A. E., Yu, L. C. & Davies, S. M. 2014. Transplantation for children with acute myeloid leukemia: a comparison of outcomes with reduced intensity and myeloablative regimens. *Blood*, 123, 1615-20.
- Bleakley, M. & Riddell, S. R. 2004. Molecules and mechanisms of the graft-versus-leukaemia effect. *Nat Rev Cancer*, 4, 371-80.
- Boitano, A. E., Wang, J., Romeo, R., Bouchez, L. C., Parker, A. E., Sutton, S. E., Walker, J. R., Flaveny, C. A., Perdew, G. H., Denison, M. S., Schultz, P. G. & Cooke, M. P. 2010. Aryl hydrocarbon receptor antagonists promote the expansion of human hematopoietic stem cells. *Science*, 329, 1345-8.
- Boland, M. J., Nazor, K. L. & Loring, J. F. 2014. Epigenetic regulation of pluripotency and differentiation. *Circ Res*, 115, 311-24.
- Boulais, P. E. & Frenette, P. S. 2015. Making sense of hematopoietic stem cell niches. *Blood*, 125, 2621-9.
- Boussif, O., Lezoualc'h, F., Zanta, M. A., Mergny, M. D., Scherman, D., Demeneix, B. & Behr, J. P. 1995. A versatile vector for gene and oligonucleotide transfer into cells in culture and in vivo: polyethylenimine. *Proc Natl Acad Sci U S A*, 92, 7297-301.
- Bradford, M. M. 1976. A rapid and sensitive method for the quantitation of microgram quantities of protein utilizing the principle of protein-dye binding. *Anal Biochem*, 72, 248-54.
- Braendstrup, P., Levine, B. L. & Ruella, M. 2020. The long road to the first FDA-approved gene therapy: chimeric antigen receptor T cells targeting CD19. *Cytotherapy*, 22, 57-69.
- Branco, A., Bucar, S., Moura-Sampaio, J., Lilaia, C., Cabral, J. M. S., Fernandes-Platzgummer, A. & Lobato da Silva, C. 2020. Tailored Cytokine Optimization for ex vivo Culture Platforms Targeting the Expansion of Human Hematopoietic Stem/Progenitor Cells. *Front Bioeng Biotechnol*, 8, 573282.

- Broxmeyer, H. E., Cooper, S. & Capitano, M. L. 2020. Enhanced collection of phenotypic and engrafting human cord blood hematopoietic stem cells at 4 degrees C. *Stem Cells*, 38, 1326-1331.
- Brudno, J. N. & Kochenderfer, J. N. 2019. Recent advances in CAR T-cell toxicity: Mechanisms, manifestations and management. *Blood Rev*, 34, 45-55.
- Burnette, W. N. 1981. "Western blotting": electrophoretic transfer of proteins from sodium dodecyl sulfate--polyacrylamide gels to unmodified nitrocellulose and radiographic detection with antibody and radioiodinated protein A. *Anal Biochem*, 112, 195-203.
- Butler, J. M., Nolan, D. J., Vertes, E. L., Varnum-Finney, B., Kobayashi, H., Hooper, A. T., Seandel, M., Shido, K., White, I. A., Kobayashi, M., Witte, L., May, C., Shawber, C., Kimura, Y., Kitajewski, J., Rosenwaks, Z., Bernstein, I. D. & Rafii, S. 2010. Endothelial cells are essential for the self-renewal and repopulation of Notch-dependent hematopoietic stem cells. *Cell Stem Cell*, 6, 251-64.
- Buza-Vidas, N., Antonchuk, J., Qian, H., Mansson, R., Luc, S., Zandi, S., Anderson, K., Takaki, S., Nygren, J. M., Jensen, C. T. & Jacobsen, S. E. 2006. Cytokines regulate postnatal hematopoietic stem cell expansion: opposing roles of thrombopoietin and LNK. *Genes Dev*, 20, 2018-23.
- Calvo, K. R., Sykes, D. B., Pasillas, M. & Kamps, M. P. 2000. Hoxa9 immortalizes a granulocyte-macrophage colony-stimulating factor-dependent promyelocyte capable of biphenotypic differentiation to neutrophils or macrophages, independent of enforced meis expression. *Mol Cell Biol*, 20, 3274-85.
- Canton, M., Sanchez-Rodriguez, R., Spera, I., Venegas, F. C., Favia, M., Viola, A. & Castegna, A. 2021. Reactive Oxygen Species in Macrophages: Sources and Targets. *Front Immunol*, 12, 734229.
- Cavazza, A., Moiani, A. & Mavilio, F. 2013. Mechanisms of retroviral integration and mutagenesis. *Hum Gene Ther*, 24, 119-31.
- Chabannon, C., Kuball, J., Bondanza, A., Dazzi, F., Pedrazzoli, P., Toubert, A., Ruggeri, A., Fleischhauer, K. & Bonini, C. 2018. Hematopoietic stem cell transplantation in its 60s: A platform for cellular therapies. *Sci Transl Med*, 10.
- Chagastelles, P. C. & Nardi, N. B. 2011. Biology of stem cells: an overview. *Kidney Int Suppl* (2011), 1, 63-67.
- Chagraoui, J., Girard, S., Spinella, J. F., Simon, L., Bonneil, E., Mayotte, N., MacRae, T., Coulombe-Huntington, J., Bertomeu, T., Moison, C., Tomellini, E., Thibault, P., Tyers, M., Marinier, A. & Sauvageau, G. 2021. UM171 Preserves Epigenetic Marks that Are Reduced in Ex Vivo Culture of Human HSCs via Potentiation of the CLR3-KBTBD4 Complex. *Cell Stem Cell*, 28, 48-62 e6.
- Chagraoui, J., Lehnertz, B., Girard, S., Spinella, J. F., Fares, I., Tomellini, E., Mayotte, N., Corneau, S., MacRae, T., Simon, L. & Sauvageau, G. 2019. UM171 induces a homeostatic inflammatory-detoxification response supporting human HSC self-renewal. *PLoS One*, 14, e0224900.
- Chan, A. K. N. & Chen, C. W. 2019. Rewiring the Epigenetic Networks in MLL-Rearranged Leukemias: Epigenetic Dysregulation and Pharmacological Interventions. *Front Cell Dev Biol*, 7, 81.
- Chanavaz, M. 1995. Anatomy and histophysiology of the periosteum: quantification of the periosteal blood supply to the adjacent bone with 85Sr and gamma spectrometry. *J Oral Implantol*, 21, 214-9.
- Chandran, S. S. & Klebanoff, C. A. 2019. T cell receptor-based cancer immunotherapy: Emerging efficacy and pathways of resistance. *Immunol Rev*, 290, 127-147.
- Chang, P. Y., Hom, R. A., Musselman, C. A., Zhu, L., Kuo, A., Gozani, O., Kutateladze, T. G. & Cleary, M. L. 2010. Binding of the MLL PHD3 finger to histone H3K4me3 is required for MLL-dependent gene transcription. *J Mol Biol*, 400, 137-44.
- Chao, M. P., Alizadeh, A. A., Tang, C., Myklebust, J. H., Varghese, B., Gill, S., Jan, M., Cha, A. C., Chan, C. K., Tan, B. T., Park, C. Y., Zhao, F., Kohrt, H. E., Malumbres, R., Briones,

- J., Gascoyne, R. D., Lossos, I. S., Levy, R., Weissman, I. L. & Majeti, R. 2010. Anti-CD47 antibody synergizes with rituximab to promote phagocytosis and eradicate non-Hodgkin lymphoma. *Cell*, 142, 699-713.
- Chao, M. P., Majeti, R. & Weissman, I. L. 2011. Programmed cell removal: a new obstacle in the road to developing cancer. *Nat Rev Cancer*, 12, 58-67.
- Chao, M. P., Weissman, I. L. & Majeti, R. 2012. The CD47-SIRPalpha pathway in cancer immune evasion and potential therapeutic implications. *Curr Opin Immunol*, 24, 225-32.
- Chapuis, A. G., Egan, D. N., Bar, M., Schmitt, T. M., McAfee, M. S., Paulson, K. G., Voillet, V., Gottardo, R., Ragnarsson, G. B., Bleakley, M., Yeung, C. C., Muhlhauser, P., Nguyen, H. N., Kropp, L. A., Castelli, L., Wagener, F., Hunter, D., Lindberg, M., Cohen, K., Seese, A., McElrath, M. J., Duerkopp, N., Gooley, T. A. & Greenberg, P. D. 2019. T cell receptor gene therapy targeting WT1 prevents acute myeloid leukemia relapse post-transplant. *Nat Med*, 25, 1064-1072.
- Chavez-Galan, L., Olleros, M. L., Vesin, D. & Garcia, I. 2015. Much More than M1 and M2 Macrophages, There are also CD169(+) and TCR(+) Macrophages. *Front Immunol*, 6, 263.
- Chen, L., Sun, Y., Wang, J., Jiang, H. & Muntean, A. G. 2016. Differential regulation of the c-Myc/Lin28 axis discriminates subclasses of rearranged MLL leukemia. *Oncotarget*, 7, 25208-23.
- Chen, W., Kumar, A. R., Hudson, W. A., Li, Q., Wu, B., Staggs, R. A., Lund, E. A., Sam, T. N. & Kersey, J. H. 2008. Malignant transformation initiated by MLL-AF9: gene dosage and critical target cells. *Cancer Cell*, 13, 432-40.
- Chen, Y., Yu, Z., Tan, X., Jiang, H., Xu, Z., Fang, Y., Han, D., Hong, W., Wei, W. & Tu, J. 2021. CAR-macrophage: A new immunotherapy candidate against solid tumors. *Biomed Pharmacother*, 139, 111605.
- Chen, Y. H., Keiser, M. S. & Davidson, B. L. 2018. Viral Vectors for Gene Transfer. *Curr Protoc Mouse Biol*, 8, e58.
- Cheshier, S. H., Morrison, S. J., Liao, X. & Weissman, I. L. 1999. In vivo proliferation and cell cycle kinetics of long-term self-renewing hematopoietic stem cells. *Proc Natl Acad Sci U S A*, 96, 3120-5.
- Chu, B. W., Banaszynski, L. A., Chen, L. C. & Wandless, T. J. 2008. Recent progress with FKBP-derived destabilizing domains. *Bioorg Med Chem Lett*, 18, 5941-4.
- Chung, K. Y., Morrone, G., Schuringa, J. J., Plasilova, M., Shieh, J. H., Zhang, Y., Zhou, P. & Moore, M. A. 2006. Enforced expression of NUP98-HOXA9 in human CD34(+) cells enhances stem cell proliferation. *Cancer Res*, 66, 11781-91.
- Cohen, S., Roy, J., Lachance, S., Delisle, J. S., Marinier, A., Busque, L., Roy, D. C., Barabe, F., Ahmad, I., Bambace, N., Bernard, L., Kiss, T., Bouchard, P., Caudrelier, P., Landais, S., Larochelle, F., Chagraoui, J., Lehnertz, B., Corneau, S., Tomellini, E., van Kampen, J. J. A., Cornelissen, J. J., Dumont-Lagace, M., Tanguay, M., Li, Q., Lemieux, S., Zandstra, P. W. & Sauvageau, G. 2020. Hematopoietic stem cell transplantation using single UM171-expanded cord blood: a single-arm, phase 1-2 safety and feasibility study. *Lancet Haematol*, 7, e134-e145.
- Connelly, J. A., Choi, S. W. & Levine, J. E. 2012. Hematopoietic stem cell transplantation for severe congenital neutropenia. *Curr Opin Hematol*, 19, 44-51.
- Cosgrove, M. S. & Patel, A. 2010. Mixed lineage leukemia: a structure-function perspective of the MLL1 protein. *FEBS J*, 277, 1832-42.
- Cozzio, A., Passegue, E., Ayton, P. M., Karsunky, H., Cleary, M. L. & Weissman, I. L. 2003. Similar MLL-associated leukemias arising from self-renewing stem cells and short-lived myeloid progenitors. *Genes Dev*, 17, 3029-35.
- Crippa, S. & Bernardo, M. E. 2018. Mesenchymal Stromal Cells: Role in the BM Niche and in the Support of Hematopoietic Stem Cell Transplantation. *Hemasphere*, 2, e151.
- Dalby, E., Christensen, S. M., Wang, J., Hamidzadeh, K., Chandrasekaran, P., Hughitt, V. K., Tafuri, W. L., Arantes, R. M. E., Rodrigues, I. A., Herbst, R., El-Sayed, N. M., Sims, G.

- P. & Mosser, D. M. 2020. Immune Complex-Driven Generation of Human Macrophages with Anti-Inflammatory and Growth-Promoting Activity. *J Immunol*, 205, 102-112.
- Danaher, P., Warren, S., Dennis, L., D'Amico, L., White, A., Disis, M. L., Geller, M. A., Odunsi, K., Beechem, J. & Fling, S. P. 2017. Gene expression markers of Tumor Infiltrating Leukocytes. *J Immunother Cancer*, 5, 18.
- de Azevedo, M. F., Gilson, P. R., Gabriel, H. B., Simoes, R. F., Angrisano, F., Baum, J., Crabb, B. S. & Wunderlich, G. 2012. Systematic analysis of FKBP inducible degradation domain tagging strategies for the human malaria parasite *Plasmodium falciparum*. *PLoS One*, 7, e40981.
- de Bruijn, M. F., Speck, N. A., Peeters, M. C. & Dzierzak, E. 2000. Definitive hematopoietic stem cells first develop within the major arterial regions of the mouse embryo. *EMBO J*, 19, 2465-74.
- De Pieri, A., Rochev, Y. & Zeugolis, D. I. 2021. Scaffold-free cell-based tissue engineering therapies: advances, shortfalls and forecast. *NPJ Regen Med*, 6, 18.
- De Ravin, S. S., Reik, A., Liu, P. Q., Li, L., Wu, X., Su, L., Raley, C., Theobald, N., Choi, U., Song, A. H., Chan, A., Pearl, J. R., Paschon, D. E., Lee, J., Newcombe, H., Koontz, S., Sweeney, C., Shivak, D. A., Zarembek, K. A., Peshwa, M. V., Gregory, P. D., Urnov, F. D. & Malech, H. L. 2016. Targeted gene addition in human CD34(+) hematopoietic cells for correction of X-linked chronic granulomatous disease. *Nat Biotechnol*, 34, 424-9.
- Dean, M., Fojo, T. & Bates, S. 2005. Tumour stem cells and drug resistance. *Nat Rev Cancer*, 5, 275-84.
- DeNardo, D. G., Andreu, P. & Coussens, L. M. 2010. Interactions between lymphocytes and myeloid cells regulate pro- versus anti-tumor immunity. *Cancer Metastasis Rev*, 29, 309-16.
- Dhingra, S., Sharma, A. K., Arora, R. C., Slezak, J. & Singal, P. K. 2009. IL-10 attenuates TNF-alpha-induced NF kappaB pathway activation and cardiomyocyte apoptosis. *Cardiovasc Res*, 82, 59-66.
- Dominici, M., Le Blanc, K., Mueller, I., Slaper-Cortenbach, I., Marini, F., Krause, D., Deans, R., Keating, A., Prockop, D. & Horwitz, E. 2006. Minimal criteria for defining multipotent mesenchymal stromal cells. The International Society for Cellular Therapy position statement. *Cytotherapy*, 8, 315-7.
- Dong, F., Hao, S., Zhang, S., Zhu, C., Cheng, H., Yang, Z., Hamey, F. K., Wang, X., Gao, A., Wang, F., Gao, Y., Dong, J., Wang, C., Wang, J., Lan, Y., Liu, B., Ema, H., Tang, F., Gottgens, B., Zhu, P. & Cheng, T. 2020. Differentiation of transplanted haematopoietic stem cells tracked by single-cell transcriptomic analysis. *Nat Cell Biol*, 22, 630-639.
- Doran, A. C., Yurdagul, A., Jr. & Tabas, I. 2020. Efferocytosis in health and disease. *Nat Rev Immunol*, 20, 254-267.
- Doulatov, S., Notta, F., Eppert, K., Nguyen, L. T., Ohashi, P. S. & Dick, J. E. 2010. Revised map of the human progenitor hierarchy shows the origin of macrophages and dendritic cells in early lymphoid development. *Nat Immunol*, 11, 585-93.
- Ebrahimi, M., Forouzesh, M., Raoufi, S., Ramazii, M., Ghaedrahmati, F. & Farzaneh, M. 2020. Differentiation of human induced pluripotent stem cells into erythroid cells. *Stem Cell Res Ther*, 11, 483.
- Eichler, F., Duncan, C., Musolino, P. L., Orchard, P. J., De Oliveira, S., Thrasher, A. J., Armant, M., Dansereau, C., Lund, T. C., Miller, W. P., Raymond, G. V., Sankar, R., Shah, A. J., Sevin, C., Gaspar, H. B., Gissen, P., Amartino, H., Bratkovic, D., Smith, N. J. C., Paker, A. M., Shamir, E., O'Meara, T., Davidson, D., Aubourg, P. & Williams, D. A. 2017. Hematopoietic Stem-Cell Gene Therapy for Cerebral Adrenoleukodystrophy. *N Engl J Med*, 377, 1630-1638.
- El Ashkar, S., Van Looveren, D., Schenk, F., Vranckx, L. S., Demeulemeester, J., De Rijck, J., Debyser, Z., Modlich, U. & Gijssbers, R. 2017. Engineering Next-Generation BET-Independent MLV Vectors for Safer Gene Therapy. *Mol Ther Nucleic Acids*, 7, 231-245.

- Erfurth, F., Hemenway, C. S., de Erkenez, A. C. & Domer, P. H. 2004. MLL fusion partners AF4 and AF9 interact at subnuclear foci. *Leukemia*, 18, 92-102.
- Ernst, P., Mabon, M., Davidson, A. J., Zon, L. I. & Korsmeyer, S. J. 2004. An Mll-dependent Hox program drives hematopoietic progenitor expansion. *Curr Biol*, 14, 2063-9.
- Fantin, A., Vieira, J. M., Gestri, G., Denti, L., Schwarz, Q., Prykhozhiy, S., Peri, F., Wilson, S. W. & Ruhrberg, C. 2010. Tissue macrophages act as cellular chaperones for vascular anastomosis downstream of VEGF-mediated endothelial tip cell induction. *Blood*, 116, 829-40.
- Fares, I., Chagraoui, J., Gareau, Y., Gingras, S., Ruel, R., Mayotte, N., Csaszar, E., Knapp, D. J., Miller, P., Ngom, M., Imren, S., Roy, D. C., Watts, K. L., Kiem, H. P., Herrington, R., Iscove, N. N., Humphries, R. K., Eaves, C. J., Cohen, S., Marinier, A., Zandstra, P. W. & Sauvageau, G. 2014. Cord blood expansion. Pyrimidoindole derivatives are agonists of human hematopoietic stem cell self-renewal. *Science*, 345, 1509-12.
- Faridi, F., Ponnusamy, K., Quagliano-Lo Coco, I., Chen-Wichmann, L., Grez, M., Henschler, R. & Wichmann, C. 2013. Aberrant epigenetic regulators control expansion of human CD34+ hematopoietic stem/progenitor cells. *Front Genet*, 4, 254.
- FDA. 2022. *Approved Cellular and Gene Therapy Products* [Online]. Available: <https://www.fda.gov/vaccines-blood-biologics/cellular-gene-therapy-products/approved-cellular-and-gene-therapy-products> [Accessed].
- Feng, Q., Chai, C., Jiang, X. S., Leong, K. W. & Mao, H. Q. 2006. Expansion of engrafting human hematopoietic stem/progenitor cells in three-dimensional scaffolds with surface-immobilized fibronectin. *J Biomed Mater Res A*, 78, 781-91.
- Fitzsimmons, R. E. B., Mazurek, M. S., Soos, A. & Simmons, C. A. 2018. Mesenchymal Stromal/Stem Cells in Regenerative Medicine and Tissue Engineering. *Stem Cells Int*, 2018, 8031718.
- Fu, J. F., Liang, D. C. & Shih, L. Y. 2007. Analysis of acute leukemias with MLL/ENL fusion transcripts: identification of two novel breakpoints in ENL. *Am J Clin Pathol*, 127, 24-30.
- Gabrusiewicz, K., Ellert-Miklaszewska, A., Lipko, M., Sielska, M., Frankowska, M. & Kaminska, B. 2011. Characteristics of the alternative phenotype of microglia/macrophages and its modulation in experimental gliomas. *PLoS One*, 6, e23902.
- Galluzzi, L., Chan, T. A., Kroemer, G., Wolchok, J. D. & Lopez-Soto, A. 2018. The hallmarks of successful anticancer immunotherapy. *Sci Transl Med*, 10.
- Gao, X., Zhang, D., Xu, C., Li, H., Caron, K. M. & Frenette, P. S. 2021. Nociceptive nerves regulate haematopoietic stem cell mobilization. *Nature*, 589, 591-596.
- Gautier, E. L., Shay, T., Miller, J., Greter, M., Jakubzick, C., Ivanov, S., Helft, J., Chow, A., Elpek, K. G., Gordonov, S., Mazloom, A. R., Ma'ayan, A., Chua, W. J., Hansen, T. H., Turley, S. J., Merad, M., Randolph, G. J. & Immunological Genome, C. 2012. Gene-expression profiles and transcriptional regulatory pathways that underlie the identity and diversity of mouse tissue macrophages. *Nat Immunol*, 13, 1118-28.
- Geissmann, F., Manz, M. G., Jung, S., Sieweke, M. H., Merad, M. & Ley, K. 2010. Development of monocytes, macrophages, and dendritic cells. *Science*, 327, 656-61.
- Gerhardt, T. & Ley, K. 2015. Monocyte trafficking across the vessel wall. *Cardiovasc Res*, 107, 321-30.
- Ghafouri-Fard, S., Niazi, V., Taheri, M. & Basiri, A. 2021. Effect of Small Molecule on ex vivo Expansion of Cord Blood Hematopoietic Stem Cells: A Concise Review. *Front Cell Dev Biol*, 9, 649115.
- Ginhoux, F., Greter, M., Leboeuf, M., Nandi, S., See, P., Gokhan, S., Mehler, M. F., Conway, S. J., Ng, L. G., Stanley, E. R., Samokhvalov, I. M. & Merad, M. 2010. Fate mapping analysis reveals that adult microglia derive from primitive macrophages. *Science*, 330, 841-5.
- Golchin, A. & Farahany, T. Z. 2019. Biological Products: Cellular Therapy and FDA Approved Products. *Stem Cell Rev Rep*, 15, 166-175.

- Gonzalez-Mejia, M. E. & Doseff, A. I. 2009. Regulation of monocytes and macrophages cell fate. *Front Biosci (Landmark Ed)*, 14, 2413-31.
- Gordon, S., Pluddemann, A. & Martinez Estrada, F. 2014. Macrophage heterogeneity in tissues: phenotypic diversity and functions. *Immunol Rev*, 262, 36-55.
- Gossen, M., Freundlieb, S., Bender, G., Muller, G., Hillen, W. & Bujard, H. 1995. Transcriptional activation by tetracyclines in mammalian cells. *Science*, 268, 1766-9.
- Gross, G., Gorochov, G., Waks, T. & Eshhar, Z. 1989a. Generation of effector T cells expressing chimeric T cell receptor with antibody type-specificity. *Transplant Proc*, 21, 127-30.
- Gross, G., Waks, T. & Eshhar, Z. 1989b. Expression of immunoglobulin-T-cell receptor chimeric molecules as functional receptors with antibody-type specificity. *Proc Natl Acad Sci U S A*, 86, 10024-8.
- Gschwandtner, M., Derler, R. & Midwood, K. S. 2019. More Than Just Attractive: How CCL2 Influences Myeloid Cell Behavior Beyond Chemotaxis. *Front Immunol*, 10, 2759.
- Gurusamy, N., Alsayari, A., Rajasingh, S. & Rajasingh, J. 2018. Adult Stem Cells for Regenerative Therapy. *Prog Mol Biol Transl Sci*, 160, 1-22.
- Gutbier, S., Wanke, F., Dahm, N., Rummelin, A., Zimmermann, S., Christensen, K., Kochl, F., Rautanen, A., Hatje, K., Geering, B., Zhang, J. D., Britschgi, M., Cowley, S. A. & Patsch, C. 2020. Large-Scale Production of Human iPSC-Derived Macrophages for Drug Screening. *Int J Mol Sci*, 21.
- Haar, J. L. & Ackerman, G. A. 1971. A phase and electron microscopic study of vasculogenesis and erythropoiesis in the yolk sac of the mouse. *Anat Rec*, 170, 199-223.
- Haas, S., Hansson, J., Klimmeck, D., Loeffler, D., Velten, L., Uckelmann, H., Wurzer, S., Prendergast, A. M., Schnell, A., Hexel, K., Santarella-Mellwig, R., Blaszkiewicz, S., Kuck, A., Geiger, H., Milsom, M. D., Steinmetz, L. M., Schroeder, T., Trumpp, A., Krijgsveld, J. & Essers, M. A. 2015. Inflammation-Induced Emergency Megakaryopoiesis Driven by Hematopoietic Stem Cell-like Megakaryocyte Progenitors. *Cell Stem Cell*, 17, 422-34.
- Haase, A., Glienke, W., Engels, L., Gohring, G., Esser, R., Arseniev, L. & Martin, U. 2019. GMP-compatible manufacturing of three iPS cell lines from human peripheral blood. *Stem Cell Res*, 35, 101394.
- Hacein-Bey-Abina, S., Von Kalle, C., Schmidt, M., McCormack, M. P., Wulffraat, N., Leboulch, P., Lim, A., Osborne, C. S., Pawliuk, R., Morillon, E., Sorensen, R., Forster, A., Fraser, P., Cohen, J. I., de Saint Basile, G., Alexander, I., Wintergerst, U., Frebourg, T., Aurias, A., Stoppa-Lyonnet, D., Romana, S., Radford-Weiss, I., Gross, F., Valensi, F., Delabesse, E., Macintyre, E., Sigaux, F., Soulier, J., Leiva, L. E., Wissler, M., Prinz, C., Rabbitts, T. H., Le Deist, F., Fischer, A. & Cavazzana-Calvo, M. 2003. LMO2-associated clonal T cell proliferation in two patients after gene therapy for SCID-X1. *Science*, 302, 415-9.
- Haddad, E. & Hoenig, M. 2019. Hematopoietic Stem Cell Transplantation for Severe Combined Immunodeficiency (SCID). *Front Pediatr*, 7, 481.
- Haeckel, E. 1873. *Natürliche Schöpfungsgeschichte: gemeinverständliche wissenschaftliche Vorträge über die Entwicklungslehre im allgemeinen und diejenige von Darwin, Goethe und Lamarck im besonderen*, Berlin.
- Hamilton, J. A. 2019. GM-CSF-Dependent Inflammatory Pathways. *Front Immunol*, 10, 2055.
- Hammond, C., Abrams, J. R. & Syrjala, K. L. 2007. Fertility and risk factors for elevated infertility concern in 10-year hematopoietic cell transplant survivors and case-matched controls. *J Clin Oncol*, 25, 3511-7.
- Hanahan, D. & Weinberg, R. A. 2011. Hallmarks of cancer: the next generation. *Cell*, 144, 646-74.
- Hart, R. & Greaves, D. R. 2010. Chemerin contributes to inflammation by promoting macrophage adhesion to VCAM-1 and fibronectin through clustering of VLA-4 and VLA-5. *J Immunol*, 185, 3728-39.

- Hartmann, J., Schussler-Lenz, M., Bondanza, A. & Buchholz, C. J. 2017. Clinical development of CAR T cells-challenges and opportunities in translating innovative treatment concepts. *EMBO Mol Med*, 9, 1183-1197.
- He, J., Abdel-Wahab, O., Nahas, M. K., Wang, K., Rampal, R. K., Intlekofer, A. M., Patel, J., Krivstov, A., Frampton, G. M., Young, L. E., Zhong, S., Bailey, M., White, J. R., Roels, S., Deffenbaugh, J., Fichtenholtz, A., Brennan, T., Rosenzweig, M., Pelak, K., Knapp, K. M., Brennan, K. W., Donahue, A. L., Young, G., Garcia, L., Beckstrom, S. T., Zhao, M., White, E., Banning, V., Buell, J., Iwanik, K., Ross, J. S., Morosini, D., Younes, A., Hanash, A. M., Paietta, E., Roberts, K., Mullighan, C., Dogan, A., Armstrong, S. A., Mughal, T., Vergilio, J. A., Labrecque, E., Erlich, R., Vietz, C., Yelensky, R., Stephens, P. J., Miller, V. A., van den Brink, M. R., Otto, G. A., Lipson, D. & Levine, R. L. 2016. Integrated genomic DNA/RNA profiling of hematologic malignancies in the clinical setting. *Blood*, 127, 3004-14.
- Heffner, G. C., Bonner, M., Christiansen, L., Piercicy, F. J., Campbell, D., Smurnyy, Y., Zhang, W., Hamel, A., Shaw, S., Lewis, G., Goss, K. A., Garijo, O., Torbett, B. E., Horton, H., Finer, M. H., Gregory, P. D. & Veres, G. 2018. Prostaglandin E2 Increases Lentiviral Vector Transduction Efficiency of Adult Human Hematopoietic Stem and Progenitor Cells. *Mol Ther*, 26, 320-328.
- Herzog, V. & Fahimi, H. D. 1973. A new sensitive colorimetric assay for peroxidase using 3,3'-diaminobenzidine as hydrogen donor. *Anal Biochem*, 55, 554-62.
- Hildinger, M., Eckert, H. G., Schilz, A. J., John, J., Ostertag, W. & Baum, C. 1998. FMEV vectors: both retroviral long terminal repeat and leader are important for high expression in transduced hematopoietic cells. *Gene Ther*, 5, 1575-9.
- Hopman, R. K. & DiPersio, J. F. 2014. Advances in stem cell mobilization. *Blood Rev*, 28, 31-40.
- Horton, S. J., Grier, D. G., McGonigle, G. J., Thompson, A., Morrow, M., De Silva, I., Moulding, D. A., Kioussis, D., Lappin, T. R., Brady, H. J. & Williams, O. 2005. Continuous MLL-ENL expression is necessary to establish a "Hox Code" and maintain immortalization of hematopoietic progenitor cells. *Cancer Res*, 65, 9245-52.
- Hsieh, J. J., Cheng, E. H. & Korsmeyer, S. J. 2003. Taspase1: a threonine aspartase required for cleavage of MLL and proper HOX gene expression. *Cell*, 115, 293-303.
- Huss, R. 2000. Isolation of primary and immortalized CD34-hematopoietic and mesenchymal stem cells from various sources. *Stem Cells*, 18, 1-9.
- International Stem Cell, I., Amps, K., Andrews, P. W., Anyfantis, G., Armstrong, L., Avery, S., Baharvand, H., Baker, J., Baker, D., Munoz, M. B., Beil, S., Benvenisty, N., Ben-Yosef, D., Biancotti, J. C., Bosman, A., Brena, R. M., Brison, D., Caisander, G., Camarasa, M. V., Chen, J., Chiao, E., Choi, Y. M., Choo, A. B., Collins, D., Colman, A., Crook, J. M., Daley, G. Q., Dalton, A., De Sousa, P. A., Denning, C., Downie, J., Dvorak, P., Montgomery, K. D., Feki, A., Ford, A., Fox, V., Fraga, A. M., Frumkin, T., Ge, L., Gokhale, P. J., Golan-Lev, T., Gourabi, H., Gropp, M., Lu, G., Hampl, A., Harron, K., Healy, L., Herath, W., Holm, F., Hovatta, O., Hyllner, J., Inamdar, M. S., Irwanto, A. K., Ishii, T., Jaconi, M., Jin, Y., Kimber, S., Kiselev, S., Knowles, B. B., Kopper, O., Kukhareenko, V., Kuliev, A., Lagarkova, M. A., Laird, P. W., Lako, M., Laslett, A. L., Lavon, N., Lee, D. R., Lee, J. E., Li, C., Lim, L. S., Ludwig, T. E., Ma, Y., Maltby, E., Mateizel, I., Maysnar, Y., Mileikovsky, M., Minger, S. L., Miyazaki, T., Moon, S. Y., Moore, H., Mummery, C., Nagy, A., Nakatsuji, N., Narwani, K., Oh, S. K., Oh, S. K., Olson, C., Otonkoski, T., Pan, F., Park, I. H., Pells, S., Pera, M. F., Pereira, L. V., Qi, O., Raj, G. S., Reubinoff, B., Robins, A., Robson, P., Rossant, J., et al. 2011. Screening ethnically diverse human embryonic stem cells identifies a chromosome 20 minimal amplicon conferring growth advantage. *Nat Biotechnol*, 29, 1132-44.
- Irving, M., Lanitis, E., Migliorini, D., Ivics, Z. & Guedan, S. 2021. Choosing the Right Tool for Genetic Engineering: Clinical Lessons from Chimeric Antigen Receptor-T Cells. *Hum Gene Ther*, 32, 1044-1058.
- Italiani, P. & Boraschi, D. 2014. From Monocytes to M1/M2 Macrophages: Phenotypical vs. Functional Differentiation. *Front Immunol*, 5, 514.

- Ivics, Z., Hackett, P. B., Plasterk, R. H. & Izsvak, Z. 1997. Molecular reconstruction of Sleeping Beauty, a Tc1-like transposon from fish, and its transposition in human cells. *Cell*, 91, 501-10.
- Iyer, S. S., Ghaffari, A. A. & Cheng, G. 2010. Lipopolysaccharide-mediated IL-10 transcriptional regulation requires sequential induction of type I IFNs and IL-27 in macrophages. *J Immunol*, 185, 6599-607.
- Jackson, Z., Roe, A., Sharma, A. A., Lopes, F., Talla, A., Kleinsorge-Block, S., Zamborsky, K., Schiavone, J., Manjappa, S., Schauner, R., Lee, G., Liu, R., Caimi, P. F., Xiong, Y., Krueger, W., Worden, A., Kadan, M., Schneider, D., Orentas, R., Dropulic, B., Sekaly, R. P., de Lima, M., Wald, D. N. & Reese, J. S. 2020. Automated Manufacture of Autologous CD19 CAR-T Cells for Treatment of Non-hodgkin Lymphoma. *Front Immunol*, 11, 1941.
- Jacobson, L. O., Marks, E. K. & Gaston, E. O. 1953. [Effect of protection of the spleen during total body irradiation on the blood in rabbit]. *Rev Hematol*, 8, 515-32.
- Jaenisch, R. & Young, R. 2008. Stem cells, the molecular circuitry of pluripotency and nuclear reprogramming. *Cell*, 132, 567-82.
- Jaffredo, T., Gautier, R., Eichmann, A. & Dieterlen-Lievre, F. 1998. Intraaortic hemopoietic cells are derived from endothelial cells during ontogeny. *Development*, 125, 4575-83.
- Jagasia, M. H., Greinix, H. T., Arora, M., Williams, K. M., Wolff, D., Cowen, E. W., Palmer, J., Weisdorf, D., Treister, N. S., Cheng, G. S., Kerr, H., Stratton, P., Duarte, R. F., McDonald, G. B., Inamoto, Y., Vigorito, A., Arai, S., Datiles, M. B., Jacobsohn, D., Heller, T., Kitko, C. L., Mitchell, S. A., Martin, P. J., Shulman, H., Wu, R. S., Cutler, C. S., Vogelsang, G. B., Lee, S. J., Pavletic, S. Z. & Flowers, M. E. 2015. National Institutes of Health Consensus Development Project on Criteria for Clinical Trials in Chronic Graft-versus-Host Disease: I. The 2014 Diagnosis and Staging Working Group report. *Biol Blood Marrow Transplant*, 21, 389-401 e1.
- Jaiswal, S., Jamieson, C. H., Pang, W. W., Park, C. Y., Chao, M. P., Majeti, R., Traver, D., van Rooijen, N. & Weissman, I. L. 2009. CD47 is upregulated on circulating hematopoietic stem cells and leukemia cells to avoid phagocytosis. *Cell*, 138, 271-85.
- Jakubzick, C., Gautier, E. L., Gibbings, S. L., Sojka, D. K., Schlitzer, A., Johnson, T. E., Ivanov, S., Duan, Q., Bala, S., Condon, T., van Rooijen, N., Grainger, J. R., Belkaid, Y., Ma'ayan, A., Riches, D. W., Yokoyama, W. M., Ginhoux, F., Henson, P. M. & Randolph, G. J. 2013. Minimal differentiation of classical monocytes as they survey steady-state tissues and transport antigen to lymph nodes. *Immunity*, 39, 599-610.
- Jan, M. & Majeti, R. 2013. Clonal evolution of acute leukemia genomes. *Oncogene*, 32, 135-40.
- Jiang, W. & Xu, J. 2020. Immune modulation by mesenchymal stem cells. *Cell Prolif*, 53, e12712.
- June, C. H., Maus, M. V., Plesa, G., Johnson, L. A., Zhao, Y., Levine, B. L., Grupp, S. A. & Porter, D. L. 2014. Engineered T cells for cancer therapy. *Cancer Immunol Immunother*, 63, 969-75.
- June, C. H., O'Connor, R. S., Kawalekar, O. U., Ghassemi, S. & Milone, M. C. 2018. CAR T cell immunotherapy for human cancer. *Science*, 359, 1361-1365.
- June, C. H., Riddell, S. R. & Schumacher, T. N. 2015. Adoptive cellular therapy: a race to the finish line. *Sci Transl Med*, 7, 280ps7.
- Junker, F., Gordon, J. & Qureshi, O. 2020. Fc Gamma Receptors and Their Role in Antigen Uptake, Presentation, and T Cell Activation. *Front Immunol*, 11, 1393.
- Katayama, Y., Battista, M., Kao, W. M., Hidalgo, A., Peired, A. J., Thomas, S. A. & Frenette, P. S. 2006. Signals from the sympathetic nervous system regulate hematopoietic stem cell egress from bone marrow. *Cell*, 124, 407-21.
- Kaushansky, K. 2006. Lineage-specific hematopoietic growth factors. *N Engl J Med*, 354, 2034-45.
- Kebriaei, P., Izsvak, Z., Narayanavari, S. A., Singh, H. & Ivics, Z. 2017. Gene Therapy with the Sleeping Beauty Transposon System. *Trends Genet*, 33, 852-870.

- Kelly, J. J., Saeed-Marand, M., Nystrom, N. N., Evans, M. M., Chen, Y., Martinez, F. M., Hamilton, A. M. & Ronald, J. A. 2021. Safe harbor-targeted CRISPR-Cas9 homology-independent targeted integration for multimodality reporter gene-based cell tracking. *Sci Adv*, 7.
- Kim, M., Rhee, J. K., Choi, H., Kwon, A., Kim, J., Lee, G. D., Jekarl, D. W., Lee, S., Kim, Y. & Kim, T. M. 2017. Passage-dependent accumulation of somatic mutations in mesenchymal stromal cells during in vitro culture revealed by whole genome sequencing. *Sci Rep*, 7, 14508.
- Klichinsky, M., Ruella, M., Shestova, O., Lu, X. M., Best, A., Zeeman, M., Schmierer, M., Gabrusiewicz, K., Anderson, N. R., Petty, N. E., Cummins, K. D., Shen, F., Shan, X., Veliz, K., Blouch, K., Yashiro-Ohtani, Y., Kenderian, S. S., Kim, M. Y., O'Connor, R. S., Wallace, S. R., Kozlowski, M. S., Marchione, D. M., Shestov, M., Garcia, B. A., June, C. H. & Gill, S. 2020. Human chimeric antigen receptor macrophages for cancer immunotherapy. *Nat Biotechnol*, 38, 947-953.
- Knapp, D. J., Hammond, C. A., Miller, P. H., Rabu, G. M., Beer, P. A., Ricicova, M., Lecault, V., Da Costa, D., VanInsberghe, M., Cheung, A. M., Pellacani, D., Piret, J., Hansen, C. & Eaves, C. J. 2017. Dissociation of Survival, Proliferation, and State Control in Human Hematopoietic Stem Cells. *Stem Cell Reports*, 8, 152-162.
- Kochenderfer, J. N., Dudley, M. E., Kassim, S. H., Somerville, R. P., Carpenter, R. O., Stetler-Stevenson, M., Yang, J. C., Phan, G. Q., Hughes, M. S., Sherry, R. M., Raffeld, M., Feldman, S., Lu, L., Li, Y. F., Ngo, L. T., Goy, A., Feldman, T., Spaner, D. E., Wang, M. L., Chen, C. C., Kranick, S. M., Nath, A., Nathan, D. A., Morton, K. E., Toomey, M. A. & Rosenberg, S. A. 2015. Chemotherapy-refractory diffuse large B-cell lymphoma and indolent B-cell malignancies can be effectively treated with autologous T cells expressing an anti-CD19 chimeric antigen receptor. *J Clin Oncol*, 33, 540-9.
- Kochenderfer, J. N., Wilson, W. H., Janik, J. E., Dudley, M. E., Stetler-Stevenson, M., Feldman, S. A., Maric, I., Raffeld, M., Nathan, D. A., Lanier, B. J., Morgan, R. A. & Rosenberg, S. A. 2010. Eradication of B-lineage cells and regression of lymphoma in a patient treated with autologous T cells genetically engineered to recognize CD19. *Blood*, 116, 4099-102.
- Kodama, H., Nose, M., Niida, S. & Yamasaki, A. 1991. Essential role of macrophage colony-stimulating factor in the osteoclast differentiation supported by stromal cells. *J Exp Med*, 173, 1291-4.
- Kohn, D. B., Booth, C., Kang, E. M., Pai, S. Y., Shaw, K. L., Santilli, G., Armant, M., Buckland, K. F., Choi, U., De Ravin, S. S., Dorsey, M. J., Kuo, C. Y., Leon-Rico, D., Rivat, C., Izotova, N., Gilmour, K., Snell, K., Dip, J. X., Darwish, J., Morris, E. C., Terrazas, D., Wang, L. D., Bauser, C. A., Paprotka, T., Kuhns, D. B., Gregg, J., Raymond, H. E., Everett, J. K., Honnet, G., Biasco, L., Newburger, P. E., Bushman, F. D., Grez, M., Gaspar, H. B., Williams, D. A., Malech, H. L., Galy, A., Thrasher, A. J. & Net, C. G. D. c. 2020. Lentiviral gene therapy for X-linked chronic granulomatous disease. *Nat Med*, 26, 200-206.
- Krivtsov, A. V. & Armstrong, S. A. 2007. MLL translocations, histone modifications and leukaemia stem-cell development. *Nat Rev Cancer*, 7, 823-33.
- Krivtsov, A. V., Twomey, D., Feng, Z., Stubbs, M. C., Wang, Y., Faber, J., Levine, J. E., Wang, J., Hahn, W. C., Gilliland, D. G., Golub, T. R. & Armstrong, S. A. 2006. Transformation from committed progenitor to leukaemia stem cell initiated by MLL-AF9. *Nature*, 442, 818-22.
- Kronstein-Wiedemann, R. & Tonn, T. 2019. Colony Formation: An Assay of Hematopoietic Progenitor Cells. *Methods Mol Biol*, 2017, 29-40.
- Krumsiek, J., Marr, C., Schroeder, T. & Theis, F. J. 2011. Hierarchical differentiation of myeloid progenitors is encoded in the transcription factor network. *PLoS One*, 6, e22649.
- Kuijk, E., Jager, M., van der Roest, B., Locati, M. D., Van Hoeck, A., Korzelius, J., Janssen, R., Besselink, N., Boymans, S., van Boxtel, R. & Cuppen, E. 2020. Publisher Correction: The mutational impact of culturing human pluripotent and adult stem cells. *Nat Commun*, 11, 3932.

- Kumar, A., Watkins, R. & Vilgelm, A. E. 2021. Cell Therapy With TILs: Training and Taming T Cells to Fight Cancer. *Front Immunol*, 12, 690499.
- Kumar, S. & Geiger, H. 2017. HSC Niche Biology and HSC Expansion Ex Vivo. *Trends Mol Med*, 23, 799-819.
- Kustikova, O. S., Baum, C. & Fehse, B. 2008. Retroviral integration site analysis in hematopoietic stem cells. *Methods Mol Biol*, 430, 255-67.
- Laemmli, U. K. 1970. Cleavage of structural proteins during the assembly of the head of bacteriophage T4. *Nature*, 227, 680-5.
- Laluppa, J. A., McAdams, T. A., Papoutsakis, E. T. & Miller, W. M. 1997. Culture materials affect ex vivo expansion of hematopoietic progenitor cells. *J Biomed Mater Res*, 36, 347-59.
- Lamers, C. H., Sleijfer, S., van Steenbergen, S., van Elzaker, P., van Krimpen, B., Groot, C., Vulto, A., den Bakker, M., Oosterwijk, E., Debets, R. & Gratama, J. W. 2013. Treatment of metastatic renal cell carcinoma with CAIX CAR-engineered T cells: clinical evaluation and management of on-target toxicity. *Mol Ther*, 21, 904-12.
- Landmann, R., Knopf, H. P., Link, S., Sansano, S., Schumann, R. & Zimmerli, W. 1996. Human monocyte CD14 is upregulated by lipopolysaccharide. *Infect Immun*, 64, 1762-9.
- Laurenti, E. & Gottgens, B. 2018. From haematopoietic stem cells to complex differentiation landscapes. *Nature*, 553, 418-426.
- Lavau, C., Szilvassy, S. J., Slany, R. & Cleary, M. L. 1997. immortalization and leukemic transformation of a myelomonocytic precursor by retrovirally transduced HRX-ENL. *EMBO J*, 16, 4226-37.
- Le Blanc, K., Frassoni, F., Ball, L., Locatelli, F., Roelofs, H., Lewis, I., Lanino, E., Sundberg, B., Bernardo, M. E., Remberger, M., Dini, G., Egeler, R. M., Bacigalupo, A., Fibbe, W., Ringden, O., Developmental Committee of the European Group for, B. & Marrow, T. 2008. Mesenchymal stem cells for treatment of steroid-resistant, severe, acute graft-versus-host disease: a phase II study. *Lancet*, 371, 1579-86.
- Lefrere, J. J. & Berche, P. 2010. [Doctor Brown-Sequard's therapy]. *Ann Endocrinol (Paris)*, 71, 69-75.
- Lehtonen, A., Ahlfors, H., Veckman, V., Miettinen, M., Lahesmaa, R. & Julkunen, I. 2007. Gene expression profiling during differentiation of human monocytes to macrophages or dendritic cells. *J Leukoc Biol*, 82, 710-20.
- Lemke, G. 2019. How macrophages deal with death. *Nat Rev Immunol*, 19, 539-549.
- Lewis, C. E. & Pollard, J. W. 2006. Distinct role of macrophages in different tumor microenvironments. *Cancer Res*, 66, 605-12.
- Li, W. 2012. Eat-me signals: keys to molecular phagocyte biology and "appetite" control. *J Cell Physiol*, 227, 1291-7.
- Li, X. & Song, Y. 2021. Structure, function and inhibition of critical protein-protein interactions involving mixed lineage leukemia 1 and its fusion oncoproteins. *J Hematol Oncol*, 14, 56.
- Li, Y., Roberts, N. D., Wala, J. A., Shapira, O., Schumacher, S. E., Kumar, K., Khurana, E., Waszak, S., Korbil, J. O., Haber, J. E., Imielinski, M., Group, P. S. V. W., Weischenfeldt, J., Beroukhi, R., Campbell, P. J. & Consortium, P. 2020. Patterns of somatic structural variation in human cancer genomes. *Nature*, 578, 112-121.
- Li, Z., Luo, R. T., Mi, S., Sun, M., Chen, P., Bao, J., Neilly, M. B., Jayathilaka, N., Johnson, D. S., Wang, L., Lavau, C., Zhang, Y., Tseng, C., Zhang, X., Wang, J., Yu, J., Yang, H., Wang, S. M., Rowley, J. D., Chen, J. & Thirman, M. J. 2009. Consistent deregulation of gene expression between human and murine MLL rearrangement leukemias. *Cancer Res*, 69, 1109-16.
- Liebermann, D. A. & Hoffman, B. 1994. Differentiation primary response genes and proto-oncogenes as positive and negative regulators of terminal hematopoietic cell differentiation. *Stem Cells*, 12, 352-69.

- Liggett, L. A. & Sankaran, V. G. 2020. Unraveling Hematopoiesis through the Lens of Genomics. *Cell*, 182, 1384-1400.
- Lin, H. D., Fong, C. Y., Biswas, A., Choolani, M. & Bongso, A. 2016. Human Umbilical Cord Wharton's Jelly Stem Cell Conditioned Medium Induces Tumoricidal Effects on Lymphoma Cells Through Hydrogen Peroxide Mediation. *J Cell Biochem*, 117, 2045-55.
- Lin, W., Huang, L., Li, Y., Fang, B., Li, G., Chen, L. & Xu, L. 2019. Mesenchymal Stem Cells and Cancer: Clinical Challenges and Opportunities. *Biomed Res Int*, 2019, 2820853.
- Liu, T., Zhang, L., Joo, D. & Sun, S. C. 2017. NF-kappaB signaling in inflammation. *Signal Transduct Target Ther*, 2.
- Loeffler, D. & Schroeder, T. 2021. Symmetric and asymmetric activation of hematopoietic stem cells. *Curr Opin Hematol*, 28, 262-268.
- Loyola, L., Achuthan, V., Gilroy, K., Borland, G., Kilbey, A., Mackay, N., Bell, M., Hay, J., Aiyer, S., Fingerman, D., Villanueva, R. A., Cameron, E., Kozak, C. A., Engelman, A. N., Neil, J. & Roth, M. J. 2019. Disrupting MLV integrase: BET protein interaction biases integration into quiescent chromatin and delays but does not eliminate tumor activation in a MYC/Runx2 mouse model. *PLoS Pathog*, 15, e1008154.
- Macarthur, C. C., Fontes, A., Ravinder, N., Kuninger, D., Kaur, J., Bailey, M., Taliana, A., Vemuri, M. C. & Lieu, P. T. 2012. Generation of human-induced pluripotent stem cells by a nonintegrating RNA Sendai virus vector in feeder-free or xeno-free conditions. *Stem Cells Int*, 2012, 564612.
- Maciejewski, J., Weber, H., Neuhaus, K., Wachter, M., Elstner, E., Seiler, F. R. & Volk, H. D. 1991. Comparative analysis of the influences of IL-1, IL-3 and GM-CSF on the commitment of granulocyte-macrophage progenitors in vitro. *Ann Hematol*, 63, 242-8.
- Maeder, M. L. & Gersbach, C. A. 2016. Genome-editing Technologies for Gene and Cell Therapy. *Mol Ther*, 24, 430-46.
- Maetzig, T., Galla, M., Baum, C. & Schambach, A. 2011. Gammaretroviral vectors: biology, technology and application. *Viruses*, 3, 677-713.
- Majzner, R. G. & Mackall, C. L. 2019. Clinical lessons learned from the first leg of the CAR T cell journey. *Nat Med*, 25, 1341-1355.
- Mantovani, A., Sica, A., Sozzani, S., Allavena, P., Vecchi, A. & Locati, M. 2004. The chemokine system in diverse forms of macrophage activation and polarization. *Trends Immunol*, 25, 677-86.
- Martinazzi, M., Paltrinieri, E. & Zappala, G. 1972. [Cytocentrifugation: a versatile technic for routine cytological diagnosis]. *Quad Sclavo Diagn*, 8, 706-21.
- Maude, S. L., Laetsch, T. W., Buechner, J., Rives, S., Boyer, M., Bittencourt, H., Bader, P., Verneris, M. R., Stefanski, H. E., Myers, G. D., Qayed, M., De Moerloose, B., Hiramatsu, H., Schlis, K., Davis, K. L., Martin, P. L., Nemecek, E. R., Yanik, G. A., Peters, C., Baruchel, A., Boissel, N., Mechinaud, F., Balduzzi, A., Krueger, J., June, C. H., Levine, B. L., Wood, P., Taran, T., Leung, M., Mueller, K. T., Zhang, Y., Sen, K., Lebwohl, D., Pulsipher, M. A. & Grupp, S. A. 2018. Tisagenlecleucel in Children and Young Adults with B-Cell Lymphoblastic Leukemia. *N Engl J Med*, 378, 439-448.
- McBlane, J. W., Phul, P. & Sharpe, M. 2018. Correction to: Preclinical Development of Cell-Based Products: a European Regulatory Science Perspective. *Pharm Res*, 35, 212.
- Mead, A. J. & Mullally, A. 2017. Myeloproliferative neoplasm stem cells. *Blood*, 129, 1607-1616.
- Medvinsky, A. & Dzierzak, E. 1996. Definitive hematopoiesis is autonomously initiated by the AGM region. *Cell*, 86, 897-906.
- Menasche, P. 2020. Cell Therapy With Human ESC-Derived Cardiac Cells: Clinical Perspectives. *Front Bioeng Biotechnol*, 8, 601560.
- Mendez-Ferrer, S., Michurina, T. V., Ferraro, F., Mazloom, A. R., Macarthur, B. D., Lira, S. A., Scadden, D. T., Ma'ayan, A., Enikolopov, G. N. & Frenette, P. S. 2010. Mesenchymal and haematopoietic stem cells form a unique bone marrow niche. *Nature*, 466, 829-34.

- Merad, M., Manz, M. G., Karsunky, H., Wagers, A., Peters, W., Charo, I., Weissman, I. L., Cyster, J. G. & Engleman, E. G. 2002. Langerhans cells renew in the skin throughout life under steady-state conditions. *Nat Immunol*, 3, 1135-41.
- Metcalfe, D. 2008. Hematopoietic cytokines. *Blood*, 111, 485-91.
- Metchnikoff, O. 1921. *Life of Elie Metchnikoff, 1845-1916.*, Constable Limited.
- Meyer, C., Burmeister, T., Groger, D., Tsaur, G., Fechina, L., Renneville, A., Sutton, R., Venn, N. C., Emerenciano, M., Pombo-de-Oliveira, M. S., Barbieri Blunck, C., Almeida Lopes, B., Zuna, J., Trka, J., Ballerini, P., Lapillonne, H., De Braekeleer, M., Cazzaniga, G., Corral Abascal, L., van der Velden, V. H. J., Delabesse, E., Park, T. S., Oh, S. H., Silva, M. L. M., Lund-Aho, T., Juvonen, V., Moore, A. S., Heidenreich, O., Vormoor, J., Zerkalenskaya, E., Olshanskaya, Y., Bueno, C., Menendez, P., Teigler-Schlegel, A., Zur Stadt, U., Lentjes, J., Gohring, G., Kustanovich, A., Aleinikova, O., Schafer, B. W., Kubetzko, S., Madsen, H. O., Gruhn, B., Duarte, X., Gameiro, P., Lippert, E., Bidet, A., Cayuela, J. M., Clappier, E., Alonso, C. N., Zwaan, C. M., van den Heuvel-Eibrink, M. M., Izraeli, S., Trakhtenbrot, L., Archer, P., Hancock, J., Moricke, A., Alten, J., Schrappe, M., Stanulla, M., Strehl, S., Attarbaschi, A., Dworzak, M., Haas, O. A., Panzer-Grumayer, R., Sedek, L., Szczepanski, T., Caye, A., Suarez, L., Cave, H. & Marschalek, R. 2018. The MLL recombinome of acute leukemias in 2017. *Leukemia*, 32, 273-284.
- Meyer, C., Burmeister, T., Strehl, S., Schneider, B., Hubert, D., Zach, O., Haas, O., Klingebiel, T., Dingermann, T. & Marschalek, R. 2007. Spliced MLL fusions: a novel mechanism to generate functional chimeric MLL-MLLT1 transcripts in t(11;19)(q23;p13.3) leukemia. *Leukemia*, 21, 588-90.
- Mills, C. D., Kincaid, K., Alt, J. M., Heilman, M. J. & Hill, A. M. 2000. M-1/M-2 macrophages and the Th1/Th2 paradigm. *J Immunol*, 164, 6166-73.
- Mishra, B. P., Zaffuto, K. M., Artinger, E. L., Org, T., Mikkola, H. K., Cheng, C., Djabali, M. & Ernst, P. 2014. The histone methyltransferase activity of MLL1 is dispensable for hematopoiesis and leukemogenesis. *Cell Rep*, 7, 1239-47.
- Mizoguchi, S., Takahashi, K., Takeya, M., Naito, M. & Morioka, T. 1992. Development, differentiation, and proliferation of epidermal Langerhans cells in rat ontogeny studied by a novel monoclonal antibody against epidermal Langerhans cells, RED-1. *J Leukoc Biol*, 52, 52-61.
- Modlich, U., Schambach, A., Brugman, M. H., Wicke, D. C., Knoess, S., Li, Z., Maetzig, T., Rudolph, C., Schlegelberger, B. & Baum, C. 2008. Leukemia induction after a single retroviral vector insertion in Evi1 or Prdm16. *Leukemia*, 22, 1519-28.
- Monkley, S., Krishnaswamy, J. K., Goransson, M., Clausen, M., Mueller, J., Thorn, K., Hicks, R., Delaney, S. & Stjernborg, L. 2020. Optimised generation of iPSC-derived macrophages and dendritic cells that are functionally and transcriptionally similar to their primary counterparts. *PLoS One*, 15, e0243807.
- Morgan, M. A., Galla, M., Grez, M., Fehse, B. & Schambach, A. 2021. Retroviral gene therapy in Germany with a view on previous experience and future perspectives. *Gene Ther*, 28, 494-512.
- Morgan, R. A., Yang, J. C., Kitano, M., Dudley, M. E., Laurencot, C. M. & Rosenberg, S. A. 2010. Case report of a serious adverse event following the administration of T cells transduced with a chimeric antigen receptor recognizing ERBB2. *Mol Ther*, 18, 843-51.
- Morotti, M., Albukhari, A., Alsaadi, A., Artibani, M., Brenton, J. D., Curbishley, S. M., Dong, T., Dustin, M. L., Hu, Z., McGranahan, N., Miller, M. L., Santana-Gonzalez, L., Seymour, L. W., Shi, T., Van Loo, P., Yau, C., White, H., Wietek, N., Church, D. N., Wedge, D. C. & Ahmed, A. A. 2021. Promises and challenges of adoptive T-cell therapies for solid tumours. *Br J Cancer*, 124, 1759-1776.
- Morrison, S. J. & Weissman, I. L. 1994. The long-term repopulating subset of hematopoietic stem cells is deterministic and isolatable by phenotype. *Immunity*, 1, 661-73.

- Morrissey, M. A., Kern, N. & Vale, R. D. 2020. CD47 Ligation Repositions the Inhibitory Receptor SIRPA to Suppress Integrin Activation and Phagocytosis. *Immunity*, 53, 290-302 e6.
- Mount, N. M., Ward, S. J., Kefalas, P. & Hyllner, J. 2015. Cell-based therapy technology classifications and translational challenges. *Philos Trans R Soc Lond B Biol Sci*, 370, 20150017.
- Muller, K., Vogiatzi, F., Winterberg, D., Rosner, T., Lenk, L., Bastian, L., Gehlert, C. L., Autenrieb, M. P., Bruggemann, M., Cario, G., Schrappe, M., Kulozik, A. E., Eckert, C., Bergmann, A. K., Bornhauser, B., Bourquin, J. P., Valerius, T., Peipp, M., Kellner, C. & Schewe, D. M. 2022. Combining daratumumab with CD47 blockade prolongs survival in preclinical models of pediatric T-ALL. *Blood*, 140, 45-57.
- Mullighan, C. G., Goorha, S., Radtke, I., Miller, C. B., Coustan-Smith, E., Dalton, J. D., Girtman, K., Mathew, S., Ma, J., Pounds, S. B., Su, X., Pui, C. H., Relling, M. V., Evans, W. E., Shurtleff, S. A. & Downing, J. R. 2007. Genome-wide analysis of genetic alterations in acute lymphoblastic leukaemia. *Nature*, 446, 758-64.
- Mulloy, J. C., Cammenga, J., Berguido, F. J., Wu, K., Zhou, P., Comenzo, R. L., Jhanwar, S., Moore, M. A. & Nimer, S. D. 2003. Maintaining the self-renewal and differentiation potential of human CD34+ hematopoietic cells using a single genetic element. *Blood*, 102, 4369-76.
- Mulloy, J. C., Cammenga, J., MacKenzie, K. L., Berguido, F. J., Moore, M. A. & Nimer, S. D. 2002. The AML1-ETO fusion protein promotes the expansion of human hematopoietic stem cells. *Blood*, 99, 15-23.
- Muntean, A. G., Tan, J., Sitwala, K., Huang, Y., Bronstein, J., Connelly, J. A., Basrur, V., Elenitoba-Johnson, K. S. & Hess, J. L. 2010. The PAF complex synergizes with MLL fusion proteins at HOX loci to promote leukemogenesis. *Cancer Cell*, 17, 609-21.
- Murray, P. J. 2017. Macrophage Polarization. *Annu Rev Physiol*, 79, 541-566.
- Nayak, D., Roth, T. L. & McGavern, D. B. 2014. Microglia development and function. *Annu Rev Immunol*, 32, 367-402.
- Nielsen, M. C., Andersen, M. N. & Moller, H. J. 2020. Monocyte isolation techniques significantly impact the phenotype of both isolated monocytes and derived macrophages in vitro. *Immunology*, 159, 63-74.
- Niu, J., Ren, Y., Zhang, T., Yang, X., Zhu, W., Zhu, H., Li, J., Li, J. & Pang, Y. 2014. Retrospective comparative study of the effects of dendritic cell vaccine and cytokine-induced killer cell immunotherapy with that of chemotherapy alone and in combination for colorectal cancer. *Biomed Res Int*, 2014, 214727.
- Notta, F., Doulatov, S., Laurenti, E., Poepl, A., Jurisica, I. & Dick, J. E. 2011. Isolation of single human hematopoietic stem cells capable of long-term multilineage engraftment. *Science*, 333, 218-21.
- Nowell, P. C. 2007. Discovery of the Philadelphia chromosome: a personal perspective. *J Clin Invest*, 117, 2033-5.
- Nowell, P. C. & Hungerford, D. A. 1960. Chromosome studies on normal and leukemic human leukocytes. *J Natl Cancer Inst*, 25, 85-109.
- Okeyo-Owuor, T., Li, Y., Patel, R. M., Yang, W., Casey, E. B., Cluster, A. S., Porter, S. N., Bryder, D. & Magee, J. A. 2019. The efficiency of murine MLL-ENL-driven leukemia initiation changes with age and peaks during neonatal development. *Blood Adv*, 3, 2388-2399.
- Okita, K., Ichisaka, T. & Yamanaka, S. 2007. Generation of germline-competent induced pluripotent stem cells. *Nature*, 448, 313-7.
- Orecchioni, M., Ghosheh, Y., Pramod, A. B. & Ley, K. 2020. Corrigendum: Macrophage Polarization: Different Gene Signatures in M1(LPS+) vs. Classically and M2(LPS-) vs. Alternatively Activated Macrophages. *Front Immunol*, 11, 234.
- Orkin, S. H. & Zon, L. I. 2008. Hematopoiesis: an evolving paradigm for stem cell biology. *Cell*, 132, 631-44.

- Pan, Y., Yu, Y., Wang, X. & Zhang, T. 2020. Tumor-Associated Macrophages in Tumor Immunity. *Front Immunol*, 11, 583084.
- Parihar, A., Eubank, T. D. & Doseff, A. I. 2010. Monocytes and macrophages regulate immunity through dynamic networks of survival and cell death. *J Innate Immun*, 2, 204-15.
- Petersdorf, E. W. 2004. HLA matching in allogeneic stem cell transplantation. *Curr Opin Hematol*, 11, 386-91.
- Petit, I., Szyper-Kravitz, M., Nagler, A., Lahav, M., Peled, A., Habler, L., Ponomaryov, T., Taichman, R. S., Arenzana-Seisdedos, F., Fujii, N., Sandbank, J., Zipori, D. & Lapidot, T. 2002. G-CSF induces stem cell mobilization by decreasing bone marrow SDF-1 and up-regulating CXCR4. *Nat Immunol*, 3, 687-94.
- Pietras, E. M., Reynaud, D., Kang, Y. A., Carlin, D., Calero-Nieto, F. J., Leavitt, A. D., Stuart, J. M., Gottgens, B. & Passegue, E. 2015. Functionally Distinct Subsets of Lineage-Biased Multipotent Progenitors Control Blood Production in Normal and Regenerative Conditions. *Cell Stem Cell*, 17, 35-46.
- Poh, A. R. & Ernst, M. 2018. Targeting Macrophages in Cancer: From Bench to Bedside. *Front Oncol*, 8, 49.
- Pourrajab, F., Zare-Khormizi, M. R., Hashemi, A. S. & Hekmatimoghaddam, S. 2020. Genetic Characterization and Risk Stratification of Acute Myeloid Leukemia. *Cancer Manag Res*, 12, 2231-2253.
- Psatha, N., Georgolopoulos, G., Phelps, S. & Papayannopoulou, T. 2017. Brief Report: A Differential Transcriptomic Profile of Ex Vivo Expanded Adult Human Hematopoietic Stem Cells Empowers Them for Engraftment Better than Their Surface Phenotype. *Stem Cells Transl Med*, 6, 1852-1858.
- Qian, B. Z. & Pollard, J. W. 2010. Macrophage diversity enhances tumor progression and metastasis. *Cell*, 141, 39-51.
- Rath, M., Muller, I., Kropf, P., Closs, E. I. & Munder, M. 2014. Metabolism via Arginase or Nitric Oxide Synthase: Two Competing Arginine Pathways in Macrophages. *Front Immunol*, 5, 532.
- Redecke, V., Wu, R., Zhou, J., Finkelstein, D., Chaturvedi, V., High, A. A. & Hacker, H. 2013. Hematopoietic progenitor cell lines with myeloid and lymphoid potential. *Nat Methods*, 10, 795-803.
- Reimer, J., Knoss, S., Labuhn, M., Charpentier, E. M., Gohring, G., Schlegelberger, B., Klusmann, J. H. & Heckl, D. 2017. CRISPR-Cas9-induced t(11;19)/MLL-ENL translocations initiate leukemia in human hematopoietic progenitor cells in vivo. *Haematologica*, 102, 1558-1566.
- Research, G. V. 2021. *Global Cell Therapy Market Size*.
- Rigall, G. J., Cadot, S., Kluin, R. J., Xue, Z., Bernards, R., Majewski, I. J. & Wessels, L. F. 2012. A regression model for estimating DNA copy number applied to capture sequencing data. *Bioinformatics*, 28, 2357-65.
- Robbins, P. F., Kassim, S. H., Tran, T. L., Crystal, J. S., Morgan, R. A., Feldman, S. A., Yang, J. C., Dudley, M. E., Wunderlich, J. R., Sherry, R. M., Kammula, U. S., Hughes, M. S., Restifo, N. P., Raffeld, M., Lee, C. C., Li, Y. F., El-Gamil, M. & Rosenberg, S. A. 2015. A pilot trial using lymphocytes genetically engineered with an NY-ESO-1-reactive T-cell receptor: long-term follow-up and correlates with response. *Clin Cancer Res*, 21, 1019-27.
- Robbins, P. F., Morgan, R. A., Feldman, S. A., Yang, J. C., Sherry, R. M., Dudley, M. E., Wunderlich, J. R., Nahvi, A. V., Helman, L. J., Mackall, C. L., Kammula, U. S., Hughes, M. S., Restifo, N. P., Raffeld, M., Lee, C. C., Levy, C. L., Li, Y. F., El-Gamil, M., Schwarz, S. L., Laurencot, C. & Rosenberg, S. A. 2011. Tumor regression in patients with metastatic synovial cell sarcoma and melanoma using genetically engineered lymphocytes reactive with NY-ESO-1. *J Clin Oncol*, 29, 917-24.
- Robinson, S. N., Ng, J., Niu, T., Yang, H., McMannis, J. D., Karandish, S., Kaur, I., Fu, P., Del Angel, M., Messinger, R., Flagge, F., de Lima, M., Decker, W., Xing, D., Champlin, R. &

- Shpall, E. J. 2006. Superior ex vivo cord blood expansion following co-culture with bone marrow-derived mesenchymal stem cells. *Bone Marrow Transplant*, 37, 359-66.
- Robinton, D. A. & Daley, G. Q. 2012. The promise of induced pluripotent stem cells in research and therapy. *Nature*, 481, 295-305.
- Roos, D. 2019. Chronic Granulomatous Disease. *Methods Mol Biol*, 1982, 531-542.
- Rosales, C. 2017. Fcγ Receptor Heterogeneity in Leukocyte Functional Responses. *Front Immunol*, 8, 280.
- Rosas, M., Osorio, F., Robinson, M. J., Davies, L. C., Dierkes, N., Jones, S. A., Reis e Sousa, C. & Taylor, P. R. 2011. Hoxb8 conditionally immortalised macrophage lines model inflammatory monocytic cells with important similarity to dendritic cells. *Eur J Immunol*, 41, 356-65.
- Rossi, L., Challen, G. A., Sirin, O., Lin, K. K. & Goodell, M. A. 2011. Hematopoietic stem cell characterization and isolation. *Methods Mol Biol*, 750, 47-59.
- Roux, E., Bougaran, P., Dufourcq, P. & Couffignal, T. 2020. Fluid Shear Stress Sensing by the Endothelial Layer. *Front Physiol*, 11, 861.
- Salim, T., Sershen, C. L. & May, E. E. 2016. Investigating the Role of TNF-α and IFN-γ Activation on the Dynamics of iNOS Gene Expression in LPS Stimulated Macrophages. *PLoS One*, 11, e0153289.
- Sanjuan-Pla, A., Macaulay, I. C., Jensen, C. T., Woll, P. S., Luis, T. C., Mead, A., Moore, S., Carella, C., Matsuoka, S., Bouriez Jones, T., Chowdhury, O., Stenson, L., Lutteropp, M., Green, J. C., Facchini, R., Boukarabila, H., Grover, A., Gambardella, A., Thongjuea, S., Carrelha, J., Tarrant, P., Atkinson, D., Clark, S. A., Nerlov, C. & Jacobsen, S. E. 2013. Platelet-biased stem cells reside at the apex of the haematopoietic stem-cell hierarchy. *Nature*, 502, 232-6.
- Saudemont, A., Jaspers, L. & Clay, T. 2018. Current Status of Gene Engineering Cell Therapeutics. *Front Immunol*, 9, 153.
- Schmidt, M., Carbonaro, D. A., Speckmann, C., Wissler, M., Bohnsack, J., Elder, M., Aronow, B. J., Nolte, J. A., Kohn, D. B. & von Kalle, C. 2003. Clonality analysis after retroviral-mediated gene transfer to CD34+ cells from the cord blood of ADA-deficient SCID neonates. *Nat Med*, 9, 463-8.
- Schofield, R. 1978. The relationship between the spleen colony-forming cell and the haemopoietic stem cell. *Blood Cells*, 4, 7-25.
- Schreiner, S., Birke, M., Garcia-Cuellar, M. P., Zilles, O., Greil, J. & Slany, R. K. 2001. MLL-ENL causes a reversible and myc-dependent block of myelomonocytic cell differentiation. *Cancer Res*, 61, 6480-6.
- Schroder, K., Hertzog, P. J., Ravasi, T. & Hume, D. A. 2004. Interferon-γ: an overview of signals, mechanisms and functions. *J Leukoc Biol*, 75, 163-89.
- Schultz, L. & Mackall, C. 2019. Driving CAR T cell translation forward. *Sci Transl Med*, 11.
- Schulz, C., Gomez Perdiguero, E., Chorro, L., Szabo-Rogers, H., Cagnard, N., Kierdorf, K., Prinz, M., Wu, B., Jacobsen, S. E., Pollard, J. W., Frampton, J., Liu, K. J. & Geissmann, F. 2012. A lineage of myeloid cells independent of Myb and hematopoietic stem cells. *Science*, 336, 86-90.
- Schuster, S. J., Svoboda, J., Chong, E. A., Nasta, S. D., Mato, A. R., Anak, O., Brogdon, J. L., Pruteanu-Malinici, I., Bhoj, V., Landsburg, D., Wasik, M., Levine, B. L., Lacey, S. F., Melenhorst, J. J., Porter, D. L. & June, C. H. 2017. Chimeric Antigen Receptor T Cells in Refractory B-Cell Lymphomas. *N Engl J Med*, 377, 2545-2554.
- Seita, J. & Weissman, I. L. 2010. Hematopoietic stem cell: self-renewal versus differentiation. *Wiley Interdiscip Rev Syst Biol Med*, 2, 640-53.
- Sessa, M., Lorioli, L., Fumagalli, F., Acquati, S., Redaelli, D., Baldoli, C., Canale, S., Lopez, I. D., Morena, F., Calabria, A., Fiori, R., Silvani, P., Rancoita, P. M., Gabaldo, M., Benedicenti, F., Antonioli, G., Assanelli, A., Cicalese, M. P., Del Carro, U., Sora, M. G., Martino, S., Quattrini, A., Montini, E., Di Serio, C., Ciceri, F., Roncarolo, M. G., Aiuti, A.,

- Naldini, L. & Biffi, A. 2016. Lentiviral haemopoietic stem-cell gene therapy in early-onset metachromatic leukodystrophy: an ad-hoc analysis of a non-randomised, open-label, phase 1/2 trial. *Lancet*, 388, 476-87.
- Seyffer, F. & Tampe, R. 2015. ABC transporters in adaptive immunity. *Biochim Biophys Acta*, 1850, 449-60.
- Shammaa, R., El-Kadiry, A. E., Abusarah, J. & Rafei, M. 2020. Mesenchymal Stem Cells Beyond Regenerative Medicine. *Front Cell Dev Biol*, 8, 72.
- Shao, W., Shan, J., Kearney, M. F., Wu, X., Maldarelli, F., Mellors, J. W., Luke, B., Coffin, J. M. & Hughes, S. H. 2016. Retrovirus Integration Database (RID): a public database for retroviral insertion sites into host genomes. *Retrovirology*, 13, 47.
- Sharma, P., Hu-Lieskovan, S., Wargo, J. A. & Ribas, A. 2017. Primary, Adaptive, and Acquired Resistance to Cancer Immunotherapy. *Cell*, 168, 707-723.
- Shi, L., Tang, G. P., Gao, S. J., Ma, Y. X., Liu, B. H., Li, Y., Zeng, J. M., Ng, Y. K., Leong, K. W. & Wang, S. 2003. Repeated intrathecal administration of plasmid DNA complexed with polyethylene glycol-grafted polyethylenimine led to prolonged transgene expression in the spinal cord. *Gene Ther*, 10, 1179-88.
- Shuman, S. 1991. Recombination mediated by vaccinia virus DNA topoisomerase I in *Escherichia coli* is sequence specific. *Proc Natl Acad Sci U S A*, 88, 10104-8.
- Shuman, S. 1994. Novel approach to molecular cloning and polynucleotide synthesis using vaccinia DNA topoisomerase. *J Biol Chem*, 269, 32678-84.
- Sica, A. & Mantovani, A. 2012. Macrophage plasticity and polarization: in vivo veritas. *J Clin Invest*, 122, 787-95.
- Sidney, L. E., Branch, M. J., Dunphy, S. E., Dua, H. S. & Hopkinson, A. 2014. Concise review: evidence for CD34 as a common marker for diverse progenitors. *Stem Cells*, 32, 1380-9.
- Sierra-Filardi, E., Nieto, C., Dominguez-Soto, A., Barroso, R., Sanchez-Mateos, P., Puig-Kroger, A., Lopez-Bravo, M., Joven, J., Ardavin, C., Rodriguez-Fernandez, J. L., Sanchez-Torres, C., Mellado, M. & Corbi, A. L. 2014. CCL2 shapes macrophage polarization by GM-CSF and M-CSF: identification of CCL2/CCR2-dependent gene expression profile. *J Immunol*, 192, 3858-67.
- Simonetta, F., Alvarez, M. & Negrin, R. S. 2017. Natural Killer Cells in Graft-versus-Host-Disease after Allogeneic Hematopoietic Cell Transplantation. *Front Immunol*, 8, 465.
- Singh, V. K., Saini, A., Kalsan, M., Kumar, N. & Chandra, R. 2016. Describing the Stem Cell Potency: The Various Methods of Functional Assessment and In silico Diagnostics. *Front Cell Dev Biol*, 4, 134.
- Sinn, P. L., Sauter, S. L. & McCray, P. B., Jr. 2005. Gene therapy progress and prospects: development of improved lentiviral and retroviral vectors--design, biosafety, and production. *Gene Ther*, 12, 1089-98.
- Sitnicka, E., Lin, N., Priestley, G. V., Fox, N., Broudy, V. C., Wolf, N. S. & Kaushansky, K. 1996. The effect of thrombopoietin on the proliferation and differentiation of murine hematopoietic stem cells. *Blood*, 87, 4998-5005.
- Slany, R. K., Lavau, C. & Cleary, M. L. 1998. The oncogenic capacity of HRX-ENL requires the transcriptional transactivation activity of ENL and the DNA binding motifs of HRX. *Mol Cell Biol*, 18, 122-9.
- Sloma, I., Imren, S., Beer, P. A., Zhao, Y., Lecault, V., Leung, D., Raghuram, K., Brimacombe, C., Lambie, K., Piret, J., Hansen, C., Humphries, R. K. & Eaves, C. J. 2013. Ex vivo expansion of normal and chronic myeloid leukemic stem cells without functional alteration using a NUP98HOXA10homeodomain fusion gene. *Leukemia*, 27, 159-69.
- Smith, B. W., Rozelle, S. S., Leung, A., Ubellacker, J., Parks, A., Nah, S. K., French, D., Gadue, P., Monti, S., Chui, D. H., Steinberg, M. H., Frelinger, A. L., Michelson, A. D., Theberge, R., McComb, M. E., Costello, C. E., Kotton, D. N., Mostoslavsky, G., Sherr, D. H. & Murphy, G. J. 2013. The aryl hydrocarbon receptor directs hematopoietic progenitor cell expansion and differentiation. *Blood*, 122, 376-85.

- Somervaille, T. C., Matheny, C. J., Spencer, G. J., Iwasaki, M., Rinn, J. L., Witten, D. M., Chang, H. Y., Shurtleff, S. A., Downing, J. R. & Cleary, M. L. 2009. Hierarchical maintenance of MLL myeloid leukemia stem cells employs a transcriptional program shared with embryonic rather than adult stem cells. *Cell Stem Cell*, 4, 129-40.
- Southall, S. M., Wong, P. S., Odho, Z., Roe, S. M. & Wilson, J. R. 2009. Structural basis for the requirement of additional factors for MLL1 SET domain activity and recognition of epigenetic marks. *Mol Cell*, 33, 181-91.
- Sreejit, G., Fleetwood, A. J., Murphy, A. J. & Nagareddy, P. R. 2020. Origins and diversity of macrophages in health and disease. *Clin Transl Immunology*, 9, e1222.
- Stadtmauer, E. A., Faitg, T. H., Lowther, D. E., Badros, A. Z., Chagin, K., Dengel, K., Iyengar, M., Melchiori, L., Navenot, J. M., Norry, E., Trivedi, T., Wang, R., Binder, G. K., Amado, R. & Rapoport, A. P. 2019. Long-term safety and activity of NY-ESO-1 SPEAR T cells after autologous stem cell transplant for myeloma. *Blood Adv*, 3, 2022-2034.
- Stavropoulou, V., Almosailleakh, M., Royo, H., Spetz, J. F., Juge, S., Brault, L., Kopp, P., Iacovino, M., Kyba, M., Tzankov, A., Stadler, M. B., Cazzaniga, G., Peters, A. & Schwaller, J. 2018. A Novel Inducible Mouse Model of MLL-ENL-driven Mixed-lineage Acute Leukemia. *Hemasphere*, 2, e51.
- Stavropoulou, V., Kaspar, S., Brault, L., Sanders, M. A., Juge, S., Morettini, S., Tzankov, A., Iacovino, M., Lau, I. J., Milne, T. A., Royo, H., Kyba, M., Valk, P. J. M., Peters, A. & Schwaller, J. 2016. MLL-AF9 Expression in Hematopoietic Stem Cells Drives a Highly Invasive AML Expressing EMT-Related Genes Linked to Poor Outcome. *Cancer Cell*, 30, 43-58.
- Stein, M., Keshav, S., Harris, N. & Gordon, S. 1992. Interleukin 4 potently enhances murine macrophage mannose receptor activity: a marker of alternative immunologic macrophage activation. *J Exp Med*, 176, 287-92.
- Stein, S., Ott, M. G., Schultze-Strasser, S., Jauch, A., Burwinkel, B., Kinner, A., Schmidt, M., Kramer, A., Schwable, J., Glimm, H., Koehl, U., Preiss, C., Ball, C., Martin, H., Gohring, G., Schwarzwaelder, K., Hofmann, W. K., Karakaya, K., Tchatchou, S., Yang, R., Reinecke, P., Kuhlcke, K., Schlegelberger, B., Thrasher, A. J., Hoelzer, D., Seger, R., von Kalle, C. & Grez, M. 2010. Genomic instability and myelodysplasia with monosomy 7 consequent to EVI1 activation after gene therapy for chronic granulomatous disease. *Nat Med*, 16, 198-204.
- Sun, J., Ramos, A., Chapman, B., Johnnidis, J. B., Le, L., Ho, Y. J., Klein, A., Hofmann, O. & Camargo, F. D. 2014. Clonal dynamics of native haematopoiesis. *Nature*, 514, 322-7.
- Sun, L., Rautela, J., Delconte, R. B., Souza-Fonseca-Guimaraes, F., Carrington, E. M., Schenk, R. L., Herold, M. J., Huntington, N. D., Lew, A. M., Xu, Y. & Zhan, Y. 2018. GM-CSF Quantity Has a Selective Effect on Granulocytic vs. Monocytic Myeloid Development and Function. *Front Immunol*, 9, 1922.
- Swerdlow, S. H., Campo, E., Pileri, S. A., Harris, N. L., Stein, H., Siebert, R., Advani, R., Ghielmini, M., Salles, G. A., Zelenetz, A. D. & Jaffe, E. S. 2016. The 2016 revision of the World Health Organization classification of lymphoid neoplasms. *Blood*, 127, 2375-90.
- Takahashi, K., Tanabe, K., Ohnuki, M., Narita, M., Ichisaka, T., Tomoda, K. & Yamanaka, S. 2007. Induction of pluripotent stem cells from adult human fibroblasts by defined factors. *Cell*, 131, 861-72.
- Takahashi, K. & Yamanaka, S. 2006. Induction of pluripotent stem cells from mouse embryonic and adult fibroblast cultures by defined factors. *Cell*, 126, 663-76.
- Tan, M. P., Gerry, A. B., Brewer, J. E., Melchiori, L., Bridgeman, J. S., Bennett, A. D., Pumphrey, N. J., Jakobsen, B. K., Price, D. A., Ladell, K. & Sewell, A. K. 2015. T cell receptor binding affinity governs the functional profile of cancer-specific CD8+ T cells. *Clin Exp Immunol*, 180, 255-70.
- Tang, C. H. & Tsai, C. C. 2012. CCL2 increases MMP-9 expression and cell motility in human chondrosarcoma cells via the Ras/Raf/MEK/ERK/NF-kappaB signaling pathway. *Biochem Pharmacol*, 83, 335-44.

- Tang, D., Kang, R., Coyne, C. B., Zeh, H. J. & Lotze, M. T. 2012. PAMPs and DAMPs: signal 0s that spur autophagy and immunity. *Immunol Rev*, 249, 158-75.
- Tauber, A. I. 2003. Metchnikoff and the phagocytosis theory. *Nat Rev Mol Cell Biol*, 4, 897-901.
- Taylor, J., Xiao, W. & Abdel-Wahab, O. 2017. Diagnosis and classification of hematologic malignancies on the basis of genetics. *Blood*, 130, 410-423.
- Teerenhovi, L., Knuutila, S., Ekblom, M., Rossi, L., Borgstrom, G. H., Tallman, J. K., Andersson, L. & de la Chapelle, A. 1984. A method for simultaneous study of the karyotype, morphology, and immunologic phenotype of mitotic cells in hematologic malignancies. *Blood*, 64, 1116-22.
- Thomas, E. D., Lochte, H. L., Jr., Lu, W. C. & Ferrebee, J. W. 1957. Intravenous infusion of bone marrow in patients receiving radiation and chemotherapy. *N Engl J Med*, 257, 491-6.
- Tichelli, A., Bucher, C., Rovo, A., Stussi, G., Stern, M., Paulussen, M., Halter, J., Meyer-Monard, S., Heim, D., Tsakiris, D. A., Biedermann, B., Passweg, J. R. & Gratwohl, A. 2007. Premature cardiovascular disease after allogeneic hematopoietic stem-cell transplantation. *Blood*, 110, 3463-71.
- Till, J. E. & Mc, C. E. 1961. A direct measurement of the radiation sensitivity of normal mouse bone marrow cells. *Radiat Res*, 14, 213-22.
- Tsou, C. L., Peters, W., Si, Y., Slaymaker, S., Aslanian, A. M., Weisberg, S. P., Mack, M. & Charo, I. F. 2007. Critical roles for CCR2 and MCP-3 in monocyte mobilization from bone marrow and recruitment to inflammatory sites. *J Clin Invest*, 117, 902-9.
- Turgeon, M. L. 2005. *Clinical hematology: theory and procedures*, Lippincott Williams and Wilkins.
- Tverdynin, M. S., Bulanova, T. P. & Chernysheva, E. S. 1980. [Pappenheim method of panoptic staining of histological sections]. *Arkh Patol*, 42, 80-1.
- Ugale, A., Norddahl, G. L., Wahlestedt, M., Sawen, P., Jaako, P., Pronk, C. J., Soneji, S., Cammenga, J. & Bryder, D. 2014. Hematopoietic stem cells are intrinsically protected against MLL-ENL-mediated transformation. *Cell Rep*, 9, 1246-55.
- Upadhaya, S., Yu, J. X., Shah, M., Correa, D., Partridge, T. & Campbell, J. 2021. The clinical pipeline for cancer cell therapies. *Nat Rev Drug Discov*, 20, 503-504.
- Ushach, I. & Zlotnik, A. 2016. Biological role of granulocyte macrophage colony-stimulating factor (GM-CSF) and macrophage colony-stimulating factor (M-CSF) on cells of the myeloid lineage. *J Leukoc Biol*, 100, 481-9.
- van der Stegen, S. J., Hamieh, M. & Sadelain, M. 2015. The pharmacology of second-generation chimeric antigen receptors. *Nat Rev Drug Discov*, 14, 499-509.
- van Furth, R. & Cohn, Z. A. 1968. The origin and kinetics of mononuclear phagocytes. *J Exp Med*, 128, 415-35.
- van Schie, R. C., Verstraten, H. G., Tax, W. J., van den Berkmortel, F. W., van de Winkel, J. G. & de Mulder, P. H. 1992. Effect of rIFN-gamma on antibody-mediated cytotoxicity via human monocyte IgG Fc receptor II (CD32). *Scand J Immunol*, 36, 385-93.
- Velten, L., Haas, S. F., Raffel, S., Blaszkiewicz, S., Islam, S., Hennig, B. P., Hirche, C., Lutz, C., Buss, E. C., Nowak, D., Boch, T., Hofmann, W. K., Ho, A. D., Huber, W., Trumpp, A., Essers, M. A. & Steinmetz, L. M. 2017. Human haematopoietic stem cell lineage commitment is a continuous process. *Nat Cell Biol*, 19, 271-281.
- Vogelstein, B., Papadopoulos, N., Velculescu, V. E., Zhou, S., Diaz, L. A., Jr. & Kinzler, K. W. 2013. Cancer genome landscapes. *Science*, 339, 1546-58.
- Volkman, A., Chang, N. C., Strausbauch, P. H. & Morahan, P. S. 1983. Differential effects of chronic monocyte depletion on macrophage populations. *Lab Invest*, 49, 291-8.
- Vosberg, S., Herold, T., Hartmann, L., Neumann, M., Opatz, S., Metzeler, K. H., Schneider, S., Graf, A., Krebs, S., Blum, H., Baldus, C. D., Hiddemann, W., Spiekermann, K., Bohlander, S. K., Mansmann, U. & Greif, P. A. 2016. Close correlation of copy number

- aberrations detected by next-generation sequencing with results from routine cytogenetics in acute myeloid leukemia. *Genes Chromosomes Cancer*, 55, 553-67.
- Vyas, M., Muller, R. & Pogge von Strandmann, E. 2017. Antigen Loss Variants: Catching Hold of Escaping Foes. *Front Immunol*, 8, 175.
- Wagner, J. E., Jr., Brunstein, C. G., Boitano, A. E., DeFor, T. E., McKenna, D., Sumstad, D., Blazar, B. R., Tolar, J., Le, C., Jones, J., Cooke, M. P. & Bleul, C. C. 2016. Phase I/II Trial of StemRegenin-1 Expanded Umbilical Cord Blood Hematopoietic Stem Cells Supports Testing as a Stand-Alone Graft. *Cell Stem Cell*, 18, 144-55.
- Wang, W., Zhong, W., Yuan, J., Yan, C., Hu, S., Tong, Y., Mao, Y., Hu, T., Zhang, B. & Song, G. 2015. Involvement of Wnt/beta-catenin signaling in the mesenchymal stem cells promote metastatic growth and chemoresistance of cholangiocarcinoma. *Oncotarget*, 6, 42276-89.
- Wang, X., Dong, F., Zhang, S., Yang, W., Yu, W., Wang, Z., Zhang, S., Wang, J., Ma, S., Wu, P., Gao, Y., Dong, J., Tang, F., Cheng, T. & Ema, H. 2018. TGF-beta1 Negatively Regulates the Number and Function of Hematopoietic Stem Cells. *Stem Cell Reports*, 11, 274-287.
- Wei, J., Wunderlich, M., Fox, C., Alvarez, S., Cigudosa, J. C., Wilhelm, J. S., Zheng, Y., Cancelas, J. A., Gu, Y., Jansen, M., Dimartino, J. F. & Mulloy, J. C. 2008. Microenvironment determines lineage fate in a human model of MLL-AF9 leukemia. *Cancer Cell*, 13, 483-95.
- Wei, Q. & Frenette, P. S. 2018. Niches for Hematopoietic Stem Cells and Their Progeny. *Immunity*, 48, 632-648.
- Wei, X., Yang, X., Han, Z. P., Qu, F. F., Shao, L. & Shi, Y. F. 2013. Mesenchymal stem cells: a new trend for cell therapy. *Acta Pharmacol Sin*, 34, 747-54.
- Weinreb, C., Rodriguez-Fraticelli, A., Camargo, F. D. & Klein, A. M. 2020. Lineage tracing on transcriptional landscapes links state to fate during differentiation. *Science*, 367.
- Weiskopf, K. & Weissman, I. L. 2015. Macrophages are critical effectors of antibody therapies for cancer. *MAbs*, 7, 303-10.
- Weissman, I. L. & Shizuru, J. A. 2008. The origins of the identification and isolation of hematopoietic stem cells, and their capability to induce donor-specific transplantation tolerance and treat autoimmune diseases. *Blood*, 112, 3543-53.
- Wen, R., Dong, C., Xu, C., Zhao, L., Yang, Y., Zhang, Z., Chen, Y., Duan, L., Chen, H., Yang, Z. & Zhang, B. 2020. UM171 promotes expansion of autologous peripheral blood hematopoietic stem cells from poorly mobilizing lymphoma patients. *Int Immunopharmacol*, 81, 106266.
- Werner, B., Case, J., Williams, M. J., Chkhaidze, K., Temko, D., Fernandez-Mateos, J., Cresswell, G. D., Nichol, D., Cross, W., Spiteri, I., Huang, W., Tomlinson, I. P. M., Barnes, C. P., Graham, T. A. & Sottoriva, A. 2020. Measuring single cell divisions in human tissues from multi-region sequencing data. *Nat Commun*, 11, 1035.
- Whitfield, J., Littlewood, T., Evan, G. I. & Soucek, L. 2015. The estrogen receptor fusion system in mouse models: a reversible switch. *Cold Spring Harb Protoc*, 2015, 227-34.
- Wilkinson, A. C., Igarashi, K. J. & Nakauchi, H. 2020. Haematopoietic stem cell self-renewal in vivo and ex vivo. *Nat Rev Genet*, 21, 541-554.
- Williams, J. W., Giannarelli, C., Rahman, A., Randolph, G. J. & Kovacic, J. C. 2018. Macrophage Biology, Classification, and Phenotype in Cardiovascular Disease: JACC Macrophage in CVD Series (Part 1). *J Am Coll Cardiol*, 72, 2166-2180.
- Wilson, A., Laurenti, E., Oser, G., van der Wath, R. C., Blanco-Bose, W., Jaworski, M., Offner, S., Dunant, C. F., Eshkind, L., Bockamp, E., Lio, P., Macdonald, H. R. & Trumpp, A. 2008. Hematopoietic stem cells reversibly switch from dormancy to self-renewal during homeostasis and repair. *Cell*, 135, 1118-29.
- Wilson, A. & Trumpp, A. 2006. Bone-marrow haematopoietic-stem-cell niches. *Nat Rev Immunol*, 6, 93-106.

- Winters, A. C. & Bernt, K. M. 2017. MLL-Rearranged Leukemias-An Update on Science and Clinical Approaches. *Front Pediatr*, 5, 4.
- Wu, S., Zhang, C., Zhang, X., Xu, Y. Q. & Deng, T. X. 2015. Is peripheral blood or bone marrow a better source of stem cells for transplantation in cases of HLA-matched unrelated donors? A meta-analysis. *Crit Rev Oncol Hematol*, 96, 20-33.
- Xuan, W., Qu, Q., Zheng, B., Xiong, S. & Fan, G. H. 2015. The chemotaxis of M1 and M2 macrophages is regulated by different chemokines. *J Leukoc Biol*, 97, 61-9.
- Xue, J., Schmidt, S. V., Sander, J., Draffehn, A., Krebs, W., Quester, I., De Nardo, D., Gohel, T. D., Emde, M., Schmidleithner, L., Ganesan, H., Nino-Castro, A., Mallmann, M. R., Labzin, L., Theis, H., Kraut, M., Beyer, M., Latz, E., Freeman, T. C., Ulas, T. & Schultze, J. L. 2014. Transcriptome-based network analysis reveals a spectrum model of human macrophage activation. *Immunity*, 40, 274-88.
- Yam, L. T., Li, C. Y. & Crosby, W. H. 1971. Cytochemical identification of monocytes and granulocytes. *Am J Clin Pathol*, 55, 283-90.
- Yamanaka, S. 2020. Pluripotent Stem Cell-Based Cell Therapy-Promise and Challenges. *Cell Stem Cell*, 27, 523-531.
- Yokoyama, A. 2017. Transcriptional activation by MLL fusion proteins in leukemogenesis. *Exp Hematol*, 46, 21-30.
- Yokoyama, A., Lin, M., Naresh, A., Kitabayashi, I. & Cleary, M. L. 2010. A higher-order complex containing AF4 and ENL family proteins with P-TEFb facilitates oncogenic and physiologic MLL-dependent transcription. *Cancer Cell*, 17, 198-212.
- Yonemura, Y., Ku, H., Lyman, S. D. & Ogawa, M. 1997. In vitro expansion of hematopoietic progenitors and maintenance of stem cells: comparison between FLT3/FLK-2 ligand and KIT ligand. *Blood*, 89, 1915-21.
- Yu, J., Vodyanik, M. A., Smuga-Otto, K., Antosiewicz-Bourget, J., Frane, J. L., Tian, S., Nie, J., Jonsdottir, G. A., Ruotti, V., Stewart, R., Slukvin, I. & Thomson, J. A. 2007. Induced pluripotent stem cell lines derived from human somatic cells. *Science*, 318, 1917-20.
- Yulyana, Y., Ho, I. A., Sia, K. C., Newman, J. P., Toh, X. Y., Endaya, B. B., Chan, J. K., Gnecci, M., Huynh, H., Chung, A. Y., Lim, K. H., Leong, H. S., Iyer, N. G., Hui, K. M. & Lam, P. Y. 2015. Paracrine factors of human fetal MSCs inhibit liver cancer growth through reduced activation of IGF-1R/PI3K/Akt signaling. *Mol Ther*, 23, 746-56.
- Zakrzewski, W., Dobrzynski, M., Szymonowicz, M. & Rybak, Z. 2019. Stem cells: past, present, and future. *Stem Cell Res Ther*, 10, 68.
- Zehn, D., Lee, S. Y. & Bevan, M. J. 2009. Complete but curtailed T-cell response to very low-affinity antigen. *Nature*, 458, 211-4.
- Zeisig, B. B., Milne, T., Garcia-Cuellar, M. P., Schreiner, S., Martin, M. E., Fuchs, U., Borkhardt, A., Chanda, S. K., Walker, J., Soden, R., Hess, J. L. & Slany, R. K. 2004. Hoxa9 and Meis1 are key targets for MLL-ENL-mediated cellular immortalization. *Mol Cell Biol*, 24, 617-28.
- Zhang, F., Parayath, N. N., Ene, C. I., Stephan, S. B., Koehne, A. L., Coon, M. E., Holland, E. C. & Stephan, M. T. 2019. Genetic programming of macrophages to perform anti-tumor functions using targeted mRNA nanocarriers. *Nat Commun*, 10, 3974.
- Zhang, X., Edwards, J. P. & Mosser, D. M. 2009. The expression of exogenous genes in macrophages: obstacles and opportunities. *Methods Mol Biol*, 531, 123-43.
- Zhang, X. B., Schwartz, J. L., Humphries, R. K. & Kiem, H. P. 2007. Effects of HOXB4 overexpression on ex vivo expansion and immortalization of hematopoietic cells from different species. *Stem Cells*, 25, 2074-81.
- Zhao, L. & Cao, Y. J. 2019. Engineered T Cell Therapy for Cancer in the Clinic. *Front Immunol*, 10, 2250.
- Zhong, W., Tong, Y., Li, Y., Yuan, J., Hu, S., Hu, T. & Song, G. 2017. Mesenchymal stem cells in inflammatory microenvironment potentially promote metastatic growth of

List of References

- cholangiocarcinoma via activating Akt/NF-kappaB signaling by paracrine CCL5. *Oncotarget*, 8, 73693-73704.
- Zhu, J. & Emerson, S. G. 2002. Hematopoietic cytokines, transcription factors and lineage commitment. *Oncogene*, 21, 3295-313.
- Zhu, X., Sun, Q., Tan, W. S. & Cai, H. 2021. Reducing TGF-beta1 cooperated with StemRegenin 1 promoted the expansion ex vivo of cord blood CD34(+) cells by inhibiting AhR signalling. *Cell Prolif*, 54, e12999.
- Zhu, Y., Knolhoff, B. L., Meyer, M. A., Nywening, T. M., West, B. L., Luo, J., Wang-Gillam, A., Goedegebuure, S. P., Linehan, D. C. & DeNardo, D. G. 2014. CSF1/CSF1R blockade reprograms tumor-infiltrating macrophages and improves response to T-cell checkpoint immunotherapy in pancreatic cancer models. *Cancer Res*, 74, 5057-69.
- Zovein, A. C., Hofmann, J. J., Lynch, M., French, W. J., Turlo, K. A., Yang, Y., Becker, M. S., Zanetta, L., Dejana, E., Gasson, J. C., Tallquist, M. D. & Iruela-Arispe, M. L. 2008. Fate tracing reveals the endothelial origin of hematopoietic stem cells. *Cell Stem Cell*, 3, 625-36.

Acknowledgements

I would like to thank all those who have contributed to the success of this dissertation through their professional and personal support.

First, I want to thank Professor Dr. Andreas Humpe for offering me the opportunity to conduct my doctoral thesis at the Division of Transfusion Medicine, Cell Therapeutics and Haemostaseology of the Ludwig-Maximilians-University Munich in the research group of PD Dr. Christian Wichmann.

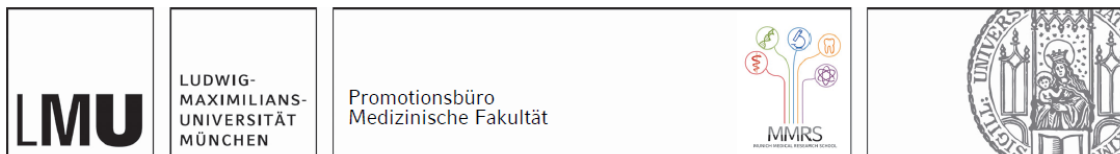
My special thanks go to my supervisors PD Dr. Christian Wichmann and PD Dr. Christian Kellner for their constant support, mentorship and guidance. I am grateful to PD Dr. Christian Wichmann for providing the exciting research topic, for planning the experiments and for excellently assisting me throughout the years. Many thanks to PD Dr. Christian Kellner for taking over the evaluation of this work, for his competent help to achieve the thesis' aims and for the critical discussion of scientific problems.

I would like to say a big thank you to the research group of the Division of Transfusion Medicine, Cell Therapeutics and Haemostaseology including all former and current members: Nina Pirschtat, Susanne Setzer, Sophie Schabernack, Sophie Kreißig, Lukas Bürtsch, Sebastian Lutz, Tobias Zeller, Ira Münnich, Dr. Irene Pauls and Patricia Hilger. Particularly, thanks to Dr. Linping Chen-Wichmann for the support and help during my experiments and Sarah Soliman for the preliminary work of this project. I would also like to thank the team of the plateletpheresis for providing donor-derived peripheral blood samples.

In the connection to the work presented in this thesis, I gratefully acknowledge the contribution of the collaborators who provided valuable primary samples, methods and devices for profound characterization of the cells. Thanks to Prof. Dr. Philipp Greif and Dr. Sebastian Vosberg from the Department of Medicine III, Prof. Dr. Jürgen Bernhagen and Dr. Adrian Hoffmann from the Institute for Stroke and Dementia Research and Dr. Luise Hartmann and Dr. Stephanie Schneider from the Laboratory for Leukemia Diagnostic.

In the end I want to thank my dear family, particularly my parents Andreas and Sabine and my brother Christian, for their immense support and trust during the entire time. In addition, I want to thank Murrel, the overweight cat of my parents, for the cuddling sessions leading to stress relaxation.

Affidavit



Eidesstattliche Versicherung

Windisch, Roland

Name, Vorname

Ich erkläre hiermit an Eides statt, dass ich die vorliegende Dissertation mit dem Titel:

From Harmful to Useful: Exploiting a Leukemia-Associated Transcription Factor for Large-Scale Manufacture of Functional Human Macrophages

selbständig verfasst, mich außer der angegebenen keiner weiteren Hilfsmittel bedient und alle Erkenntnisse, die aus dem Schrifttum ganz oder annähernd übernommen sind, als solche kenntlich gemacht und nach ihrer Herkunft unter Bezeichnung der Fundstelle einzeln nachgewiesen habe.

Ich erkläre des Weiteren, dass die hier vorgelegte Dissertation nicht in gleicher oder in ähnlicher Form bei einer anderen Stelle zur Erlangung eines akademischen Grades eingereicht wurde.

München, 10.05.2023

Ort, Datum

Roland Windisch

Unterschrift Doktorandin bzw. Doktorand

List of Publications

Peer-Reviewed Publications:

Original Research Articles:

1. Zeller T, Lutz S, Muennich IA, **Windisch R**, Hilger P, Herold T, Tahiri N, Banck J, Weigert O, Moosmann A, von Bergwelt-Baildon M, Bruns H, Wichmann C, Valerius T, Schewe D, Peipp M, Rösner T, Humpe A, Kellner C: Dual Checkpoint Blockade of CD47 and LILRB1 Enhances CD20 Antibody-Dependent Phagocytosis of Lymphoma Cells by Macrophages. (*Frontiers in Immunology*, Accepted, doi: 10.3389/fimmu.2022.929339). **IF 8.8**
2. Kunz P, Stuckenberger E, Hausmann K, Gentiluomo L, Neustrup M, Michalakis S, Rieser R, Romeijn S, Wichmann C, **Windisch R**, Hawe A, Jiskoot W, Menzen T: Understanding opalescence measurements of biologics – a comparative study of methods, standards, and molecules. (*International Journal of Pharmaceutics*, Accepted, IJP_122321). **IF 6.5**
3. Redondo Monte E, Leubolt G, **Windisch R**, Kerbs P, Dutta S, Landspersky T, Istvánffy R, Oostendorp R, Chen-Wichmann L, Cusan M, Schotta G, Wichmann C, Greif PA: Specific effects of somatic GATA2 zinc finger mutations on erythroid differentiation. **Experimental Hematology** 2022, 108:26-35. **IF 3.2**
4. Chen-Wichmann L, Shvartsman M, Preiss C, Hockings C, **Windisch R**, Redondo Monte E, Leubolt G, Spiekermann K, Lausen J, Brendel C, Grez M, Greif PA, Wichmann C: Compatibility of RUNX1/ETO fusion protein modules driving CD34+ human progenitor cell expansion. **Oncogene**. 2019, 38(2):261-272. **IF 8.7**

Unpublished Articles:

1. **Windisch R**, Soliman S, Hoffmann A, Chen-Wichmann L, Vosberg S, Lutz S, Kellner C, Redondo Monte E, Hartmann L, Schneider S, Beier F, Strobl CD, Weigert O, Peipp M, Schuendeln M, Bernhagen J, Humpe A, Klump H, Brendel C, Greif PA, Wichmann C: Engineering an inducible leukemia-associated transcription factor enables large-scale *ex vivo* production of functional human phagocytes. (*In Preparation*).
2. Swoboda A, **Windisch R**, Kerbs P, Redondo Monte E, Bagnoli JW, Chen-Wichmann L, Caroleo A, Cusan M, Krebs S, Blum H, Enard W, Herold T, Wichmann C, Greif PA: CSF3R T618I collaborates with RUNX1-RUNX1T1 to expand hematopoietic progenitors and sensitizes to GLI-Inhibition. (*HemaSphere*, Under Review). **IF 8.3**
3. Schabernack S*, **Windisch R***, Setzer S, Chen-Wichmann L, Kreissig S, Maenner D, Schuendeln M, Humpe A, Kellner C, Wichmann C: A dual-mode iCasp9-RQR8 expression cassette to improve targeted eradication of transduced cells. **equal contribution* (*Cytotherapy*, Under Review). **IF 6.2**

Reviews:

1. **Windisch R**, Pirschtat N, Kellner C, Chen-Wichmann L, Lausen J, Humpe A, Krause DS, Wichmann C: Oncogenic deregulation of cell adhesion molecules in leukemia. **Cancers**. 2019, Mar 5;11(3), 311. **IF 6.6**

Book Chapters:

1. **Windisch R**, Kreissig S, Wichmann C: Defined Human Leukemic CD34+ Liquid Cultures to Study HDAC/Transcriptional Repressor Complexes, In: Krämer OH (ed.): HDAC/HAT Function Assessment and Inhibitor Development. Humana Press, New York. **Methods in Molecular Biology**. 2023;2589:27-49. **IF 1.3**

Abstracts:

Hilger P, Zeller T, Vogiatzi F, Muennich IA, **Windisch R**, Wichmann C, Nimmerjahn F, Valerius T, Peipp M, Schewe D, Humpe A, Kellner C: Enhancing CD38 Antibody-Mediated Phagocytosis of T-ALL Cells by Fc engineering and CD47 blockade. **Jahrestagung der Deutschen, Österreichischen und Schweizerischen Gesellschaften für Hämatologie und Medizinische Onkologie, Vienna**, October 7-10, 2022. *Oncol Res Treat* 45 (Suppl. 2): 92.

Zeller T, Lutz S, Muennich IA, **Windisch R**, Hilger P, Herold T, Tahiri N, Banck J, Weigert O, Moosmann A, von Bergwelt-Baildon M, Bruns H, Wichmann C, Valerius T, Schewe D, Peipp M, Rösner T, Humpe A, Kellner C: Immune Checkpoint Co-Blockade of CD47 and HLA Receptors to Enhance CD20 Antibody-Dependent Cellular Phagocytosis of Lymphoma Cells. **Jahrestagung der Deutschen, Österreichischen und Schweizerischen Gesellschaften für Hämatologie und Medizinische Onkologie, Vienna**, October 7-10, 2022. *Oncol Res Treat* 45 (Suppl. 2): 162.

Zeller T, Lutz S, Muennich IA, **Windisch R**, Hilger P, Herold T, Tahiri N, Banck J, Weigert O, Moosmann A, von Bergwelt-Baildon M, Bruns H, Wichmann C, Valerius T, Schewe D, Peipp M, Rösner T, Humpe A, Kellner C: Dual Immune Checkpoint Blockade of LILRB1 and CD47 Enhances Antibody-Dependent Cellular Phagocytosis of Lymphoma Cells by CD20 Antibodies. **Joint Meeting of the German Society of Immunology (DGfI) & the Austrian Society for Allergology & Immunology (ÖGAI), Hannover**, September 7-10, 2022. *Eur J Immunol* 52 (Suppl. 1): 118.

Roesch A, **Windisch R**, Wichmann C, Wolkers WF, Kersten G, Menzen T: Membrane permeability of Jurkat cells to cryoprotective agents determined by flow imaging microscopy. **CRYO2022 Joint Meeting of the Society for Cryobiology and the Society for Low Temperature Biology, Dublin**, July 19-22, 2022.

Windisch R, Soliman S, Hoffman A, Chen-Wichmann L, Lutz S, Kellner C, Redondo Monte E, Vosberg S, Hartmann L, Schneider S, Beier F, Strobl CD, Weigert O, Peipp M, Schuendeln M, Bernhagen J, Humpe A, Brendel C, Klump H, Greif PA, Wichmann C: From harmful to useful: exploiting a leukemic transcription factor for large-scale *ex vivo* manufacture of human macrophages. **ISCT 2022 Annual Meeting, San Francisco**, May 4-7, 2022. *Cytotherapy* 24(5): S100-S101.

Windisch R, Soliman S, Hoffman A, Chen-Wichmann L, Lutz S, Kellner C, Redondo Monte E, Vosberg S, Hartmann L, Schneider S, Beier F, Strobl CD, Weigert O, Peipp M, Schuendeln M, Bernhagen J, Humpe A, Brendel C, Klump H, Greif PA, Wichmann C: An inducible leukemia-associated transcription factor facilitates large-scale *ex vivo* generation of functional human macrophages. **63rd ASH Annual Meeting and Exposition, Atlanta**, December 11-14, 2021. *Blood* 138 (Suppl. 1): 2805.

Swoboda A, **Windisch R**, Kerbs P, Redondo Monte E, Bagnoli JW, Chen-Wichmann L, Caroleo A, Cusan M, Krebs S, Blum H, Enard W, Herold T, Wichmann C, Greif PA: CSF3R T618I collaborates with RUNX1-RUNX1T1 to expand hematopoietic progenitors and sensitizes to GLI-Inhibition. **63rd ASH Annual Meeting and Exposition, Atlanta**, December 11-14, 2021. *Blood* 138 (Suppl. 1): 2233.

Windisch R, Schabernack S, Chen-Wichmann L, Maenner D, Hildebrandt M, Humpe A, Kellner C, Wichmann C: Efficient CAR T cell generation starting with LRS-chambers of thrombocyte apheresis-sets. **54. Jahrestagung der deutschen Gesellschaft für Transfusionsmedizin und Immunhämatologie (DGTI), Vienna**, September 22-24 2021. *Transfus Med Hemother* 48 (Suppl 1): 65.

Schabernack S, **Windisch R**, Setzer S, Chen-Wichmann L, Humpe A, Kellner C, Wichmann C: An engineered iCas9-T2A-RQR8 suicide cassette for efficient 2-step purification and controllable eradication of gene-modified cells. **54. Jahrestagung der deutschen Gesellschaft für Transfusionsmedizin und Immunhämatologie (DGTI), Vienna**, September 22-24, 2021. *Transfus Med Hemother* 48 (Suppl. 1): 13.

Windisch R, Soliman S, Hoffmann A, Chen-Wichmann L, Lutz S, Kellner C, Redondo Monte E, Vosberg S, Hartmann L, Schneider S, Beier F, Strobl CD, Weigert O, Schuendeln M, Bernhagen J, Humpe A, Brendel C, Klump H, Greif PA, Wichmann C: Converting a leukemic transcription factor into a powerful tool for large-scale *ex vivo* production of human phagocytes. **ISCT 2021 Annual Meeting, New Orleans**, May 26-28, 2021. *Cytotherapy* 23(5): S76.

Windisch R, Soliman S, Hoffmann A, Chen-Wichmann L, Kellner C, Redondo-Monte E, Hartmann L, Schneider S, Bernhagen J, Weigert O, Klump H, Brendel C, Humpe A, Greif PA, Wichmann C: Converting a leukemic transcription factor into a powerful tool for large-scale *ex vivo* production of lymphoma cell engulfing macrophages. **53. Jahrestagung der deutschen Gesellschaft für Transfusionsmedizin und Immunhämatologie (DGTI), Berlin**, September 16-18, 2020. **Best Abstract Award**. *Transfus Med Hemother* 47 (Suppl. 1): 35.

Windisch R, Soliman S, Hoffmann A, Chen-Wichmann L, Kellner C, Redondo-Monte E, Hartmann L, Schneider S, Bernhagen J, Klump H, Humpe A, Greif PA, Wichmann C: Tricking the devil with an engineered protein switch for *ex vivo* blood cell production. **ISCT 2020 Annual Meeting, Paris**, May 28-29, 2020. *Cytotherapy* 22: S26S186.

Windisch R, Soliman S, Hoffmann A, Kellner C, Chen-Wichmann L, Bernhagen J, Klump H, Humpe A, Greif P.A, Wichmann C: An engineered MLL-ENL protein switch facilitates *ex vivo* expansion and monocytic differentiation of CD34+ progenitors. **52. Jahrestagung der deutschen Gesellschaft für Transfusionsmedizin und Immunhämatologie (DGTI), Mannheim**, September 18-20, 2019. *Transfus Med Hemother* 46 (Suppl. 1): 26.

Setzer S, Chen-Wichmann L, **Windisch R**, Dick A, Humpe A, Kellner C, Wichmann C: Development of a dual iCas9-RQR8 inducible suicide cassette for efficient purification and eradication of gene-modified cells. **52. Jahrestagung der deutschen Gesellschaft für Transfusionsmedizin und Immunhämatologie (DGTI), Mannheim**, September 18-20, 2019. *Transfus Med Hemother* 46 (Suppl. 1): 36.

Windisch R, Pirschtat N, Soliman S, Chen-Wichmann L, Kellner C, Setzer S, Shvartsman M, Herold T, Humpe A, Greif PA, Wichmann C: Unexpected properties of a novel t(11;19) out-of-frame MLL fusion gene in expanding human CD34+ blood progenitor cells resembling acute myelomonoblastic leukemia AML M4/5. **ACUTE LEUKEMIAS XVII Biology and Treatment Strategies, Munich**, February 24-27, 2019. *Ann Hematol* 98 (Suppl. 1):S5.

Soliman S, **Windisch R**, Pirschtat N, Setzer S, Chen-Wichmann L, Humpe A, Wichmann C: Engineering of inducible transcription factors (iTFs) to explore human ex vivo CD34+ cell expansion and differentiation. **51. Jahrestagung der deutschen Gesellschaft für Transfusionsmedizin und Immunhämatologie (DGTI), Lübeck**, September 19-21, 2018. *Transfus Med Hemother* 45 (Suppl. 1): 9.

Windisch R, Chen-Wichmann L, Shvartsman M, Preiss C, Hockings C, Redondo Monte E, Leubolt G, Spiekermann K, Lausen J, Brendel C, Grez M, Greif PA, Wichmann C: Dissecting an aberrant transcription factor: Convertibility of RUNX1/ETO fusion protein modules driving CD34+ human progenitor cell expansion. **XXII. Wilsede Meeting, Wilsede**, June 30-July 03, 2018.

Pirschtat N, Soliman S, **Windisch R**, Chen-Wichmann L, Kellner C, Humpe A, Greif P.A., Wichmann C: A t(11;19) out-of-frame MLL fusion gene expands human CD34+ blood progenitor cells resembling acute myelomonoblastic leukemia AML M4/5. **International Symposium Cancer Evolution, Munich**, March 1-3, 2018.